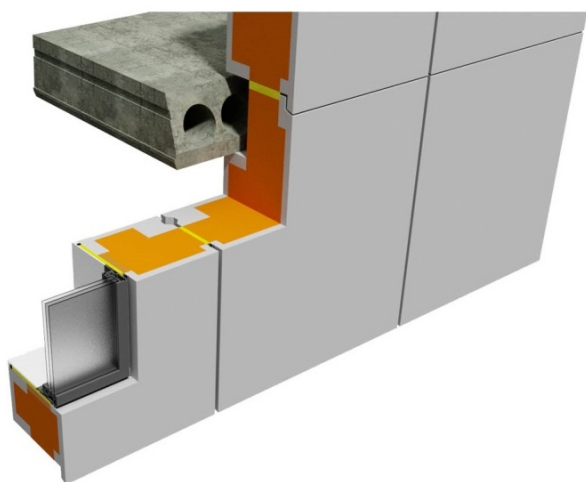


# Analysis and Development of Advanced Sandwich Elements for Sustainable Buildings

Kamil Hodicky



DTU Civil Engineering report R-332  
September 2015

# Analysis and Development of Advanced Sandwich Elements for Sustainable Buildings

Kamil Hodicky

Ph.D. Thesis

Department of Civil Engineering  
Technical University of Denmark

2015

Figure front page:  
Generic view of thin-walled High Performance Concrete Sandwich Panels (Connovate, 2015).

## Analysis and Development of Advanced Sandwich Elements for Sustainable Buildings

Copyright ©, Kamil Hodicky, 2015

Printed by Rosendahls-Schultz Grafisk

Department of Civil Engineering

Technical University of Denmark

ISBN: 9788778774224

ISSN: 1601-2917

Report: Byg R-332

# Preface

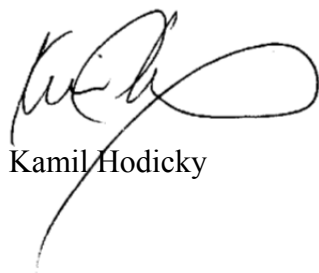
This thesis is submitted as a partial fulfilment of the requirements for the Danish Ph.D. degree. The thesis is based on experimental and numerical investigations carried out as a subproject in the main The Danish National Advanced Technology Foundation-project focusing on optimization of structural behaviour of advanced sandwich elements for sustainable buildings. The project was undertaken at the Department of Civil Engineering at the Technical University of Denmark (DTU Byg), Kgs. Lyngby, Denmark between July 2011 and June 2015.

The project included an external research stay at the North Carolina State University, USA and a leave of absence; twelve months in connection with the industrial Conelto project ([www.conelto.dk](http://www.conelto.dk)) regarding optimization and development of new types Ultra High Performance Fiber Reinforced Concretes for Conelto wind mill towers.

The principal supervisor of the Ph.D. project was Professor Henrik Stang from DTU Byg with co-supervisor Associate Professor Jacob Wittrup Schmidt, also from DTU Byg.

Financial support was provided by The Danish National Advanced Technology Foundation.

Kgs. Lyngby the 30<sup>th</sup> of June 2015



Kamil Hodicky





# Acknowledgments

The presented work would not have been achieved without the help and support of a range of people and I would like to take the opportunity to express them my gratitude.

First of all, I would like to acknowledge the supervision of Professor Henrik Stang. He was the one who guided me all my way through and provided me numerous useful advices and feedbacks. Next, I would like to name several of my colleagues that contributed significantly to the present work. They are Associate Professor Jacob Wittrup Schmidt, Assistant Professor Jens Henrik Nielsen and PhD student Thomas Hulin.

Secondly, I would like to thank to my spouse Barbora for her support, love and understanding she has had for me all the time. Barbora has been always my biggest motivation to overcome any obstacles that I encountered.

Furthermore, I would like to thank to whole team of Connovate for great collaboration and support during the development of High Performance Concrete Sandwich Panels. Special thanks go to PhD student Natalie Williams Portal from Chalmers University of Technology, Sweden for her help and guidance with modelling work.

Further, I need to express my gratitude to Professor Sami Rizkalla and colleagues from Constructed Lab Facilities at North Carolina State University, who made my external stay pleasant and fruitful.

I gratefully acknowledge support from Danish Technological Institute for funding this Ph.D. project. Financial contributions supporting experimental investigations, traveling, and conference attendance from Otto Mønsted Fond, Oticon Fonden, Larsen and Nielsen Fond, G.A. Hagemanns Mindefond, Reinholdt W. Jorck og Hustrus Fond, Torben og Alice Frimodts Fond, COWIfonden, and USA-Danish Networking programme were also very much appreciated.

Finally, I would like to thank to my family and friends who encouraged me throughout the entire project. Even though they were in another country, I could feel their support every day.



# Abstract

Building industry represents nearly 40 % of primary energy consumption in most countries registered in the International Energy Agency. This makes the building sector the highest energy consuming sector in industry worldwide. To fulfil energy reduction objectives, European Union (EU) countries and companies are looking for solutions to lower the energy demands from the building sector. Therefore, ambitious targets for energy consumption of new buildings are being implemented, and by the year 2020 nearly zero energy buildings will become a requirement in the EU. As a consequence of these requirements as well as general requirements for increased efficiency and sustainability, the building sector is experiencing a growing demand for modular, lightweight building elements having a high degree of insulation, a long life time, a low CO<sub>2</sub> emission, a low consumption of raw material, and an attractive surface with minimum maintenance. The need for improvement, innovative structures and production methods therefore grows. In this challenging environment, precast thin-walled High Performance Concrete (HPC) Sandwich Panels offer an interesting solution to all actors involved in the value chain of the building, from the architects and the manufacturers to the end owners. However, the literature available with respect to analysis and/or design of thin-walled HPC sandwich panels is scarce.

The goal of this work was to develop a framework for analysis and optimization of the precast thin-walled High Performance Concrete Sandwich Panels. The present framework was led at three levels.

The first level experimentally investigated material and mechanical properties of shear connectors, insulation layer and HPC. Material characterization included assessment of time dependent strength, fracture properties, stiffness and shrinkage for HPC.

In a second stage, the structural level was described to study the influence of the various constituents of the sandwich panel on the behaviour of the panel under shear and bending loading. The experimental investigations focused on using the metallic, Basalt Fiber Reinforced Polymer (BFRP) and Carbon Fiber Reinforced Polymer (CFRP) connecting systems in combination with rigid foam. The experimental program included testing of small-scale specimens by applying shear (push-off) loading and semi-full scale specimens by flexural loading. Further, two full-scale thin-walled HPC sandwich panels were exposed to flexural loading.

Both the material level and the structural level were described through experimental and numerical investigations. A non-linear 3-D FEM model was developed using commercial programme Diana. Results of FEM analysis were found in good agreement with the experimental results. The FEM model was capable predicting behaviour of HPC sandwich panel exposed to shear and flexural loading with reasonable accuracy.

cy. Further, numerical study was performed to assess the risk of early age cracking and to analyse the robustness of thin-walled sandwich panels at early ages. The approach investigates the constrained shrinkage that the external HPC plate is subjected to. The modelling approach studied crack propagation in dependence on the stiffness of the restraints as well as distance between the restraints. The analysis predicts when cracking occurs and, if it occurs, how severe the consequences are.

Finally, the third level was concerned about structural and cost optimization of the proposed sandwich system. The optimization procedure was performed to find the structurally and thermally efficient design of load-carrying thin-walled precast HPC sandwich panels with an optimal economical solution. The optimization approach was based on the selection of material's performances and panel's geometrical parameters as well as on material cost functions in the sandwich panel design. The strength based design of sandwich panels is in competence with the format of Eurocode 2. The optimization process outcomes in complex of design recommendations, which fulfil the requirement of minimum cost for those elements.

# Resumé (in Danish)

Bygningsindustrien producerer næsten 40 % af det primære energiforbrug i de fleste lande registreret i det International Energi Agentur. Dette gør bygningssektoren til den største forbruger af energi verden over. For at nå målsætningerne til energireduktion, er EU lande og virksomheder på udkig efter løsninger der kan reducere energibehovet i bygningssektoren. Ambitiøse mål for energiforbrug i nybyggeri bliver implementeret, og fra 2020 vil det blive et krav om nul energi bygninger i EU. En konsekvens af disse krav, i tillæg til generelle krav til højere effektivisering og bæredygtighed i byggeriet, oplever bygningssektoren en voksende efterspørgsel af modulbyggeri med letvægtslementer med høj isoleringsevne, lang levetid, lavt CO<sub>2</sub> udslip, lavt forbrug af råmaterialer og en attraktiv og vedligeholdelsesfri overflade.

Behovet for forbedringer, innovative konstruktionsløsninger og produktionsmetoder er derfor stærkt stigende. I denne sammenhæng tilbyder præfabrikerede tyndvæggede sandwichelementer ved brug af højstyrkebeton interessante muligheder til alle involverede aktører i byggeriets værdikæde. Fra arkitekter og producenter til slutkunden. Den tilgængelige litteratur vedrørende strukturel analyse og dimensionering af tyndvæggede højstyrkebeton elementer er dog begrænset.

Målet med dette arbejde er at udvikle en rationel metode for analyse og optimering af præfabrikerede tyndvæggede højstyrkebeton elementer. For at nå denne målsætning er dette studie inddelt i tre faser.

Den første fase indeholder eksperimentelle forsøg af materiale- og mekaniske egenskaber for forskydningssamlinger, isolering og højstyrkebeton. Undersøgelsen inkluderer en vurdering af tidsafhængige styrkeegenskaber, brudegenskaber, stivhed, samt svind for højstyrkebeton.

I den næste fase, er den strukturelle opførsel beskrevet, for at studere sensitiviteten af forskellige bestanddele i sandwichelementet under forskydning og bøjning. Forsøgene fokuserer på brug af stålfiber, bassalt fiberarmeret polymer og karbon fiberarmeret polymer som samlingssystemer i kombination med stiv skum. Eksperimenterne inkluderer små-skala forsøg med prøvelegemer udsat for forskydning og semi-fuldskala forsøg med prøvelegemer udsat for bøjning. Endvidere, er der udført to fuld-skala forsøg med tyndvæggede højstyrkebeton elementer udsat for bøjning.

Både materiale-og strukturelt niveau er beskrevet gennem eksperimentelle og numeriske undersøgelser. En ikke-lineær 3-D Finite Element (FE) model blev udviklet ved brug af det kommercielle programmet DIANA. FE-modellen viser god overensstemmelse mellem numeriske og eksperimentelle resultater. FE-modellen kan beskrive opførslen af højstyrkebeton elementer udsat for forskydning- og bøjning med tilfredsstillende nøjagtighed. Endvidere, blev numeriske studier benyttet til at vurdere risikoen for tidlig revnedannelse og til at analysere holdbarheden af tyndvæggede sandwich

elementer i dens tidlige levealder. Denne metode undersøger det svind højstyrkebetonen pladerne er udsat for når de er indspændt. Modellerings metoden studerer revneudvikling afhængig af stivheden af tilstødende materialer, i tillæg til afstanden mellem understøtninger. Analysen estimerer når revnedannelse opstår, og hvis den opstår, hvor alvorlige konsekvenserne er.

Tredje fase, koncentrerer sig om optimering af konstruktion og omkostninger for det foreslåede sandwichsystem. Optimeringsprocessen blev udført for at finde et effektivt design med hensyn til strukturelle egenskaber og temperatur egenskaber for præfabrikerede tyndvæggede højstyrkebeton elementer, der samtidig er økonomisk attraktiv. Optimeringsstrategien blev baseret på en udvælgelse af materialernes funktion og elementernes geometriske parametre, i tillæg til materialeomkostninger i dimensionering af sandwich elementer. Dimensioneringen af sandwich elementer er i overensstemmelse med Eurocode 2. Optimeringsprocessen resulterer i anbefalinger til dimensionering af præfabrikerede tyndvæggede højstyrkebeton elementer som opfylder kravet til lavest mulig pris.

# Table of Contents

|          |   |           |
|----------|---|-----------|
| <b>1</b> | <b>Introduction</b>                             | <b>1</b>  |
| 1.1      | State of art of sandwich panels .....           | 1         |
| 1.1.1    | FRP shear connectors .....                      | 4         |
| 1.1.2    | Degree of composite action .....                | 7         |
| 1.2      | Background .....                                | 11        |
| 1.3      | Objectives .....                                | 12        |
| 1.4      | Scope.....                                      | 14        |
| 1.4.1    | Research approach.....                          | 14        |
| 1.4.2    | Limitations and assumptions .....               | 15        |
| 1.5      | Organization of thesis .....                    | 16        |
| <b>2</b> | <b>High Performance Concrete</b>                | <b>21</b> |
| 2.1      | Introduction.....                               | 21        |
| 2.2      | Fiber Reinforcement .....                       | 23        |
| 2.2.1    | Loose Fibers .....                              | 24        |
| 2.2.2    | FRP Grids .....                                 | 27        |
| 2.3      | Material and mechanical properties of HPC ..... | 30        |
| 2.3.1    | Compressive properties .....                    | 30        |
| 2.3.2    | Tensile properties .....                        | 31        |
| 2.3.3    | Shear properties .....                          | 33        |
| 2.3.4    | Fracture properties.....                        | 34        |
| 2.3.5    | Shrinkage behaviour .....                       | 35        |
| <b>3</b> | <b>Journal paper 1/Conference paper 1</b>       | <b>39</b> |
| 3.1      | Introduction.....                               | 40        |
| 3.2      | Modelling.....                                  | 41        |
| 3.3      | Experimental procedure.....                     | 46        |
| 3.4      | Results and discussion .....                    | 47        |
| 3.5      | Conclusions.....                                | 50        |
| 3.6      | Acknowledgement .....                           | 50        |
| <b>4</b> | <b>Conference paper 2</b>                       | <b>51</b> |
| 4.1      | Introduction.....                               | 52        |
| 4.2      | Experimental procedure .....                    | 53        |
| 4.3      | Mechanical properties.....                      | 54        |
| 4.3.1    | Compressive strength .....                      | 54        |
| 4.3.2    | Tensile strength .....                          | 55        |
| 4.3.3    | Static elastic modulus .....                    | 55        |
| 4.3.4    | Fracture energy .....                           | 56        |
| 4.3.5    | Autogenous shrinkage-induced stresses .....     | 56        |



|          |   |           |
|----------|---|-----------|
| 4.4      | Assessment risk of fracture.....                          | 59        |
| 4.5      | Conclusions.....  | 61        |
| <b>5</b> | <b>Conference paper 3</b>                                 | <b>63</b> |
| 5.1      | Introduction.....   | 64        |
| 5.2      | Experimental program .....                                | 66        |
| 5.3      | Test setup .....  | 66        |
| 5.3.1    | Push-off specimen details.....                            | 66        |
| 5.3.2    | Flexural specimen details .....                           | 67        |
| 5.4      | Test instrumentation .....                                | 67        |
| 5.4.1    | Push-off test instrumentation.....                        | 67        |
| 5.4.2    | Flexural test instrumentation .....                       | 68        |
| 5.5      | Test results and failure modes .....                      | 69        |
| 5.5.1    | Push-off test results and failure modes.....              | 69        |
| 5.5.2    | Flexural test results, modelling and failure modes.....   | 70        |
| 5.6      | Conclusions.....  | 71        |
| 5.6.1    | Push-off test.....  | 71        |
| 5.6.2    | Flexural test .....                                       | 71        |
| 5.6.3    | Numerical modelling.....                                  | 72        |
| <b>6</b> | <b>Journal paper 2</b>                                    | <b>73</b> |
| 6.1      | Introduction.....   | 74        |
| 6.2      | Experimental investigation .....                          | 77        |
| 6.2.1    | Material properties.....                                  | 78        |
| 6.2.2    | Panel configurations .....                                | 79        |
| 6.2.3    | Fabrication of the panels .....                           | 81        |
| 6.2.4    | Test setup.....   | 81        |
| 6.2.5    | Test instrumentation .....                                | 82        |
| 6.3      | Finite element analysis.....                              | 83        |
| 6.3.1    | Concrete - element and constitutive relationships.....    | 83        |
| 6.3.2    | Rigid Foam - element and constitutive relationships ..... | 83        |
| 6.3.3    | CFRP Grid - element and constitutive relationships .....  | 84        |
| 6.3.4    | Rigid foam/concrete interface .....                       | 84        |
| 6.3.5    | CFRP grid/concrete interface .....                        | 85        |
| 6.3.6    | Loading and boundary conditions .....                     | 86        |
| 6.4      | Results and Discussion .....                              | 86        |
| 6.4.1    | Failure modes - all panels.....                           | 86        |
| 6.4.2    | Panels without CFRP grid .....                            | 87        |
| 6.4.3    | Debonded panels .....                                     | 88        |
| 6.4.4    | Panels with CFRP grid .....                               | 89        |
| 6.5      | Design Equation.....                                      | 91        |
| 6.6      | Parametric Study.....                                     | 92        |
| 6.7      | Conclusions.....  | 93        |

|          |  |            |
|----------|--|------------|
| 6.8      | Acknowledgement .....  | 94         |
| <b>7</b> | <b>Full scale testing and modelling</b>                        | <b>95</b>  |
| 7.1      | Introduction.....  | 95         |
| 7.2      | Experimental investigation .....                               | 96         |
| 7.2.1    | Material properties.....                                       | 96         |
| 7.2.2    | Panel configuration.....                                       | 97         |
| 7.2.3    | Fabrication of the panels .....                                | 98         |
| 7.2.4    | Test setup.....  | 99         |
| 7.2.5    | Test instrumentation .....                                     | 101        |
| 7.3      | Finite element analysis.....                                   | 104        |
| 7.3.1    | Concrete - element and constitutive relationships.....         | 104        |
| 7.3.2    | Rigid insulation - element and constitutive relationships..... | 104        |
| 7.3.3    | Steel - element and constitutive relationships .....           | 104        |
| 7.3.4    | BFRP grid - element and constitutive relationships .....       | 105        |
| 7.3.5    | Rigid insulation/concrete interface.....                       | 105        |
| 7.3.6    | Rigid insulation/rigid insulation interface .....              | 105        |
| 7.3.7    | Steel/concrete interface .....                                 | 105        |
| 7.3.8    | BFRP grid/concrete interface .....                             | 106        |
| 7.3.9    | Loading and boundary conditions .....                          | 106        |
| 7.4      | Results and discussion .....                                   | 107        |
| 7.4.1    | Failure modes .....  | 107        |
| 7.4.2    | Experimental and numerical results .....                       | 109        |
| 7.4.3    | Crack development.....   | 109        |
| 7.5      | Conclusion .....   | 110        |
| <b>8</b> | <b>Journal paper 3</b>   | <b>111</b> |
| 8.1      | Optimization problem.....                                      | 112        |
| 8.2      | Theoretical background .....                                   | 114        |
| 8.2.1    | Fictitious Crack Model.....                                    | 114        |
| 8.3      | Basic hypothesis .....   | 115        |
| 8.4      | Parametric study .....   | 116        |
| 8.4.1    | Non-linear FE model .....                                      | 117        |
| 8.4.2    | Linear elastic FE model.....                                   | 118        |
| 8.5      | Results and discussion .....                                   | 118        |
| 8.6      | Case study .....   | 120        |
| 8.6.1    | Material properties.....                                       | 120        |
| 8.6.2    | FE model .....   | 122        |
| 8.6.3    | Results and discussion.....                                    | 124        |
| 8.7      | Conclusion .....   | 126        |
| 8.8      | Acknowledgments .....  | 126        |

|  |            |
|--|------------|
| <b>9 Journal paper 4</b>   | <b>127</b> |
| 9.1 Introduction.....  | 128        |
| 9.2 Optimization problem.....                                      | 131        |
| 9.2.1 Formulation of the optimization problem.....                 | 132        |
| 9.2.2 Objective function .....                                     | 133        |
| 9.2.3 Design prerequisites .....                                   | 133        |
| 9.2.4 Constraints.....   | 134        |
| 9.3 Ultimate and serviceability limit state analysis of HPCSP..... | 136        |
| 9.3.1 Flexural failure mode .....                                  | 137        |
| 9.3.2 Shear failure mode.....                                      | 140        |
| 9.3.3 Global HPCSP buckling.....                                   | 140        |
| 9.3.4 Local HPC plate buckling .....                               | 141        |
| 9.3.5 Deflections and cracking in the HPCSP .....                  | 142        |
| 9.4 Material cost function .....                                   | 142        |
| 9.4.1 HPC plates .....   | 142        |
| 9.4.2 Insulation layer .....                                       | 143        |
| 9.4.3 Shear connectors and reinforcement .....                     | 144        |
| 9.5 Optimization procedure .....                                   | 144        |
| 9.6 Results and discussion .....                                   | 146        |
| 9.7 Parametric study .....   | 151        |
| 9.7.1 Local HPC plate buckling .....                               | 151        |
| 9.7.2 Global HPCSP buckling.....                                   | 151        |
| 9.8 Conclusions.....   | 153        |
| 9.9 Acknowledgments .....  | 154        |
| <b>10 Conclusions and recommendations for further work</b>         | <b>155</b> |
| 10.1 Conclusions.....  | 155        |
| 10.2 Recommendations for further work.....                         | 160        |
| <b>Additional publications (not included in the thesis)</b>        | <b>163</b> |
| <b>Bibliography</b>  | <b>165</b> |

# Chapter 1

## Introduction

### 1.1 State of art of sandwich panels

In 1849, French gardener Joseph Monier wanted to make a more durable flowerpot, so he used iron mesh to reinforce garden pots and tubs. That was the beginning of reinforced concrete and the basis of precast concrete structures. In the early years of the 20th century, concrete was rapidly becoming the most popular building material. At those times no cranes were available and concrete was solely produced off-site and walls were built vertically. The earliest application of precast elements is dated around 1893 at Camp Logan Rifle Range, Illinois, USA. Instead of using the usual method in making concrete walls vertically, Robert Aiken designed and built retaining wall using steel tipping table. After concrete hardened the panels were tilted up onto a prepared foundation to form the walls as shown in Figure 1.1. Aiken's steel tipping table made tilt-up construction easier. However, the precast industry started to gain popularity after development of mobile crane in the late 1940s. The mobile crane allowed building much larger panels than before. Also ready-mix concrete was developed around the same time, which allowed even more effectively utilize the construction of commercial precast structures. The biggest boom came after World War II, there was a great need for family, commercial and industrial buildings. Further development led designers and contractors to an idea of tilt-up concrete sandwich panels. The panels were constructed with 50 mm sand layer placed between two layers of concrete plates and tied together by metallic reinforcement. The sand was eventually washed out as the wall was lifted into place, creating a hollow core sandwich panel. Early generations of concrete sandwich wall panels used different kind of materials to separate the

two concrete plates such as woodchips, sand, lightweight concrete and cellular glass (Collins, 1954).



Figure 1.1 *Tilt-slab concrete construction for La Jolla Woman's Club built between years 1912 to 1914 (Schaffer, 1998).*

Collins (1954) suggested that a wood fiber filler material could possibly be used without shear connectors. Nevertheless, most of designers chose to use minimum shear ties for panels. Examples of shear ties used up to this time period are shown in Figure 1.2.

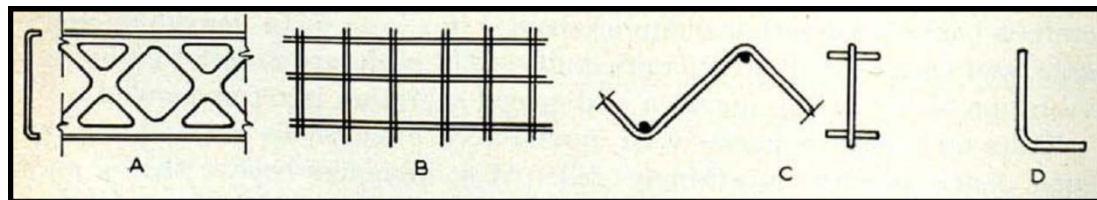


Figure 1.2 *Examples of shear ties placed between two layers of concrete plates (Collins, 1954).*

The utilization of the precast concrete system for single family house is dated to 1938. These precast panels were not sandwich panels and provided only the façade of the structure whilst a wood frame was used to support the panels and to supply the main structure for the home.

Another type of early precast concrete system was developed and patented by Quentin Twachtman in 1935. The system was casted based on similar principles used today. A steel mesh 150/150 mm was cast into concrete layer on wooden formwork. Crimped metal plate was used to form ribs (see Figure 1.3). An insulating layer was placed on concrete layer, followed by another layer of mesh and finally another 30 mm of concrete was cast. The wall thickness was 200 mm and ribs were vertically reinforced. The large wall units were taken to the building site by lorry and assembled in place (Zippodt, 1935). Though the materials used in constructing sandwich panels have

improved significantly, the basic method of producing the panels remains very similar to this early version.

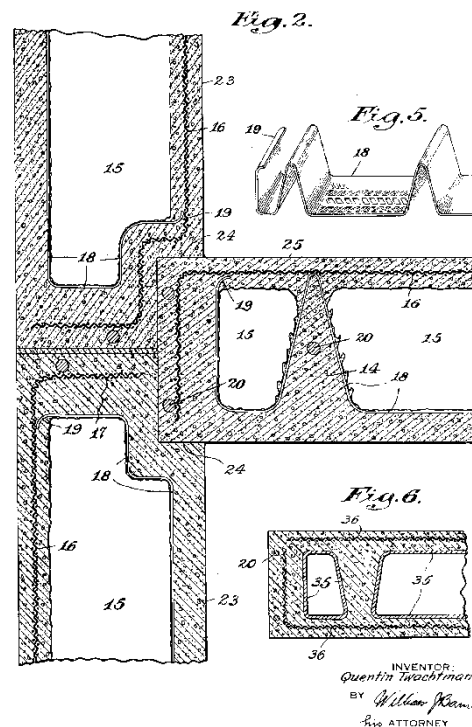


Figure 1.3 *Precast concrete system was developed and patented by Quentin Twachtman (Twachtman, 1936).*

Further utilization of this technique enabled to develop 1000-family houses in 1951-1952 at Great Lakes, Illinois (Lorman & Wiehle, 1953). It was the first large scale use of precast concrete sandwich panels. Steel pin shear connectors were used for construction as shown in Figure 1.2 D. The shear connectors became to ideal for concrete sandwich panels and several variations were used at those times as shown in Figure 1.2. Through development precast concrete sandwich panels became fire-proof. As part of the initiative, Inter Industries, Inc. produced a house made up of concrete sandwich wall panels in which insulation was provided by inserting mineral wool in waterproof bags between two concrete plates. By this time ideal insulation materials were established. Pre-requirements for these materials are to have low density, relatively high compressive strength, high shear strength, good bonding characteristics, high insulative qualities, and low cost. At the time insulation materials used were cellular glass materials, plastic foam, compressed and treated wood fibers in cement, foam, and lightweight concrete. Cellular glass or compressed wood fibers were used for the precision-made type of sandwich wall panel whilst the lightweight concrete mixes were suggested for the cast-in-place large tilt-up sandwich wall panel in order to achieve economic design. The concept of designing of sandwich panels started in the 1960s with solid concrete zones used as core shear transfer mechanism to create full composite action. Nevertheless, the thermal efficiency of these panels was significantly reduced due to thermal bridging caused by the concrete ribs connecting the two

concrete plates through the insulation layer. To reduce thermal losses and maintain the full composite action, metal trusses were used to replace the solid concrete ribs. Although, steel trusses provided an improvement in comparison with solid concrete shear zones, its conductivity still affected the thermal efficiencies of these panels (Glech, 2007).

It was stated that monolithically-cast concrete ribs, concrete shear connectors, or mechanical shear ties should connect the two concrete plates in a sandwich wall panel which are separated by a nonstructural insulation layer. The nonstructural insulation layer should not transfer any shear stresses and only the concrete plates should carry the compressive and bending stresses. Connecting two concrete plates with sufficient shear connectors allows them to act together, as one structural unit in composite action. Non-metallic ties started to be used in the late 1980s to produce thermally efficient non-composite panels; however, structural efficiency was sacrificed. To this time, increase of structural efficiency hampered thermal efficiency and vice versa. Therefore, increasing one desired property was at the expense of the other. Concrete sandwich panel technology leaped forward over past decade with introducing Fiber Reinforce Polymer (FRP) shear reinforcement due to the relatively high stiffness combined with its relatively low thermal conductivity compared to steel (Erki & Rizkalla, 1993; Soriano & Rizkalla, 2013). The proper design with FRP shear reinforcement, concrete sandwich panel can achieve the desired combination of composite action and thermal efficiency.

### 1.1.1 FRP shear connectors

Many efforts have been made to increase the thermal efficiency of precast concrete sandwich wall panels, while maintaining structural efficiency. Wade et al. (1988) and Einea et al. (1994) performed the first attempt to use Glass Fiber Reinforced Polymer (GFRP) connectors for insulated concrete sandwich walls. Salmon et al. (1997) introduced GFRP bars formed in a truss orientation in place of metal wire trusses. The experimental investigation showed that the use of GFRP resulted in 84% composite action compared to 88% for steel truss connectors. The proposed system used in this study is shown in Figure 1.4. To prevent concrete ribs from forming around the FRP bent bar system, thus forming thermal bridges, a small block of insulation was placed around the bar prior to construction as shown in Figure 1.4.

Following the same concept Morcous et al. (2010), Lameiras et al. (2013a, 2013b), Maximos et al. (2007) and Woltman et al. (2013) studied different shapes of GFRP shear connectors to obtain the full composite action. These research programs have indicated that FRP shear connectors can provide the dual purpose of improving the thermal capabilities of a building envelope, while at the same time, providing the desired structural integrity and efficiency.

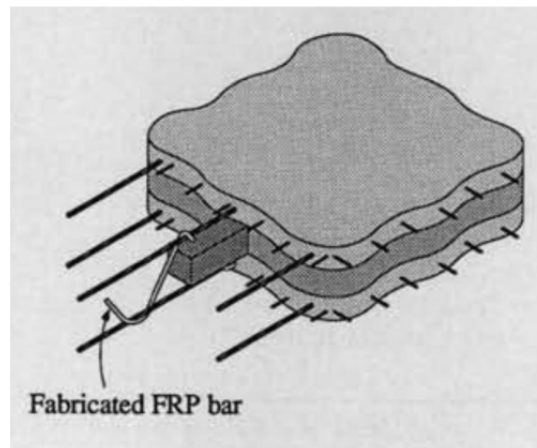


Figure 1.4 *FRP Bent Bar Shear Connector* (PCI Committee on Precast Sandwich Wall Panels, 2011).

Pantelides et al. (2008) presented another innovative technique containing GFRP shells, as shown in Figure 1.5 for shear transfer mechanism. Test results indicated that 97 - 99 % composite action could be attained in precast concrete sandwich wall panels using GFRP shells. It was observed that the panels failed in a ductile manner, suggesting that the GFRP shells provided sufficient shear transfer mechanism between the external and internal concrete plates.



Figure 1.5 *Photo of GFRP Shell with reinforcement and foam insulation installed* (Pantelides et al., 2008).

Frankl et al. (2008, 2011) performed an experimental program to determine the behavior of precast, prestressed concrete sandwich wall panels reinforced with Carbon Fiber Reinforced Polymer (CFRP) shear grid. The use of CFRP grids as trusses enabled significant improvements of mechanical and thermal performances. It was observed that the desired composite action is possible to achieve using either Expanded Polystyrene (EPS) or Extruded Polystyrene (XPS) rigid foam insulation in combination with CFRP grid. Nevertheless, panels constructed using EPS insulation, provided a better shear transfer mechanism and achieved higher percent composite action than XPS insulation due to better bond between EPS foam and concrete. This required higher amount of CFRP shear connectors for combination with XPS in comparison



with EPS insulation. Detail of the panel cross-section and elevation, using CFRP grids, are shown in Figure 1.6.

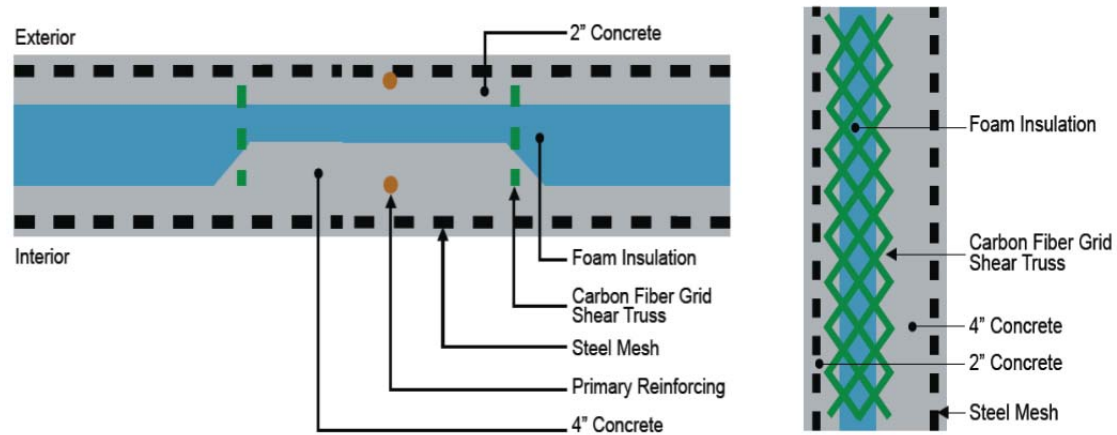


Figure 1.6 Cross section views of panels with CFRP shear grid; 1" = 25.4 mm (Glech, 2007).

The objective of the research by (Frankl et al., 2008, 2011), was to determine the appropriate CFRP shear grid quantity and configuration to achieve optimal structural performance of the sandwich panel for lateral loads. Predicting of shear transfer mechanism for a certain CFRP shear grid in combination with insulation combination is essential to evaluate the structural behavior of a precast concrete sandwich wall panel. The behavior of any shear transfer mechanism must be well quantified in order to predict the ultimate response of a sandwich panel subjected to lateral loading.

Naito et al. (2012) conducted a series of push tests to investigate the shear capacity, failure modes and response of fourteen commercially produced shear ties. The shear connectors tested included those made of carbon steel, stainless steel, galvanized carbon steel, CFRP, GFRP and basalt fiber reinforced polymer (BFRP). Simplified engineer level multi-linear strength curves were developed for each connection. The results indicated that shear ties used in sandwich wall panels have considerable variation in strength, stiffness, and deformability. The maximum shear strength of the discrete ties averaged 10.5 kN with a minimum of 5.52 kN and maximum of 18.4 kN.

Hassan & Rizkalla (2010) and Rizkalla et al. (2009) performed further analyses of the results from experimental program conducted by Frankl et al. (2011). The shear flow capacity of the CFRP shear grid with insulation  $q$  was expressed using the following equation:

$$q = \frac{F}{L} \quad (1.1)$$

where  $q$  is shear flow capacity,  $F$  is the maximum force at the interface at the critical section at the ultimate-load level and  $L$  represent the length of CFRP grid along the width of the panel up to the critical section. The nominal shear flow capacity of the CFRP grid with XPS insulation layer was found to be 33 N/mm, while the CFRP grid

with EPS produced 70 N/mm. Higher values of shear flow strength form EPS insulation was attributed to the superior bond that EPS rigid foam insulation forms at the concrete interface when compared with that of XPS. During post testing inspection of the panels, XPS foam was easily removed by hand as it was completely separated from the concrete plates.

Kim et al. (2010) performed another experimental program using CFRP grid on scaled down specimens. The study was performed to investigate the effect of several parameters such as grid embedment length, insulation thickness and type, shear grid density, and the effect of repeated loading, on the shear flow strength of the composite connector. Results indicated that the shear transfer strength depends on both the shear grid density (spacing), and the insulation type and thickness.

### 1.1.2 Degree of composite action

The structural efficiency of sandwich wall panels depends on degree of composite action. Sandwich wall panels may be designed with various degrees of composite action: non-composite, partially composite or full composite (Rizkalla et al., 2009). Full composite action is developed when the shear forces that are built up at the face of one concrete plate can be transferred to the other plate through action of the shear connectors. This action allows to the both concrete plates work together and resists to the applied forces as a single unit, as shown in Figure 1.7. It is more than obvious that the most effective design is achieved when the predicted full composite behavior matches the actual structural behavior (PCI Committee on Precast Sandwich Wall Panels, 2011). However, the predicted behaviour is highly dependent on the degree of composite action achieved by the concrete sandwich panel.

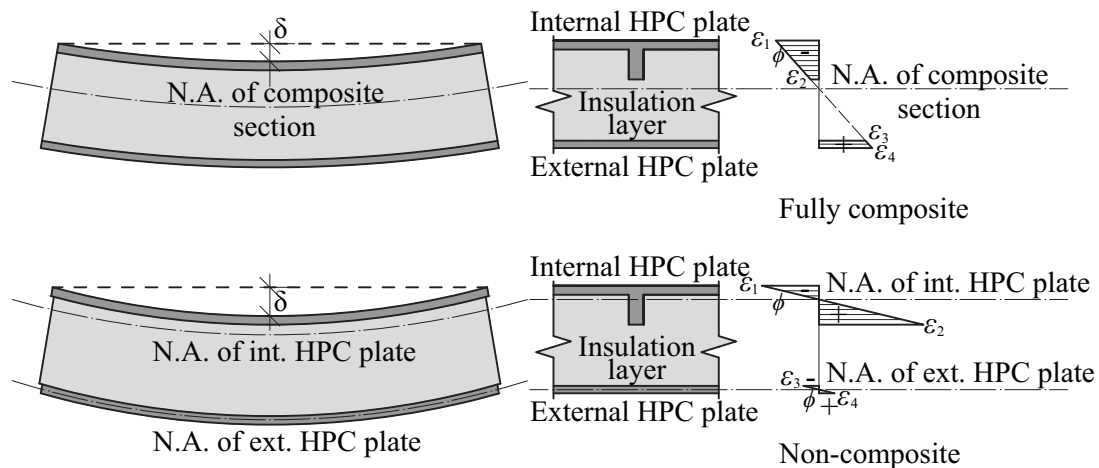


Figure 1.7 Depiction of strain distribution in sandwich panel with full composite and non-composite action.

Until the last decade, knowledge on the performance and behavior of concrete sandwich walls was limited to observation of panels in service and limited testing up to structural failure. Recently, several studies on sandwich wall panel behavior have

been carried out to study diverse parameters believed to affect their behavior (Kazem et al., 2014; Rizkalla et al., 2012; Sopal, 2013; Sopal et al., 2013). These experimental works have been performed in order to better understand the composite behavior of sandwich panels and in effort to develop predictions of their behavior.

Non-composite sandwich wall panels are typically constructed with a thick internal structural concrete plate, whilst the external plate is thin and non-structural. These panels are usually used as architectural cladding. In Figure 1.8 some examples of architectural load-carrying panels are shown (Freedman, 1999). The reason of using these panels instead of full composite panels is due to shear connecting system is kept to a minimum in order to minimize thermal bridging. As a result, panels provide superior thermal capabilities. The self-weight of the external non-structural concrete plate have to be transferred to the internal structural concrete plate through insulation layer.

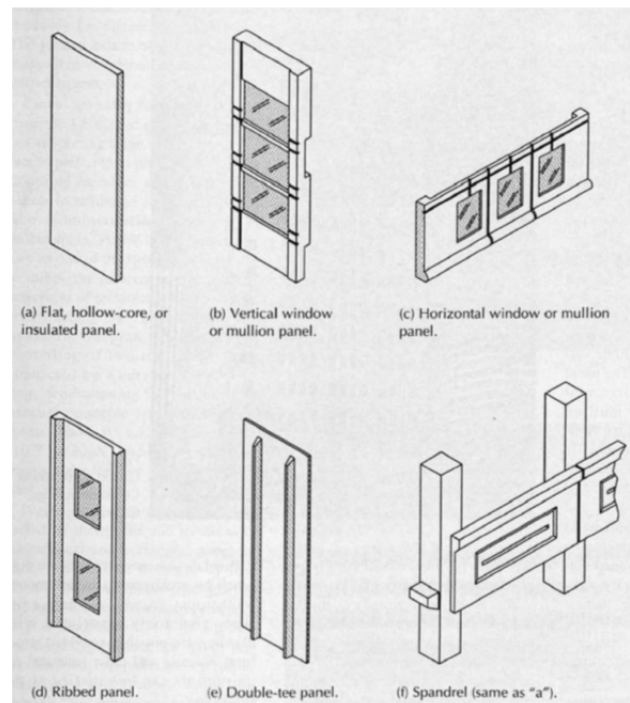


Figure 1.8 *Several examples of Architectural load-carrying sandwich wall panels* (Freedman, 1999).

Transfer and maintaining of structural integrity between the two concrete plates has typically been done by using steel pins and ties, or solid concrete zones. In order to minimize the thermal bridging effect and improve the effective thermal properties of these panels, FRP pins started to be used (Naito et al., 2012). FRP materials have much lower thermal conductivity in comparison with steel and concrete, therefore, effectively breaks the thermal bridge and improves the panel's thermal performance while maintaining structural integrity. Typical non-composite connectors, including FRP connectors, are shown in Figure 1.9.

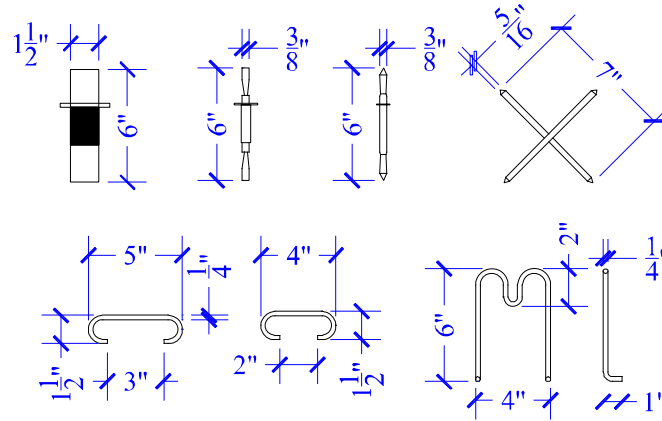


Figure 1.9 Examples of typical non-composite connectors, including FRP connectors; 1" = 25.4 mm (Naito et al., 2012).

Sandwich wall panels with partial degree of composite represents compromise between full composite and non-composite design. These panels are usually thinner than the one designed with non-composite action. The partial composite action can be achieved by connecting the two concrete plates with one-way shear connectors, including wire trusses (Figure 1.10).

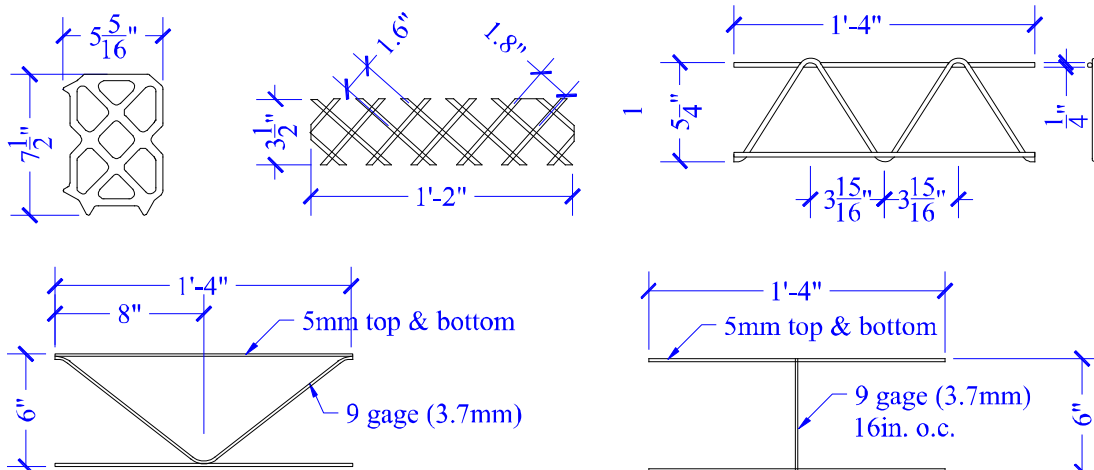


Figure 1.10 Examples of shear connectors used for concrete sandwich walls with partial degree of composite action; 1" = 25.4 mm (Naito et al., 2012).

Nijhawan (1998) showed in his paper that using steel trusses is possible to reach nearly full composite action with proper design approach. He also presented an alternative method for determining the interface shear force in a typical insulated wall panel. Further, he highlighted the urgent need for an appropriate method to evaluate the shear flow characteristics of any shear transfer mechanism used in prestressed precast concrete sandwich wall panels. The pre-requirement for evaluation achieved percentage of composite action is to determine load carrying capacity and stiffness of the shear connectors. Although composite action has many advantages, some disadvantages should mention as well. Bowing of sandwich panels should be taken into consideration during design process. However, bowing of sandwich panels is a complicated issue, and highly dependent on temperature load, humidity gradients and shrinkage of

concrete (Losch, 2003). In some cases, the design of sandwich wall panels can be ultimately controlled by secondary moment effects caused by bowing of these elements. Non-composite sandwich wall panels typically do not experience the thermal bowing due to thermal strain in the external concrete plate is not transferred to the internal plate, i.e. each concrete plates deform independently. The magnitude of precast sandwich wall bowing is governed by degree of composite action; therefore the need of prediction the shear transfer mechanism across the insulation layer is crucial. Bush Jr. & Stine (1994) performed the study on the flexural behavior of non-loadbearing precast concrete sandwich panels using steel truss girders as shear connectors. The tested panels were produced with 50 mm EPS insulation layer and the two 75 mm concrete plates. The two types of panels were constructed, the one type with the truss girders placed in the transverse direction, and the one type with the truss girders placed in the longitudinal direction. The panels with the truss girders oriented longitudinally were able to reach nearly full composite action. Whilst, the panels constructed with truss girders oriented transversely behaved in partial composite manner (60 % composite action). Bush Jr. & Wu (1998) made an effort in estimation of service load deflections and bending stresses for non-loadbearing partial composite sandwich panels. The authors developed a closed form elastic continuum approach for discrete steel truss connectors. The data from experimental work were directly compared with closed form solution and finite element models. The both methods overestimated the prediction of the deflection at mid-span for the two-truss and three-truss panels by approximately 60 and 50 percent, respectively. Further, Bush Jr. & Wu (1998) emphasized the need for better characterization of any shear transfer mechanism used in sandwich wall panels and improves in the prediction of panel performance and behavior. The structural behavior of precast full composite sandwich panels subjected to axial loading and eccentric axial loading was presented by Benayoune et al. (2006; 2007). The panels were behaving in nearly full composite manner, showing the adequacy of the steel truss shear connectors. Shear forces were developed by the bending stresses from the eccentric load.

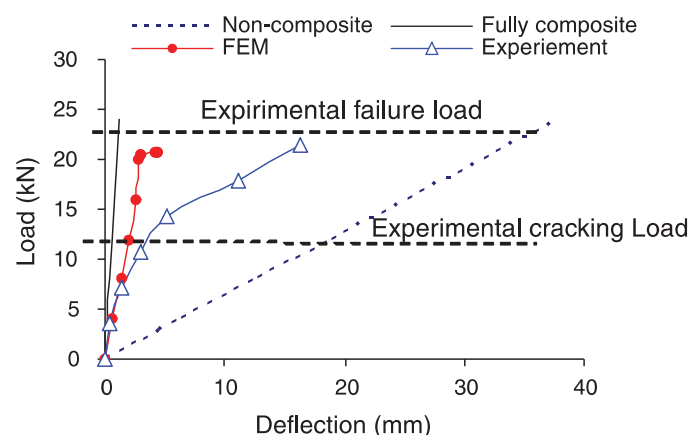


Figure 1.11 Load-deflection profiles at mid-span for panel P11 (Benayoune et al., 2008).

Benayoune et al. (2008) further presented experimental program on the flexural behavior of precast sandwich panels. Finite element analysis was performed and directly compared with experimental results. The results showed that the truss girders were able to transfer a significant amount of shear and create a high degree of composite action, as shown in Figure 1.11.

## 1.2 Background

Building industry represent nearly 40 % of primary energy consumption in most countries registered in the International Energy Agency (IEA - Energy efficiency, 2015). This makes the building sector the highest energy consuming sector in industry worldwide. To fulfil energy reduction objectives, EU countries and companies are looking for solutions to lower the energy demands from the building sector. Therefore, ambitious targets for energy consumption of new buildings are being implemented, and by the year 2020 nearly zero energy buildings will become a requirement in the European Union (European Commission, 2015). As a consequence of these requirements as well as general requirements for increased efficiency and sustainability, the building sector is experiencing a growing demand for modular, lightweight building elements having a high degree of insulation, a long life time, a low CO<sub>2</sub> emission, a low consumption of raw material, and an attractive surface with minimum maintenance. The need for improvement, innovative structures and production methods therefore grows. In this challenging environment, precast thin-walled High Performance Concrete Sandwich Panels (Figure 1.12) offer an interesting solution to all actors involved in the value chain of the building, from the architects and the manufacturers to the end owners.

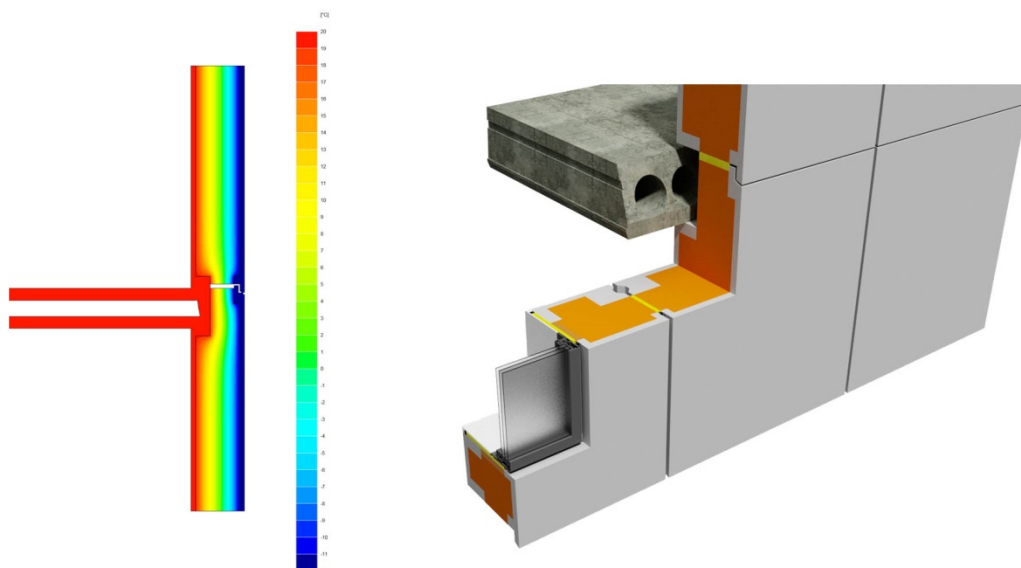


Figure 1.12 *Generic view of thin-walled High Performance Concrete Sandwich Panels and temperature profile throughout the panel (Connovate, 2015).*

The term of sandwich panels comes from the way how they are constructed. They consist of two outer plates of concrete framing a layer of insulation material. The inner concrete plate may be load-carrying, whilst the function of the outer layer is usually to protect the insulation layer from the outside environment and provide an aesthetic exterior aspect. The thickness and type of insulation can be adjusted according to the targeted thermal performance (U-value) of the building. The two concrete plates are usually connected, and the shear forces coming from the dead weight of the outer plate must be transferred to the main structural panel through specific shear connectors.

Sandwich panels have several beneficial features from their structure and manufacturing process. They are made in production plants, which bring a high level of reproducibility and quality control, and production efficiency with a skilled workforce and optimised production methods (Salmon et al., 1997). They are easily transportable and fast to mount on site, which reduces building time since earthworks, foundations and others can be done during panel production. Further, they provide structural efficiency for both low- and high-rise buildings. Finally, they ensure a connected insulation layer through the building including roof and corners, and provide a customisable solution to the end user (Morcous et al., 2010; PCI Committee on Precast Sandwich Wall Panels, 2011). Usually sandwich panels are made of a thick load-carrying plate (150 to 200 mm) of ordinary reinforced concrete (PCI Committee on Precast Sandwich Wall Panels, 2011). This may result in particularly thick walls (up to 600 mm) when combined with a 300 mm thick insulation layer. Therefore, the panels are heavy which allow transporting only few elements at a time, resulting in high transportation costs. In addition, assembly cost may be high due to heavy weight of the sandwich panels and need for heavy weight cranes.

Those issues may be eliminated by using thinner concrete plates, made possible by the use of High Performance Concrete (HPC), as has been investigated by several authors. Recently, Benayoune et al. (2006) studied 40 mm thick structural concrete plates for a case of eccentric loading, Gara et al. (2012) experimentally investigated sandwich panels with wall thickness of 35 mm, and Lameiras et al. (2013a, 2013b) went also for thin profiles.

### 1.3 Objectives

The presented work is part of a wider The Danish National Advanced Technology Foundation research project focussed on the study of the above described sandwich panels. A part of the research project focussed on study of sandwich elements using HPC thin plates exposed to high temperatures (Hulin, 2015), another part studied insulation properties (Hansen, 2015), and a last part examined the effects of using such panels on the indoor environment of buildings (Mikeska, 2014).



The vision and objective of the research project is to develop a new sustainable building system using fiber reinforced HPC for sandwich elements. The system should meet the visions of low energy use, low material consumption, material recycling and low CO<sub>2</sub> emission throughout the entire life cycle, contributing to Denmark fulfilling its international obligations as well as expanding Denmark's international position through export of an innovative building technology. Further, the system should represent the next step in the construction industry's increasing use of prefabricated elements, making it possible to offer to the end user better solutions for insulation, increased living space and better indoor air quality at a competitive price.

The panels are usually consisted of 300 mm thick Kingspan Kooltherm K3 phenolic foam insulation or EPS. The load-carrying plate is made of HPC and reinforced with a steel mesh. The thickness of the plate is 30 mm and is stiffened with steel reinforced structural concrete ribs. The front plate (thus named since it is in contact with the outside environment) has a thickness of 20 to 30 mm, protects the insulation layer and provides exterior aesthetics. The two concrete plates framing the insulation layer are connected using shear transferring connectors. They can be placed in the structural ribs or in the thin plates directly according to the static analysis and handling requirements. The connectors are made of steel or fibre reinforced polymers (FRP) of which several types can be chosen according to performances and cost. A view of the panel geometry is presented in Figure 1.13.

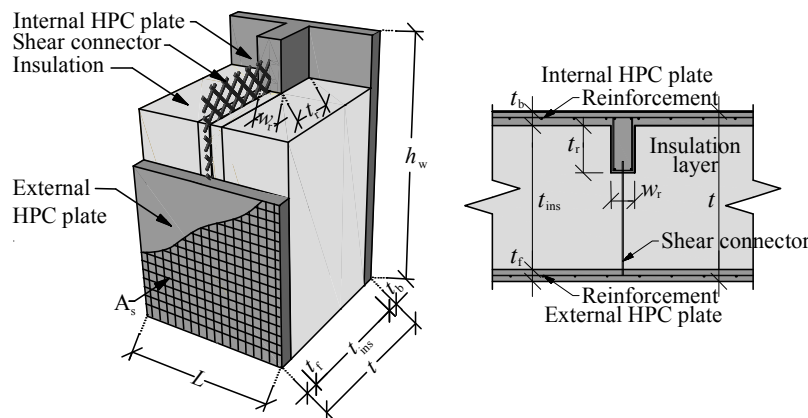


Figure 1.13 View of thin-walled HPC sandwich element geometry considered in the present work.

In Figure 1.13, the panel height is ( $h_w$ ) and length ( $L$ ), respectively;  $t_b$ ,  $t_f$ ,  $t_r$  and  $t_{ins}$  are the thicknesses of the internal HPC plate, external HPC plate, rib structure and insulation layer, respectively;  $w_r$  denotes width of the rib structure;  $t$  is the total thickness of the panel.

Such elements, among other requirements, must comply with standards for concrete properties (Bamforth et al., 2007), standards for design of concrete structures (CEN, 2010) and national building regulations (Byggningsreglementet - BR10, 2014). Further,



the elements must fulfil the fire safety regulations by providing sufficient fire resistance.

Considering the aforementioned considerations, the objectives of this Ph.D. project were:

#### *Material characterization*

- Material characterization of HPC including time dependent strength, fracture properties, stiffness and shrinkage

#### *Experimental verification*

- Present a preliminary experimental study of segments and full-scale sandwich elements using HPC thin plates exposed to shear and flexural loading

#### *FEM modelling*

- Assessment of risk of early age cracking and residual stresses in HPC plates
- Evaluate shear transfer mechanism of HPC sandwich panels
- Development of non-linear model capable predicting behaviour of HPC sandwich panel exposed to shear and flexural loading

#### *Structural optimization*

- Develop a model for optimizing manufacturing techniques, geometrical configuration and use of materials with respect to price, mechanical, and thermal performance

## 1.4 Scope

### 1.4.1 Research approach

The study of the precast thin-walled High Performance Concrete Sandwich Panels is led at three levels. The first level investigated material and mechanical properties of shear connectors, insulation and HPC. In a second stage, the structural level is described to study the influence of the various constituents of the sandwich panel on the behaviour of the panel under shear and bending loading. Both the material level and the structural level are described through experimental and modelling work. Finally, the third level is concerned about structural and cost optimization of the proposed sandwich system.

#### *Testing*

All constituents of the sandwich panel have to be independently characterized to provide the correct material input to FEM modelling. So far in the literature, sandwich panels are usually made of a thick load-carrying plate (150 to 200 mm) of ordinary

reinforced concrete. The testing procedure must therefore include segments and full-scale sandwich elements using HPC thin plates exposed to shear loading and bending.

### *Modelling*

Several authors have attempted to develop numerical models to simulate the behaviour of precast sandwich panel under axial, shear and flexural loading. The behaviour of precast sandwich panel is rather complicated due its highly non-linear behaviour of the constituent materials. Some researchers simplified their models by using linear material models and linear elastic analysis (Einea et al., 1994; Hassan & Rizkalla, 2010). Most of the other researchers approached the problem using non-linear 2-D (Benayoune et al., 2006; Benayoune et al., 2007 and Gara et al., 2012) or 3-D (Benayoune et al., 2008; Lameiras et al., 2013b and Sopal, 2013). However, 2D and 3D modelling approaches significantly simplified the behaviour of precast sandwich panel. With used simplifications, the numerical analysis resulted in an overestimation of the precast sandwich panel behaviour in comparison to experimental data. It has been emphasized by several authors that there is a need for better characterization of any shear transfer mechanism used in sandwich wall panels and improve in the prediction of panel performance and behaviour.

An attempt is to develop a non-linear 3-D FEM model, which is capable to describe the structural behaviour of the panel with reasonable accuracy. This model will be compared to the test results for calibration. Further, the model will be used as design tool assisting decision processes.

The second part of the study attempts to present a rough approach to analyze the robustness of thin-walled sandwich panels at early ages. The analysis predicts when cracking occurs and, if it occurs, how severe the consequences are.

### *Optimization*

Finally, the third level is concerned about the procedure to find the structurally and thermally efficient design of load-carrying thin-walled precast HPC sandwich panels with an optimal economical solution. The optimization approach should take into account the selection of material's performances and sandwich panel's geometrical parameters as well as material cost function in the sandwich panel design. The proposed optimization process outcomes in complex of HPCSP design recommendations, which fulfil the requirement of minimum cost for those elements.

More detailed state-of-the-art reviews of the various processes and phenomena associated with the testing, modelling and optimization are given in the corresponding chapters of this Ph.D. thesis.

## 1.4.2 Limitations and assumptions

The main limitation of the present works lays in the testing possibility. Indeed, testing and especially the full scale testing remains an expensive process where many things

can go wrong, which makes repetitions costly. Building statistically relevant test results would take many more tests.

Further, the work has been limited to investigating HPC sandwich panels reinforced with metallic, BFRP and CFRP grids in combination with loose Glass and Polypropylene fibers. The loading conditions investigated have been limited to shear and bending, and only the short-term response has been investigated (i.e. no creep).

The presented work relies on the tests, which were performed at Technical University of Denmark and North Carolina State University during the Ph.D. studies. The results presented here should be interpreted as preliminary observations and guidelines, rather than definite conclusions.

The literature available in the field of HPC is quite extensive, but little work has been done with respect to thin plates or sandwich structures. Literature is therefore, used for general background and theories.

Finally, the correspondence between the scales and the observable components of the material structure and their interactions are specified on macro-level.

## 1.5 Organization of thesis

An overview of the chapters, the relevant papers associated to them and the eventual collaborations are briefly presented in Table 1.1.

- Chapter 1: “Introduction”
  - This section introduces the research topic of the thesis. A brief state-of-the-art of sandwich panels is given with a primary focus on the various aspects, which influence structural integrity.
- Chapter 2: “High Performance Concrete”
  - This chapter provides an overview of the most important parameters characterizing HPC and fiber reinforcement. The intention is to introduce common terms and concepts related to the work carried out during this Ph.D. study.
- Chapter 3: “Journal paper 1/Conference paper 1”
  - The first journal and conference paper discuss the wedge splitting test setup and inverse analysis algorithm for various multi-linear softening curves. The fracture mechanics parameters of three fiber reinforced and regular HPC are presented. These data were consequently used as material input for FEM modelling.

- Chapter 4: “Conference paper 2”
  - The second conference paper contains a description of experimental setup that allows measurement of effective shrinkage in HPC, which develops on an elastic inhomogeneity embedded in HPC matrix undergoing shrinkage during hydration (autogenous shrinkage). The paper also presents the analysis necessary to perform an interpretation of the experimental results and to determine effective shrinkage in the HPC matrix. Furthermore, the mechanical properties of three fiber reinforced and regular HPC were investigated in detail as function of time. The measured data provides direct input for FEM modelling.
- Chapter 5: “Conference paper 3”
  - The third conference paper discusses experimental and numerical investigation of thin-walled concrete sandwich panel system using the BFRP and CFRP connecting systems. The experimental program included testing of small scale specimens by applying shear (push-off) loading and semi-full scale specimens by flexural loading. Numerical investigations were based on 3-D linear elastic finite element analysis.
- Chapter 6: “Journal paper 2”
  - The second journal paper investigates the composite action of segments representing concrete sandwich panels using the Carbon Fiber Reinforcement Polymer (CFRP) grid/rigid foam as shear mechanism. The experimental program examined the effect of various parameters believed to affect the shear flow strength for this CFRP grid/foam system. A non-linear 3-D FEM analysis was performed to model the behaviour of the tested segments and to study the behaviour of concrete sandwich panels. Results of FEM analysis were found in good agreement with the experimental results. Design equation was developed to determine the shear flow strengths for given CFRP grid/foam systems. The parametric study was performed to predict shear flow strength of different fiber reinforced polymer materials, rigid foam thickness and spacing between vertical lines of the grid.
- Chapter 7: “Full scale testing and modelling”
  - This chapter discusses experimental and numerical investigation of full scale thin-walled HPC sandwich panel system exposed to flexural loading. A non-linear 3-D FEM analysis was performed to model the behaviour of the tested full scale panels. Results of FEM analysis were found in good agreement with the experimental results.

- Chapter 8: “Journal paper 3”
  - The third journal paper presents a rough approach to analyze the robustness of thin-walled sandwich panels at early ages. The approach investigates the constrained shrinkage that the external HPC plate is subjected to. Parametric study is analyzed for a large number of parameter variations. The non-linear FE model was developed using the finite element analysis software DIANA. The modelling approach studied crack propagation in dependence on the stiffness of the restraints as well as distance between the restraints. The results of non-linear FE analysis outcome into the plots assessing crack propagation of concrete elements with the geometry comparable to infinite sheet. Furthermore, the case study was performed for novel thin-walled sandwich elements made of fiber-reinforced HPC. The results of the case study proved that the proposed approach fits reasonably well with the observations on site, i.e. the ability to predict when crack growth becomes unstable and when structural macro-cracking is expected to appear.
- Chapter 9: “Journal paper 4”
  - The fourth journal paper addresses procedure to find the structurally and thermally efficient design of load-carrying thin-walled precast HPC sandwich panels with an optimal economical solution. The optimization approach is based on the selection of material’s performances and panel’s geometrical parameters as well as on material cost functions in the sandwich panel design. The strength based design of sandwich panels is in competence with the format of Eurocode 2. The optimization process outcomes in complex of design recommendations, which fulfil the requirement of minimum cost for those elements.
- Chapter 10: “Conclusions and recommendations for further work”
  - Conclusions together with recommendations for future work of the presented research project are given in this chapter.

Table 1.1 *An overview of the chapters and the relevant papers associated to them in collaboration with others throughout the Ph.D. project.*

| Chapter | Paper   | Information on  | In collaboration with   |
|---------|---------|---|---|
| I       |         | Introduction  |   |
| II      |         | Characterization of HPC and fiber reinforcement   |   |
| III     | JP1/CP1 | All experimental<br>Material characterization of HPC including time dependent fracture properties                     | <u>Thomas Hulin</u> , <i>Technical University of Denmark (DTU), Denmark</i>   |
| IV      | CP2     | All experimental<br>Material characterization of HPC including time dependent free and autogenous shrinkage           | <u>Thomas Hulin</u> , <i>Technical University of Denmark (DTU), Denmark</i>   |
| V       | CP3     | Modelling and experimental<br>Study of segments and full-scale sandwich elements exposed to shear loading and bending | <u>Thomas Hulin</u> , <i>Technical University of Denmark (DTU), Denmark</i>   |
| VI      | JP2     | Modelling and experimental<br>Shear transfer mechanism of HPC sandwich panels   | <u>Dr. Gautam Sopal</u> , <i>Tower Engineering Professionals, Inc., Raleigh, North Carolina, USA</i><br><u>Professor Sami Rizkalla</u> , <i>North Carolina State University, Department of Civil, Construction and Environmental Engineering, Raleigh, North Carolina, USA</i><br><u>Thomas Hulin</u> , <i>Technical University of Denmark (DTU), Denmark</i> |
| VII     |         | Modelling and experimental<br>Full scale testing and modelling  |   |
| VIII    | JP3     | Modelling<br>Assessment of risk of early age cracking in thin-walled concrete sandwich panels                         | <u>Natalie William Portal</u> , <i>Chalmers University of Technology/Swedish Cement and Concrete Research Institute, Denmark</i><br><u>Thomas Hulin</u> , <i>Technical University of Denmark (DTU), Denmark</i>   |
| IX      | JP4     | Modelling<br>Structural and cost optimization process of load carrying thin-walled sandwich panels                    | <u>Sanne Hansen</u> , <i>Technical University of Denmark (DTU), Denmark</i><br><u>Thomas Hulin</u> , <i>Technical University of Denmark (DTU), Denmark</i>  |
| X       |         | Conclusions and recommendations for future work   |   |



## Chapter 2

# High Performance Concrete

### 2.1 Introduction

This chapter provides an overview of the most important parameters characterizing HPC. The chapter is comprised of several sections. In Sections 2.2 and 2.3, the fundamentals of fiber technology, mechanical and material properties of HPC are presented. However, the intention of the sections is not to give a complete review of the various processes, standards and principles as they can be found elsewhere, see e.g. (Bache, 1989; Brandt, 1994; Li, 1995; Aïtcin, 2000; Bennett, 2002; Dhir et al., 2002; Bentur, 2002; Bamforth et al., 2007; Brandt, 2009; CEN, 2010). The intention is to introduce common terms and concepts related to the work carried out during this Ph.D. study.

The main feature of HPC lays in its high strength. A concrete with a compressive strength of 60 MPa or above will be considered as having a high strength (Neville & Aïtcin, 1998; Neville, 2011). HPC is a type of concrete, which meets special performance and uniformity requirements, typically related to enhanced concrete strength, improved crack control and durability that cannot always be achieved by conventional materials, normal mixing, casting and curing practices. Special performance requirements using conventional materials can be achieved only by adopting low water to binder ratio (below 0.4), which necessitates high cement content. Judicious choice of chemical and mineral admixtures can reduce the cement content and results in economical HPC. However, the effect of a mineral admixture on the strength of concrete varies significantly with its properties and replacement levels (Bharatkumar et al., 2001). The influence of supplementary cementitious materials (SCM), namely silica



fume, metakaolin, fly ash and ground granulated blast-furnace slag, on the engineering properties of HPC has been investigated with results showing that the inclusion of the different SCM has considerable influence on the workability of HPC (Megat et al., 2011). Silica fume and metakaolin significantly enhanced the strength of HPC. Fly ash reduced the early-age strength; however, it enhanced the long-term strength of the HPC. Likewise, ground granulated blast-furnace slag impaired the early-age strength, but marginally improved the long-term strength at low replacement levels. The general effect of the different SCM on the elastic modulus of HPC is rather small compared to their effect on strength.

Recently, many authors performed studies on multi-objective mix proportioning optimization of HPC (Lim et al., 2004; Baykasoğlu et al., 2009; Ozbay et al., 2010; Aït-cin, 2011; Lee et al., 2012). The purpose was to study water to binder ratio, total binder content, silica fume replacement ratio, fine to total aggregate ratio, and amount of superplasticizer to determine their effects on the transport and mechanical properties of HPC. Using mix proportion variables, mathematical formulations were obtained for the slump, mechanical and permeation properties via mathematical regression.

Precise mix design methodologies with various degrees of complexity can be followed to obtain needed characteristics in terms of early age behaviour, strength and strength development, and shrinkage (de Larrard & Sedran, 2002; Alves et al., 2004; Ozbay et al., 2010). The higher strength in HPC is not followed by the same rise in fracture energy, which leads to a much more brittle material than ordinary concrete. This property will have its importance in the following discussion.

HPC seems to be very promising material, however, several issues arise from using it in a thin load-carrying sandwich panels. The thin walled sandwich panels studied in the present research typically use thicknesses of the plates between 20 mm to 30 mm. On a material level, shrinkage due to hydration of the cement paste and autogenous shrinkage can lead to crack initiation in restrained areas (around shear connectors). On a structural level, the slenderness of the panel may lead to severe buckling of the loaded structure, which needs to be stiffened by reinforced ribs in the transverse direction. The slenderness of the plates can also lead to potential cracking at the junction with shear connectors due to the thin concrete cover of their embedded parts. In conventional reinforced concrete, limits for cracking are mainly established to prevent corrosion. When using non-corrosive reinforcement or FRP, those limits no longer apply. However, depending on the client, requirements for crack widths can be set for aesthetic purposes and those can sometimes exceed the requirements for corrosion resistance. For a rough surface, a crack width of 0.25 mm can be accepted (ACI Committee 533, 2012). For surfaces with higher architectural importance such as smooth interior surfaces, the crack width should not exceed 0.10 mm or for polished surfaces not appear at all.

In Eurocode 2 (CEN, 2010), a couple of variables such as exposure class, water-cement ratio and reinforcement diameter determine the cover layer thickness. This is to ensure sufficient adhesion and corrosion resistance. When non-corrosive materials are used the variable for corrosion resistance can be ignored and the cover layer thickness can be reduced down to 1 mm (Yin et al., 2013) if only bond properties are regarded. However, to achieve a reasonable production procedure, a cover layer thickness of approximately 15 mm is assumed to be sufficient.

## 2.2 Fiber Reinforcement

Section 2.1 indicates thin-walled HPC sandwich panels are prone to structural cracking. The sandwich panels have high architectural importance and cracks on the surface should be limited or completely prevented. HPC usually exhibits a large number of microcracks, especially at the interface between coarser aggregates and mortar, even before subjection to any load. These microcracks influence the mechanical behaviour of HPC, and their propagation during loading contributes to the non-linear behaviour at low stress levels and causes volume expansion near failure. Many of these microcracks are caused by segregation, shrinkage or thermal expansion of the mortar. Additionally, microcracks develop during loading because of the difference in stiffness between aggregates and mortar, and since the aggregate-mortar interface usually constitutes the weakest link in the composite system. In general, cement-based materials have a relatively low tensile strength but more importantly a low tensile strain capacity, which leads to brittle behaviour and the fact that cracks are almost inevitable in any concrete structures. Therefore, there is a need to reinforce the thin-walled sandwich panel in order to enhance fracture properties of HPC. Ordinary steel reinforcement has very limited use due the thinness of HPC plates. A recent innovative attempt to improve the sustainability of HPC is the development of Fiber Reinforced High Performance Concrete (FRHPC) and HPC reinforced with FRP grids (so-called Textile Reinforced Concrete). It is now generally accepted that the primary effect of fibres and FRP grids is that they improve the post-cracking behaviour and the toughness – i.e. the capacity of transferring stresses after matrix cracking and the tensile strains at rupture – rather than the tensile strength; see e.g. Shah (1992), Naaman & Reinhardt (1996), Li & Maalej (1996). In some of the early work on FRHPC it was thought that the tensile strength could be increased due to an assumption that fibres delay the widening of microcracks (initiated at flaws) – and that the closer the fibres were spaced, the more resistance to cracking (Romualdi & Batson, 1963). This concept was adapted from the model for fracture mechanics of materials with points of discontinuity developed by Griffith (1921). However, as the fibres that were used in the study were large compared to the flaw size and the amount of fibres that could be mixed without problems was rather limited (up to 3.0 volume percent), this mechanism is not likely to have contributed to the strength of the material. Rather, as Romualdi & Batson (1963) and Romualdi & Mandel (1964) used indirect test meth-

ods (i.e. splitting test and flexural tests) to determine the tensile strength, it is more likely that the interpreted increase in tensile strength was an effect of the increased toughness after matrix cracking resulting in a higher peak load. On the other hand, more recent investigations on the mechanics of fibres have shown that these actually can delay the widening of microcracks, see e.g. Betterman et al. (1995), Banthia & Sheng (1996), Nelson et al. (2002) and Lawler et al. (2003). Three main factors controlling the performance of fibers and FRP grids are: (1) the physical properties of fibres and matrix; (2) the strength and bond between fibres and matrix; and (3) the amount of fibres (volume fraction) and their distribution and orientation (Ingemar Löfgren, 2005a). In the following subsections 2.2.1 and 2.2.2, loose fibers and FRP grids will be described in more detail, respectively.

### 2.2.1 Loose Fibers

There is a wide range of the materials used for fibre production. Steel fibres have been used for a considerable time, but modern steel fibres have higher slenderness and more complex geometries, and are often made of high-strength steel. Furthermore, synthetic fibres are becoming more attractive as they can provide effective reinforcement comparable to that of steel fibres. Types of synthetic fibres that have been incorporated into HPC include: polyethylene (PE), polypropylene (PP), acrylics (PAN), polyvinyl acetate (PVA), polyamides (PA), aramid, polyester (PES), glass, basalt and carbon. Some examples of different commercially available fibres can be seen in Figure 2.1.



Figure 2.1. *Some examples of different commercially available fibres.* (Löfgren, 2005)

The mechanical and geometrical properties of fibres vary widely and different effects on the properties of HPC. Some types of fibre are mainly used to improve the toughness and reduce crack widths, while others are there to reduce plastic shrinkage cracking or to mitigate spalling of concrete during fire, see e.g. Bentur et al. (2006), Khoury (2008) and Knack (2011).

Several important terms, definitions, parameters, and features serve to characterise the wide variety of existing fibres; for more information see e.g. ACI Committee 544 (2002), Löfgren (2005), Arnon Bentur & Mindess (2006) and Mortensen (2006)

- *aspect ratio* - is the ratio of length to diameter (or equivalent diameter for non-circular fibres) of a fibre
- *bundled fibres* - usually are strands consisting of several hundreds or thousands of filaments of microfibres
- *chopped strand* - contains fibres chopped to various lengths
- *collated* - refers to fibres bundled together either by cross-linking or by chemical means
- *fibrillated* - referring to continuous networks of fibre, in which the individual fibres have branching fibrils
- *filament* - which is a continuous fibre, i.e. one with an aspect ratio approaching infinity
- *monofilament* - a large-diameter continuous fibre, generally with a diameter greater than 100  $\mu\text{m}$
- *multifilament* - a yarn consisting of many continuous filaments or strands

These definitions and features are generally independent of fibre type, i.e., polymeric, metallic, glass, etc., and depend on the geometry rather than any material characteristics. From a geometrical point of view, fibres used in cementitious composites may be classified as:

- *macro-fibres* - the length is larger than the maximum aggregate size (at least by a factor of two for coarse aggregates) and if their cross-section diameter is much greater than that of the cement grains (which typically means less than 50  $\mu\text{m}$ ) and an aspect ratio less than 100.
- *microfibers* - the cross-section diameter is of the same order as the cement grains and their length is less than the maximum aggregate size.

Prerequisites for fibers to be effective in HPC, it has been found that fibers should have the following properties (see e.g. Naaman, 2003; Löfgren, 2005).

- Tensile strength of fibers should be significantly higher than the HPC (two or three order magnitude)
- The bond between fiber and HPC should be the same order as, or higher, than the tensile strength of HPC
- Elastic modulus should be significantly higher than that of HPC (at least 2-3 times)
- Sufficient ductility so that fibre does not fracture due to fibre abrasion or bending
- The coefficient of thermal expansion and Poisson's ratio should be in the same order as HPC
- The fiber has to be durable to withstand the high alkaline environment

Generally, the cross section of an individual fibre can be flat, polygonal, rectangular, diamond, square, triangular or any substantially polygonal shape. In order to improve the bond characteristic between fiber and HPC, a fibre can be modified along its length by roughening its surface or by including mechanical deformations. Thus, fibre can be smooth, indented, deformed, crimped, coiled, twisted, with end hooks, paddles, buttons, or other anchorage.

In accordance with the standard EN 14889-1 and EN 14889-2 (CEN, 2006a, 2006b), fibers are divided to classes according the intended use, which are:

- *Class I* - is intended primarily to improve the short-term plastic properties of HPC by controlling plastic shrinkage, settlement cracks, and reducing bleeding, but not adversely affecting the long-term properties.
- *Class II* - is intended primarily to improve the durability of HPC by improving abrasion and impact resistance and by reducing damage caused by cycles of freezing and thawing.
- *Class III* - fibres, which are primarily used to increase the residual strength of HPC.
- *Class IV* - fibres which are primarily used to improve the fire resistance of HPC.

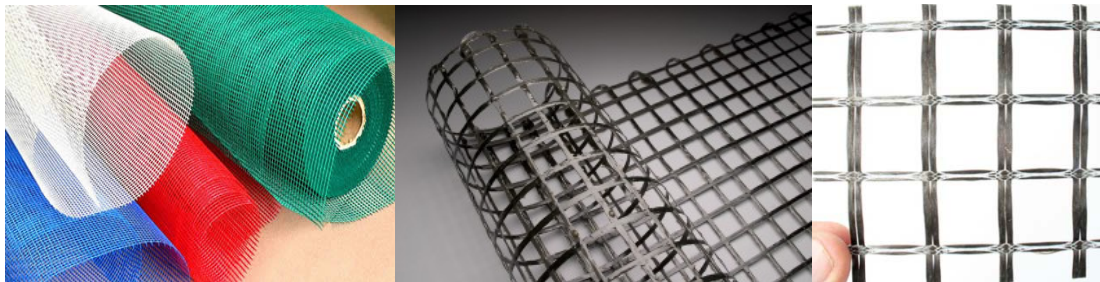
The properties of fibre vary considerably, in particular with respect to the modulus of elasticity. An overview of physical properties of some fibres is presented in Table 2.1. In this thesis, it is primarily of interest to explore the use of loose PP and glass fibres as these are currently the most readily available and applied materials.

Table 2.1 *Physical properties of some fibres*

| Type of fiber              | Diameter<br>[ $\mu\text{m}$ ] | Specific<br>gravity<br>[ $\text{g}/\text{cm}^3$ ] | Tensile<br>strength<br>[MPa] | Elastic<br>modulus<br>[GPa] | Ultimate<br>elongation<br>[%] |
|----------------------------|-------------------------------|---|------------------------------|-----------------------------|-------------------------------|
| <i>Metallic</i>            |                               |   |                              |                             |                               |
| Steel                      | 5-1000                        | 7.85  | 200-2600                     | 195-210                     | 0.5-5                         |
| <i>Synthetic</i>           |                               |   |                              |                             |                               |
| Acryl (PAN)                | 5-17                          | 1.18  | 200-1000                     | 14.6-19.6                   | 7.5-50.0                      |
| Aramid (e.g. Kevlar)       | 10-12                         | 1.4-1.5   | 2000-3500                    | 62-130                      | 2.0-4.6                       |
| Carbon (low modulus)       | 7-18                          | 1.6-1.7   | 800-1100                     | 38-43                       | 2.1-2.5                       |
| Carbon (high modulus)      | 7-18                          | 1.7-1.9   | 1500-4000                    | 200-800                     | 1.3-1.8                       |
| Nylon (polyamide)          | 20-25                         | 1.16  | 965                          | 5.17                        | 20.0                          |
| Polyester (e.g. PET)       | 10-80                         | 1.34-1.39   | 280-1200                     | 10-18                       | 10-50                         |
| Polyethylene (PE)          | 25-1000                       | 0.96  | 80-600                       | 5.0                         | 12-100                        |
| Polyethylene (HPPE)        | -                             | 0.97  | 3000-4100                    | 80-150                      | 2.9-4.1                       |
| Polypropylene (PP)         | 10-200                        | 0.90-0.91   | 310-760                      | 3.5-4.9                     | 6-15.0                        |
| Polyvinyl acetate (PVA)    | 3-8                           | 1.2-2.5   | 800-3600                     | 30-80                       | 4-12                          |
| <i>Glass</i>               |                               |   |                              |                             |                               |
| E glass                    | 8-15                          | 2.54  | 2000-4000                    | 72                          | 3.0-4.8                       |
| AR glass                   | 8-20                          | 2.70  | 1500-3700                    | 80                          | 2.5-3.6                       |
| <i>Natural - organic</i>   |                               |   |                              |                             |                               |
| Cellulose (wood)           | 15-125                        | 1.50  | 300-2000                     | 10-50                       | 20                            |
| Coconut                    | 100-400                       | 1.12-1.15   | 120-200                      | 19-25                       | 10-25                         |
| Bamboo                     | 50-400                        | 1.50  | 50-350                       | 33-40                       | -                             |
| Jute                       | 100-200                       | 1.02-1.04   | 250-350                      | 25-32                       | 1.5-1.9                       |
| <i>Natural - inorganic</i> |                               |   |                              |                             |                               |
| Asbestos                   | 0.02-25                       | 2.55  | 200-1800                     | 164                         | 2-3                           |
| Wollstonite                | 25-40                         | 2.87-3.09   | 2700-4100                    | 303-530                     | -                             |

### 2.2.2 FRP Grids

In thin-walled HPC sandwich elements, bi- or multi-axial 2D FRP grids can be used as reinforcement (Figure 2.2). For a simple bi-axial case, the grid is made of two groups of textile fibre yarns, warp ( $0^\circ$ ) and weft ( $90^\circ$ ), interwoven perpendicularly to each other. Yarns are composed of multiple single fibres of continuous length, also designed as filaments; grouping of continuous fibres is primarily done to obtain the desired thickness of yarn (Mahadevan, 2009).

Figure 2.2. *Examples of AR-glass, carbon and basalt FRP grids.*

The fineness of a yarn is measured in tex (g/1000 m) and is a function of the number of filaments, average filament diameter and density. Moreover, the fabrication method and applied sizing to fibres have a significant effect on the interaction between the assembled filaments, as such, the mechanical properties of a fibre filament decrease when is yarn formed (Brameshuber, 2006). The choice of fibre material for use in HPC is based on various factors such as materials properties, corrosion and temperature resistance, bond quality, demand/production cost and even environmental impact. In terms of mechanical behaviour, tensile strength, breaking elongation and modulus of elasticity superior to those related to the cementitious matrix is essential. The reinforcement ratio and placement of the textile reinforcement will also have a great impact on the composite behaviour of a TRC member (Brameshuber, 2006). Fibre materials, which have generally been used and explored in sandwich panels include, but are not limited to: alkali resistant glass (AR-glass), carbon, basalt, aramid, polyvinyl-alcohol (PVA) with polyvinyl chloride (PVC) coating. In this thesis, it is primarily of interest to explore the use of AR-glass, basalt and carbon FRP grids as these are currently the most readily available and applied materials. Furthermore, a qualitative assessment of general mechanical and chemical properties including corrosion and temperature resistance, bond quality, in addition to demand and production cost for each of selected reinforcements is summarized in Table 2.2. Each criterion is assessed on a scale from Low to High based on a relative comparison between conventional steel reinforcement, AR-glass, carbon and basalt FRP grids for use in HPC. This assessment is primarily based on data retrieved from Brameshuber (2006), Van de Velde et al. (2003), Scheffler et al. (2009), Wei et al. (2010), Vetrotex (2011), Saertex (2013) and Smarter Building Systems (2010).

In summary, it is challenging to simply select an optimal reinforcement material from this qualitative assessment partially due to rather comparable properties highlighted for each alternative. Conventional steel reinforcement appears to be a relatively good solution, but history of the breakdown of its corrosion resistance and related deterioration in itself is an aspect motivating the use of alternative solutions. When comparing the novel materials, namely AR-glass, carbon and basalt, AR-glass appears to be the most effective option. Carbon presents many advantages but its high initial cost and relatively low availability in regards to FRP grids are drawbacks. Basalt is comparable to AR-glass, but is still in need of much research in terms of use as reinforcement in cementitious matrices.

More comprehensive information on different types of fibres, their properties and use can be found in the following references: in general textbooks on fibre-reinforced composites, e.g. Balaguru & Shah (1992) and Arnon Bentur & Mindess (2006); in textbooks on fibres, e.g. Phillips & Hongu (1997) and Hearle (2001); in ACI Committee 544 (2002), a state-of-the-art report on fibre-reinforced concrete; in Zheng & Feldman (1995), a review article on synthetic fibre-reinforced concrete.

Table 2.2 *Qualitative Assessment of Selected Reinforcements* (Williams et al., 2014)

| Reinforcement Material     | Basalt Reinforcement   | Carbon  | AR-Glass  | Conventional Steel  |
|----------------------------|--|---|---|---|
| Corrosion Resistance       | -Comparable to unsized E-glass and AR-glass in high alkaline solutions (Scheffler et al. 2009)**<br>- <b>High</b> to neutral or realistic acidic conditions (Wei et al. 2010) and alkaline outdoor conditions (Van de Velde et al. 2003) | - <b>High</b> to acid, alkaline and organic solvents (inert)  | - <b>Average-High</b> to alkali attack<br>- <b>High</b> to neutral or realistic acidic outdoor conditions   | - <b>High</b> to high alkaline solutions (passive film)<br>- <b>Low</b> to low alkaline, neutral or realistic acidic outdoor conditions |
| Temperature Resistance     | - <b>High</b> resistance<br>- <b>Low</b> thermal expansion (Smarter Building Systems 2010)<br>- <b>Low</b> thermal conductivity (Smarter Building Systems 2010)  | - <b>High</b> thermal expansion, shortens when heated<br>- <b>Average</b> thermal conductivity (Saertex 2013) | - <b>Low</b><br>- <b>Average</b> thermal expansion (Saertex 2013; Vetrotex 2011)<br>- <b>Low</b> thermal conductivity (Saertex 2013; Vetrotex 2011) | - <b>Average</b><br>- <b>High</b> thermal expansion and conductivity (Saertex 2013)   |
| Bond Quality               | - <b>Average</b><br>-Unsize filaments (Scheffler et al. 2009)<br>-Low friction coefficient, improve with coatings (Scheffler et al. 2009)  | - <b>Low-Average</b><br>-Smaller filament diameter leads to weaker adhesion<br>-Improve with coatings         | - <b>Average</b> , depends on density of yarn<br>-Improve with coatings   | - <b>Low-High</b> , based on mechanical deformations  |
| Demand/Production Cost     | - <b>Low/Average</b> , easily extractable natural resource (Smarter Building Systems 2010)   | - <b>Low/High</b> , compared to all other reinforcement materials   | - <b>Average/Average</b> , particularly produced for use in alkaline environments   | - <b>High/Average</b> , commonly used   |
| Total Score* (Norm. score) | 9.25 (1.09)  | 9.5 (1.12)  | 7.75 (0.91)   | 8.5 (1.00)  |

\* Low = 1, Low to Average = 1.5, Low to High = 2, Average = 2, Average to High = 2.5, High = 3.

\*\*Uncertainties exist due to unknown chemical formulation of basalt and fiber sizings, which as result caused observations of high standard deviation values in tensile strength after ageing (Scheffler et al. 2009)



## 2.3 Material and mechanical properties of HPC

In HPC design and quality control, compressive strength is the property generally specified and by which concrete is classified (Bamforth et al., 2007). The main reason for this is that, compared to most other properties, testing of compressive strength is relatively easy. Furthermore, many properties of HPC, such as modulus of elasticity, tensile strength, permeability, etc., are believed to be dependent on the compressive strength and may therefore be deduced from the strength data. Though, the compressive strength cannot be utilised as a replacement for all properties, especially not for the increase of toughness observed in fibre-reinforced HPC. This means that for fibre-reinforced HPC some sort of toughness property is required, and that other test methods have to be utilised to characterise it. In addition, the type of properties required depends on the constitutive models that are used to describe the material in numerical analyses. The ranges of some mechanical properties of cement-based materials, such as cement paste and HPC, are listed in Table 2.3. In the table, values of the following properties are listed: the compressive strength  $f_c$ ; the tensile strength  $f_t$ ; the modulus of elasticity  $E$ ; the fracture energy  $G_F$ ; and the characteristic length  $l_{ch}$ . The characteristic length is an indication of the material's brittleness and is defined as:

$$l_{ch} = \frac{E_c G_F}{f_t^2} \quad (2.1)$$

Table 2.3 *Range of mechanical properties of cement-based materials*

| Material             | $f_c$<br>[MPa] | $f_t$<br>[MPa] | $E$<br>[GPa] | $G_F$<br>[N/m] | $l_{ch}$<br>[mm] |
|----------------------|----------------|----------------|--------------|----------------|------------------|
| Cement paste         | 10 - 25        | 2.0 - 10.0     | 10 - 30      | $\approx 10$   | 5 - 15           |
| Mortar               | 25 - 50        | 1.0 - 10.0     | 10 - 30      | 10 - 50        | 100 - 200        |
| HPC                  | 60 - 120       | 4.0 - 5.5      | 40 - 50      | 100 - 150      | 150 - 200        |
| Fibre-reinforced HPC | 60 - 120       | 4.0 - 5.5      | 40 - 55      | > 150          | > 200            |

### 2.3.1 Compressive properties

The stress–strain relation of plain HPC exhibits nearly linear elastic response up to about 30% of the compressive strength. This is followed by gradual softening up to the HPC compressive strength; beyond the compressive strength, the HPC stress–strain relation exhibits strain softening until failure takes place by crushing. Experimental observations have suggested that the macroscopic behaviour under compression is due to frictional sliding along pre-existing flaws, resulting in formation of tensile cracks at the tips of these flaws; see e.g. Vonk (1992) and Van Mier (1996). Cracking starts as sliding on the aggregate–cement paste interface (the weak zone) and propagates into the matrix as tensile cracks; these tensile cracks grow with increasing compression and become parallel to the direction of the principal compressive stress. The final failure is due to interaction of the tensile cracks. The main explanation, as proposed by Neville (2011), of the largely curvilinear stress–strain relation of concrete lies in the presence of interfaces between the aggregate and the hardened cement

paste, in which micro-cracks develop even under modest loading. The behaviour of concrete changes and as the compressive strength increases and it becomes more brittle. For a normal-strength concrete, the aggregate is significantly stronger and stiffer than the cement paste, while for a HPC the strength and stiffness are alike. As a result, some cracks extend through the aggregates resulting in a smooth crack surface, compared to the more tortuous crack surface in normal-strength concrete. In HPC, the tensile strength of the aggregate, rather than the interface between paste and aggregates, may become the weak link (Rao & Prasad, 2002). With fibres present in the matrix, the HPC become more ductile (see Figure 2.3), and the main effect of fibres appears to be that they offer resistance against the longitudinal crack growth. Though, the effect of fibres is highly dependent on the type of fibre used, the size and properties of the fibres, the volume fraction added, and the properties of the matrix. Glavind (1992), for example, found that the addition of fibres was particularly advantageous for improving the mechanical properties of HPC loaded in compression, as the inherent brittleness was significantly reduced. Generally, it can be concluded that fibres at moderate dosages ( $< 1\%$ ) do not affect the pre-peak properties, whereas the strain at crack localisation and the failure strain increase. However, with microfibres (e.g. carbon) and for high fibre volumes ( $> 1\%$ ) it is possible to increase the compressive strength (Löfgren, 2005).

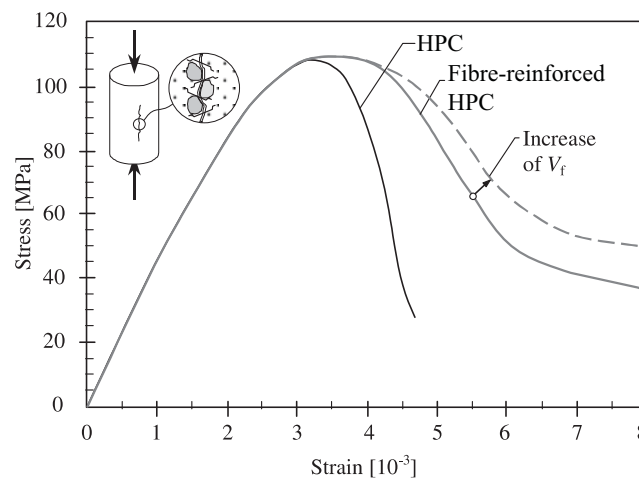


Figure 2.3. *Schematic description of the behaviour of HPC in compression.*

### 2.3.2 Tensile properties

It is generally accepted that the most appropriate classification of the tensile behaviour is based on the uni-axial response; see e.g. Hillerborg et al. (1976), Van Mier (1996) and Stang et al. (2007). The tensile behaviour of cement-based materials may be classified as either strain-softening (a quasi-brittle material) or pseudo strain-hardening; see Figure 2.4. For strain-softening materials, a localised single crack determines the post-peak behaviour and once the matrix cracks the stress will start to decrease. The pseudo strain-hardening material is characterised by the stress-strain curve with a quasi-strain hardening (or pseudo-strain hardening) behaviour

(i.e. a post-cracking strength larger than the cracking strength, or elastic-plastic response). Based on this classification, tensile properties for strain-softening materials will be discussed.

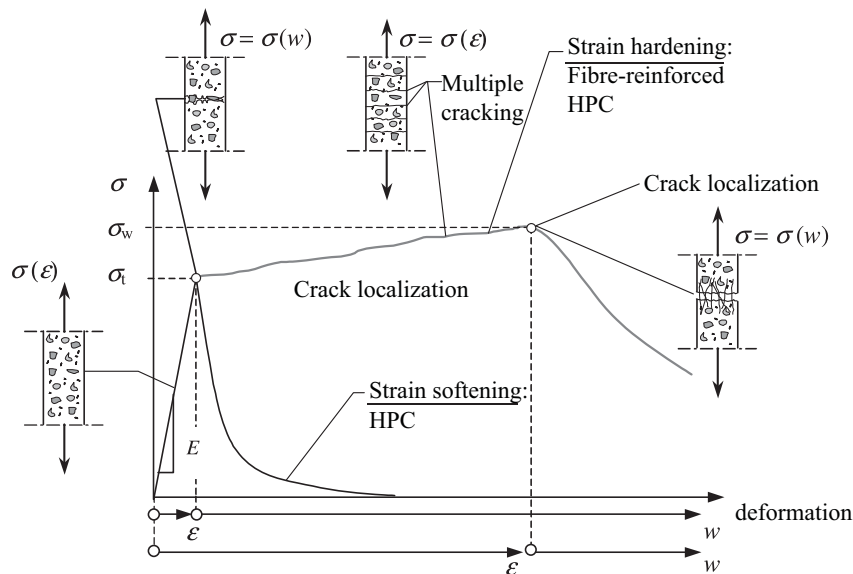


Figure 2.4. *Classification of tensile behaviour of HPC.*

Plain HPC is a strain-softening material, and results from a number of researchers – e.g. Cornelissen et al. (1986), Hordijk & Reinhardt (1991) and Stang & Østergaard (2003). They indicate that the experimental data for the stress-crack opening curve lie in a relatively narrow band when the stress is normalised with respect to the tensile strength. This means that, despite the complexity of the various mechanisms involved, experimental data can be fitted quite accurately with relative simple expressions; see e.g. Cotterell & Mai (1995), Karihaloo (1995), Shah (1995) and Van Mier (1996). The tensile fracture behaviour can be characterised by the tensile stress versus crack opening curve, which can be used in a cohesive crack model, for example the so-called fictitious crack model originally suggested by Hillerborg et al. (1976), or a crack band model (Bažant, 2002).

In the fictitious crack model, the main parameters are the tensile strength, the modulus of elasticity, the fracture energy  $G_F$ , and the shape of the  $\sigma$ - $w$  curve; see Figure 2.5. As the shape of the  $\sigma$ - $w$  curve does not vary too much for plain HPC, it is for most practical engineering applications usually sufficient to determine the fracture energy,  $G_F$ , and the tensile strength and to select an appropriate  $\sigma$ - $w$  relationship. The fracture energy can be determined experimentally in: uni-axial tension tests, which yield the complete  $\sigma$ - $w$  curve; three-point bending tests, or other fracture test methods, such as the wedge-splitting test method, see e.g. Löfgren et al. (2005) and Skocek & Stang (2008). If no experimental results exist, values of the fracture energy have been recommended in CEB-FIP Model Code 1990 (1993). When the fracture energy and tensile strength have been determined, the  $\sigma$ - $w$  relationship can be approximated as: linear (see e.g. Hillerborg et al. 1976); bi-linear (see e.g. CEB-FIP Model Code 1990, 1993; Olesen, 2001); multi- or polylinear (see e.g. Nanakorn & Horii, 1996; Skocek &

Stang, 2008); polynomial or exponential (see e.g. Cornelissen et al., 1986; Reinhardt, 1984 and Stang & Østergaard, 2003). For most practical applications, it has been found that the bi-linear relationship is a sufficient approximation (see e.g. Cotterell & Mai, 1995).

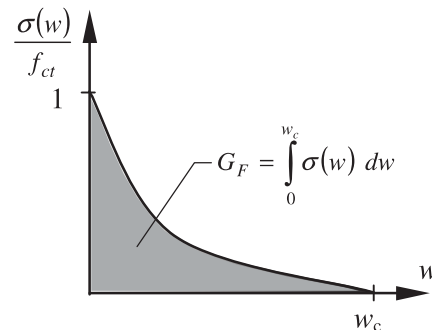


Figure 2.5. *Concept of the fictitious crack model.*

Fibre-reinforced HPC, with low and moderate volume fractions of fibres, can also be regarded as a strain-softening material. As already pointed out, the tensile strength and modulus of elasticity are not significantly affected. Although, the fibres have a considerable impact on the tensile fracture behaviour, and the fracture energy and shape of the  $\sigma$ - $w$  curves vary considerably depending on type and amount of fibres used, the quality of the concrete, etc.; see e.g. (Li, 1993). Furthermore, as pointed out by (Hillerborg, 1980), the complete fracture energy is of no interest since the stress-free crack opening,  $w_c$ , occurs at very large crack openings for most fibre-reinforced HPC, while for most HPC (without fibres) it is seldom larger than 0.3 mm. Consequently, with the fictitious crack model as a framework, to completely characterise the mechanical behaviour of fibre-reinforced concrete in tension it is necessary to determine the  $\sigma$ - $w$  relationship. As the shape of the  $\sigma$ - $w$  curve will be more or less complex, it may be necessary to simplify the relationship in a similar manner as for plain HPC. Exactly how the  $\sigma$ - $w$  relationship should be approximated depends, among other things, on its shape, the constitutive model used, and the type of analysis (i.e. whether it is for determining the structural behaviour in service state or ultimate limit state); see (Hillerborg, 1980; Rossi & Chanvillard, 2000).

### 2.3.3 Shear properties

The principal action responsible for transferring shear stresses across a crack in plain concrete is often explained as aggregate interlock and friction at the crack faces. For fibre-reinforced concrete, at low and moderate fibre dosages the cracking strength is not affected but, as soon as the matrix cracks, the fibres are activated and start to be pulled out, resulting in a significant toughening behaviour (see Barragán, 2002). Allos (1989) reported that the shear transfer capacity could be significantly increased, as much as up to 60 % of the compressive strength. Barragán (2002) found that the maximum shear strength increased with the fibre volume fraction (for high-strength concrete the increase was significant, close to 100 % with 40 kg/m<sup>3</sup> steel fibres). For rein-

forced concrete it is known that the amount of reinforcement crossing the shear plane influences the shear friction and the shear capacity due to dowel effects and a similar effect is observed for FRC. Barragán (2002) evaluated the dowel action of fibres by evaluating the residual shear stresses at different slip limits and found that this increased with the fibre volume fraction.

#### 2.3.4 Fracture properties

During the past four decades, different methods have been proposed and used to characterise the tensile behaviour of HPC: e.g. by measuring the flexural strength, as in the early work of Romualdi & Batson (1963), or by determining the behaviour in terms of dimensionless toughness indices (as prescribed in ASTM C1018-97 (1997)) to determine residual flexural strengths at prescribed deflections; see RILEM TC 162-TDF (2002). In addition, the splitting test (also known as the Brazilian test) has been used to determine the splitting tensile strength. The main test setups used are:

- Uni-axial tension test or direct tensile test.
- Flexural test
- Panel or plate test.

Other test methods exist, e.g. the wedge-splitting test (WST) method, the compact tension test, etc., but the most common test approach appears to be the flexural test on beams/prisms. Beam/prism specimens are loaded in either three-point or four-point bending and can be equipped with a notch. Flexural beam tests are used in a number of national standards/guidelines: see e.g. ASTM C1018-97 (1997), ACI Committee 544 (2002) and CEN (2006a). Panel/plate tests are typically used for shotcrete and can be either square panels, e.g. the EFNARC panel test (EFNARC, 1996), or round panels (ASTM 1550-02, 2003). Panel/plate tests are typical application-specific tests where the loading condition of the test method simulates a design situation in a real structure. For determining tensile fracture properties of HPC and fibre-reinforced HPC, the three-point bending test on a notched beam is probably the most widespread method. For a review of different test methods, see e.g. ACI Committee 544 (2002), Balaguru & Shah (1992), Bentur & Mindess (2006), Gopalaratnam et al. (1991), Shah & Carpinteri (1990), Stang et al. (2000), Banthia & Trottier (1995), Barr et al. (1996), Gopalaratnam & Gettu (1995), Hassan et al. (2014), Marti et al. (1999), Rossi & Chanvillard (2000), Taylor et al. (1997), Van Mier (1996) and Löfgren (2005).

The fracture behaviour of fibre-reinforced concrete can be described by the stress-crack opening ( $\sigma$ - $w$ ) relationship, as was shown in the previous section, but to obtain this it is necessary to have appropriate test methods that can be used to determine this fundamental relationship. But determining the  $\sigma$ - $w$  relationship is an intricate problem, especially in a flexural test for which it may also be necessary to have a proce-

ture for interpreting the test results, for example by conducting inverse analysis (see Chapter 3).

### 2.3.5 Shrinkage behaviour

Concrete shrinks as a result of drying, self-desiccation, chemical reaction, or temperature reduction. The appearance of tensile stresses in the menisci created in the fresh concrete as it is drying (plastic shrinkage) or in the hardened concrete due to self-desiccation (autogenous shrinkage) and due to drying (drying shrinkage) (Springenschmid, 1994; Aïtcin, 2003).

Autogenous shrinkage is a consequence of the chemical contraction occurring in the cement paste when water hydrates cement particles. In fact, the absolute volume of the hydrates formed is smaller than the sum of the absolute volume of the cement particles and the water that have reacted. Hydration creates some 8 % voids (Neville, 2011). This very fine porosity drains water from the coarser capillaries where water is not as strongly bonded. Consequently, as hydration progresses it is observed that the coarse capillaries are being emptied (as in the case of drying shrinkage) but without any mass loss. This phenomenon is called self-desiccation. Self-desiccation is due to the movement of the water that is moving from the preexisting coarse capillaries towards the very fine porosity created by cement hydration.

Drying shrinkage occurs when concrete dries in dry air, as concrete loses some of its internal water; menisci appear within the coarse superficial capillaries. In the case of drying shrinkage there is a mass loss. In ordinary concrete with  $W/C$  ratio greater than 0.50, for example, there is more water than required to fully hydrate the cement particles and a large amount of this water is contained in well-connected large capillaries so that the menisci created by self-desiccation appear in large capillaries where they generate only very low tensile stresses. Therefore, the hydrated cement paste barely shrinks when self-desiccation develops (40–60 microstrains) (Jensen & Hansen, 2001).

In the case of HPC with a  $W/B$  ratio of 0.35 or less, significantly more cement and less mixing water have been used, so that the initial pore network is essentially composed of very fine capillaries. When self-desiccation starts to develop, as soon as hydration begins, menisci rapidly develop into small capillaries if no external water is added. Since many cement grains start to hydrate simultaneously in HPC, the drying of the very fine capillaries can generate high tensile stresses that shrink the hydrated cement paste. This early shrinkage is referred to as autogenous shrinkage. Autogenous shrinkage is as large as drying shrinkage observed in ordinary concrete when these two types of drying develop in capillaries of the same diameter (Aïtcin et al., 1997).

But, when there is an external supply of water, the capillaries do not dry out as long as they are connected to this external source of water (Caldarone, 2008). The result is that no menisci, no tensile stress, and no autogenous shrinkage develop within a HPC

thin element having a  $W/C$  ratio of 0.35 that is constantly water cured from the moment of its setting. But when the  $W/C$  ratio is lower than 0.35 or at the center of a large concrete element made with a 0.35  $W/C$  ratio HPC, concrete microstructure can be so dense that water penetration can be stopped and self-desiccation can develop in certain parts of concrete. In fact, when cement particles are hydrating with water coming from an external source there is an increase in the absolute volume of the cement that leads to the filling of some pores and capillaries. In this case, it would be more appropriate to speak of isothermal (differential) shrinkage rather than autogenous, since autogenous shrinkage refers to the shrinkage of a closed system.

Thus, the essential difference between ordinary concrete and HPC is that ordinary concrete exhibits practically no autogenous shrinkage, whether it is water cured or not, whereas HPC can experience significant autogenous shrinkage if it is not water cured during the hydration process. Autogenous shrinkage does not develop in HPC as long as the pores and capillaries are interconnected and have access to external water, but, when the continuity of the pore and capillary systems is broken, then, and only then does autogenous shrinkage start to develop within the hydrated cement paste of a HPC, as shown in Figure 2.6.

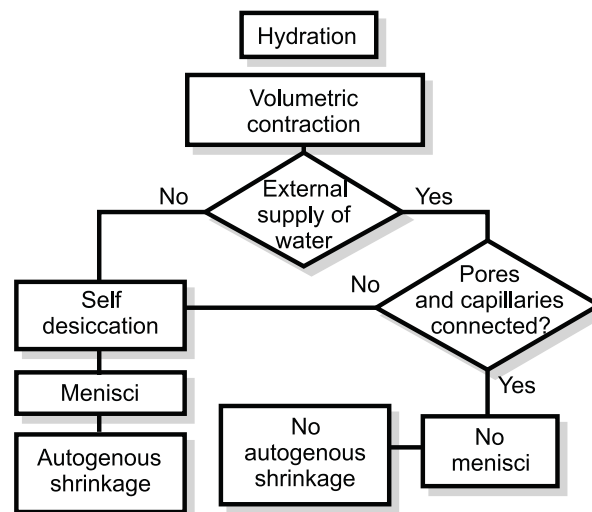


Figure 2.6. *Influence of curing conditions on the occurrence of autogenous shrinkage.* (Aïtcin, 2003)

Drying shrinkage of the hydrated cement paste begins at the surface of the concrete and progresses more or less rapidly through the concrete, depending on the relative humidity of the ambient air and the size of capillaries. Drying shrinkage of ordinary concrete is therefore rapid because the capillary network is well connected and contains open capillaries at the surface of the concrete. Drying shrinkage in HPC is slow because capillaries are very fine and soon get disconnected. Another major difference between drying shrinkage and autogenous shrinkage is that drying shrinkage develops from the surface inwards, while autogenous shrinkage is homogeneous and isotropic, insofar as the cement particles and water are well dispersed within the concrete. Thus, there are considerable differences between ordinary concrete and HPC with respect to

their shrinkage behavior. The cement paste of an ordinary concrete exhibits rapid drying shrinkage progressing from the surface inwards, whereas HPC cement paste can develop a significant isotropic autogenous shrinkage when not water cured. This difference in the shrinkage behavior of the cement paste has very important consequences for concrete curing and concrete durability.

Based on above, it is obvious that autogenous shrinkage plays a big role in the problem of early-age cracking in many HPC. Autogenous shrinkage should be limited because it may induce microcracking or macrocracking and impair the concrete quality. Autogenous shrinkage of concrete is a phenomenon known from the beginning of the 20th century, but its practical importance has only been recognized in recent years. Despite the growing interest in autogenous deformation, no consensus has yet been reached in the scientific community on standard test methods and on the terminology, although some attempts have been made in this direction (see e.g. Bentur, 2003; Dela, 2000; Jensen & Hansen, 2001; Lura & Jensen, 2006; Østergaard, 2003; Stang, 1996; Yun et al., 2012). However, the mechanisms leading to autogenous shrinkage are still poorly understood. While there is general agreement about the existence of a relationship between autogenous shrinkage and relative humidity changes in the pores of the hardening cement paste, the actual mechanisms are unknown.

For more information on different test methods for determination autogenous shrinkage and autogenous shrinkage induced stresses see Chapter 4.





## Chapter 3

### Journal paper 1

Title: Wedge Splitting Test and Inverse Analysis on Fracture Behaviour of Fiber Reinforced and Regular High Performance Concretes

Authors: Kamil Hodicky, Thomas Hulin, Jacob W. Schmidt and Henrik Stang

Published in: Journal of Civil Engineering and Architecture, 2014, 8(5), 595-603.

### Conference paper 1

Title: Wedge Splitting Test on Fracture Behaviour of Fiber Reinforced and Regular High Performance Concretes

Authors: Kamil Hodicky, Thomas Hulin, Jacob W. Schmidt and Henrik Stang

Conference: In Proceedings of the 13<sup>th</sup> International Conference on Fracture (IFC), Beijing, China, 2013.

## Abstract

The fracture behaviour of three fiber reinforced and regular High Performance Concretes (HPC) is presented in this paper. Two mixes are based on optimization of HPC whereas the third mix was a commercial mix developed by CONTEC ApS (Denmark). The wedge splitting test setup with 48 cubical specimens was used experimentally and the cracked non-linear hinge model based on the fictitious crack model was applied for the interpretation of the results. The stress-crack opening relationships were extracted by using inverse analysis algorithm for various multi-linear softening curves. The fracture mechanics parameters such as crack opening displacement (COD), fracture energy and characteristic length were experimentally determined. Experiments were performed at 1, 3, 7 and 28 days. Fracture energy,  $G_f$ , was found to increase with age, while the characteristic length,  $L_{ch}$ , was found to decrease.

## 3.1 Introduction

Development of fiber reinforced concrete plays important role in industrialization of the building industry. The possibility of replacement of ordinary reinforcement is presently very important topic (Löfgren et al. 2007). The number of practical applications of fiber-reinforced High Performance Concrete (HPC) is increasing like foundation slabs, foundations and walls. The fibres are likely to replace the ordinary reinforcement completely (Jansson et al. 2010). While the other structures like beams and slab, fibers can be used in combination with ordinary reinforcement or pre-stressed reinforcement. The both cases show improvement of working environment at the construction site and potential benefits due to economic factors. The one of main benefits of fiber reinforcement is an ability to transfer stress across a crack. However, if fiber-reinforced HPC is to be a more widely used material, general simple test method is needed for the concrete industry. This is necessary for fiber-reinforced HPC, where industry lacks such a method to verify their daily production quality control. Further, it would provide relevant material data allowing to the structural engineers design of structures that are safe and cost-efficient. As design tools seem to become more advanced and the design requirements are more complex, the need of fracture properties is required for structural analysis. Therefore, there is a need of simple test method that allows determining the fracture properties of fiber-reinforced HPC with acceptable accuracy, which can be used by companies in their daily production without expensive investment to testing equipment.

In last two decades the tensile behaviour of non-fiber and fiber reinforced concretes is mostly described by the concepts of the fictitious crack model. The most often used non-linear fictitious crack model was originally developed by Hillerborg et al. (1976). This model is able to closely describe the fracture properties of concrete. However, determination of softening curves of stress-crack opening relationships can cause

particular difficulties like in case of uniaxial tensile test and three point bending (Østergaard et al. 2004). Another option is the wedge splitting test setup (WST), which is made for indirect determination of the softening curve. The WST was originally proposed by Linsbauer & Tschegg (1986) and later developed by Brühwiler & Wittmann (1990). The researchers have greatly used the WST-method, and recently interest in the method increased rapidly. Its main advantage lies in its simplicity and stability. Furthermore, a standard cube is used, but the test can also be performed on core-drilled samples from the existing structure. Moreover, it was proven by Østergaard et al. (2004) and Hansen et al. (1998) that the test is suitable for early-aged concretes because it doesn't suffer problems caused by self-weight of the specimen. The work of Elser et al. (1996) should be mentioned as well. Their work presented the fracture behaviour of polypropylene fiber-reinforced concrete.

The present paper focuses on the inverse analysis of WST approach developed by Østergaard et al. (2004) for bi-linear softening curve and the approach, which comes out of Skoceck & Stang (2008) work for multi-linear softening curve. So far, Østergaard's bi-linear softening curves are mostly used to approximate the softening behaviour of concretes. It is expected that refinement of the softening curves will reflect in improved accuracy of the WST simulation. For that purpose the semi-analytical approach is used as the background for inverse analysis of the WST. The inverse analysis is capable in estimating both elastic and fracture properties from the WST. Fracture energy,  $G_f$ , was found to increase with age, while the characteristic length,  $L_{ch}$ , was found to decrease.

## 3.2 Modelling

Loading of the specimen by wedge leads to splitting force and subsequently initiation of a crack at the bottom of the notch. Furthermore with increase of load stable crack propagation is observed. The control of the experiment may be performed by crack mouth opening displacement or by constant displacement rate of the wedge. The crack hinge model (CHM) to the WST geometry was developed by Ulfkjær et al. (1995) and later extended by Olesen (2001). The CHM simulates the area closely surrounded by propagated crack. The hinge is modelled as array of springs, which are attached to the rigid boundaries of the element. The stress transferred by the spring is assumed to be linear elastic in the pre-cracked state, whereas the cracked state is determined by the stress-crack opening relationship as shown in Eq. (3.1)

$$\sigma = \begin{cases} \sigma(\varepsilon) = E\varepsilon & \text{Pre-cracked State} \\ \sigma_w(w) = g(w)f_t & \text{Cracked State} \end{cases} \quad (3.1)$$

where  $E$  represent elastic modulus,  $\varepsilon$  denotes elastic strain,  $\sigma_w(w)$  denotes stress-crack opening relationship with crack opening  $w$ , and  $f_t$  represents tensile strength. In Figure

3.1 the function  $g(w)$  is for the  $N$ -linear ( $N \geq 2$ ) softening curve is shown and is defined as:

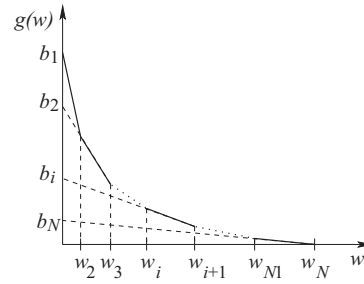


Figure 3.1. The scheme of multi-linear softening curve.

$$g(w) = b_i - a_i w; \quad w_{(i-1)} < w < w_i \quad (3.2)$$

where  $w_i$  corresponds to the intersection of  $i$ -th and  $i + 1$ th line and has the form:

$$w_i = \frac{b_i - b_{i+1}}{a_i - a_{i+1}} \quad \text{where } i < N \quad (3.3)$$

The critical crack width (width at which  $g(w) = 0$ ) is calculated by:

$$w_N = w_c = \frac{b_N}{a_N} \quad (3.4)$$

with  $N$  equals to number of lines in the softening curve. Figure 3.2 shows hinge model geometry, which is described by the half of the angular deformation  $\varphi$  and depth of the neutral axis  $y_0$ .

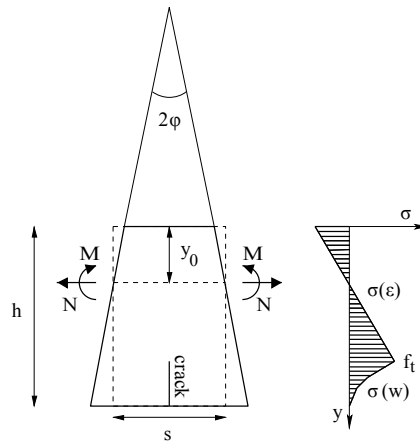


Figure 3.2. The hinge model and assumed stress distribution.

Olesen (2001) analytically determined crack opening  $w(y)$  for each point  $y$  for known stress  $\sigma(y)$ . The mean of longitudinal strains,  $\varepsilon^*(y)$  is then calculated as:

$$\varepsilon^*(y) = (y - y_0) 2\varphi / s \quad (3.5)$$

Then deformation of an incremental strip of the hinge is given by  $u(y) = s\varepsilon^*(y)$ , where  $s$  is the length of the hinge ( $s = 0.5h$ ). Once crack occurs,  $u(y)$  can be computed as the sum of the elastic deformation and the crack opening according Eq. (3.6).

$$u(y) = s\varepsilon^*(y) = s \frac{\sigma_w(w(y))}{E} + w(y) \quad (3.6)$$

The stress distribution equation can be obtained by combining Eq. (3.5) and (3.6) as follows:

$$\sigma_w(w(y)) = \frac{\varsigma_i - 2\varphi(y - y_0)\beta_i}{1 - \beta_i} \frac{E}{s} \quad (3.7)$$

Solving Eq. (3.7) by introducing cohesive law (Eq. 3.1) with respect to  $w(y)$  and  $\sigma_w(w(y))$  the following solution is observed:

$$\sigma_w(w(y)) = \frac{\varsigma_i - 2\varphi(y - y_0)\beta_i}{1 - \beta_i} \frac{E}{s} \quad (3.8)$$

$$w(y) = \frac{2\varphi(y - y_0) - \varsigma_i}{1 - \beta_i} \quad (3.9)$$

where  $\varsigma_i$  and  $\beta_i$  are dimensionless factors:

$$\beta_i = \frac{f_t a_i s}{E} \quad \text{and} \quad \varsigma_i = \frac{f_t b_i s}{E} \quad (3.10)$$

For additional information on the development and implementation of the CHM see the following references Olesen (2001), Østergaard et al. (2004) and Skocek & Stang (2008). However, two equations have to be fulfilled to determine the material properties from the CHM:

$$M_{ext} - M_{hinge} = 0 \quad \text{and} \quad CMOD_{obs} - CMOD_{WST} = 0 \quad (3.11)$$

where  $M_{ext}$  is the external bending moment and  $M_{hinge}$  stands as bending moment transferred by hinge. The  $CMOD_{obs}$  represents the observed  $CMOD$  and  $CMOD_{WST}$  is computed  $CMOD$ . The external bending moment,  $M_{ext}$  can be calculated as follow:

$$M_{ext} = P_{sp}(d_2 - y_0) + \frac{1}{2}P_v d_1 + \frac{1}{2}mge \quad (3.12)$$

where

$$P_v = P_{sp} \frac{2 \tan \alpha_w + \mu_c}{1 - \mu_c \tan \alpha_w} \quad (3.13)$$

refers to splitting load,  $P_{sp}$ , and vertical load  $P_v$ ;  $\alpha_w$  stands for wedge angle,  $\mu_c$  for friction in the roller bearing,  $m$  denotes mass of the specimen,  $g$  is the acceleration of gravity and  $e$  represents the horizontal distance between the axis of symmetry of the specimen and the centre of gravity of one half of the specimen. The bending moment transferred by hinge,  $M_{hinge}$  is computed by:

$$M_{hinge} = \int_0^h \sigma(y)(y - y_0) dy \quad (3.14)$$

where  $\sigma$  stands for cohesive law from Eq. (3.1). The  $CMOD_{WST}$  is defined as sum of elastic deformation of the specimen,  $\delta_e$ ; deformation due to presence of the crack opening,  $\delta_w$ ; and deformation caused by geometrical amplification,  $\delta_g$ .

$$CMOD_{WST} = \delta_e + \delta_w + \delta_g \quad (3.15)$$

The evaluation of the elastic deformation,  $\delta_e$  can be found in Tada et al. (2000) as

$$\delta_e = \frac{P_{sp}}{Et} v_2 \quad (3.16)$$

where  $t$  = specimen thickness and  $v_2$  is a function of the ratio between the length of the initial notch and the distance from the loading line to the bottom of the specimen.

$$v_2 = \frac{x}{(1-x)^2} (38.2 - 55.4x + 33.0x^2) \quad (3.17)$$

The ratio is given by  $x = 1 - h/b$  (See Figure 3.3).

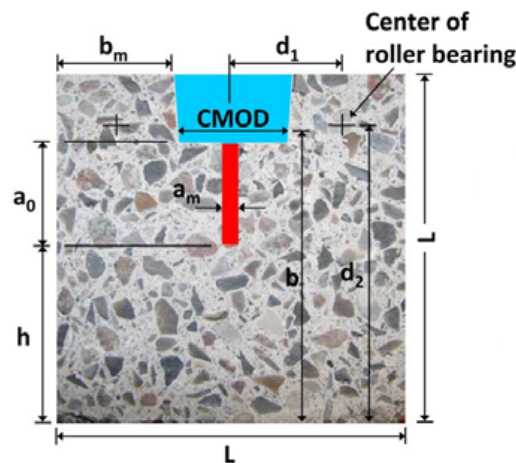


Figure 3.3. *WST specimen geometry with the blue area indicating the groove and the red area indicating 4.5mm notch.*

The deformation due to presence of the crack opening,  $\delta_w$  can be directly computed from Eq. (3.9) at  $y = h$ . Finally, deformation caused by geometrical amplification,  $\delta_g$  is derived as

$$\delta_g = 2(b-h) \left( \frac{\delta_w}{2d} - \frac{\varphi^{el}}{1-\beta_i} \right) \quad (3.18)$$

where  $\varphi^{el}$  is denoted as maximum elastic angular deformation of the hinge and  $\beta_i$  is dimensionless factors defined in Eq. (3.10).

The computation of inverse analysis is based on three steps that are repeated until convergence criteria are obtained. The first step involves computation of elastic modulus,  $E$ . Therefore, only data corresponding to the elastic loading are considered. Determination of elastic modulus is very fast and reliable since the part of working diagram is governed by  $E$ . Once elastic modulus is found, the tensile strength  $f_t$  and the first decreasing branch of softening curve  $a_1$  are searched. Furthermore,  $N-1$  searchings are performed in order to find  $a_i$  and  $b_i$ , where  $i \geq 2$ . The process of inverse analysis can be written as:

$$\begin{aligned} & \text{while (convergence is not achived)} \\ & \min_E \sum_{j=1}^{K^{el}} \|P_{j,obs} - P_{j,hinge}\| \\ & \min_{f_t, a_1} \sum_{j=1}^K \|P_{j,obs} - P_{j,hinge}\| \\ & \text{for } i \geq 2 \\ & \min_{a_i, b_i} \sum_{j=1}^K \|P_{j,obs} - P_{j,hinge}\| \\ & \text{check convergence} \end{aligned} \quad (3.19)$$

where  $K$  is total number of recorded load-crack opening pairs in the experiment,  $K^{el}$  is number of recorded load-crack opening pairs corresponding to elastic part of loading,  $P_{j,obs}$  denotes splitting force in  $j$ -th recorded load-crack opening pair,  $P_{j,hinge}$  is optimized splitting force in  $j$ -th computed load-crack opening pair.

The each measurement can be influenced by errors, and it is impossible to fit the model exactly to the measurements, which means that the choice of the suitable robust form  $\|P_{obs} - P_{hinge}\|$  plays important role. The iterative process minimizes the difference between observed loads applied in the experiments,  $P_{obs}$ , and the load predicted by CHM,  $P_{hinge}$  according to the error normalization function as:

$$\|P_{obs} - P_{hinge}\| = \sqrt{1 + \frac{(P_{obs} - P_{hinge})^2}{2}} - 1 \quad (3.20)$$



The stopping criteria for the maximum relative difference for two subsequent sets were used fracture energy;  $G_f$  obtained from Eq. (3.21) and the characteristic length,  $L_{ch}$  from Eq. (3.22).

$$G_f = \frac{f_t}{2} \sum_{i=1}^N [(2b_i - a_i(w_{i-1} + w_i))(w_i - w_{i-1})] \quad (3.21)$$

$$L_{ch} = \frac{EG_f}{f_t^2} \quad (3.22)$$

The points obtained from the experimental load-CMOD data used by the inverse analysis program to determine the cohesive laws were selected equidistantly in regards to arch length in the normalized coordinate system. The linear interpolation is used for points selected between measured data. The arc length increment used for given analysis was 0.05.

### 3.3 Experimental procedure

The present work represents three fiber reinforced and regular HPC mixes. The first mix was a commercial mix developed by CONTEC ApS and was denoted as Contec mix. Another two HPC mix designs were based on research work of Ozbay et al. (2010). These two mixes were denoted as DTU mixes. The DTUI mix was designed to correspond to the mechanical properties of the Contec mix. The DTUII mix was adjusted by bauxite sand and fly ash to obtain better mechanical properties than Contec and DTUI. The mix designs are shown in Table 3.1. A 60l pan mixer was used for mixing; mixing time was 2 minutes for the dry mixing and 5 minutes with water and super-plasticizer. The vibrating time was chosen to be 30s. After casting, the specimens were left to harden in a climate chamber ( $22 \pm 2$  °C and  $65 \pm 5\%$  RH). Specimens were demoulded after 24h and put in the water at 20 °C for curing. The experimental programme presented in this paper included 48 wedge splitting tests.

WST-specimens were casted in special PVC moulds with groove and notch made for this purpose. The geometry of the WST-specimen is shown in Figure 3.3. The WST-cube has length  $L = 100$  mm and thickness  $t = 100$  mm. The height of the ligament was  $h = 50$  mm. The mean width of notch  $a_m = 4.5$  mm, however, the walls of a real notch were a little bit inclined in order to avoid demoulding problems. The length of notch was  $a_0 = 28$  mm. Position of center of roller bearing, where splitting load is applied was  $d_1 = 39.5$  mm and  $d_2 = 85.4$  mm. Figure 3.4 shows WST experimental setup, where the rotational joints are used to prevent unwanted restrained. The rotational joint (a rectangular bar) was placed below specimen combined with roller bearing above the wedge.

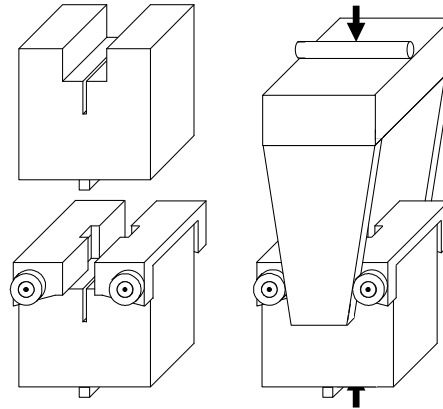


Figure 3.4. *Schematic showing of experimental WST test setup.*

Loading is controlled by displacement measurements from a clip gage inserted into the groove of the WST specimen to measure the CMOD. Distance  $b = 83.5$  mm describes contact position of the clip gage. The clip gage was modified by using brass feet to contact the side of the groove. The vertical load was recorded by the testing machine, and subsequently used for calculation of the splitting load. The wedge angle from the vertical axis was used  $15^\circ$ . The constant displacement rate of the wedge was kept initially of  $0.05$  mm/s to a CMOD of  $0.5$  mm. After reaching a CMOD of  $0.5$  mm, the displacement rate was increased to  $0.10$  mm/s to minimize testing time.

Table 3.1 *Mix designs (kg/m<sup>3</sup>)*

| Mix                                | Contec | DTUI  | DTUII  | Contec-F | DTUIF | DTUIIF |
|------------------------------------|--------|-------|--------|----------|-------|--------|
| Cement (CEM I 52.5 R)              | /      | 495   | 460    | /        | 495   | 460    |
| Binder Contop S 105-2              | 582.3  | /     | /      | 582.3    | /     | /      |
| CA, granite, 02-05 mm              | 832.3  | 868.4 | 1015.6 | 832.3    | 868.4 | 1015.6 |
| FA, sea gravel, 0.1-1.5 mm         | 763.7  | 781.6 | /      | 763.7    | 781.6 | /      |
| FA, bauxite sand, 0-1 mm           | /      | /     | 609.4  | /        | /     | 609.4  |
| Silica fume                        | /      | 55    | 57.5   | /        | 55    | 57.5   |
| Fly ash                            | /      | /     | 57.5   | /        | /     | 57.5   |
| Superplasticizer                   | /      | 11    | 25.9   | /        | 11    | 25.9   |
| Glass fibers                       | /      | /     | /      | 4.04     | 4.0   | 3.5    |
| Polypropylene fibers               | /      | /     | /      | 2.02     | 2.0   | 1.78   |
| Total dry mass                     | 2178.3 | 2200  | 2200   | 2184.4   | 2206  | 2205.3 |
| Water-cementitious material ratio  | 0.304  | 0.25  | 0.25   | 0.304    | 0.25  | 0.25   |
| Water-cementitious material ratio* | /      | 0.27  | 0.295  | /        | 0.27  | 0.295  |

\*including the water content of the superplasticizer

### 3.4 Results and discussion

Figure 3.5a shows the load-CMOD curves demonstrate the performance of the model and of the inverse analysis (Example for DTUIF at 28 day maturity). It is visible that computation based on softening curve for  $N = 3$  provide better approximation compared to the bi-linear curve. The computational time was approximately 15 minutes with softening curve for  $N = 2$  and approximately 25 minutes with softening curve for  $N = 3$ . The increase in computational time is compensated with increase in accuracy of the model. Figure 3.5b shows an example of stress-crack opening relationships at different ages for DTUIF. Furthermore, it shows the fracture energy given by the area under the curves is increasing with age.

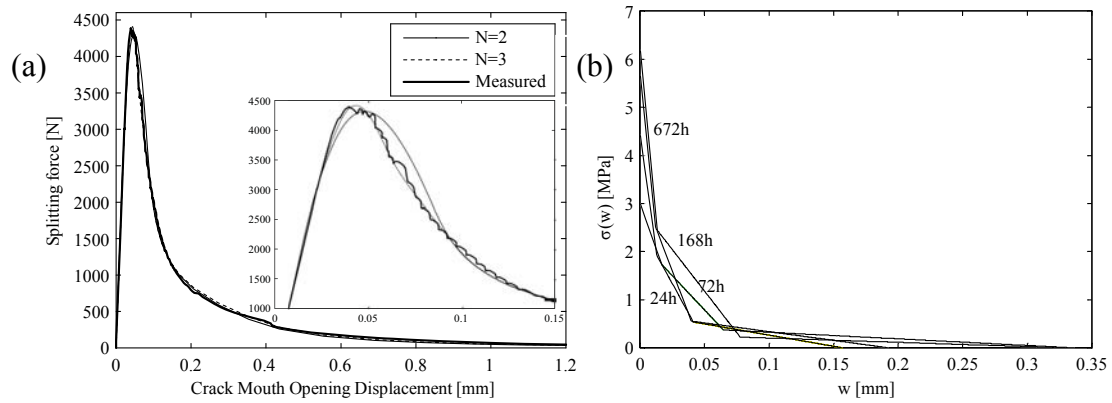


Figure 3.5. Example of comparison of the measured and the computed load-CMOD curves for DTUIF at 28 day maturity (a) and stress-crack opening relationships for DTUIF for different ages (b).

The development of modulus of elasticity  $E$  seen in Figure 3.6 shows some scatter and furthermore, a drop in  $E$  is seen for DTUII mix. With the exception of the Contec mixes, the mean static elastic modulus of the concretes  $E_{cm}$ , reached about 60 GPa after 28 days. The static elastic modulus of the Contec mixes was at 40 GPa, thus significantly lower. This seems to be caused by discontinues grain size distribution curve and by a disadvantageous pore size distribution of the hardened concrete. The static elastic modulus of the DTU mixes developed significantly faster than Contec mixes.

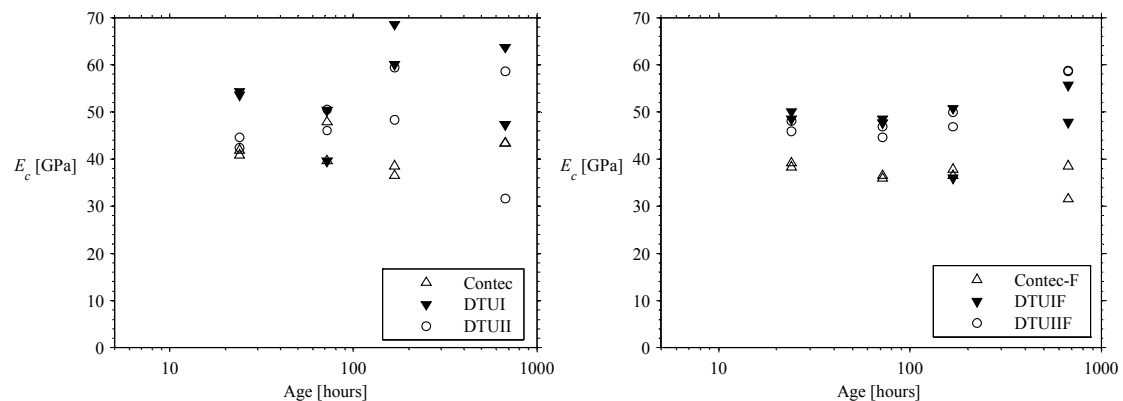
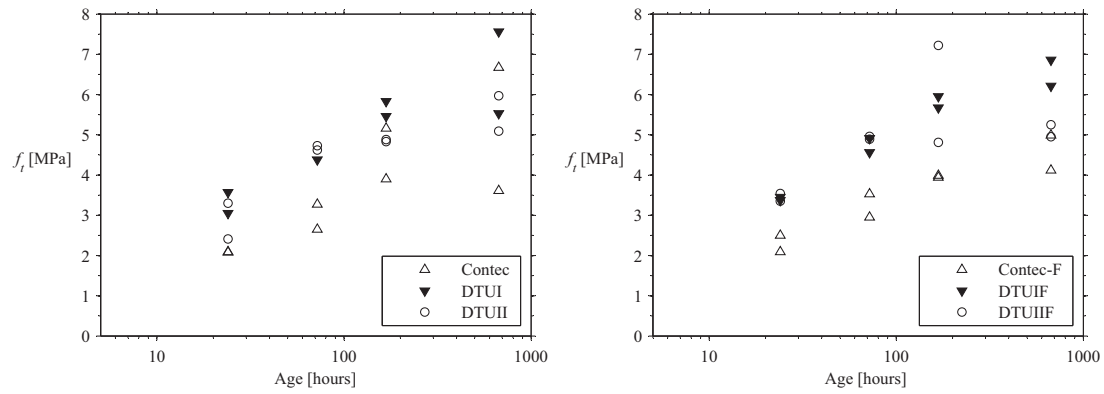


Figure 3.6. Development in modulus of elasticity.

Figure 3.7 shows the development in the tensile strength,  $f_t$ . The 28 days tensile strength of all HPC mixes was high around 6 MPa. The tensile strength of the DTU mixes made with silica fume, fly ash and cement with rapid hardening was observed to develop faster. After three days it was at roughly 5 MPa - well above the strength of the Contec mixes, 3 MPa. Tensile strength development of Contec mixes tended to increase slower than DTU mixes. There was no obvious change of tensile strength caused by adding fibers to HPC matrix.

In general results of development of elastic modulus  $E$  and tensile strength  $f_t$  follow the literature, see e.g. Østergaard et al. (2004). Their results also indicate a drop in the modulus of elasticity at 28 days.

Figure 3.7. *Development in tensile strength.*

Development in fracture energy with age is shown in Figure 3.8. The development of this property is in agreement with observation found in literature see e.g. Østergaard et al. (2004) and Löfgren et al. (2007). Same as at these papers the fracture energy is found to increase with age.

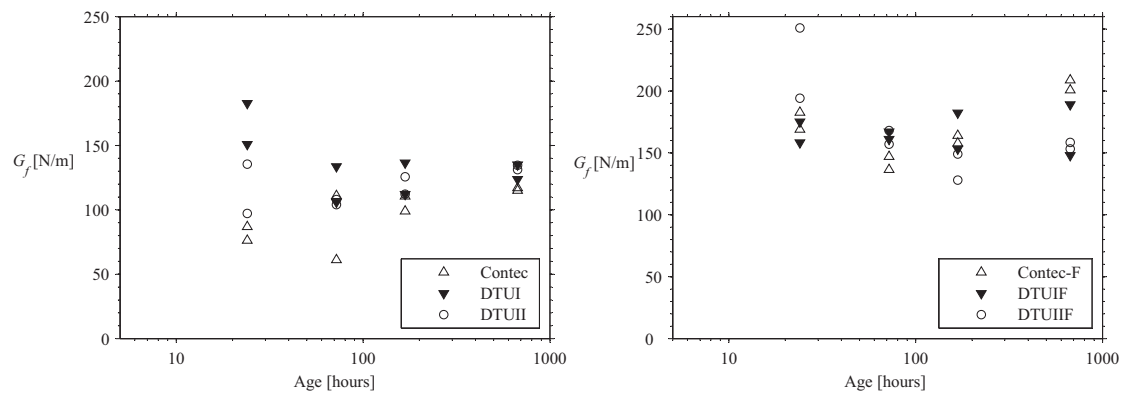
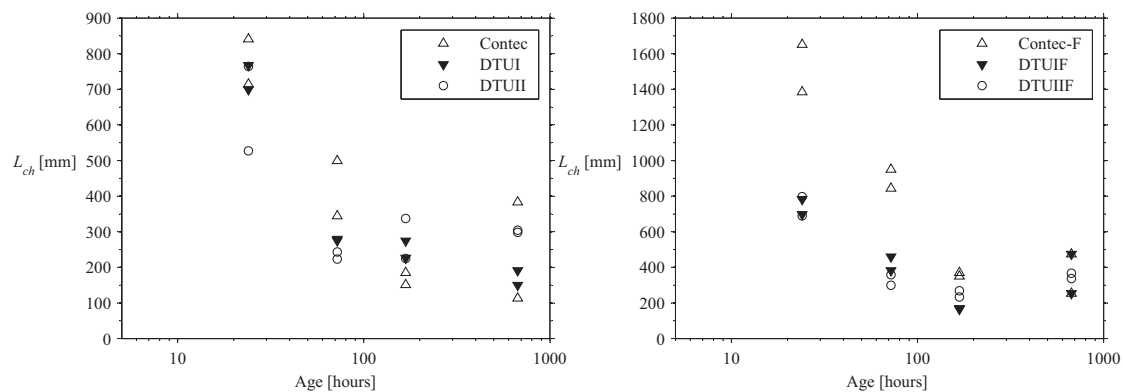
Figure 3.8. *Development in fracture energy.*

Figure 3.9 shows the development in characteristic length. The general trend in the development of the characteristic length despite the scatter was observed to decrease with maturity. The same results were also found in literature, e.g. Østergaard et al. (2004).

Figure 3.9. *Development in characteristic length.*

### 3.5 Conclusions

This paper presents current knowledge of the inverse analysis of the WST. In particular it addresses the question about the amount of information that can be retrieved from the WST using inverse analysis. The fracture behaviour of three fiber reinforced and regular HPC were investigated. The wedge splitting test setup with 48 cubical specimens was used experimentally and the cracked non-linear hinge model based on the fictitious crack model was applied for the interpretation of the results. The stress-crack opening relationships were extracted by using inverse analysis algorithm for various multi-linear softening curves. The fracture mechanics parameters such as crack opening displacement (COD), fracture energy and characteristic length were experimentally determined. Experiments were performed at 1, 3, 7 and 28 days. Fracture energy,  $G_f$ , was found to increasing with age, while the characteristic length,  $L_{ch}$ , was found to decrease.

The conclusions that can be drawn from this study are that:

- The wedge splitting test is suitable test method for assessment of fracture properties of regular and glass-polypropylene fiber reinforced HPC.
- The test method is easy to handle and the execution is relatively fast.
- Using the inverse analysis, the both elastic and fracture properties may be interpreted from the test results as a bi-linear or multi-linear stress-crack opening relationship.
- The refinement of the softening curves reflects in improved accuracy of the WST simulation in comparison with bi-linear softening curves with acceptable increase of computational time.

The suggested future work is to investigate the effect to varying material parameters on the fracture behavior as determined by the WST and inverse analysis, i.e. different volumes of carbon and basalt fiber reinforced polymers in HPC.

### 3.6 Acknowledgement

The authors greatly thank to the Danish National Advanced Technology Foundation and Connovate for the financial support.

## Chapter 4

### Conference paper 2

- Title: Assessment risk of fracture in thin-walled fiber reinforced and regular High Performance Concretes sandwich elements
- Authors: Kamil Hodicky, Thomas Hulin, Jacob W. Schmidt and Henrik Stang
- Conference: In Proceedings of the 8<sup>th</sup> International Conference on Fracture Mechanics of Concrete and Concrete Structures, International Center for Numerical Methods in Engineering (CIMNE), p. 1257-1266, Toledo, Spain, 2013.

## Abstract

High Performance Concrete Sandwich Elements (HPCSE) are an interesting option for future low or plus energy building construction. Recent research and development work, however, indicate that such elements are prone to structural cracking due to the combined effect of shrinkage and high temperature load. Due to structural restraints, autogenous shrinkage may lead to high self-induced stresses. Therefore, autogenous shrinkage plays important role in design of HPCSE. The present paper assesses risk of fracture due to autogenous shrinkage-induced stresses in three fiber reinforced and regular High Performance Concretes (HPC). The research work described in this paper contains a description of experimental setup that allows measurement of effective shrinkage in HPC, which develops on an elastic inhomogeneity embedded in HPC matrix undergoing shrinkage during hydration (autogenous shrinkage). The test setup is based on direct measurement of the hydrostatic pressure developed in a simple pressure sensor embedded in the same matrix and a subsequent analysis based on Eshelby's solution for an ellipsoidal inhomogeneity embedded in an infinite matrix. The paper also presents the analysis necessary to perform an interpretation of the experimental results and to determine effective shrinkage in the HPC matrix. Furthermore, the mechanical properties of all the mixes – static elastic modulus, compression strength, tensile strength as well as fracture energy were investigated in detail as function of time. Finally, the paper describes the modeling work with HPCSE predicting structural cracking provoked by autogenous shrinkage. It was observed that risk of cracking due to autogenous shrinkage rapidly rises after 3 days in case of regular HPC and after 7 days in case of fiber reinforced HPC.

## 4.1 Introduction

Thin-walled High Performance Concrete Sandwich Elements (HPCSE) undergo volume changes. These changes are generated by high thermal load applied on the concrete plates in the hardened state combined with autogenous and drying shrinkage during hardening. HPCSE are particularly sensitive to self-desiccation of the cement paste during hydration process, which leads to autogenous shrinkage. If a restraint is present, autogenous shrinkage may lead to high self-induced stresses (Gilbert, 2001; Sule & van Breugel, 2004; Maruyama et al., 2006). In practice, restraint of HPCSE arises from rigid inhomogeneities, reinforcement, temperature gradients over the specimen thickness and subgrade friction that limits the volumetric changes. The prediction of shrinkage cracking due to restraint is a complex phenomenon dependent on the interaction of several factors such as: free shrinkage, creep relaxation, material stiffness, fracture resistance, environmental conditions, time dependence, and degree of restraint (Shah et al., 1997; Shah & Weiss, 2000). Autogenous shrinkage should be limited because it may possibly cause surface and even through-thickness micro-

cracking or macro-cracking and impair the concrete quality (Lura et al., 2003) Therefore autogenous shrinkage plays important role in design of HPCSE. The present paper is case study of 3.59 m wide and 4.48 m high load carrying HPCSE. These HPCSE were subjected to structural cracking approximately 6 months after assembly. The HPCSE consist of an internal layer of insulation and two external High Performance Concrete (HPC) plates. The connectors are used to keep the plates together and the panel intact during handling. The prediction of shrinkage cracking is a complex problem dependent on several factors as was already mentioned. The experimental investigations and monitoring of all these factors could lead to high financial cost and long-term measurement.

This work presents a low cost experiment which can combine several factors into one. The experimental work is based on direct measurement of the autogenous shrinkage-induced stresses. In former studies some experiments of self-induced stresses in concrete were performed. Nielsen (1971) in his doctoral study developed a stress sensor to measure the stresses in an aggregate in a uniaxial creep test. The technique of measurement was based on change in the mutual inductance between two coils which are displaced in relation to each other. Furthermore, Sato et al. (1999) attempted to measure self-induced stress with an embedded deformed bar and inspection of micro-crack in concrete at the vicinity of rebar. Dela (2000) used massive porcelain spheres encircled with manganin wire glued to the surface as stress sensor to predict the magnitude of eigenstresses around aggregates in hardening cement paste. Her study is based on linear elastic solution and stepwise calculation taking into account change in the stiffness but disregarding the relaxation. Finally, the work by Stang (1996) should be mentioned. In this work, the shrinkage-induced clamping pressure acting on aggregates and different fiber types embedded in cement pastes were investigated as a function of time. The estimation is based on direct measurement of the pressure developed in a simple pressure sensor embedded in the same matrix and a subsequent analysis based on Eshelby's solution for an ellipsoidal inhomogeneity embedded in an infinite matrix (Eshelby, 1957).

The main motivation of the present work is to demonstrate that autogenous shrinkage of the HPC contributes to the potential structural cracking of the front plate of the HPCSE. Three fiber reinforced and regular HPC mixes were analyzed in order to assess risk of fracture and eventually foresee whether cracks will be propagated stably or unstably. Additionally the mechanical properties of all mixes – Static elastic modulus, compressive strength, tensile strength as well as fracture energy were investigated in detail as function of time.

## 4.2 Experimental procedure

The present work represents three fiber reinforced and regular HPC mixes. The first mix was a commercial mix developed by CONTEC ApS and will be denoted as Con-



tec mix. Another two HPC mix designs were based on research work of Ozbay et al. (2010). These two mixes were denoted as DTU mixes. The DTUI mix was designed to correspond to the mechanical properties of the Contec mix. The DTUII mix was adjusted by bauxite sand and fly ash to obtain better mechanical properties than Contec and DTUI. The mix designs are shown in Table 4.1. A 60l pan mixer was used for mixing; mixing time was 2 minutes for the dry mixing and 5 minutes with water and super-plasticizer. The vibrating time was chosen to be 30s. After casting, the specimens were left to harden in a climate chamber ( $22 \pm 2$  °C and  $65 \pm 5\%$  RH). Specimens were demoulded after 24h and put in the water at 20 °C for curing. Beams for determination of the mechanical properties were casted in one use polystyrene moulds.

Table 4.1 *Mix designs (kg/m<sup>3</sup>)*

| Mix                                | Contec | DTUI  | DTUII  | Contec-F | DTUIF | DTUIIF |
|------------------------------------|--------|-------|--------|----------|-------|--------|
| Cement (CEM I 52.5 R)              | /      | 495   | 460    | /        | 495   | 460    |
| Binder Contop S 105-2              | 582.3  | /     | /      | 582.3    | /     | /      |
| CA, granite, 02-05 mm              | 832.3  | 868.4 | 1015.6 | 832.3    | 868.4 | 1015.6 |
| FA, sea gravel, 0.1-1.5 mm         | 763.7  | 781.6 | /      | 763.7    | 781.6 | /      |
| FA, bauxite sand, 0-1 mm           | /      | /     | 609.4  | /        | /     | 609.4  |
| Silica fume                        | /      | 55    | 57.5   | /        | 55    | 57.5   |
| Fly ash                            | /      | /     | 57.5   | /        | /     | 57.5   |
| Superplasticizer                   | /      | 11    | 25.9   | /        | 11    | 25.9   |
| Glass fibers                       | /      | /     | /      | 4.04     | 4.0   | 3.5    |
| Polypropylene fibers               | /      | /     | /      | 2.02     | 2.0   | 1.78   |
| Total dry mass                     | 2178.3 | 2200  | 2200   | 2184.4   | 2206  | 2205.3 |
| Water-cementitious material ratio  | 0.304  | 0.25  | 0.25   | 0.304    | 0.25  | 0.25   |
| Water-cementitious material ratio* | /      | 0.27  | 0.295  | /        | 0.27  | 0.295  |

\*including the water content of the superplasticizer

### 4.3 Mechanical properties

The developments of the mechanical properties - Static elastic modulus, compression strength, tensile strength (wedge splitting test) as well as fracture energy were investigated in detail as function of time. All the tests were performed at room temperature ( $20 \pm 2$  °C). The compressive strength and static elastic modulus were determined according to EN 1992-1-1 (Bamforth et al., 2007). Specimen geometry for mechanical tests is shown in Table 4.2.

Table 4.2 *Specimen geometry for different tests*

| Test                   | Specimen geometry      |
|------------------------|------------------------|
| Compressive strength   | W/H/L = 40/40/40 mm    |
| Tensile strength       | W/H/L = 100/100/100 mm |
| Static elastic modulus | W/H/L = 100/100/100 mm |

#### 4.3.1 Compressive strength

The mean compressive strength at 28 days was observed to range roughly between 75 to 110 MPa. DTU mixes have significantly higher development of compressive strength during the first days. This phenomenon can be explained by the use of the cement with rapid hardening together with silica fume and fly ash in case of DTUIIF.

There was not found any significant difference in compressive strength between regular HPC mixes and the fiber reinforced. Development of compression strength for all HPC mixes is shown in Table 4.3.

### 4.3.2 Tensile strength

The 28 days splitting tensile strength of all HPC mixes was high around 5.5 MPa. The tensile strength of the DTU mixes made with silica fume, fly ash and cement with rapid hardening was observed to develop faster. After three days it was at roughly 5 MPa - well above the strength of the Contec mixes, 3 MPa (Table 4.3). Tensile strength development of Contec mixes tended to increase slower than DTU mixes. There was no obvious change of tensile strength caused by adding fibers to HPC matrix.

### 4.3.3 Static elastic modulus

With the exception of the Contec mixes, the mean static elastic modulus of the concretes  $E_{cm}$ , reached about 60 GPa after 28 days. The static elastic modulus of the Contec mixes was at 40 GPa, thus significantly lower. This seems to be caused by discontinues grain size distribution curve and by a disadvantageous pore size distribution of the hardened concrete. The static elastic modulus of the DTU mixes developed significantly faster than Contec mixes (Table 4.3).

Table 4.3 *Mechanical properties*

| Mix      | Age (days) | $f_{cm,cube}$ – SD (MPa) | $f_{ctm,sp}$ – SD (MPa) | $E_{cm}$ – SD (GPa) | $L_{chm}$ – SD (mm) | $G_{fm}$ – SD (N/m) |
|----------|------------|--------------------------|-------------------------|---------------------|---------------------|---------------------|
| Contec   | 1          | 31.4 – 4.8               | 2.1 – 0.0               | 41.3 – 0.8          | 777 – 89            | 81.5 – 7.6          |
|          | 3          | 43.6 – 8.2               | 3.0 – 0.4               | 43.7 – 5.8          | 430 – 109           | 86.1 – 35.2         |
|          | 7          | 59.1 – 3.2               | 5.1 – 0.9               | 36.5 – 1.4          | 115 – 24            | 110.6 – 8.2         |
|          | 28         | 72.3 – 8.4               | 5.2 – 2.1               | 43.3 – 0.0          | 186 – 49            | 115.9 – 1.4         |
| DTUI     | 1          | 61.5 – 3.5               | 3.6 – 0.4               | 53.5 – 0.5          | 768 – 48            | 182.7 – 22.6        |
|          | 3          | 65.6 – 2.2               | 4.4 – 0.0               | 44.9 – 7.5          | 281 – 3             | 119.8 – 19.5        |
|          | 7          | 73.1 – 6.9               | 5.6 – 0.3               | 60.0 – 6.0          | 234 – 34            | 124.3 – 17.2        |
|          | 28         | 89.2 – 3.7               | 6.5 – 1.4               | 55.5 – 11.6         | 168 – 29            | 129.3 – 8.0         |
| DTUII    | 1          | 60.9 – 10.2              | 2.9 – 0.6               | 43.5 – 1.5          | 621 – 167           | 116.4 – 27.1        |
|          | 3          | 81.8 – 4.3               | 4.7 – 0.1               | 48.3 – 3.1          | 234 – 14            | 106.0 – 2.9         |
|          | 7          | 84.2 – 6.3               | 4.9 – 0.0               | 53.8 – 7.8          | 279 – 79            | 121.9 – 9.5         |
|          | 28         | 102.7 – 9.0              | 5.5 – 0.6               | 58.6 – 19.0         | 258 – 4             | 134.6 – 2.4         |
| Contec-F | 1          | 38.0 – 5.2               | 2.1 – 0.3               | 39.1 – 0.5          | 1652 – 188          | 184.8 – 9.7         |
|          | 3          | 52.1 – 2.5               | 3.3 – 0.4               | 36.5 – 0.4          | 464 – 76            | 136.5 – 7.4         |
|          | 7          | 60.3 – 4.0               | 3.9 – 0.0               | 36.4 – 0.9          | 370 – 14            | 157.8 – 4.4         |
|          | 28         | 71.9 – 1.5               | 4.6 – 0.6               | 35.0 – 4.9          | 346 – 156           | 204.8 – 5.7         |
| DTUIF    | 1          | 47.4 – 3.5               | 3.4 – 0.1               | 50.0 – 1.1          | 697 – 60            | 158.2 – 11.8        |
|          | 3          | 64.9 – 5.8               | 4.8 – 0.2               | 48.5 – 0.6          | 344 – 54            | 161.0 – 4.2         |
|          | 7          | 65.0 – 5.4               | 5.9 – 0.2               | 43.3 – 10.4         | 209 – 3             | 167.8 – 20.6        |
|          | 28         | 81.6 – 2.3               | 6.5 – 0.5               | 52.3 – 5.6          | 223 – 156           | 168.9 – 29.1        |
| DTUIIF   | 1          | 58.1 – 7.3               | 3.5 – 0.1               | 48.1 – 1.5          | 894 – 76            | 222.5 – 40.1        |
|          | 3          | 75.1 – 5.8               | 5.0 – 0.0               | 46.8 – 1.6          | 299 – 42            | 157.0 – 7.8         |
|          | 7          | 83.8 – 5.3               | 5.1 – 1.7               | 46.8 – 2.1          | 245 – 25            | 135.8 – 14.8        |
|          | 28         | 111.9 – 4.6              | 5.2 – 0.2               | 58.7 – 0.1          | 338 – 21            | 155.8 – 3.7         |

#### 4.3.4 Fracture energy

An experimental investigation completed as part of this study were using the Wedge splitting test (WST) to ascertain the fracture behaviour of the concrete mixtures used throughout this work. The specimen geometry and analysis needed to evaluate the WST were published in Skocek & Stang (2008). The fracture energy  $G_f$ , characterize the material's resistance to fracture. The mean fracture energy  $G_{fm}$ , was found to increasing with age for all the mixes. The brittleness of cohesive material can be described by the characteristic length,  $L_{ch}$ . The general trend in the development of the mean characteristic length  $L_{chm}$ , was observed to decrease with maturity. The same results were also found in literature, e.g. (Hariri, 2000; Østergaard et al., 2004).

#### 4.3.5 Autogenous shrinkage-induced stresses

The experimental setup proposed by Stang (1996) was used to determine autogenous shrinkage-induced stresses. As stress sensor a laboratory mercury thermometer with temperature scale going from 0 to 50 °C and a precision of 0.1 °C was chosen. The stress sensors were calibrated for hydrostatic pressure by using the so-called Budenberg instrument. The Budenberg was loaded stepwise until reaching 50 bars, and then unloaded. The average calibration factor  $\alpha$ , was found to be 1.67 MPa/°C. Furthermore, the amount of mercury in the capillary tube was measured by weighing the tube with and without mercury and the calibration factor  $\beta$  (g/°C), was determined related to apparent temperature change to mass of mercury. The equivalent compression modulus of the stress sensor  $\kappa^e$ , was determined according Eq. (4.1):

$$\kappa^e = \frac{\alpha \gamma_{hg}}{\beta} v \quad (4.1)$$

where  $\gamma_{hg}$  is density of mercury and  $v$  is the total volume of mercury cell (glass and mercury). Based on modelling the mercury cell as an axis-symmetric ellipsoidal shell with wall thickness  $h$ , the linear elastic solution for the equivalent compression modulus  $\kappa^{e*}$ , can be determined as shown in Eq.(4.2) (Stang, 1996)

$$\kappa^{e*} = \frac{2E^s h}{3bI} \quad (4.2)$$

where  $E^s$  is static elastic modulus and  $I$  is function of  $a/b$  ( $a$  is the length of the half-axis in the direction of symmetry and  $b$  is radius of the cell) and Poisson's ration  $\nu^s$ . The calculated bulk moduli based on linear elastic shell solution were compared with measured one. It was found that results of measured and calculated bulk moduli,  $\kappa^e$  and  $\kappa^{e*}$ , are close with 10 % differences between them.

To record properly the stresses due to autogenous shrinkage, the thermometer should disturb the concrete as little as possible. The glass tube protecting the mercury-filled

capillary is removed leaving only the mercury container and the capillary (see Figure 4.1a). Before casting, the 18 cylinders (3 cylinders per mix) were oiled to allow the HPC freely shrink without applying tension on the cylinder. After calibration, the stress sensors were casted into the center of PVC cylindrical mould filled with the HPC. The cylinders had a diameter of 100 mm and a height of 200 mm. The recording of the temperature during long-term testing was performed by thermocouples inserted in the concrete cylinder. To compensate the 0.2 °C precision of the couples, two couples were inserted close to the thermometer and the average of their readings was considered. After casting, the top of the cylinder was covered with a thin layer of oil to preserve the water from evaporating (see Figure 4.1b). Thus, the HPC experience only autogeneous shrinkage and temperature variation associated with the hydration process.

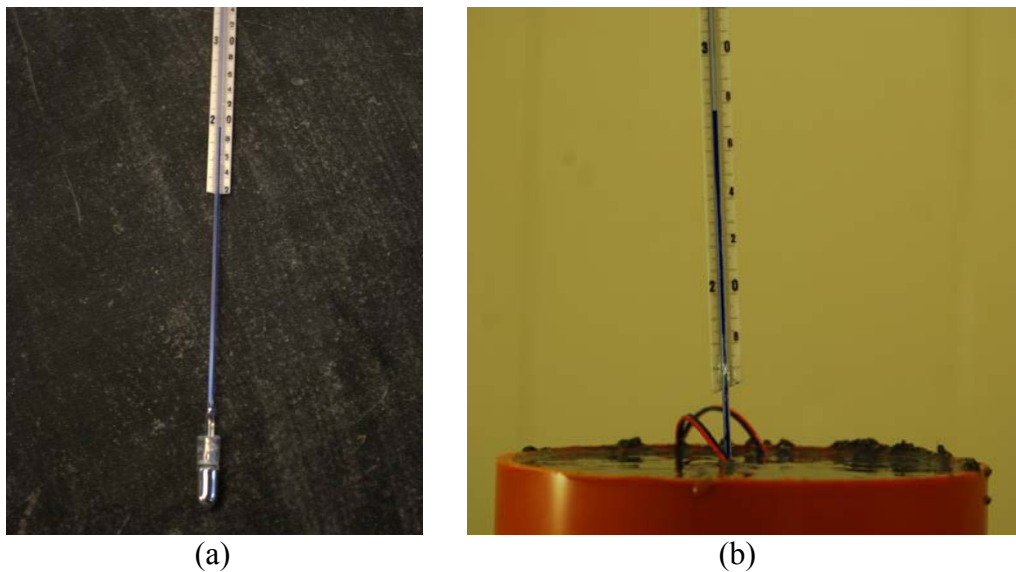


Figure 4.1. *a) Photograph showing the different parts of the mercury thermometer used as a pressure sensor in the experimental investigations. b) Photograph showing the experimental setup, the PVC mould, the stripped thermometer, and the thermocouple module.*

The output of observation was based on temperature differences  $\Delta T$ , between the stress sensor and average value of the two thermocouples observed over time  $t$ , where  $t = 0$  corresponds to the beginning of experiment (30 minutes after mixing). Using the calibration factor  $\alpha$ , the observed  $\Delta T$  was readily transformed to an equivalent hydrostatic stress state  $\sigma_{hyd}^e$ , in the equivalent elastic inhomogeneity:

$$\sigma_{hyd}^e(t) = \alpha(\Delta T(t) - \Delta T(t = 0)) \quad (4.3)$$

The development in equivalent hydrostatic stress state for six different mixes is shown in Figure 4.2. Figure 4.2 clearly shows that there is a significant difference between the DTU and Contec mixes. A much higher hydrostatic stress develops in the sensors embedded in DTU mixes. Furthermore, the hydrostatic stress keeps rising in the Con-

tec mixes and then after approximately 600 hours drops to an almost constant level. The hydrostatic stress of the DTU mixes keeps constantly rising up to 2000 hours then the curve is flattened. All fiber reinforced mixes showed the same tendency in development of the hydrostatic stresses as regular HPC mixes. However, there is a lack of information in literature whether increase of the hydrostatic stresses in fiber reinforced HPC mixes is significant or not. The experimental programme with more specimens would be necessary to statistically confirm this phenomenon.

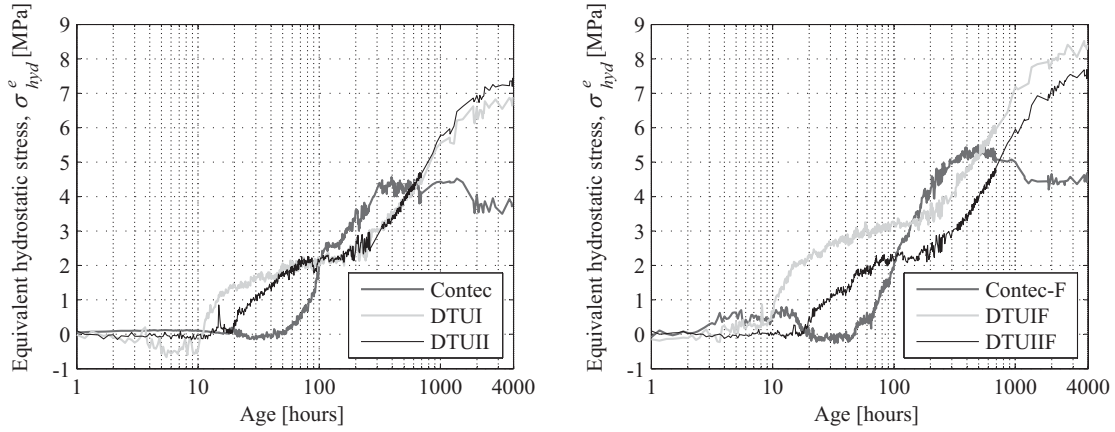


Figure 4.2. *Development in equivalent hydrostatic stress  $\sigma_{hyd}^e$ , in the pressure sensors.*

The analysis in Stang (1996) based on Eshelby's original superposition scheme with homogeneous infinite medium and an inclusion undergoing a stress-free strain was utilized in interpretation of the experimental results. The concept of effective shrinkage  $\varepsilon^{s,e}$ , was defined as a function of time according Eq. 4.4. The effective shrinkage can be defined as the autogenous shrinkage that in linear elastic system interpret the correct stress state in an embedded equivalent inhomogeneity.

$$\varepsilon^{s,e}(t) = \frac{\sigma_{hyd}^e(t)}{E_c(t)} \left( \frac{1 + \nu_c}{1 + \nu_i} + \frac{E_c(t)}{3K^{e*}} \right) \quad (4.4)$$

where  $E_c(t)$  is static elastic modulus of the HPC mixes as function of time. The Poisson's ratio of the HPC mixes,  $\nu_c$  of 0.2, is assumed to be equal to Poisson's ratio of embedded inhomogeneity,  $\nu_i$ .

Looking at Figure 4.3, it has to be noted that static elastic modulus of the HPC mixes was measured at certain time steps of maturity as shown in Table 4.3. To build up the effective shrinkage curves, the static elastic modulus of the HPC mixes as function of time was linearly interpolated between the measured ones. The effective shrinkage of the Contec mixes rises to  $2.5 \cdot 10^{-4}$  -  $3.0 \cdot 10^{-4}$  and after approximately 600 hours drops to an almost constant level of about  $2.0 \cdot 10^{-4}$  -  $2.5 \cdot 10^{-4}$ . The significant drop can be explained by relaxation, which plays an important role in Contec mixes. In the case of the DTU mixes the effective shrinkage keeps rising, however, with a much lower rate.

The effective shrinkage at 4000 hours almost reaches double of the Contec mixes, about  $3.0 \cdot 10^{-4}$  -  $4.0 \cdot 10^{-4}$ .

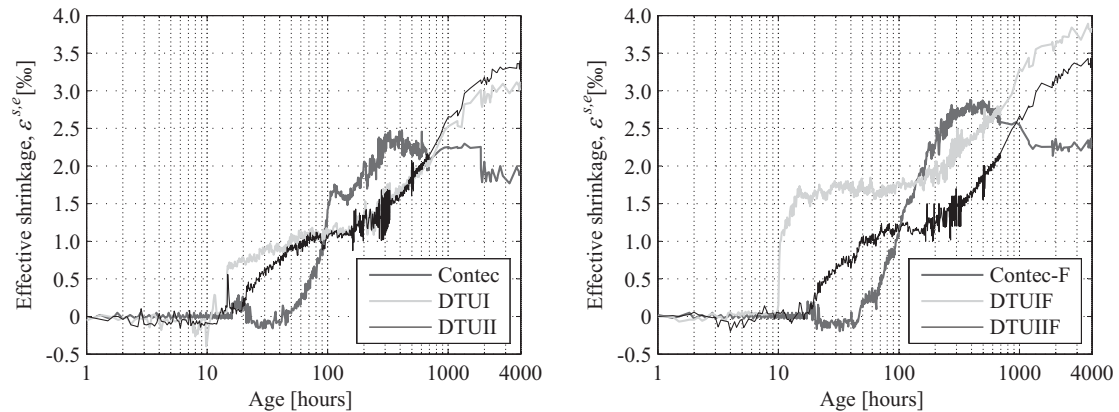


Figure 4.3. Development in effective shrinkage,  $\varepsilon^{s,e}$  for different inhomogeneities.

## 4.4 Assessment risk of fracture

In the case of HPCSE embedded steel connectors cause restrain to the HPC plates, see Figure 4.4. The finite element program Abaqus was used to calculate the response of the concrete front plate to autogenous shrinkage. The plate has a width of 3.584 m and a height of 4.48 m. The thickness of the plate is 20 mm. The shear connectors were implemented in the middle of the plate thickness. The calculations made the assumption of linear elastic behaviour/small displacements. A quarter of the panel was modelled, accounting for symmetry. The numerical model consists of two types of element: C3D8T: An 8-node thermally coupled brick for concrete front plate and T3D2T: A 2-node 3-D thermally coupled truss for welded wire truss shear connectors. All the investigated mixes were analyzed in order to assess risk of fracture and eventually foresee weather crack will be propagated stably or unstably. The material data from experiments (Static elastic modulus,  $E$ , and coefficient of thermal expansion for HPC mixes,  $\alpha_c$ ) were used as input to the Abaqus model.

To obtain the right response of the front plate, the analysis has to include autogeneous shrinkage of the front plate as well as an effect of differential shrinkage between front plate and back plate. The effect of differential shrinkage between front plate and back plate was extracted from experimental setup in Section 4.3.5 as the largest effective shrinkage difference between 3 cylinders of the same mix. The load induced by autogenous shrinkage was applied homogenously over the plate. In order to model autogenous shrinkage, this can be achieved using an extension of Hooke's law for temperature as:

$$\Delta T = \frac{\varepsilon^{s,e}(t)}{\alpha_c} \quad (4.5)$$

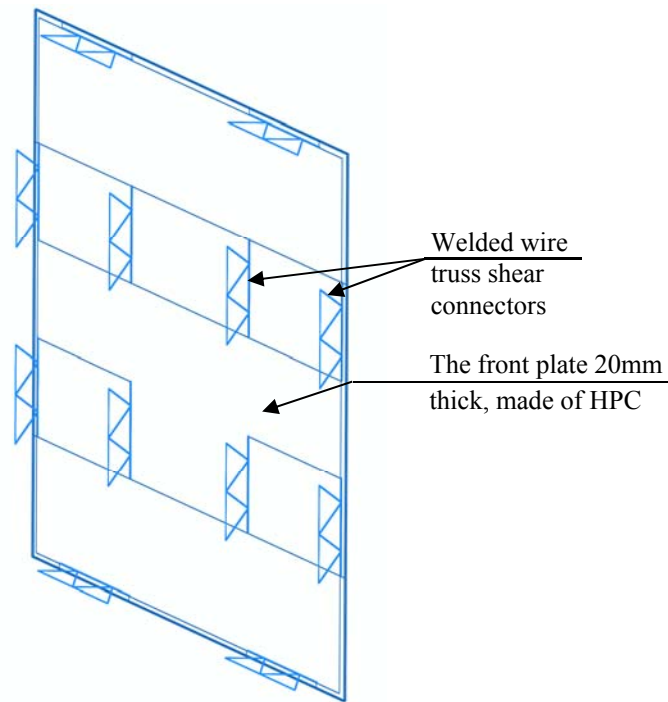


Figure 4.4. *The front plate with an arrangement of the shear connectors.*

The models were analysed for the same maturity as fracture properties were investigated. All of the results showed stresses exceeded the tensile capacity of concrete. The stress distribution was found to be highly localized in vicinity of shear connectors. These highly localized areas can correspond to the crack opening in the infinite sheet. Stang et al. (2007) performed a numerical investigation on crack propagation in an infinite sheet for a material with a linear cohesive law. They observed that a crack propagates stably as long as the crack length is smaller than characteristic length,  $L_{ch}$ . For larger crack length the crack growth becomes unstable. Dick-Nielsen (2008) study illustrates the development of the crack opening and showed that magnitude of the stable crack opening is approximately  $5\mu\text{m}$ , thus very fine crack, which is not visible by naked eye. This knowledge was used as first order approximation that linear elastic stresses will introduce crack. To predict the behaviour of the crack, the gray areas were compared with the characteristic lengths shown in Table 4.3. The crack propagation in the front plate for all the mixes was summarized in Table 4.4.

Table 4.4 *The crack propagation in the front plate*

| Mix    |    | Contec   | DTUI     | DTUII    | Contec-F | DTUIF    | DTUIIF   |
|--------|----|----------|----------|----------|----------|----------|----------|
|        | 1  | stable   | stable   | stable   | stable   | stable   | stable   |
| Age    | 3  | stable   | stable   | unstable | stable   | stable   | stable   |
| (days) | 7  | unstable | unstable | unstable | stable   | unstable | stable   |
|        | 28 | unstable | unstable | unstable | unstable | unstable | unstable |

In Figure 4.5 is shown example of output of 3D FE-analysis for DTUIF mix at 28 days maturity. The splitting tensile strength for DTUIF mix was set up to 6.5MPa (see Table 4.3). The red circle in the Figure 4.5 depicts the characteristic length which is in this case smaller than area where the tensile strength of concrete is exceeded. This observation leads to prediction that the cracks propagates unstably.

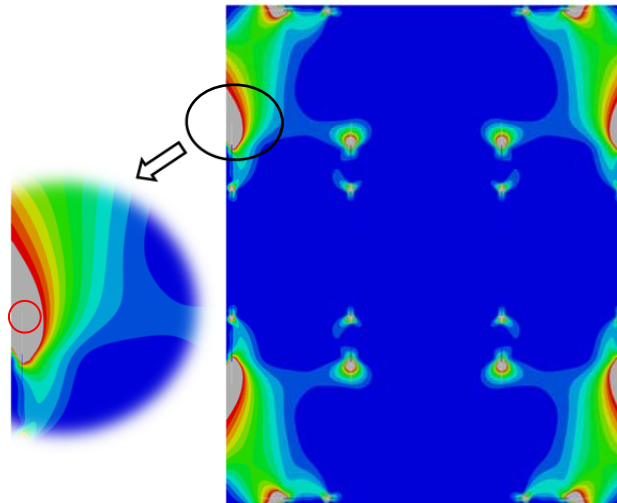


Figure 4.5. *Output of 3D FE-analysis for DTUIF mix at 28 days.*

## 4.5 Conclusions

The main assumption motivating this work is that a combination of autogenous shrinkage of the concrete and thermal load from the outside environment could lead to the cracking of the front plate of the HPCSE. In this paper, the risk of cracking related to autogenous shrinkage of the HPCSE made using three fiber reinforced and regular HPC was investigated. In the laboratory, different investigations were carried out in order to determine the characteristics of the concrete to be used as an input for the modelling work. The laboratory experiments and modelling work predicts the risk of cracking and crack propagation with relatively simple means by using the characteristic lengths. The combination of experimental and modelling work leads to the present conclusions.

The risk of cracking due to autogenous shrinkage rapidly rises after 3 days in case of regular HPC mixes and after 7 days in case of mixes with fibers. The stresses due to autogenous shrinkage have a large role to play also but minor compared to the one of the environmental conditions. The combination of autogenous shrinkage and thermal load from outside environment may lead to massive structural cracking. Furthermore, the stiffness of the shear connectors have a significant role in design of HPCSE. Therefore, their stiffness should be studied in detail and new types of shear connector for HPCSE should be developed to avoid of structural cracking.





## Chapter 5

### Conference paper 3

Title: Structural performance of new thin-walled concrete sandwich panel system reinforced with BFRP shear connectors

Authors: Kamil Hodicky, Thomas Hulin, Jacob W. Schmidt and Henrik Stang

Conference: In Proceedings of the Asia-Pacific Conference on FRP in structures (APFIS 2013), Melbourne, Victoria, Australia, 2013.

## Abstract

This paper presents a new thin-walled concrete sandwich panel system reinforced with basalt fiber-reinforced plastic (BFRP) with optimum structural performances and a high thermal resistance developed by Connovate and Technical University of Denmark. The shear connecting system made of a BFRP grid is described and provides information on the structural design with its advantages. Experimental and numerical investigations of the BFRP connecting systems were performed. The experimental program included testing of small scale specimens by applying shear (push-off) loading and semi-full scale specimens by flexural loading. Numerical investigations were based on 3-D linear elastic finite element analysis. Results from the numerical investigations were compared with experimental results of small and semi-scale specimens for the validation of the design procedure. Experimental and numerical results based on finite element modelling showed that the developed panel system meets the objectives of the research and is expected to have promising future.

## 5.1 Introduction

According to European Union (EU, 2010) residential and commercial buildings are responsible for about 40% of the total energy consumption and CO<sub>2</sub> emissions in Europe. Therefore, ambitious targets for energy consumption of new buildings are being implemented, and by the year 2020 nearly zero energy buildings will become a requirement in the European Union. As a consequence of these requirements as well as general requirements for increased efficiency and sustainability, the building sector experiencing a growing demand for modular, light and strong building elements having a high degree of insulation, a long life time, a low CO<sub>2</sub> emission, a low consumption of raw material, and an attractive surface with minimum maintenance. Thin-walled High Performance Concrete Sandwich Panels (HPCSPs) are an interesting option for future low or plus energy building constructions.

The HPCSPs have several beneficial features such as high quality, proven durability, fast erection, and attractive architectural appearance (Einea et al., 1994). A typical HPCSP consists of two precast High Performance Concrete (HPC) plates and layer of insulation separates the two HPC plates. The connectors penetrate the insulation layer and join the two HPC plates.

The HPCSPs may be designed with various degrees of composite action: non-composite, partially composite or fully composite (Rizkalla et al., 2009). The degree of composite action depends on the nature of the connection between two HPC plates. Two main categories of connectors exist: non-shear connectors and shear connectors. Non-shear connectors are used in non-composite HPCSPs primarily to resist the tensile forces required to maintain integrity of the panel by keeping two HPC plates attached. Shear connectors must provide adequate stiffness and strength to create signif-

icant composite behaviour in the panel and resist the ultimate and service loads on the panel. The connector design represents trade-off between establishment of full composite action for resisting lateral loads, and reduction of composite action to limit thermal deflections. The connections between the plates have been traditionally made by using bent reinforcing bars or various specially-designed steel or non-metallic connectors (Frankl et al., 2008). Increasing degree of composite action between two HPC plates using any type of these connectors increases the structural capacity of the HPCSP making it more efficient. However, increasing degree of composite action typically leads to significantly lower thermal efficiency of the panel due to the creation of thermal bridges (Wade et al., 1988). The stiffness of the connectors is proportional to the thermal deflection and thus has significant role in the design of HPCSPs.

Recently, the sandwich panel design concept has leaped forward by introducing fiber reinforced polymer (FRP) shear reinforcement due to the relatively high stiffness combined with its relatively low thermal conductivity compared to steel (Soriano & Rizkalla, 2013). Wade et al. (1988) performed the first attempt to use Glass-fiber reinforced polymer (GFRP) connectors for insulated concrete sandwich walls. Salmon et al. (1997) introduced GFRP bars formed in a truss orientation in place of metal wire trusses. The experimental investigation showed that the use of GFRP resulted in a high level of composite action. Following the same concept, Morcous et al. (2010) and Maximos et al. (2007) studied different shapes of GFRC shear connectors to obtain the full composite action. In past few years Rizkalla et al. (2009) focused on use Carbon Fiber Reinforced Polymer (CFRP) shear connector grids. The use of CFRP grids as trusses has enabled significantly improve mechanical and thermal performances. Therefore, the insulation between to concrete plates can deliver 100 percent of its rated performance without the hot or cold spots typically found in connection with metal trusses.

This paper presents the research program performed to investigate the behaviour of thin-walled HPCSPs reinforced with basalt FRP (BFRP) shear connectors. There is a major potential for using BFRP grid or so called basalt geo-grid at a much lower cost, since the thermal conductivity and mechanical properties are similar to GFRP and the cost of BFRP is significantly cheaper than CFRP.

Previous generations of a HPCSP system studied at Department of Civil Engineering, Technical University of Denmark (DTU) showed a high level of thermal efficiency. However, these panels were not structurally efficient due to their non-composite behaviour (Figure 5.1a). Improvements were made to these panels to create partial composite action while maintaining sufficient thermal efficiency. Using a BFRP grid as shear reinforcement redefined limits of HPCSP performance. Non-corrosive BFRP grid is shaped to look like a truss, and then casted into the panel. The new insulation products enabled to use large solid blocks instead of several layers of insulation. This step significantly accelerates the production process, decreases the amount of waste

product and especially provides direct transfer of shear stresses between two HPC plates (Figure 5.1b).

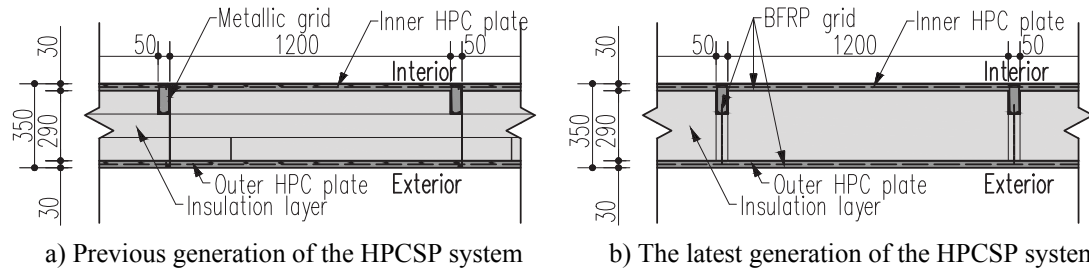


Figure 5.1. *Evolution of the HPCSP system.*

## 5.2 Experimental program

This paper describes an experimental research program performed at DTU to characterize the mechanical performance of the improved system. The program involved 25 small and semi-scale HPCSPs, which represent the panels that could be found installed on site. The first phase of experimental program consisted of material testing (insulation, HPC and BFRP grid) and pure shear (push off) test. The push-off testing was performed primarily to investigate shear transfer capacity of the insulation and BFRP grid. The push-off test has been used by a several researchers for similar purposes (Einea et al., 1994 and Salmon et al., 1997). The second phase of testing investigated flexural composite behaviour provided by the BFRP shear connectors. The specimen used to determine the level of composite action achieved by BFRP/insulation shear transfer mechanism are described in detail in the next section. Different parameters considered in the program included the type of BFRP grid used, insulation, rib structure, and the contact surface area of the insulation to HPC plate per strip of BFRP grid. Various parameters were established as part of experimental program that were believed to affect the overall structural performance and shear capacity of the BFRP shear connector transfer mechanism. All experimental investigations were also performed using Carbon FRP (CFRP) grid for direct comparison with BFRP grid.

## 5.3 Test setup

### 5.3.1 Push-off specimen details

Twenty one specimens were produced; the size of each push-off specimen was 310 by 650 mm with total thickness of 350 mm. The specimen comprised two HPC plates and one layer of insulation (Sundolitt Expanded Polystyrene or Kingspan Free Rigid Phenolic insulation). The thickness of the insulation was 290 mm. The top and bottom plate were casted using 110 MPa HPC directly against insulation boards with thickness of 30 mm. Shear connecting system was performed using BFRP or CFRP grid.

The grid is made of 100 % basalt or carbon continuous filament roving. The silane sizing was selected when making the fibers, which had component to ensure elasticity of the yarn during textile process. The grid was sized 25 by 25 mm with thickness of 0.9 mm and coated with styrene-acrylic resin, and afterwards shaped to look like a truss. The push-off tests were performed by placing each specimen in a horizontal position and pushing the bottom plate relative to the top plate in a specially designed steel frame (Figure 5.2). The specimens were supported horizontally along the top plate, while the bottom plate was placed on low friction cylindrical roller bearings to move freely with the applied load. The load was applied by a 25 kN hydraulic jack through a 30 mm steel plate to provide a uniform distribution of the load to the HPC plate in three cycles; preloading in elastic range, unloading and loading until failure was reached under displacement control (speed rate 5 mm/minute). The applied load was measured as well as the relative horizontal/vertical displacement between HPC plates at 7 locations. To compare the shear capacity, the different configurations (rib structure/connector type/insulation) were used, see Table 5.1.

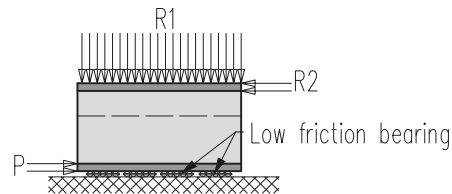


Figure 5.2. *Test setup for push off specimens.*

### 5.3.2 Flexural specimen details

The setup for all flexural specimens is shown in Figure 5.4a. 8 specimens were produced; the size of flexural specimen was 400 by 2000 mm with a total thickness of 350 mm. The panels were simply supported with a roller and pin configuration 110 mm from the ends, creating a span length of 1780 mm. The load was applied through a hydraulic actuator up to failure. The spreader beam made of two welded steel UPN profiles was used to distribute the load from the actuator to two 300 mm long steel bars. The bars pressed directly on the interior HPC plate and produced two line loads. The applied load was measured as well as vertical deflection at four locations.

## 5.4 Test instrumentation

### 5.4.1 Push-off test instrumentation

Two types of instrumentation were used to monitor the behaviour of each specimen. A 25 kN load cell measured the applied load, and 7 LVDT displacement transducers recorded the vertical and horizontal displacements of the HPC plates at various locations. The measurement was performed by placing the push-off specimen in a hori-

zontal position to the specially designed steel frame. The HPC plate with smooth surface corresponding to the exterior side was put on low friction cylindrical roller bearings to minimize friction between HPC plate and bearings. The top steel plate was lowered to the specimen and tied with 50 kN tie-down strap to eliminate vertical movements of the steel plate during testing. One LVDT was attached to the steel plate to monitor any unforeseen vertical movements. The measurement of horizontal displacements was determined by two LVDTs placed on the exterior HPC plate on one end and by one LVDT placed directly to the hydraulic jack. The vertical displacements were measured on the opposite side of each panel. Thin steel plates were fixed by two component epoxy glue at three locations to the specimens. Two LVDTs were attached on the left side to the thin steel plates connected to the interior HPC plate (Figure 5.3a). The last LVDT was placed on the thin steel plate as shown in Figure 5.3b.

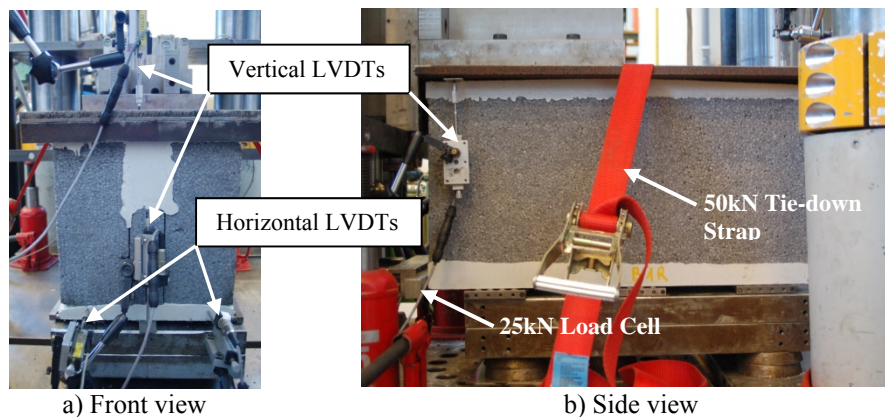


Figure 5.3. *Instrumentation for push-off specimens.*

#### 5.4.2 Flexural test instrumentation

A 100 kN load cell recorded the applied load throughout the flexural testing of the HPCSPs. The specimens were positioned to the setup with interior HPC plate on top in order to avoid local cracking under load points. 8 LVDT displacement transducers measured vertical deformations. The exterior HPC plate was instrumented with LVDTs placed at mid span, each of the two load points and supports.

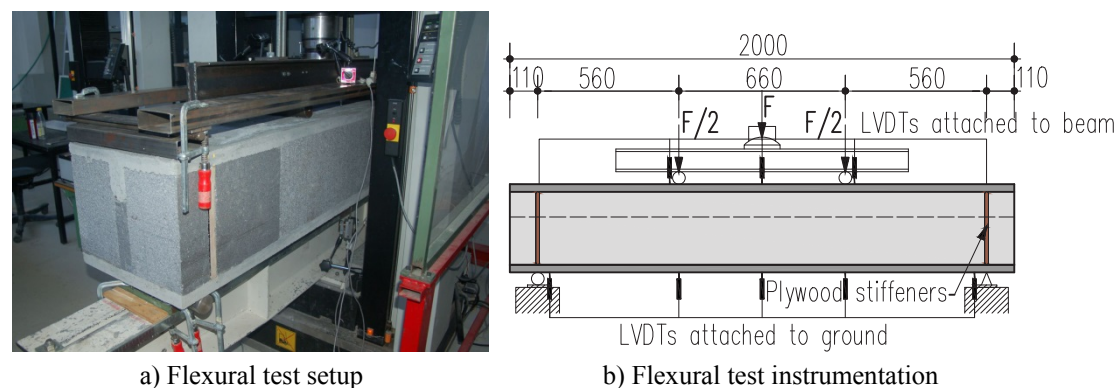


Figure 5.4. *Test setup for flexural specimens.*

The additional three LVDTs were attached to the interior HPC plate at mid span and each of the two load points as shown in Figure 5.4b.

## 5.5 Test results and failure modes

### 5.5.1 Push-off test results and failure modes

The push-off test results indicate that all testing configurations had an effect on the shear strength of the proposed shear transfer mechanism. Nevertheless, the specimens did not exhibit pure shear failure due to the moment created by the eccentricity of the applied load and the two HPC plates. Therefore, results obtained from push-off testing can only be used for verification of the FE model and then correct boundary conditions applied to simulate the real panel behaviour under pure shear loading. The 3-D linear elastic FE model was performed using commercial software Abaqus. The HPC plate and insulation was modelled as eight-node solid elements whereas FRP was modelled as two-node beam elements. The results for 14 specimens (each configuration was duplicated) tested in push-off test are shown in Table 5.1.

Table 5.1 *Push off test: Samples and results*

| Insulation Type                                  | Rib structure | Connector Type | Initial Shear Stiffness<br>[kN/mm] |
|--|---------------|----------------|------------------------------------|
| Sundolitt Expanded Polystyrene (EPS)             | No            | No             | 0.61                               |
|  | No            | BFRP grid      | 0.75                               |
|  | No            | CFRP grid      | 0.79                               |
|  | Yes           | BFRP grid      | 1.00                               |
|  | Yes           | CFRP grid      | 0.95                               |
| CFC/HCFC Kingspan Free Rigid Phenolic insulation | No            | No             | 0.77                               |
|  | Yes           | BFRP grid      | 0.95                               |

The HPCSPs made of CFC/HCFC Kingspan Free Rigid Phenolic insulation showed higher initial shear stiffness in comparison with those made with expanded polystyrene (EPS). Nevertheless, the panels with EPS reached higher ultimate shear strength. This difference in shear behaviour was caused by greater bond characteristic of EPS than CFC/HCFC Kingspan Free Rigid Phenolic insulation. The panels reinforced with BFRP grid reached similar initial shear stiffness as well as ultimate shear strength as the panels reinforced with CFRP grid. The configuration with CFC/HCFC Kingspan Free Rigid Phenolic insulation and BFRP led to a decrease of ultimate shear stiffness due to debonding between the insulation and HPC.

All push-off test specimens exhibited failure due to combination of debonding of insulation, rupture of tension cords in the BFRP and CFRP grid as well as buckling of the compression cords within the grid. In the case of CFC/HCFC Kingspan Free Rigid Phenolic insulation with BFRP and CFRP grid it was observed that grid was pulled out from HPC layer as depicted in Figure 5.5. All the specimens were shredded after testing; insulation layer was removed to the depth of BFRP and CFRP grid connectors. Furthermore, HPC faces were examined; it was observed that the specimens with



EPS insulation remained bonded, whereas the specimens with CFC/HCFC free rigid phenolic insulation showed clean HPC faces (Figure 5.6).

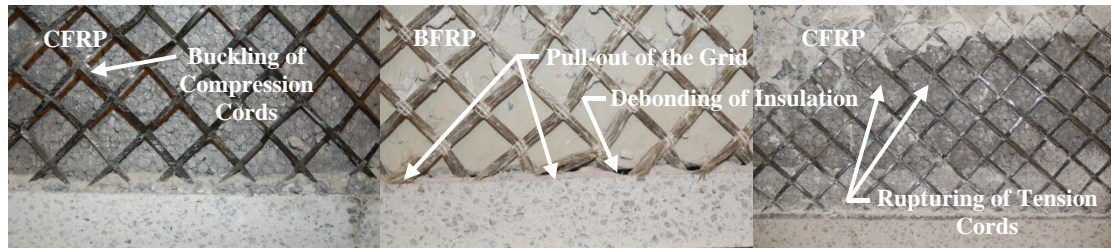


Figure 5.5. Typical failure modes of push-off test specimens.



Figure 5.6. Typical HPC faces of push-off test specimens after failure.

### 5.5.2 Flexural test results, modelling and failure modes

The testing of the first flexural specimen indicated that the panel did not provide meaningful results to examine the level of composite action which can be achieved by using BFRP and CFRP grid. It was observed that the insulation layer was compressed from 290 mm to almost 230 mm at supports and load points. Therefore, it was decided to adjust the remaining panels by placing 15 mm thick plywood to eliminate compression of insulation at supports. The load-deflection curve of the flexural specimens, compared to the theoretical one in case of full composite and non-composite action cross section is shown in Figure 5.7.

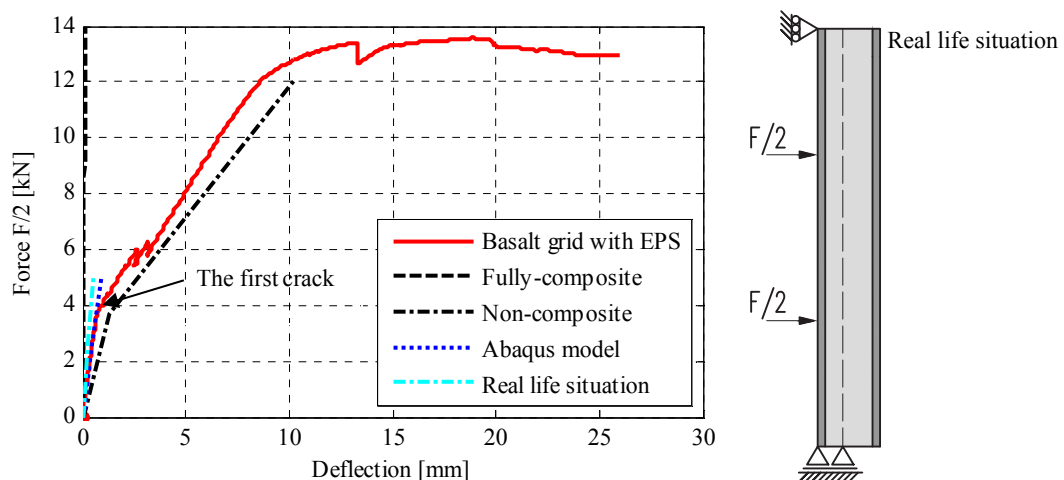


Figure 5.7. Typical load-deflection curve for flexural specimens.

When comparing the panels subjected to four-point bending with EPS insulation and BFRP grid, and the specimens with CFRP grid, the results showed no obvious difference in overall capacity. In general, the specimens with EPS insulation provided higher overall bending capacity in comparison with the CFC/HCFC Kingspan Free Rigid Phenolic insulation.

The observed flexural behaviour in comparison with the theoretical full composite and non-composite action indicated that the specimens behave only with partial composite action, i.e. 53 % composite action. The partial composite behaviour is caused by compression of insulation. Furthermore, buckling of FRP grid was observed within insulation layer, which prevented the panel from obtaining the expected composite action. Moreover, the shear slip between insulation layer and HPC plates was observed as a typical fracture mode, often experienced with a partial composite action. The obtained composite level is not representative of the expected composite behaviour. The used boundary conditions were different than in the HPCSPs mounted at the building site. In general, only the interior plate is constrained and the exterior is free to move. Therefore, the results obtained from flexural testing can only be used for verification of the FE model and then correct boundary conditions applied to simulate the real panel behaviour.

## 5.6 Conclusions

### 5.6.1 Push-off test

The HPCSPs made of CFC/HCFC Kingspan Free Rigid Phenolic insulation showed higher initial shear stiffness in comparison with those made with expanded polystyrene (EPS). Nevertheless, the panels with EPS reached higher ultimate shear strength likely due to higher bond capacity. The panels reinforced with BFRP grid reached similar initial shear stiffness as well ultimate shear strength as the panels reinforced with CFRP grid.

### 5.6.2 Flexural test

The results of the panels subjected to four-point bending showed no obvious difference in the overall capacity between the specimens with EPS insulation and BFRP grid, and the specimens with CFRP grid. In general, the specimens with EPS insulation provided a higher overall bending capacity in comparison with the CFC/HCFC Kingspan Free Rigid Phenolic insulation. The observed flexural behaviour in comparison with the theoretical composite and non-composite action indicated that the specimens behave only with partial composite action i.e. 53 % composite action. The partial composite behaviour is caused by a combination of buckling of FRP grid, compression of insulation and shear slip between insulation layer and HPC plates.

### 5.6.3 Numerical modelling

Numerical investigations were based on 3-D linear elastic finite element analysis using commercial software Abaqus. Results from the numerical investigations were compared with experimental results of small and semi-scale specimens for the validation of the design procedure. A good correlation was observed between the results in the linear elastic range.

Experimental and numerical results based on finite element modelling showed that the developed panel system meets the objectives of the research and is expected to have promising future.

## Chapter 6

### Journal paper 2

Title: Experimental and Numerical Investigation of FRP Shear Mechanism for Concrete Sandwich Panels

Authors: Kamil Hodicky, Gautam Sopal, Sami Rizkalla, Thomas Hulin and Henrik Stang

Published in: ASCE Journal of Composites for Construction, 2014.

## Abstract

This paper investigates the composite action of 46 segments representing precast concrete sandwich panels (PCSPs) using a fiber-reinforced polymer [FRP; specifically, a carbon fiber-reinforced polymer (CFRP)] grid/rigid foam as a shear mechanism. The experimental aspect of the research reported in this paper examined the effect of various parameters believed to affect the shear flow strength for this CFRP grid/foam system. The parameters that were considered are the spacing between vertical lines of CFRP grids and the thickness of the rigid foam. Results of the experimental aspect of the research reported in this paper indicated that increasing the spacing between vertical lines of CFRP grid increase the overall shear flow strengths due to the increase of the bonded contact area of the rigid foam to the concrete surface. However, the overall shear stresses were decreased due to the increase of this interface surface area. Test results also indicated that increasing the rigid foam thickness decreases the overall shear flow strength when compared with the same quantity of CFRP grid spacing. A nonlinear three-dimensional (3D) FEM analysis was performed to model the behaviour of the tested segments and to study the behaviour of PCSPs. Results of FEM analysis were in good agreement with the experimental results. A design equation was developed to determine the shear flow strengths for the given CFRP grid/foam systems. The parametric study of the research reported in this paper was performed to predict shear flow strength of different FRP materials, rigid foam thickness, and spacing between vertical lines of the grid.

## 6.1 Introduction

Precast concrete sandwich panels (PCSPs) are typically used as exterior walls for multiunit residential, commercial, and warehouse buildings. A typical PCSP consists of two concrete wythes and one layer of insulation in between the two concrete wythes. Typically, connectors penetrate the insulation layer and join the two concrete wythes. The panels are designed to carry gravity loads from floors or roofs, as well as to resist lateral loads caused by wind. The rigid foam is provided to insulate the structure; therefore, PCSPs are structurally and thermally efficient. Typical PCSPs are fabricated with heights up to 13.7 m and with widths up to 4.0 m (Einea et al., 1991). The concrete wythe thickness ranges from 50 to 150 mm, with overall panel thicknesses ranging from 125 to 300 mm (PCI Committee on Precast Sandwich Wall Panels, 2011). The PCSPs have several beneficial features such as (1) high quality in comparison to onsite made concrete elements, (2) proven durability, (3) fast erection, and (4) attractive architectural appearance (Einea et al., 1994). The PCSP may be designed with various degrees of composite action, as follows: (1) noncomposite, (2) partially composite, or (3) fully composite (Rizkalla et al., 2009). Composite action is achieved when the shear forces that are developed at the face of one wythe are trans-

ferred to the other wythe through the shear connectors. This allows both wythes to work together to resist the applied forces as a single section. Providing a composite action can significantly increase the structural efficiency and reduce both initial and lifecycle costs of these types of panels (Einea et al., 1994). The degree of composite action depends on the nature of the connection between two concrete wythes. Precast concrete sandwich panels were first introduced during the 1960s as double tee sandwich panels. Solid concrete zones were used between the double tees to develop full composite action. Double tee sandwich panels provided a robust structural wall but sacrificed the potential thermal savings. In order to reduce the concrete material, optimize the structural performance, and reduce overall cost, flat concrete slabs were soon used in place of double tees. More recently, steel ties connecting the two concrete wythes were introduced to replace solid concrete zones in an attempt to enhance the thermal performance of the PCSP. The use of steel ties improved the thermal efficiency in comparison to solid concrete zones (Glech, 2007). Increasing the degree of composite action may lead to lower thermal efficiency of the panel due to the creation of thermal bridges (Wade et al., 1988). Furthermore, undesirable thermal bowing may occur due to different temperatures between interior and exterior surfaces. The thermal deflections in long PCSPs can be significant and may cause cracking due to southern exposure, especially at building corners. Noncomposite panels were introduced in the 1980s and aimed to address the thermal deficiencies created by the steel ties. Noncomposite panels contained minimal shear connectors required for handling loads only; however, a lack of shear transfer compromised the structural integrity of the system. Recent tests by Lee & Pessiki (2008) showed that a panel with staggered solid concrete zones exhibited similar behavior to a fully composite panel. The bond between the insulation and concrete wythes provides some shear transfer (Bush Jr. & Stine, 1994; Bush Jr. & Wu, 1998; Pessiki & Mlynarczyk, 2003); however, the bond diminishes over time and will not provide full strength over the service life of the panel (Salmon et al., 1997). Recently, the PCSP design concept has leaped forward by introducing fiber-reinforced polymer (FRP) shear reinforcement. Fiber-reinforced polymers have a relatively high strength and stiffness combined with a relatively low thermal conductivity, compared to steel (Soriano & Rizkalla, 2013). Wade et al. (1988) and Einea et al. (1994) performed the first attempt to use glass fiber-reinforced polymer (GFRP) connectors for insulated concrete sandwich walls. Salmon et al. (1997) introduced GFRP bars formed in a truss orientation in place of metal wire trusses. The experimental investigation showed that the use of GFRP resulted in 84 % composite action compared to 88 % for steel truss connectors. In accordance with the same concept, Maximos et al. (2007), Lameiras et al., (2013a, 2013b), Naito et al. (2012), Morcous et al. (2010) and Woltman et al. (2013) studied different shapes of GFRC shear connectors to obtain the full composite action. These research programs have indicated that FRP shear connectors can provide a dual purpose of improving the thermal capabilities of a building envelope, while at the same time providing the desired structural integrity and efficiency. Most recently, Bunn (2011), Frankl et al.

(2008, 2011), Hassan & Rizkalla (2010), Rizkalla et al. (2009) and Sopal (2013) investigated the use of a carbon fiber-reinforced polymer (CFRP), and Hodicky et al. (2013) investigated the use of a basalt fiber-reinforced polymer (BFRP) material configured as a grid. The grid was placed in composite action with rigid foam insulation to serve as the main shear transfer mechanism for PCSP. The desired composite action can be achieved using either expanded polystyrene (EPS) or extruded polystyrene (XPS) rigid foam insulation in combination with a CFRP grid. Since carbon and basalt fibers have a thermal conductivity approximately 14 % that of steel, connecting concrete wythes with the grid allows a panel to develop composite structural action with minimum thermal bridges, therefore maintaining the insulating value of the panel. Several researchers have attempted to develop numerical models to simulate the behaviour of PCSP under axial, shear, and flexural loading (Benayoune et al., 2007, 2006, 2008; Gara et al., 2012; Hodicky et al., 2013; Mackerle, 2002; Metelli et al., 2011; Sopal, 2013). The behavior of PCSP is rather complicated due to the highly nonlinear behavior of the constituent materials and the interaction of the FRP grid and the rigid foam. Some researchers simplified their models by using linear material models and linear elastic analysis (Einea et al., 1994; Hassan & Rizkalla, 2010). Most of the other researchers approached the problem using nonlinear two-dimensional (2D; Gara et al. 2012; Benayoune et al. 2006, 2007) or three-dimensional (3D; Lameiras et al. 2013b; Sopal 2013; Hodicky et al. 2013; Benayoune et al. 2008) models. However, 2D and 3D modeling approaches significantly simplify the behaviour of PCSP. Some researchers disregarded the insulation layer from their FEM analysis (Salmon et al. 1997; Benayoune et al. 2006, 2007, 2008). Additionally, some researchers ignored the relative slip between the concrete and reinforcement/shear connector (Mackerle 2002; Benayoune et al. 2006, 2007, 2008; Hassan and Rizkalla 2010; Metelli et al. 2011; Gara et al. 2012; Sopal 2013), the effect of bond slip and dowel action, and the slip of steel reinforcement (Benayoune et al. 2006, 2007, 2008). With these assumptions, the numerical analysis resulted in an overestimation of the PCSP behaviour in comparison to experimental data (Salmon et al. 1997; Benayoune et al. 2006, 2007, 2008; Gara et al. 2012; Sopal 2013). It was reported by several researchers (Frankl et al. 2008, 2011; Hassan and Rizkalla 2010; Bunn 2011; Sopal 2013) that the rigid foam has a significant contribution to the shear transfer mechanism and it is essential to include its effect in the prediction of the behaviour of PCSP.

This paper presents an experimental and numerical investigation of small segments representing a typical PCSP (as shown in Figure 6.1), using the CFRP grid/rigid foam as a shear mechanism to achieve the composite action of the panel. The research reported in this paper investigated the effect of several parameters believed to affect the shear flow strength of the CFRP grid/rigid foam shear connection. The parameters that were considered are the spacing between vertical lines of CFRP grids and the thickness of the rigid foam. A comprehensive experimental program was conducted to determine the characteristics of the shear transfer mechanism of the CFRP grid/rigid

foam. Test results were used to develop an equation to estimate the shear flow strength using the CFRP grid/rigid foam as affected by these parameters. A nonlinear 3D FEM analysis was performed to model the behaviour of the test specimens and to study the behaviour of PCSP.

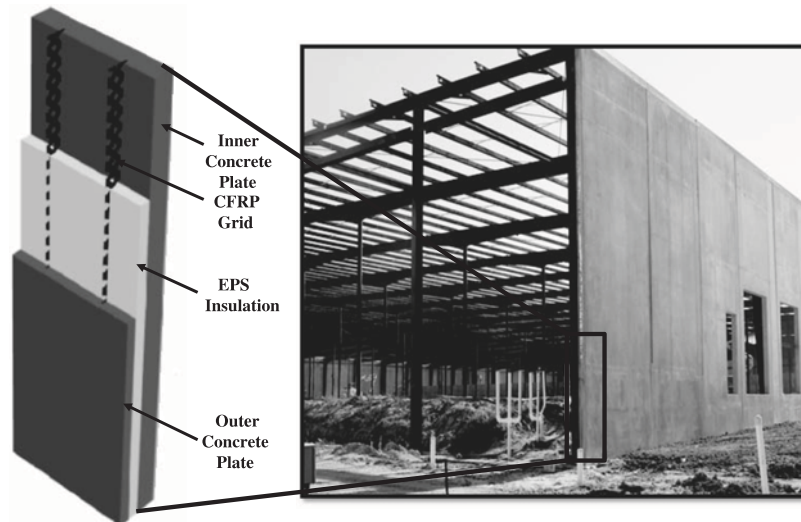


Figure 6.1. *Field application of typical wall panel.*

## 6.2 Experimental investigation

A total of 46 panel specimens were tested in push-through configuration to examine various parameters relevant to the behavior and strength of the CFRP grid/rigid foam shear transfer mechanism.

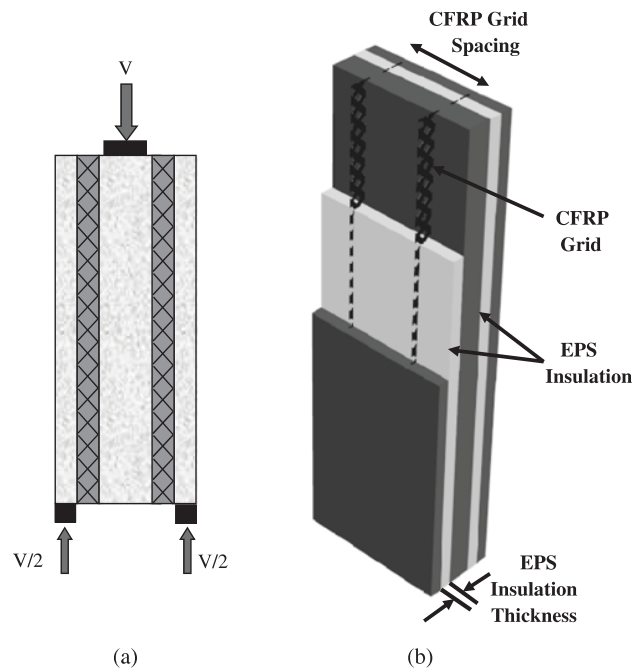


Figure 6.2. *(a) Typical specimen tested in double shear; (b) cut away of typical CFRP grid push test specimen.*



All panels built for the research reported in this paper were 1830 mm high, while the width of panels ranged from 610 - 2440 mm to accommodate the required spacing of vertical lines of the CFRP grid. All specimens were configured with three concrete wythes (50 mm outer wythes and a 100 mm center wythe) and two EPS insulation layers as shown in the cut-away rendering in Figure 6.2.

### 6.2.1 Material properties

The subsequent sections provide brief description of the material properties of the three materials used to construct the panels.

#### 6.2.1.1 Concrete

All test specimens were constructed using self-consolidating concrete (SCC). Concrete cylinders were produced at the time of casting and were stored and transported with the panels. Compression tests were conducted on 100 × 200 mm diameter concrete cylinders in accordance with ASTM C39 [ASTM C39/C39M-14 (ASTM, 2014a)], confined with neoprene caps and loaded in a universal compression testing machine. The tensile strength and modulus of elasticity were determined in accordance with ASTM C496 [ASTM C496/C496M-11 (ASTM, 2011)] and ASTM C469 [ASTM C469/C469M-14 (ASTM, 2014b)], respectively. Typical test results for the compressive concrete strength  $f_{co}$ , tensile strength of concrete  $f_t$ , and concrete modulus of elasticity  $E_c$  are given in Table 6.1.

Table 6.1 *Mechanical properties of concrete*

| Concrete | $f_{co}$ - SD [MPa] | $f_t$ - SD [MPa] | $E_c$ - SD [MPa] | Number of specimens |
|----------|---------------------|------------------|------------------|---------------------|
| SCC      | 41.4 - 4.3          | 2.4 - 0.28       | 35 000 - 3 585   | 10                  |

#### 6.2.1.2 Rigid foam

Lightweight EPS insulation was used as the rigid foam insulation material due to its cost-efficiency and availability. The polystyrene sheet was cut into pieces and inserted between the inner and the outer concrete wythes, and between the CFRP grids. Small segment of EPS insulation were tested in shear and compression. The average mechanical properties of three specimens for the rigid foam thicknesses 50 mm (EPS.2), 100 mm (EPS.4), and 150 mm (EPS.6) are summarized in Table 6.2. In Table 6.2,  $f_{cf}$ ,  $E_{rf}$  and  $G_{rf}$  are the compression strength, modulus of elasticity, and shear modulus of the EPS rigid foam, respectively.

Table 6.2 *Mechanical properties of EPS foam*

| Test Designation | Thickness [mm] | Width [mm] | Height [mm] | $f_{cf}$ - SD [kPa] | $E_{rf}$ - SD [MPa] | $G_{rf}$ - SD [MPa] | Number of specimens |
|------------------|----------------|------------|-------------|---------------------|---------------------|---------------------|---------------------|
| EPS.2            | 50             | 50         | 100         | 47 - 4              | 3.67 - 0.2          | 1.91 - 0.2          | 3                   |
| EPS.4            | 100            | 100        | 200         | 45 - 3              | 3.23 - 0.3          | 1.88 - 0.1          | 3                   |
| EPS.6            | 150            | 150        | 300         | 44 - 4              | 3.20 - 0.3          | 1.87 - 0.2          | 3                   |

### 6.2.1.3 Carbon fiber-reinforced polymer grid

The reinforcement selected for the experimental aspect of the research reported in this paper was composed of pultruded carbon fibers. A patented CFRP grid was custom-engineered in rolled forms of an orthogonal grid. The thickness of strand was 0.9 mm and average spacing between individual strands was 40 mm. The roll of the CFRP grid was then cut at 45° of an orthogonal grid to produce truss with 45° members and facilitate shear transfer between the concrete wythes, as shown in Figure 6.3.

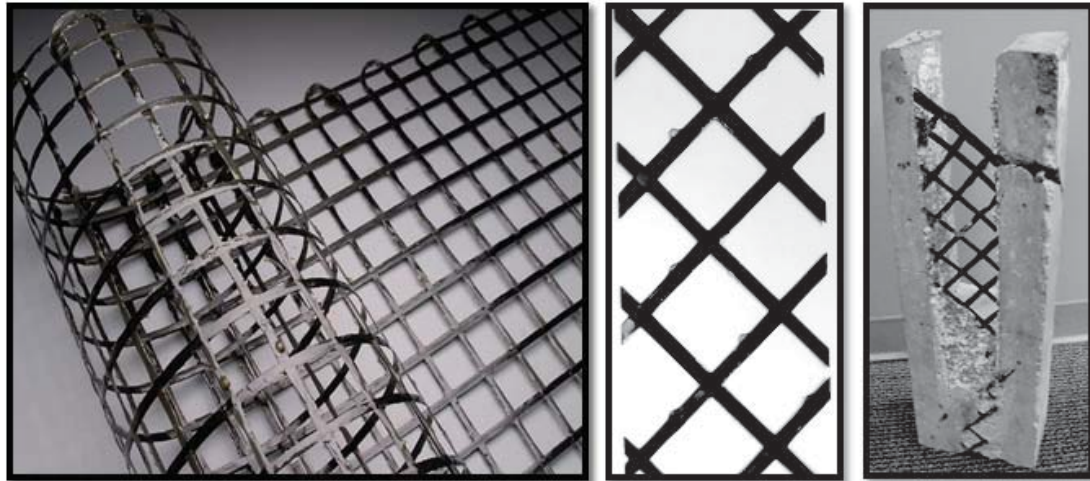


Figure 6.3. *Typical CFRP grid reinforcement as shear connectors.* (reprinted from Sopal, 2013)

Figure 6.3 shows also a piece cut from PCSP tested to failure from Sopal (2013). To determine the ultimate tensile strength and tensile modulus of elasticity, tests were conducted in accordance with ASTM D3039 [ASTM D3039D3039M-14 (ASTM, 2014c)] on individual strands of CFRP grid cut from a roll of sample material. Prior to testing, aluminum tabs were bonded to both ends of the CFRP grid test strand to grip the strand by a universal testing machine. The average mechanical properties including tensile strength  $f_{t,CFRP}$ , modulus of elasticity  $E_{CFRP}$ , and the strain at failure for the CFRP grid are given in Table 6.3.

Table 6.3 *Mechanical properties of CFRP grid*

| Textile material | $f_{t,CFRP}$ - SD [MPa] | $E_{CFRP}$ - SD [MPa] | Strain at failure - SD [%] | Number of specimens |
|------------------|-------------------------|-----------------------|----------------------------|---------------------|
| CFRP             | 1760 - 52               | 234 000 - 1300        | 0.76 - 0.02                | 180                 |

### 6.2.2 Panel configurations

Three different panel configurations were considered, as follows: (1) panels without a CFRP grid, (2) panels with a CFRP grid, and (3) panels with a CFRP grid and debonded EPS insulation. Configurations of the various panels considered in the research reported in this paper are described in detail in the subsequent subsections.

### 6.2.2.1 Panels without CFRP grid

The two panel configurations were tested without any CFRP grid to examine the shear flow contribution from the EPS insulation without a CFRP grid. Details of the dimensions and foam thicknesses for the panels without CFRP grid are given in Table 6.4. Two panels were tested for each configuration.

Table 6.4 *Panels without CFRP grid*

| Test Specimen<br>Designation | EPS Thickness<br>[mm] | Panel Height<br>[mm] | Panel Width<br>[mm] |
|------------------------------|-----------------------|----------------------|---------------------|
| 24.EPS.NONE.2                | 50                    | 1830                 | 610                 |
| 48.EPS.NONE.2                | 50                    | 1830                 | 1220                |
| 24.EPS.NONE.4                | 100                   | 1830                 | 610                 |
| 48.EPS.NONE.4                | 100                   | 1830                 | 1220                |
| 24.EPS.NONE.6                | 150                   | 1830                 | 610                 |
| 48.EPS.NONE.6                | 150                   | 1830                 | 1220                |

### 6.2.2.2 Panels with CFRP grid

Table 6.5 provides details of the 30 panels tested with a typical vertical grid. The effects of the type of rigid foam insulation, the thickness of the insulation, and the spacing between vertical rows of the CFRP grid were examined.

Table 6.5 *Panels with CFRP grid*

| Test Specimen<br>Designation | EPS Thickness<br>[mm] | CFRP grid spacing<br>[mm] | Panel Height<br>[mm] | Panel Width<br>[mm] | Number<br>of specimens |
|------------------------------|-----------------------|---------------------------|----------------------|---------------------|------------------------|
| 24.EPS.12.2                  | 50                    | 305                       | 1830                 | 610                 | 2                      |
| 48.EPS.24.2                  | 50                    | 610                       | 1830                 | 1220                | 2                      |
| 96.EPS.48.2                  | 50                    | 1220                      | 1830                 | 2440                | 5                      |
| 24.EPS.12.4                  | 100                   | 305                       | 1830                 | 610                 | 2                      |
| 48.EPS.24.4                  | 100                   | 610                       | 1830                 | 1220                | 5                      |
| 96.EPS.48.4                  | 100                   | 1220                      | 1830                 | 2440                | 5                      |
| 24.EPS.12.6                  | 150                   | 305                       | 1830                 | 610                 | 2                      |
| 48.EPS.24.6                  | 150                   | 610                       | 1830                 | 1220                | 2                      |
| 96.EPS.48.6                  | 150                   | 1220                      | 1830                 | 2440                | 5                      |

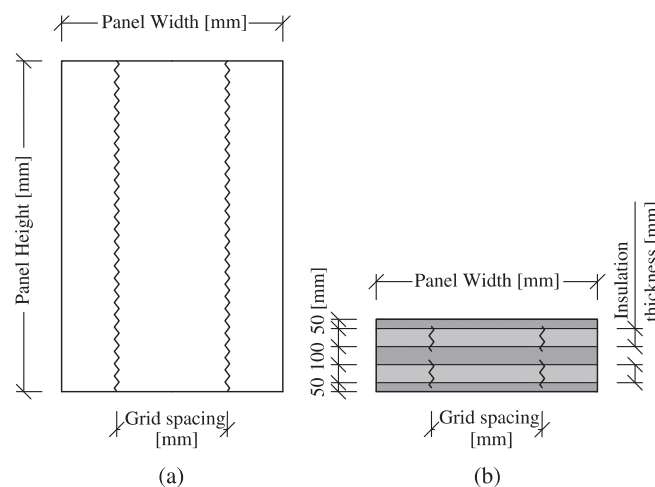


Figure 6.4. *Typical panel with CFRP grid: (a) elevation; (b) top view.*

A typical specimen with a CFRP grid is shown schematically in Figure 6.4.

### 6.2.2.3 De-bonded panels

Table 6.6 presents the panels that were tested to examine the effect of the bond between concrete and the EPS insulation, on the shear strength and behaviour. Two specimens of each type were tested for a total of four specimens. All specimens were fabricated in the same manner as the panels with a CFRP grid, except the bond between concrete and insulation was intentionally broken.

Table 6.6 *Tests of de-bonded panels*

| Test Specimen Designation | EPS Thickness [mm] | CFRP grid spacing [mm] | Panel Height [mm] | Panel Width [mm] |
|---------------------------|--------------------|------------------------|-------------------|------------------|
| 48.EPS.24.2               | 50                 | 610                    | 1830              | 1220             |
| 48.EPS.24.4               | 100                | 610                    | 1830              | 1220             |

This was achieved by using two layers of thin plastic placed between each insulation surface and the fresh concrete, as shown in Figure 6.5.

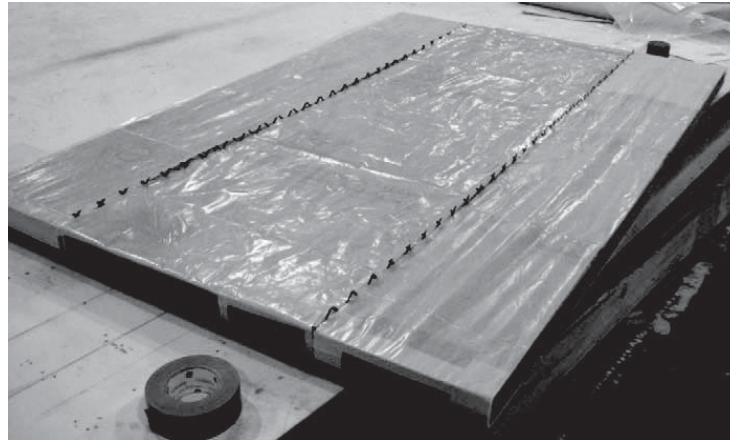


Figure 6.5. *Insulation for debonded panels with plastic layers prior to casting.*

### 6.2.3 Fabrication of the panels

All test specimens were constructed by local precast concrete producers. All EPS insulation layers were cut into three sections according to the spacing of vertical lines of the CFRP grid. The precut CFRP grid in truss configuration was then locally glued to the outer two sections of EPS using insulation board adhesive to ensure a 20 mm embedment depth of the CFRP grid into the concrete wythes. All panels were fabricated horizontally. More details about the fabrication of the panels can be found in Sopal (2013).

### 6.2.4 Test setup

Each specimen was tested in a push-through configuration, with the bottom surfaces of the outer two concrete wythes supported vertically, leaving a 50 mm gap under the middle concrete wythe to allow for vertical deflection. The push-out test has been

used by a several researchers for similar purposes (Bunn, 2011; Gara et al., 2012a; Naito et al., 2012; Woltman et al., 2013). Load was applied vertically to the top surface of the middle concrete wythe to test panels in a double shear configuration, in turn to minimize the effect of moment due to the eccentric location of the applied shear. The typical push test setup used for testing all specimens is shown in Figure 6.6. The three-wythe panels were supported vertically at the bottom edge of the two outer concrete wythes by a  $50 \times 50$  mm steel bar stock. Load was uniformly distributed to the top surface of the center concrete wythe using 600 kN hydraulic jacks and square hollow structural steel (HSS) tubes, forcing the middle wythe downwards with respect to the two outer concrete wythes. The load rate used was 1.2 mm/min.

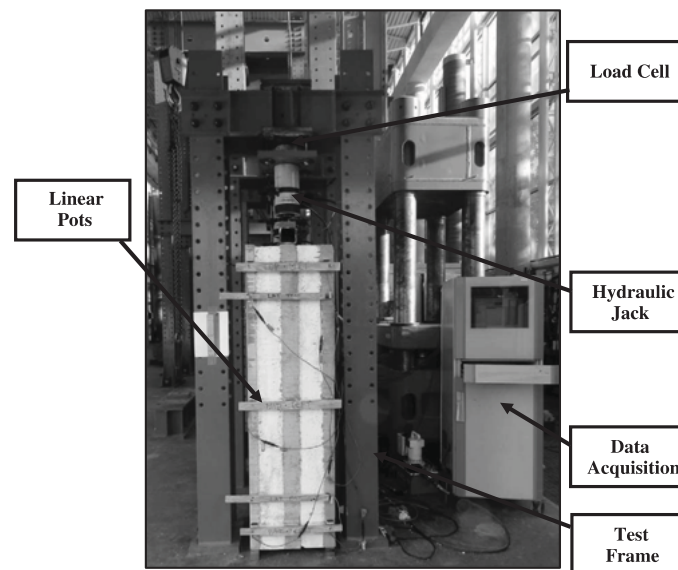


Figure 6.6. *Test setup.*

### 6.2.5 Test instrumentation

The applied load was measured until failure. The relative vertical and horizontal deflection between the concrete wythes were measured by 10 linear potentiometers at selected locations. All instruments were connected to an electronic data acquisition system. Data was recorded continuously at a sample rate of 1 Hz during loading. Measurements were taken by fixing a support block to the center concrete wythe and extending a bar to both outer concrete wythes. Two linear potentiometers were attached to the bar, one on each end. The opposite ends of these potentiometers rested on blocks fixed to the outer concrete wythe. Relative vertical displacements between the inner and outer concrete wythes were monitored on the left side of each panel at 75 mm below the top, 75 mm above the bottom, and at the midheight, as shown in Figure 6.6. The relative vertical displacement was also measured at the midheight on the right side of each panel. Left and right sides were determined while looking at the smooth concrete wythe that was cast down on the casting bed. Two linear potentiometers were also added on the left side of the specimens, as follows: (1) one 225 mm below the top, and (2) another 225 mm above the bottom. These additional potentiometers

ters were included to measure the relative horizontal deflection between the outer concrete wythes.

### 6.3 Finite element analysis

A 3D nonlinear macro-scale finite-element (FE) model of sandwich panels was developed to further investigate its structural behavior under shear stress. The model was developed using the finite element analysis software DIANA version 9.4.4 with pre-processor and postprocessor FX+ (TNO DIANA, 2011). The mesh size was adopted to provide satisfactory convergence. The nonlinear solution was based on the Newton-Raphson procedure. The subsequent subsections present various elements utilized to model the different materials used in typical push-out test specimen simulating the behaviour of PCSP.

#### 6.3.1 Concrete - element and constitutive relationships

The three concrete wythes were modeled using eight-node elements (HX24L). The standard size of the element was  $10 \times 10 \times 10$  mm with adaptive remeshing around CFRP grid connections. Multilinear isotropic material input was used to approximate the nonlinear constitutive relationship for concrete in compression. The multilinear diagram fully describes the relationship between the compressive stress and the equivalent strain. Brittle tension softening model was included to define concrete behaviour in tension as shown in Figure 6.7.

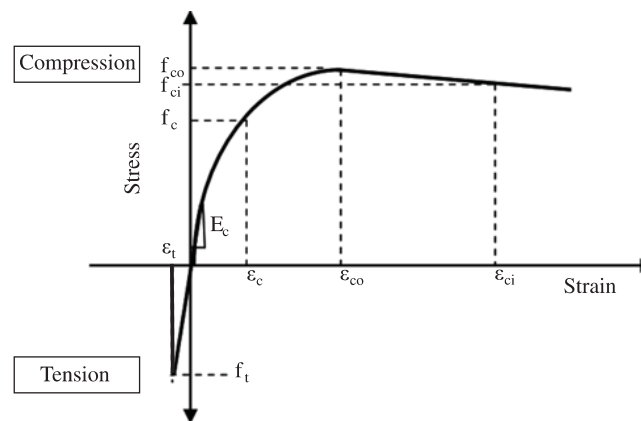


Figure 6.7. *Multilinear stress-strain constitutive model of concrete.*

#### 6.3.2 Rigid Foam - element and constitutive relationships

The two layers of rigid foam were modeled using the same eight node elements used for concrete (HX24L). The standard size of the element was  $10 \times 10 \times 10$  mm. To model the behaviour of rigid foam material in shear, the stress-strain parameters were input in DIANA version 9.4.4 using a multilinear isotropic material model based on values obtained by the experimental programs of Bunn (2011) and Soriano & Rizkalla (2013).



### 6.3.3 CFRP Grid - element and constitutive relationships

Material properties of individual strands of CFRP grid connectors tested in tension were reported in the Material Properties section. Test results indicated linear elastic behavior before rupture of the single strands of CFRP grid. The overall response of CFRP grid has not been straightforward when used as connectors between concrete wythes, as compared to the response from a single strand in a tension test. This is partially due to complex nature of CFRP grid geometry. As the fibers are subjected to tension and compression, they are also clamped against the concrete, resulting in shearing of individual strands at lower strengths as compared to the observed ultimate tensile strengths measured by the tension tests. To capture this complex behaviour, some panels were specially designed and tested in pure tension and axial compression to evaluate CFRP grid response (Bunn, 2011). The individual strands of CFRP grid connecting three concrete wythes were modeled with a fournode, three-side isoparametric solid pyramid elements (TE12L), considering the intermediate joints. The complex behavior of CFRP grid was modeled through the input parameters of stress-strain curves representing compression and tension behaviour as shown in Figure 6.8. The three curves are for 50, 100, and 150 mm thick rigid foam used for these specially designed segments.

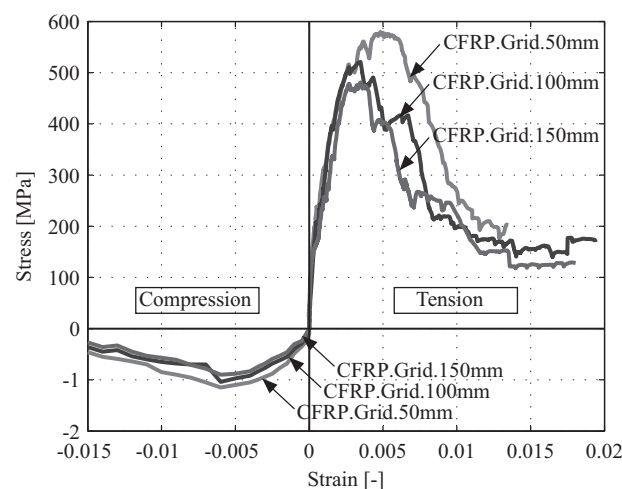


Figure 6.8. *Behavior of CFRP grid within rigid foam subjected to pure tension and compression tests.*

### 6.3.4 Rigid foam/concrete interface

Bond strength between foam and concrete interfaces was modeled using contact elements. Four interfaces between the foam and the concrete were modeled using 3D interface elements (Q24IF). The purpose of these contact pairs was to account for shear sliding and separation that could occur along the interface of solid elements. The shear strength of the interface was extracted from experimental results of panels without CFRP grid. The measured shear force from these results was translated into a shear stress-displacement relationship

$$\tau = \frac{P}{b \cdot h} \quad (6.1)$$

where  $\tau$  = shear stress;  $P$  = load from push-out tests; and  $b$  and  $h$  = width and height of the panel, respectively. Shear stress-displacement relationship inputs used to model rigid foam/concrete interfaces are shown in Figure 6.9.

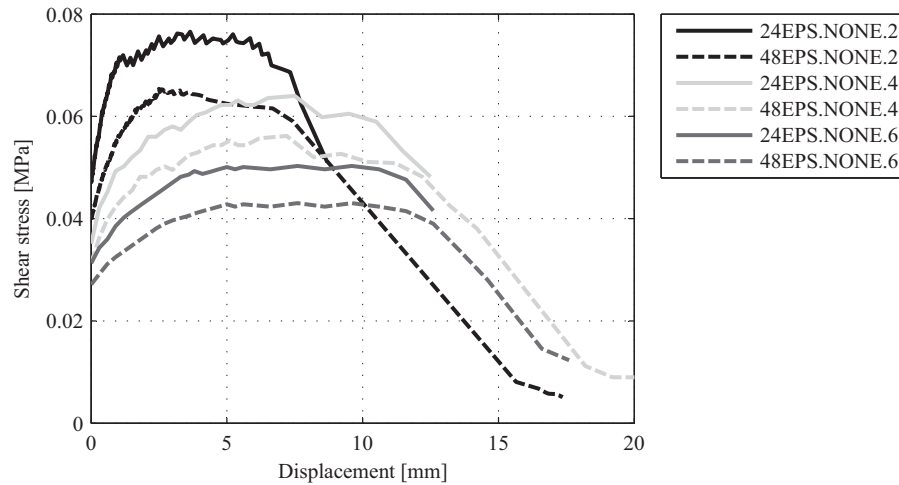


Figure 6.9. *Rigid foam/concrete interface constitutive relationships.*

### 6.3.5 CFRP grid/concrete interface

The bond-slip relationship between the CFRP grid and concrete was also incorporated in the model to simulate the bond. This data is typically obtained by means of pull-out tests; however, it was not included in the experimental aspect of the research reported in this paper. A bond-slip relationship for a similar combination of CFRP grid obtained from Schladitz et al. (2012) was thus included in the model. The CFRP grid/concrete interface was modeled using a 3D interface element (T18IF). The detail of the connection between CFRP grid and concrete is shown in Figure 6.10, where  $\tau_i$  denotes interface shear stresses.

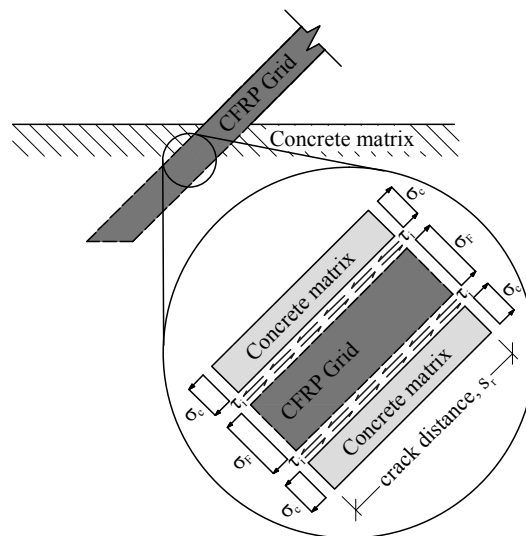


Figure 6.10. *Connection CFRP grid to concrete.*



The bond-slip relationship is defined according to a multilinear model in DIANA version 9.4.4 and is depicted in Figure 6.11.

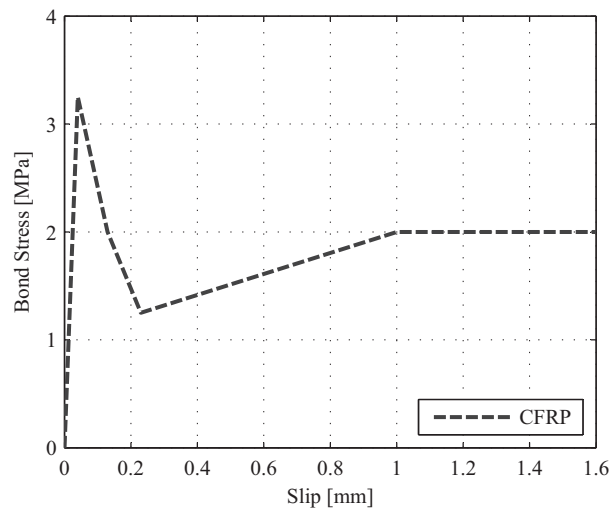


Figure 6.11. *Bond-slip relationship for CFRP grid/concrete interface.*

### 6.3.6 Loading and boundary conditions

The symmetry of the mounting and loading of the tested specimens allowed for only one-fourth of the panel to be considered in the FE model. The bottoms of the outer wythes were restrained against vertical and horizontal movements. Rotation was allowed in all direction to simulate rigid body rotation of the outer wythes and to avoid any moments at the support. Loading until failure was applied uniformly to the center concrete wythe by means of displacement control, such that an imposed displacement was applied at the location of loading. The displacement was increased in small increments up to a desired level and then the analysis was terminated.

## 6.4 Results and Discussion

Test result for each specimen is given by a single curve based on the average relative vertical deflections measured from eight instruments. The variation in the eight instruments was negligible. A total of two or five curves are obtained for tested specimens in a group. The results of the FE analysis were compared with the results of the experimental aspect of the research reported in this paper to determine the effectiveness of the analysis to simulate the panel behaviour. Furthermore, test results are summarized in various subsections to compare the behaviour and to discuss the effects of selected parameters.

### 6.4.1 Failure modes - all panels

Typical failure modes observed during testing of concrete wall panels are shown in Figure 6.12. Inspection of the specimens after testing revealed that foam failed with shear cracking and/or shear sliding. After testing, several panels were cut along a line

50 mm away from the vertical strip of CFRP grid. The foam layer was then mechanically removed along the cut to expose the CFRP grid over the height of the panel.

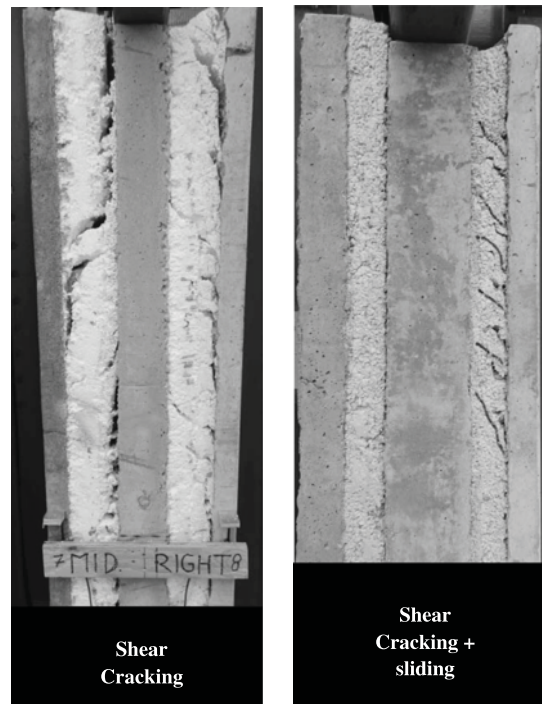


Figure 6.12. *Typical failure modes of the tested panels.*

All panels exhibited rupturing of the CFRP grid in tension and buckling of the CFRP grid in compression, as shown in Figure 6.13. Several panels also showed signs of CFRP grid pull-out from the concrete as a result of insufficient embedment depth, i.e., less than 20 mm. Some parts of EPS foam remained well bonded to the concrete after they were pulled apart.

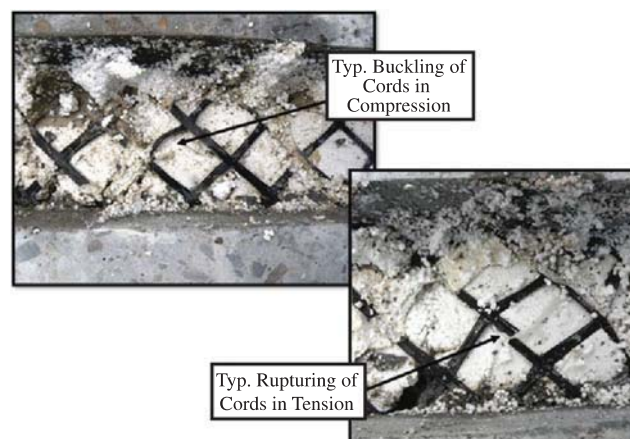


Figure 6.13. *Typical failure modes of CFRP grid.*

#### 6.4.2 Panels without CFRP grid

Results of the analysis using the DIANA version 9.4.4 FE program were postprocessed to obtain load-displacement curves and are compared with measured values for the panels with 50 mm EPS insulation in Figure 6.14. Comparisons with the experi-

mental results indicated that the overall behaviour of the rigid foam materials is well-predicted by the multilinear isotropic material model in combination with a shear stress-displacement relationship at the concrete/rigid foam interface.

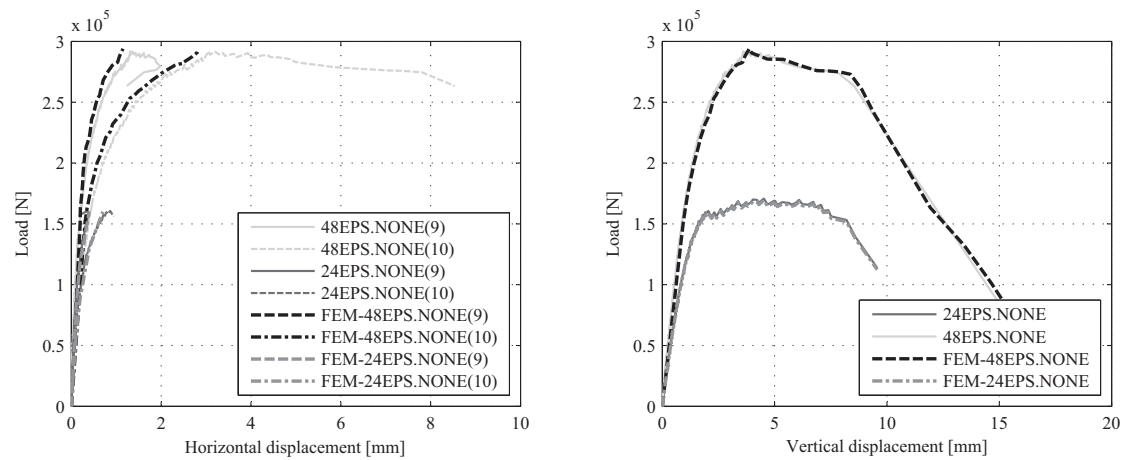
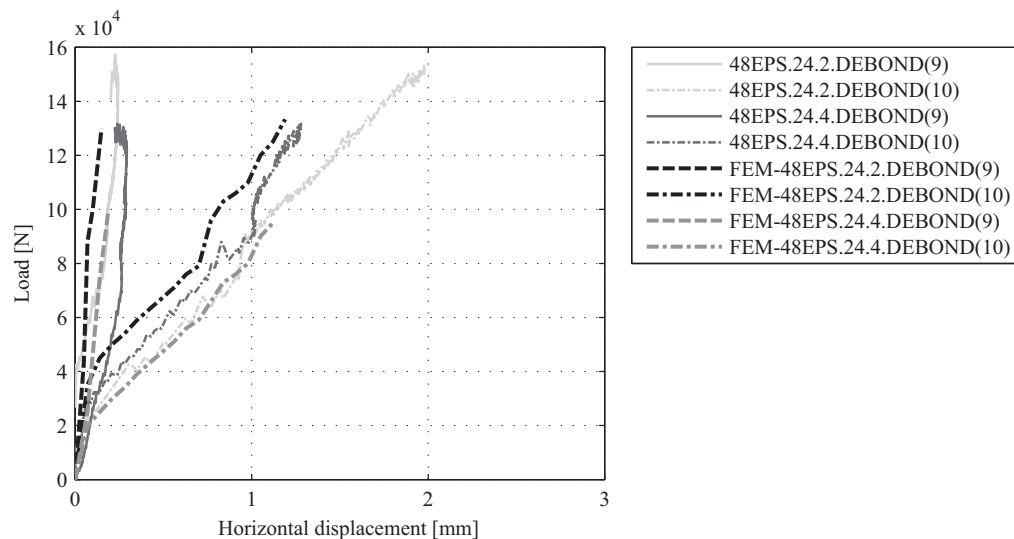


Figure 6.14. *Comparison of experimental and numerical results for panels without CFRP grid.*

### 6.4.3 Debonded panels

Comparisons of experimental and numerical results for debonded panels are shown in Figure 6.15. The FE analysis showed reasonable agreement with the measured values for the initial phase of the load-deflection curves. However, the accuracy of the ultimate strength prediction for the FE model shows a considerable amount of variation. This difference is attributed to the fact that the FE model assumed no interaction between the concrete and rigid foam. Despite using two layers of thin plastic, some interaction between the concrete and thin plastic occurred during testing.



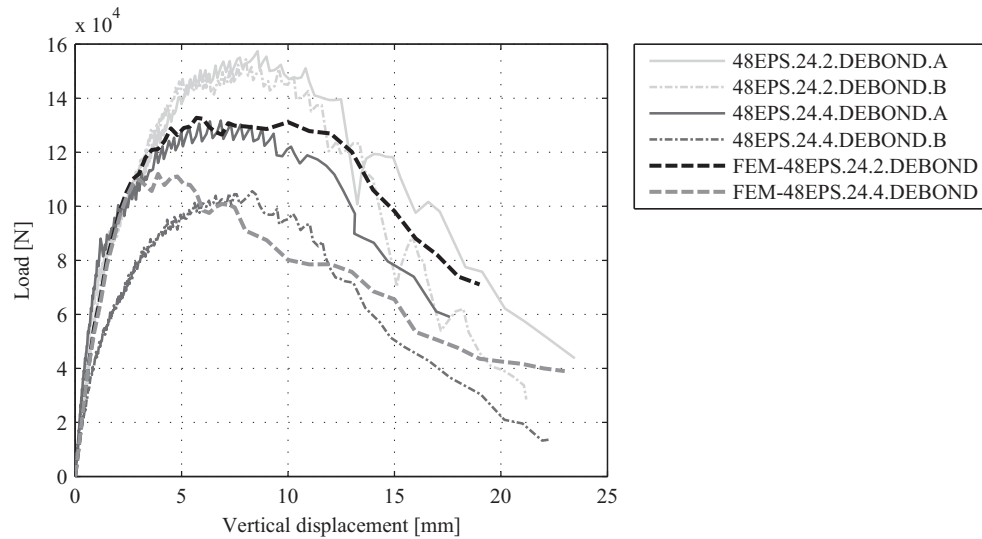


Figure 6.15. *Comparison of experimental and numerical results for debonded panels.*

#### 6.4.4 Panels with CFRP grid

Figs. 6.16-18 depict comparisons of experimental and numerical load-displacement curves for the panels with 50 mm thick EPS insulation and CFRP grid spacing of 305, 610, and 1220 mm, respectively.

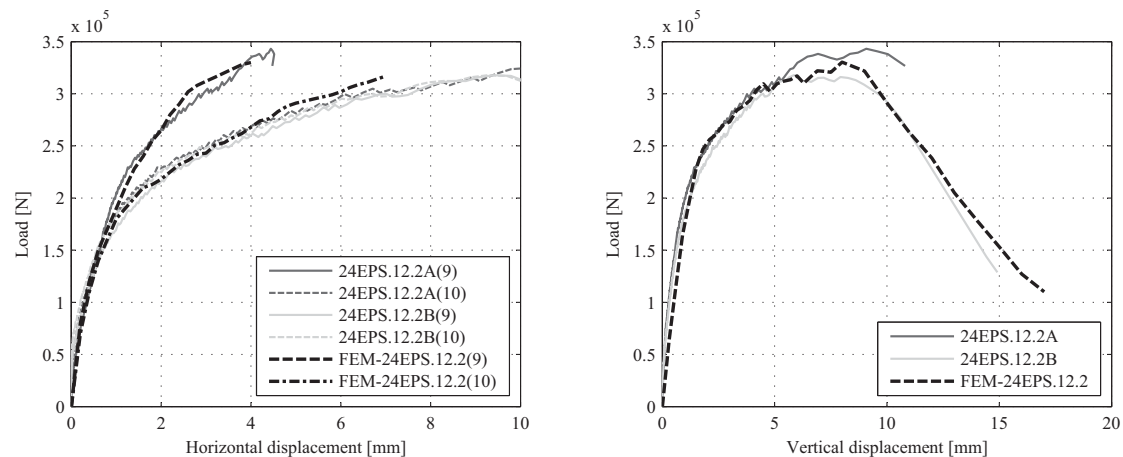


Figure 6.16. *Comparison of experimental and numerical results for panels with CFRP grid, 24EPS.12.2.*

Generally, FE analyses showed reasonable agreement with the measured values. The model predicts the initial phase of the load-deflection curves as well as the ultimate strength and postfailure behavior well for the panels with CFRP grid spacing of 305 and 610 mm. In respect to the panel with a CFRP grid spacing of 1220 mm, the FE model reasonably predicts the initial phase of the load-deflection curves and the ultimate strength. However, interpretation of the postfailure behavior of the panels showed discrepancies in comparison with experimental data (Figure 6.18). These discrepancies could be attributed to problems during construction of the panels such as formation of air pockets at the concrete/rigid foam interface. Presence of air pockets result in a weaker bond at the highly nonlinear regime. Additionally, the effect of

foam thickness and CFRP grid spacing was studied. Test results indicate that increasing the thicknesses of the EPS insulation tends to decrease the shear flow strength of the panel when compared with the same quantity of CFRP grid spacing.

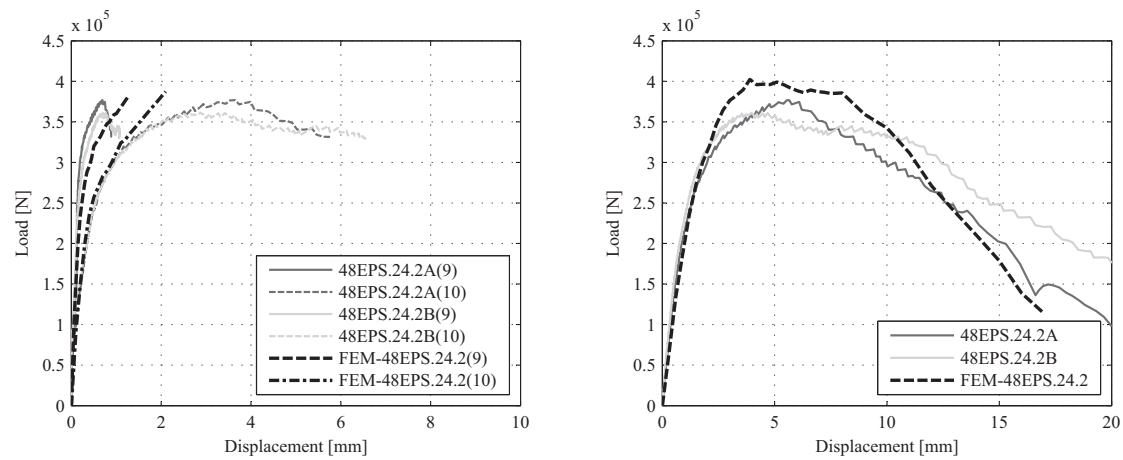


Figure 6.17. Comparison of experimental and numerical results for panels with CFRP grid, 48EPS.24.2.

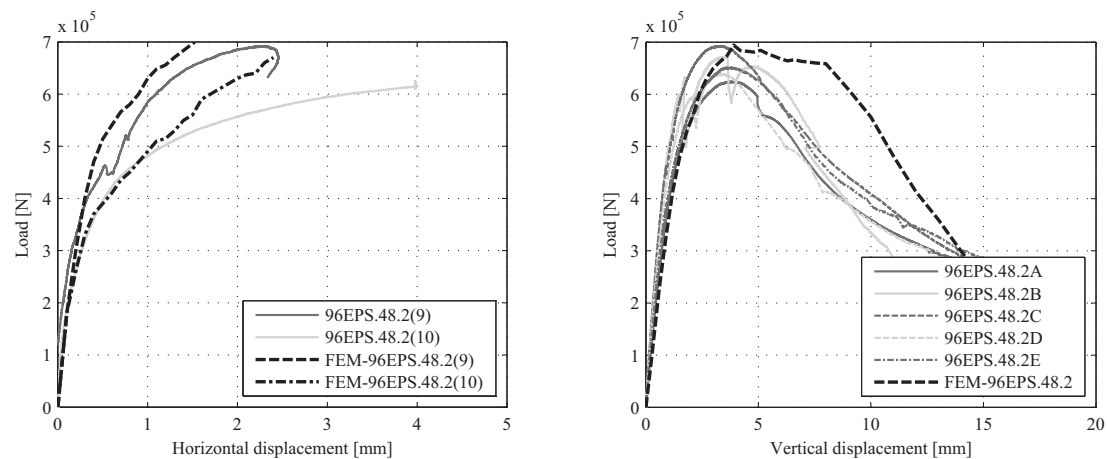


Figure 6.18. Comparison of experimental and numerical results for panels with CFRP grid, 96EPS.48.2.

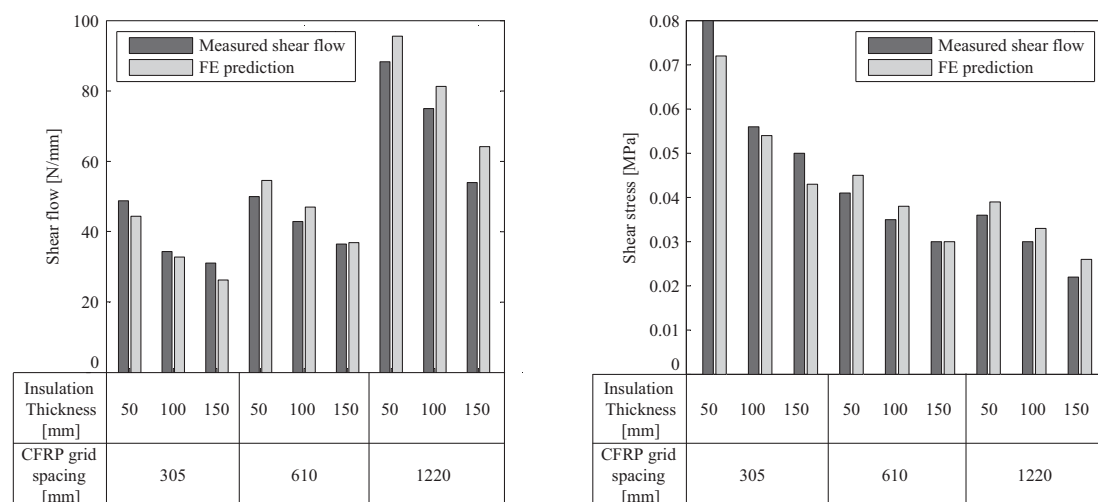


Figure 6.19. Summary of experimental and numerical results for panels with CFRP grid.

In general, a loss of shear flow strength about 35 and 45 % was observed, for the thicknesses of the EPS insulation 100 and 150 mm, respectively, when compared with 50 mm thick EPS insulation. Furthermore, test results indicate increasing the CFRP grid spacing increases the overall shear flow strength of the panel due to increased bonded area. However, it tends to decrease the overall shear stress due to the increase of interface surface area in comparison to the increase of the measured load capacity. An overall summary of experimental and numerical results for panels with a CFRP grid is presented in Figure 6.19.

## 6.5 Design Equation

To achieve full composite action, it is necessary to provide an adequate amount of CFRP grid connectors and specify a foam type that is capable of transferring the shear force induced by the applied loading. The overall nominal shear flow capacity of panel tested in the research reported in this paper is

$$q = \frac{F}{L} \quad (6.2)$$

where  $q$  = shear flow capacity;  $F$  = maximum force at the interface of the critical section at the ultimate-load level; and  $L$  = total length of the CFRP grid connecting the concrete wythes along the height of the panel. A design equation [Eq. (6.3)] is proposed to assist designers in calculating the shear flow capacity of CFRP grid/foam used as a shear transfer mechanism for any combination of the parameters considered in this paper. The overall average shear flow capacity of the CFRP grid/EPS rigid foam shear mechanism is calculated using

$$q_{\text{average shear flow}} = q_{\text{baseline}} \cdot f_{\text{type}} \cdot f_{\text{thickness}} \cdot f_{\text{spacing}} \quad (6.3)$$

where  $q_{\text{average shear flow}}$  = predicted shear flow capacity of CFRP grid/ foam;  $q_{\text{baseline}}$  = shear flow strength of CFRP grid alone; and  $f_{\text{type}}$ ,  $f_{\text{thickness}}$ , and  $f_{\text{spacing}}$  are the factors for the type of foam, insulation thickness, and CFRP grid spacing, respectively. Testing of debonded panels helped to evaluate the shear flow capacity of the CFRP grid with no contribution from the bond between the rigid foam to the concrete. Test results reported that the shear flow capacity of debonded panels was nearly 17.5 N/mm. Hence, this obtained value was considered as a baseline for this design equation approach. Eq. (6.3) modifies the baseline shear flow capacity of the panels based on established factors for the type of foam, thickness of the foam, and spacing between the vertical lines of CFRP grids. Based on the results of a total of 46 panels tested in the research reported in this paper, in combination with panels tested previously (Bunn, 2011), a spreadsheet program was used to establish the factors for all the various tested parameters. Originally, all the factors were set to a value of 1.00, with  $q_{\text{baseline}}$  equal to 17.5 N/mm. The initial analysis resulted in a shear flow capacity of 17.5 N/mm for all pan-

els. The absolute error of the predicted nominal shear flow value, in comparison to the measured values was determined for each panel. The absolute error was squared and summed for all panels. A multivariable solver tool was used to minimize the summed error by first adjusting the factors for the foam type. After the minimization routine was complete, the factors were rounded to two decimal places for these values. The same procedure was used for the remaining parameters to determine the other factors. In each case, the factors were rounded to two decimal places and the process was repeated to minimize the error. The same process was also repeated to set the values for  $f_{type}$ ,  $f_{thickness}$ , and  $f_{spacing}$ . The analysis resulted in the factors for the different parameters as given in Table 6.7. The shear flow strengths obtained from the proposed equation [Eq. (6.3)] are nominal values and should be reduced using proper strength reduction factors. Further research on the other types of rigid foam and an example to demonstrate the method can be found in Sopal (2013).

Table 6.7 *Factors for each parameter of design equation*

| Foam type | $f_{type}$ | Insulation Thickness [mm] | $f_{thickness}$ | CFRP grid spacing [mm] | $f_{spacing}$ |
|-----------|------------|---------------------------|-----------------|------------------------|---------------|
| EPS       | 2.81       | 50                        | 1.46            | 305                    | 0.68          |
|           |            |                           |                 | 610                    | 0.69          |
|           |            |                           |                 | 1220                   | 1.23          |
|           |            | 100                       | 1.03            | 305                    | 0.68          |
|           |            |                           |                 | 610                    | 0.84          |
|           |            |                           |                 | 1220                   | 1.47          |
|           |            | 150                       | 0.94            | 305                    | 0.69          |
|           |            |                           |                 | 610                    | 0.79          |
|           |            |                           |                 | 1220                   | 1.16          |

## 6.6 Parametric Study

A parametric study was conducted to predict shear flow strength of different FRP materials. In addition to CFRP grid, the parametric study of the research reported in this paper focused on BFRP and GFRP grids. The sandwich panels used in the parametric study had the same overall dimensions as the panels tested in the experimental aspect of the research reported in this paper. The BFRP and GFRP grids were assumed to have the same overall dimensions as the CFRP grid reported in this paper. The FE model developed in the Finite-Element Analysis section was used to perform the parametric study of the research reported in this paper. Material properties obtained from the literature are included in the model (Wu et al., 2012). The BFRP grids and GFRP grids had a modulus of elasticity equal to 90000 and 70000 MPa, respectively. Results of the performed parametric study for various types of FRP grids are shown in Figure 6.20. The results showed that panels with CFRP grid have higher shear flow strength in comparison with panels with vertical BFRP and GFRP grids. In general, a loss between 5 and 10 % of shear flow strength was observed for panels with vertical BFRP grids, and between 10 and 25 % for panels with vertical GFRP grids. Increasing the EPS thickness leads to a decrease of the shear flow strength of the panel. Figure 6.20

also shows that increasing the FRP grid spacing increases the overall shear flow strength of the panel due to increased bonded area.

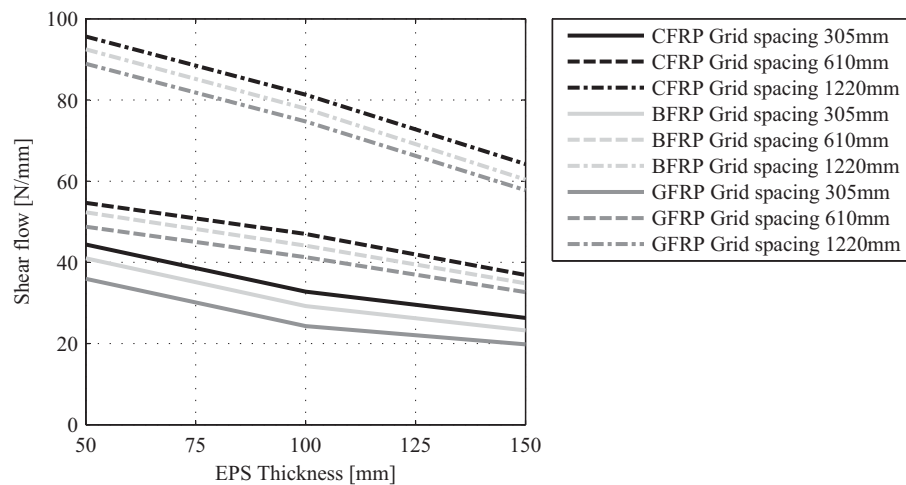


Figure 6.20. *Parametric study for various types of FRP grids.*

## 6.7 Conclusions

The research reported in this paper includes an experimental program designed to investigate the behaviour of 46 small segments representing typical sandwich panels using the CFRP grid/rigid foam as shear mechanism. Various parameters believed to affect the shear flow strength for this CFRP grid/foam system were examined. The parameters that were considered are the spacing between lines of CFRP grids and the thickness of the rigid foam. The research reported in this paper was conducted to determine the characteristics of the shear transfer mechanism of the CFRP grid/rigid foam. The observed failure modes were shear cracking and/or shear sliding for rigid foam, whereas the CFRP grid exhibited rupturing of the CFRP grid in tension and buckling of the CFRP grid in compression. Increasing the spacing between the vertical lines of the CFRP grid increased the overall shear flow strengths due to an increase of the bonded contact concrete/rigid foam interface area. However, it showed a decrease in overall shear stresses due to the increase of the interface surface area in comparison to the increase of the measured load capacity. A nonlinear 3D FEM analysis was performed to model the behaviour of the test specimens and to study the behaviour of PCSP. The FEM results were in good agreement with measured values. A spreadsheet program was used to establish the factors for design equations to predict the shear flow strengths for given CFRP grid/EPS foam systems. A parametric study was performed to predict the shear flow strength of different FRP materials. The results showed that panels with a CFRP grid have higher shear flow strength in comparison with panels with vertical BFRP and GFRP grids. Panels with vertical BFRP and GFRP grids have lower shear flow strength than panels with CFRP grids by 5 - 10 and 10 - 25 %, respectively, using the same cross section of the strands and spacing of the grid.



## 6.8 Acknowledgement

The authors would like to acknowledge the contributions of AltusGroup and Metromont Corporation for providing support to the experimental programs presented in this paper. Further, the authors are grateful for financial support of the Danish Agency for Science, Technology and Innovation on Danish-USA network programme on Innovation and Development of Advanced Sandwich Elements for Sustainable Buildings using High Performance Concrete, grant number 1370-00008A. The authors would also like to thank to Otto Mønsted Fund and Cowi Fonden for financial support of Kamil Hodicky during his external stay at North Carolina State University.

# Chapter 7

## Full scale testing and modelling

### 7.1 Introduction

In previous Chapter 6, a nonlinear 3D FE model was developed to model the shear transfer mechanism and the behaviour of the test specimens under shear loading. The FEM results were in good agreement with measured values. The aim of this chapter is to perform an experimental and numerical investigation of two full scale specimens exposed to uniformly distributed flexural loading. Further, the intention of this chapter is to develop a nonlinear 3D FE model capable to predict flexural behaviour of the precast concrete sandwich panels with a reasonable accuracy.

In the literature, several researchers have studied flexural behaviour of precast concrete sandwich panels using 3-point bending test (see e.g. Maximos et al., 2007), 4-point bending test (see e.g. Benayoune et al., 2008; Bush Jr. & Stine, 1994; Bush Jr. & Wu, 1998; Frankl et al., 2008; Hassan & Rizkalla, 2010; Kabir, 2005; Lameiras et al., 2013b; Kim & You, 2015) and uniformly distributed pressure test (see e.g. Rizkalla et al., 2012; Salmon et al., 1997).

Several researchers have attempted to develop numerical models to simulate the behaviour of precast concrete sandwich panels under flexural loading (see e.g. Benayoune et al., 2008; Salmon et al., 1997; Hassan & Rizkalla, 2010; Rizkalla et al., 2009; Mackerle, 2002; Metelli et al., 2011; Kang et al., 2011). However, their modelling approaches significantly simplified the behaviour of precast concrete sandwich panels and the numerical analysis resulted in an overestimation of the sandwich panel behaviour in comparison to experimental data.

## 7.2 Experimental investigation

A total of two full scale panel specimens were tested in flexural loading (wind loading) configuration to investigate the crack development, stiffness and the capacity of the panels. The panels built for the research reported in this chapter were 2615 mm high, 4030 mm wide and 360 mm thick.

### 7.2.1 Material properties

The subsequent sections provide brief description of the material properties of the four materials used to construct the panels.

#### 7.2.1.1 Concrete

The HPC used for construction of the full scale panels was DTUI mix. The average mechanical and fracture properties of DTUI specimens are summarized in Table 4.3.

#### 7.2.1.2 Rigid insulation

Lightweight Kingspan Kooltherm 37 insulation was used as the rigid foam insulation material due to its high insulating properties. The insulation sheet was cut into pieces and inserted between the inner and the outer HPC plates. Small segments of foam were tested in compression, see Figure 7.1.

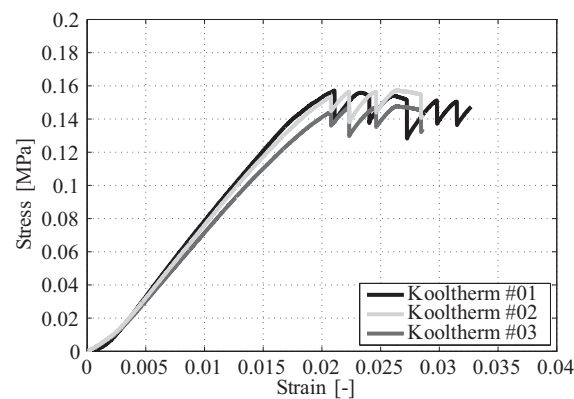


Figure 7.1. *Compression curves for Kingspan Kooltherm 37 insulation.*

The average mechanical properties of three specimens for the rigid foam are summarized in Table 7.1. In Table 7.1,  $f_{c,KK}$ ,  $f_{t,KK}$ ,  $E_{KK}$  and  $\nu_{KK}$  are the compression strength, tensile strength, modulus of elasticity and Poisson's ratio of the Kingspan Kooltherm 37 rigid foam, respectively. The values of tensile strength were not measured in this campaign and were obtained from the producer of the foam (Kingspan, 2015).

Table 7.1 *Mechanical properties of Kingspan Kooltherm 37*

| Insulation            | $f_{c,KK}$ [MPa] | $f_{t,KK}$ [MPa] | $E_{KK}$ [MPa] | $\nu_{KK}$ [MPa] | Number of specimens |
|-----------------------|------------------|------------------|----------------|------------------|---------------------|
| Kingspan Kooltherm 37 | 0.15             | 0.15             | 8.2            | 0.3              | 3                   |

### 7.2.1.3 Steel

Two types of connectors were used, i.e. the net and wire connector. The net connector is made of stretched stainless steel (thickness of the plate is 0.5 mm), see Figure 7.2 left. The connector takes shear forces in the panel and keeps the front plate in place. The net is 500 mm long, and embedded in the rib and the front plate. The wire connector is designed to take the perpendicular tension in the panel, keeps the HPC plates in place during handling and adds stiffness to the structure when it is exposed to a wind load. The connector is consisted of a stainless steel wire ( $\varnothing 4$ ) bended four times as shown in Figure 7.2 right. The parts marked with the red and yellow circle are embedded in HPC plates. The wire connector is 300 mm long.

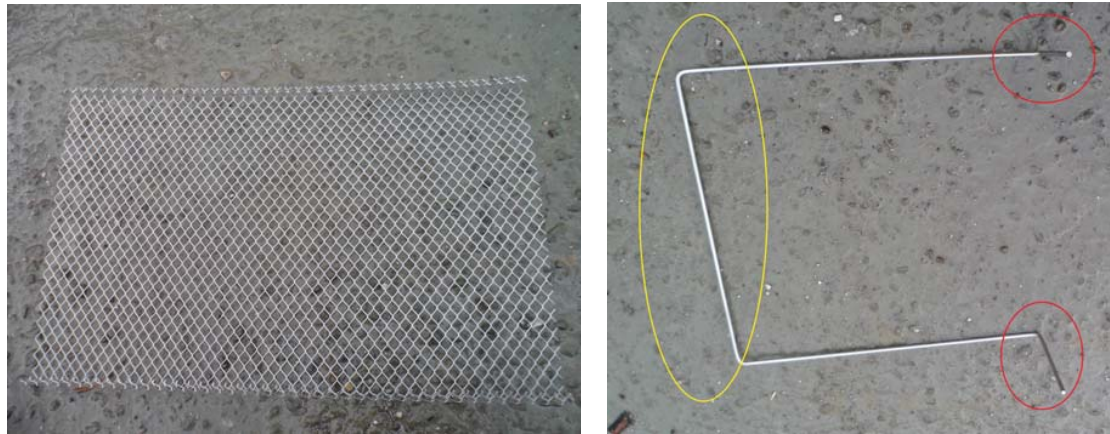


Figure 7.2. The net and wire connector.

All steel members had yield strength  $f_y = 550 \text{ N/mm}^2$ , and elastic modulus  $E_s = 215\,000 \text{ N/mm}^2$ .

### 7.2.1.4 BFRP grid

The BFRP grid used in this study was made of 100 % basalt continuous filament roving. The grid was sized 25 by 25 mm with thickness of 0.9 mm and coated with styrene-acrylic resin. The grid was cut to proper size from 100 m long roll prior casting process. The mechanical properties of BFRP grid are summarized in Table 7.2. In Table 7.2,  $f_{t,\text{BFRP}}$  and  $E_{\text{BFRP}}$  are the tensile strength and modulus of elasticity of the BFRP grid, respectively. The mechanical properties of the BFRP grid were not measured in this study and were taken directly from the producer of the BFRP grid (Zhejiang GBF Basalt Fiber Co., LTD., 2015).

Table 7.2 Mechanical properties of BFRP grid

| Textile material | $f_{t,\text{BFRP}}$ [MPa] | $E_{\text{BFRP}}$ [MPa] | Strain at failure [%] |
|------------------|---------------------------|-------------------------|-----------------------|
| BFRP             | 1200                      | 50                      | 0.24                  |

## 7.2.2 Panel configuration

Each panel is made of four net connectors and twelve wire connectors. The dimensions of the panel and locations of the connectors are shown in Figure 7.3.

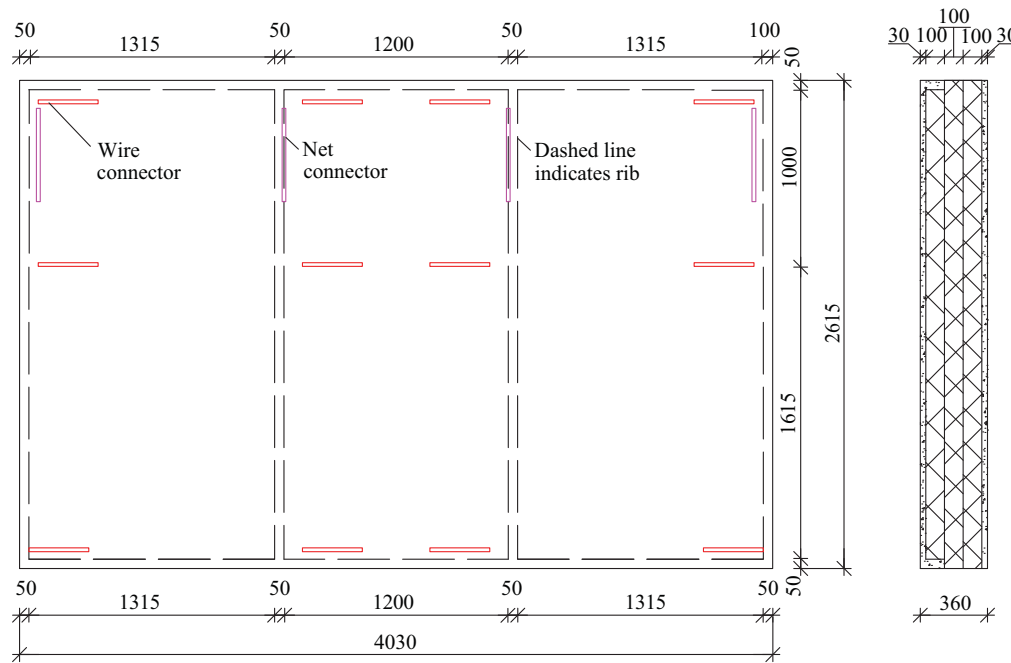


Figure 7.3. *The overall geometry of the full scale panels.*

The panels were reinforced with 2Y10 steel bars in each rib. The front and back HPC plate was reinforced with a BFRP grid placed in the middle of the HPC plate.

### 7.2.3 Fabrication of the panels

All test specimens were constructed by local precast concrete producer Ambercon A/S. All insulation layers were cut into required sections according to the spacing of shear connectors. The panels were fabricated horizontally.

The fabrication process for the panels is described below:

1. Steel forms were constructed on the steel casting platform in proper size.
2. HPC was poured in the steel forms 15 mm high and vibrated.
3. A BFRP grid was placed then on the layer of HPC and another 15 mm of HPC was poured.
4. Insulation layer and shear connectors in proper location were placed.
5. Steel reinforcement of the ribs was placed on insulation with 15 mm cover.
6. Lifting devices were installed in the ribs.
7. HPC was poured to cover the ribs and the insulation layer (15 mm above insulation layer). HPC was consequently vibrated.
8. A BFRP grid was placed then on the layer of HPC and another 15 mm of HPC was poured.
9. The HPC surface was then mechanically polished to obtain required architectural appearance.

### 7.2.4 Test setup

The testing of the full scale panels was performed in a vertical position using a test frame built at DTU (see Figure 7.4). Two test setups were used (see section 7.2.5). The tested panels were loaded by air controlled pressure pads. The load rate used was 8 Pa/s.



Figure 7.4. *Test setup.*

The panel is supported along the top and bottom. The supports are attached to the main frame of the setup to secure horizontal and vertical displacements. A sketch of the two supports is presented in Figure 7.5.

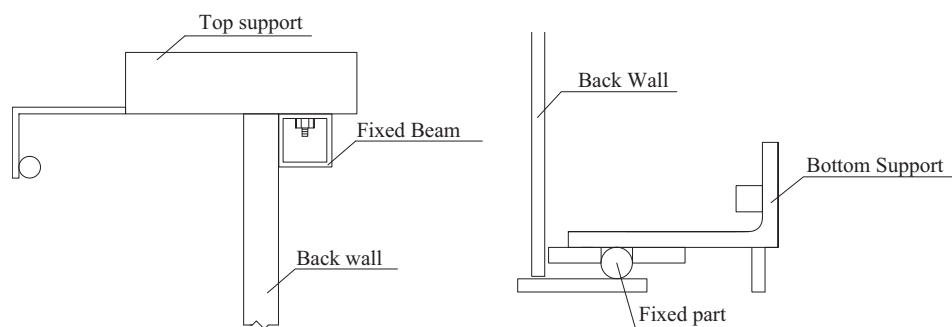


Figure 7.5. *Principle sketch of the supports.*

The pressure in the pads is controlled by a control panel, see Figure 7.6, which is linked to the program created in LabView (National Instruments, 2013).

The different elements on the control panel are:

- *Pressure transducer*: The actual air pressure in the pressure pads is measured by the pressure transducer. The signal is sent back to LabView, which evaluates the pressure and sends a signal to the magnet valve, that opens or closes depending on whether the pressure is higher or lower than desired.
- *Outlet valve*: As the magnet valve can only let air into the pads, the outlet valve allows to leave the air anytime.

- *Magnet valve*: The magnet valve controls the pressure in the system by opening or closing, and thereby pumping air into the system or letting air out. It is controlled by a signal from LabView.
- *Regulator valve*: The regulator valve controls the overall pressure in the system. The initial pressure is 8 Pa in the system. The valve is installed to 2.5 Pa, which makes fine-tuning of the pressure easier to control. The fine-tuning is controlled by the magnet valve and LabView.
- *Labview and Benchlink*: Labview is built up over a code, which will not be explained in this thesis. The Labview and Bechlink run simultaneously, and the interface of each program is shown in Figure 7.7.

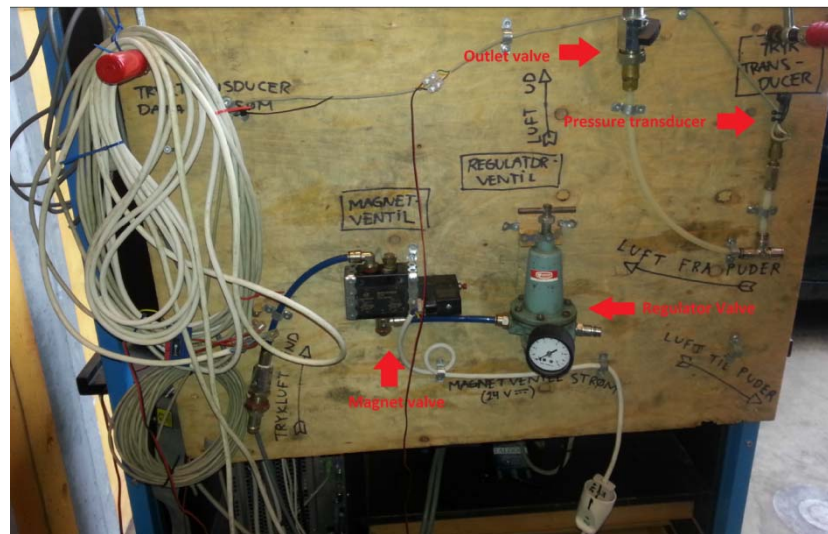


Figure 7.6. *Control panel for full scale test.*

Labview contains the following elements marked with a colour (Figure 7.7):

- *Red*: Pressure curves as a function of time. The red curve is the wanted pressure while the white curve is the actual pressure. The values are also written in numbers in the upper right corner.
- *Blue*: The slope of the wanted pressure is entered in (MPa/ds).
- *Green*: Control buttons. The 'Right arrow' starts the test. 'Stop' stops the test and if the outlet valve is open, the pads will be emptied. 'Hold' will pause the test, stopping the increase of the wanted pressure. The magnet valve will try to hold the pressure at the actual value.
- *Yellow*: The number of seconds between each measurement is entered to the left. The right box shows the time to the next measurement.

The trigger system is connected to Benchlink, so each time a pressure is registered in Labview, it is logged in Benchlink along with the values for each extensometer. After the test is done, the measurements from Benchlink can be saved and exported.



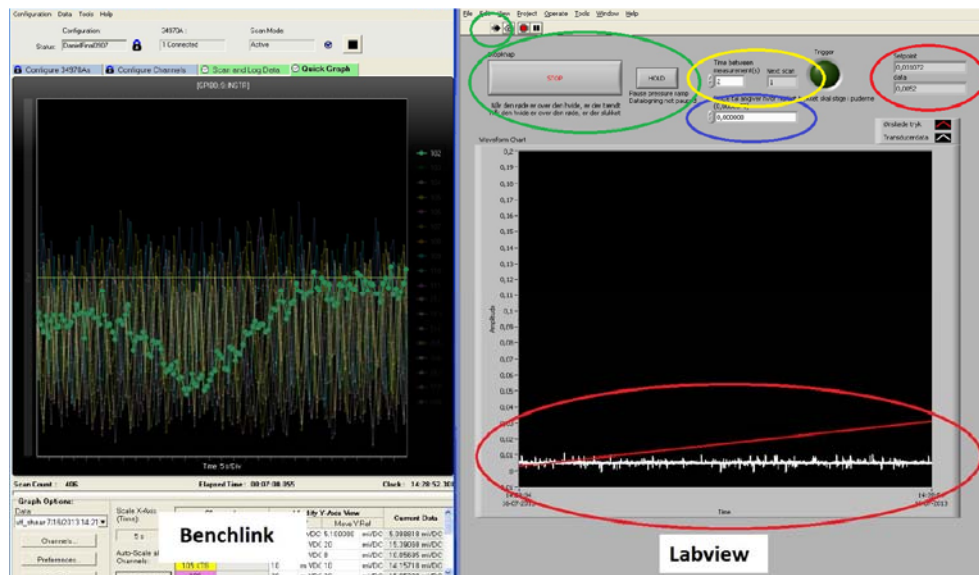


Figure 7.7. Left: Benchlink. Right: Labview.

### 7.2.5 Test instrumentation

Two setup configurations were used to study different boundary conditions, as shown in Figure 7.8. The applied load was measured until failure. The relative horizontal deflection between the HPC plates were measured by 15 (test setup 1) and 17 (test setup 2) linear extensometers at selected locations. All instruments were connected to an electronic data acquisition system. Data was recorded continuously at a sample rate of 1 Hz during loading. For safety reasons two straps were placed around the panel to keep it in place in case the panel would jump out from the setup.

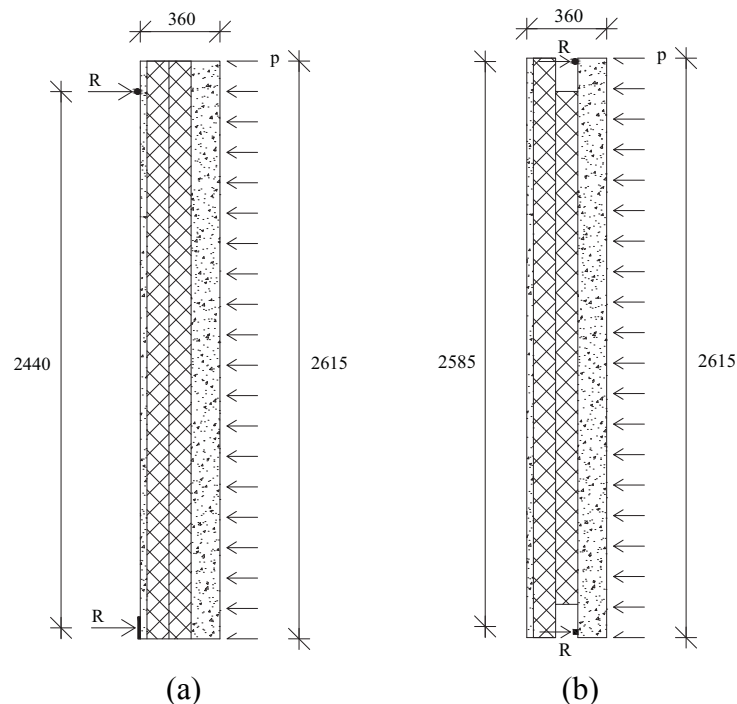


Figure 7.8. Principle sketch of forces acting on the panels; (a) Test setup 1 (b) Test setup 2.



### Test setup 1

In the first setup, panel #01 was supported on the front-plate as shown in Figure 7.8a. The pressure was applied on the back plate. In the test setup 1, all extensometers were placed to monitor the front plate as shown in Figure 7.9. The extensometers were located in 4 vertical lines. Two lines monitored the edges of the panel, one vertical line was placed in the center of the panel. The last line was located to monitor vicinity of the rib. The locations of the extensometers were top support, 400 mm above mid-plane, midplane, 400 mm below midplane and bottom support as presented in Figure 7.10.



Figure 7.9. Picture of the panel #01 - test setup 1 prior testing.

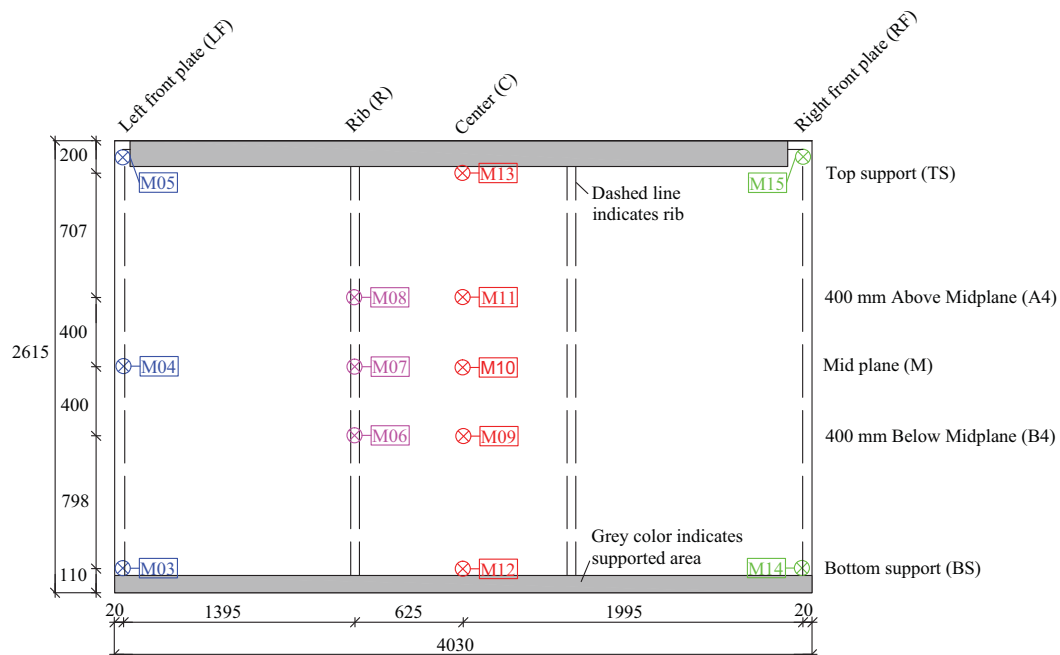


Figure 7.10. Test instrumentation of the panel #01 - test setup 1.

### Test setup 2

In the second setup - panel #02, the support conditions were changed in comparison with test setup 1. The panel was designed in a way that only the back plate is load carrying. Therefore, the support conditions were changed that only the back plate was restrained as shown in Figure 7.8b. The part of insulation had to be removed in vicinity of the supports to attach the supports to the back plate. The pressure was applied on the back plate. The Aramis optical strain measurement (GOM mbH, 2015) was used to determine the crack development at given location, see Figure 7.11. The extensometers were located in 3 vertical lines as depicted in Figure 7.12. Two lines monitored the edges of the panel, one vertical line was placed in the center of the panel. Additionally, 4 extensometers were placed to monitor the deflections of the back plate.



Figure 7.11. Picture of the panel #02 - test setup 2 prior testing.

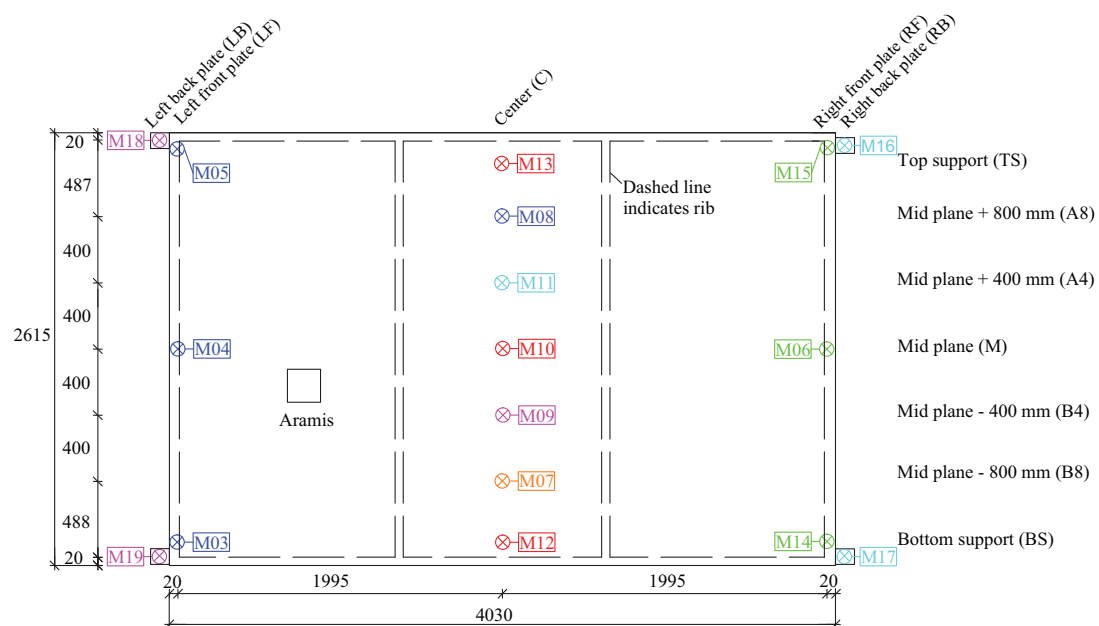


Figure 7.12. Test instrumentation of the panel #02 - test setup 2.

## 7.3 Finite element analysis

A 3D nonlinear macro-scale finite-element (FE) model of sandwich panels was developed to further investigate its structural behaviour under flexural loading. The model was developed using the finite element analysis software DIANA version 9.4.4 with pre-processor and postprocessor FX+ (TNO DIANA, 2011). The mesh size was adopted to provide satisfactory convergence. The nonlinear solution was based on the Newton-Raphson procedure. The subsequent subsections present various elements utilized to model the different materials used in full scale specimens simulating the behaviour of precast sandwich panels.

### 7.3.1 Concrete - element and constitutive relationships

The HPC plates were modeled using a four-node, three-side isoparametric solid pyramid element (TE12L). The standard size of the element was 10 mm with adaptive remeshing around shear connectors. Multilinear isotropic material input was used to approximate the nonlinear constitutive relationship for the HPC in tension. The multilinear diagram fully describes the relationship between the tensile stress and the equivalent strain. The full compression curve was not measured in this study. Thus, Thorenfeldt compression curve (Thorenfeldt et al., 1987) was used to model the crushing behaviour of the HPC. A constant shear retention factor = 0.01 was considered for the reduction of shear stiffness of concrete due to cracking.

### 7.3.2 Rigid insulation - element and constitutive relationships

The layers of rigid foam were modeled using the same four-node, three-side isoparametric solid pyramid elements as used for concrete (TE12L). The standard size of the element was 10 mm. To model the behaviour of rigid foam material in compression and tension, the stress-strain parameters were input in DIANA version 9.4.4 using a multilinear isotropic material model based on values obtained by the experimental programs (see section 7.2.1.1).

### 7.3.3 Steel - element and constitutive relationships

The steel shear connectors were also modeled using the same four-node, three-side isoparametric solid pyramid elements as used for concrete (TE12L). The stress-strain relationship of steel can be largely divided into elastic, plastic, and strain hardening regions. In structural design, it is customary to neglect the strain hardening of the material and to utilize mainly the elastic and plastic parts of the stress-strain relationship. To this end, a simple bilinear approximation is usually adopted. This results in the elastic-perfectly plastic stress-strain model as shown in Figure 7.13.

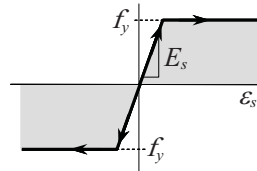


Figure 7.13. *Stress-strain curve for an elastic-perfectly plastic material.*

#### 7.3.4 BFRP grid - element and constitutive relationships

Mechanical properties of individual strands of BFRP grid connectors were reported in the section 7.2.1.4. The individual strands of CFRP grid were modelled with a four-node, three-side isoparametric solid pyramid elements (TE12L), considering the intermediate joints. The behaviour in tension was assumed linear elastic before rupture of the single strands of BFRP grid. Behaviour of BFRP grid in compression was for sake of simplicity disregarded.

#### 7.3.5 Rigid insulation/concrete interface

Bond strength between foam and concrete interfaces was modeled using contact elements. The interfaces between the foam and the concrete were modeled using 3D interface elements (T18IF). After the testing the rigid foam remained well bonded to the HPC plates. Hence, the bond between the foam and HPC was assumed for simplicity rigid.

#### 7.3.6 Rigid insulation/rigid insulation interface

There is no bonding between the individual layers of rigid foam, besides a natural friction. The contact between the layers of foam were modeled using 3D interface elements (T18IF). Coulomb friction coefficient  $\mu = 0.1$  was assigned to define sliding behaviour between the layers.

#### 7.3.7 Steel/concrete interface

The FE model was created with bond slip interaction between steel and concrete. The interfaces between steel and the concrete were modeled using 3D interface elements (T18IF). A model for the bond stress-slip behaviour is required to be able to make calculations of the crack pattern and crack widths. The bond-slip curve for good bond conditions; Ceb-Fib Model Code 1990 (fib Special Activity Group 5, 1999) was adopted. It consists of an increasing first branch up to the ultimate bond stress. This branch is followed by a plateau during which slip is increasing for constant bond stress, after which bond stress starts to decrease for increasing slip values. Finally, a constant residual bond strength is reached which is due to pure friction between the reinforcing bar with the cracked concrete lugs and the surrounding concrete. Bond-slip relationship for steel/concrete interface is shown in Figure 7.14.

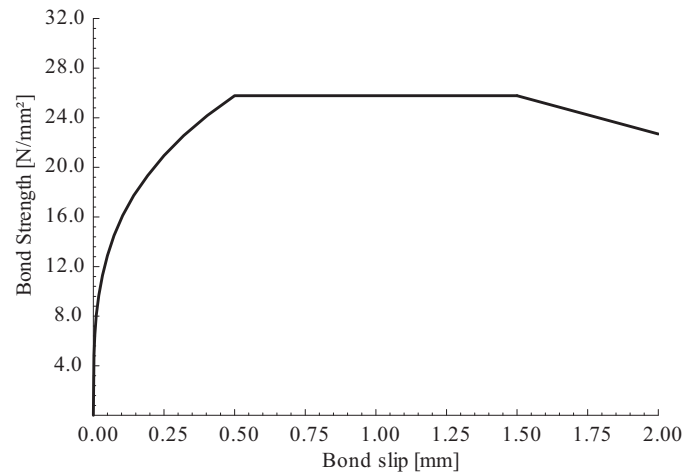


Figure 7.14. *Bond-slip relationship for steel/concrete interface.*

### 7.3.8 BFRP grid/concrete interface

The bond-slip relationship between the BFRP grid and concrete was also incorporated in the model to simulate the bond. This data is typically obtained by means of pull-out tests; however, it was not included in the experimental campaign. A bond-slip relationship for a similar combination of BFRP grid obtained from Schladitz et al. (2012) was thus included in the model. The BFRP grid/concrete interface was modeled using a 3D interface element (T18IF). The bond-slip relationship is defined according to a multilinear model in DIANA version 9.4.4 and is depicted in Figure 7.15.

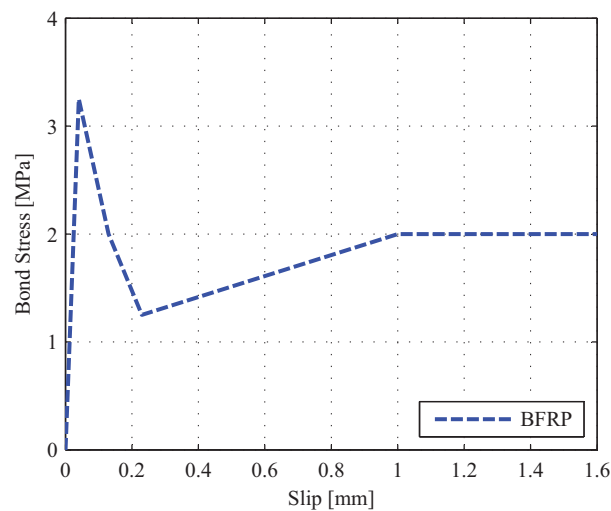


Figure 7.15. *Bond-slip relationship for BFRP grid/concrete interface.*

### 7.3.9 Loading and boundary conditions

The symmetry of the mounting and loading of the tested specimens allowed for only one-half of the panel to be considered in the FE model. The bottoms of the panels were restrained against vertical and horizontal movements, while tops of the panels were restrained against horizontal movements. Rotation was allowed in all directions to simulate rigid body rotation of the panels and to avoid any moments at the sup-

ports. Loading until failure was applied uniformly on the back plate of the sandwich panels by means of displacement control, such that an imposed displacement was applied at the location of loading. The displacement was increased in small increments up to a desired level and then the analysis was terminated.

## 7.4 Results and discussion

Test results for each panel are given by a single curve based on the average relative horizontal deflections measured from three instruments in midplane. The variation in the three instruments was negligible. The results of the FE analysis were compared with the results of the experimental aspect of the research reported in this chapter to determine the effectiveness of the analysis to simulate the panel behaviour. Furthermore, test results are summarized in various subsections to compare and discuss the behaviour of the panels.

### 7.4.1 Failure modes

Typical failure modes observed during testing of concrete wall panels are shown in Figure 7.16 and Figure 7.17.



Figure 7.16. *Typical failure modes of the panel #01 - test setup 1.*



Inspection of the panels after testing revealed that foam failed with combination of cracking and/or shear sliding. Some parts of foam remained well bonded to the concrete after testing. The back plate of the panels in general exhibited horizontal cracking in the rib structure as shown in Figure 7.16 (bottom right) and Figure 7.17 (bottom right). However, panel #01 - test setup 1 also experienced one significant vertical crack in the rib, see Figure 7.16 bottom left. The front plate of the panels in general failed due to horizontal cracking with combination of vertical cracking around ribs and shear connectors. None of the panels exhibited pull-out of BFRP grid from the concrete or rupturing of BFRP grid.



Figure 7.17. *Typical failure modes of the panel #02 - test setup 2.*

### 7.4.2 Experimental and numerical results

Figure 7.18 depicts comparisons of experimental and numerical load-displacement curves for the panel #01 and panel #02. Generally, FE analyses showed reasonable agreement with the measured values. The model predicts the initial phase of the load-deflection curves as well as the ultimate strength and postfailure behaviour of the panels. In respect to the panel #02, the FE model reasonably predicts the initial phase of the load-deflection curves and the ultimate strength. However, interpretation of the postfailure behaviour of the panels showed discrepancies in comparison with experimental data. These discrepancies could be attributed to the fact that the FE model assumed each layer of foam as single unit. However, the construction of the panels required several pieces of foam for single layer. Due to this problem, the panel #02 showed some discrepancies at the highly nonlinear regime in comparison with experimental data. The first cracks started to appear at the load level of  $10 \text{ kN/m}^2$ . Further, it should be noted an increase of stiffness in the panel #01 approximately at the load level of  $60 \text{ kN/m}^2$ . This behaviour can be explained that the foam in test setup 1 is highly compressed and it results in increase of stiffness of the foam, see Figure 7.1. This phenomenon also explains the reason why the panel #01 sustained higher load level than panel #02.

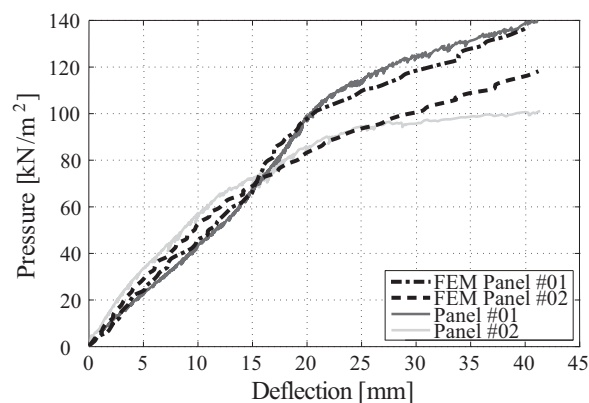


Figure 7.18. *Comparison of experimental and numerical results of the panels.*

Moreover, it should be highlighted that FE model assumed average mechanical and fracture properties for the HPC. Taking into account all the aspects of the model, FE analyses showed reasonable agreement with the measured values.

### 7.4.3 Crack development

The crack development was studied using Aramis optical strain measurement in the panel #02. The measurement was performed at given location (see Figure 7.12) for the loads up to approximately  $20 \text{ kN/m}^2$ . Comparisons of experimental and numerical load-crack opening curves for the panel #02 are shown in Figure 7.19. Generally, FE analysis showed reasonable agreement with the Aramis measurements. The model predicts the initial phase of the load-crack opening curves up to the load of  $7.5 \text{ kN/m}^2$ .



With further increase of load above  $7.5 \text{ kN/m}^2$ , FE result starts to deviate from the Aramis measurements. This deviation could be attributed to several factors: (1) A bond-slip relationship between BFRP grid and HPC was not measured in this campaign and was obtained from the literature for similar BFRP grid, (2) FE model assumed average mechanical and fracture properties for the HPC and (3) mesh size dependency on fracture propagation. The mesh size was adopted to provide satisfactory convergence with respect to the simulation time.

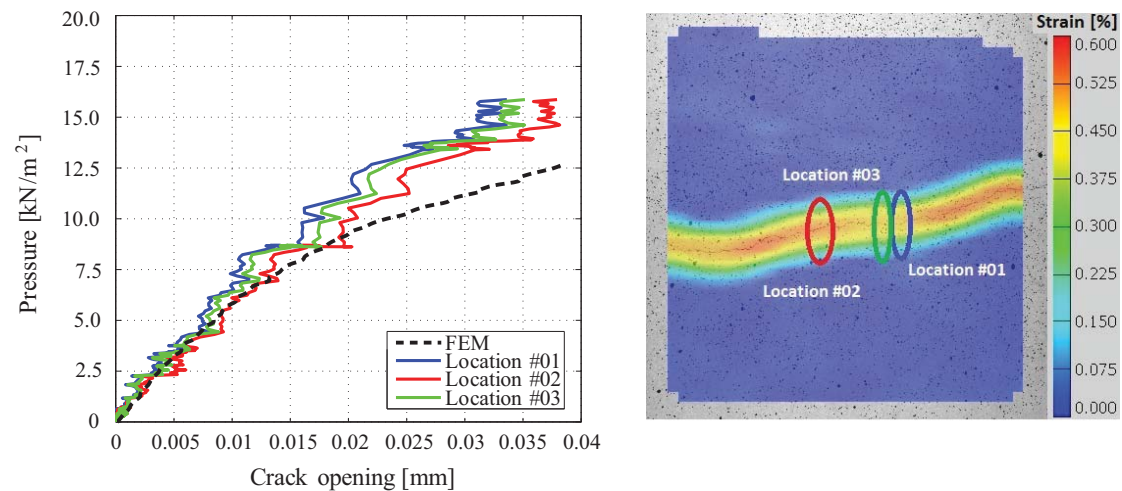


Figure 7.19. Comparison of Aramis measurements and numerical results for the panel #02.

## 7.5 Conclusion

This chapter reports an experimental and numerical investigation of two full scale precast concrete sandwich panels exposed to uniformly distributed flexural loading. The testing of the panels was performed in a vertical position using a test frame built at DTU. Two setup configurations were used to study different boundary conditions. The observed failure modes of the panels were horizontal cracking in the rib structure of the back plates and horizontal cracking with combination of vertical cracking around ribs and shear connectors in the front plates. The panel #01 - test setup 1 also experienced one significant vertical crack in the rib. That foam failed with combination of cracking and/or shear sliding. Some parts of foam remained well bonded to the concrete after testing. None of the panels exhibited pull-out of BFRP grid from the concrete or rupturing of BFRP grid. A nonlinear 3D FEM analysis was performed to model the behaviour of the test specimens and to study the behaviour of precast concrete sandwich panels. The FEM results were found in good agreement with measured values. The crack development was studied using Aramis optical strain measurement in the panel #02. The results of FE analysis showed reasonable agreement with the Aramis measurements.

## Chapter 8

### Journal paper 3

Title: Assessment of risk of early age cracking in thin-walled concrete sandwich panels

Authors: Kamil Hodicky, Natalie W. Portal, Thomas Hulin, Jacob W. Schmidt and Henrik Stang

Submitted in: Journal of Engineering Fracture Mechanics

## Abstract

The present paper presents a rough approach to analyze the robustness of thin-walled sandwich panels at early ages. The approach investigates the constrained shrinkage that the external HPC plate is subjected to. Parametric study is analyzed for a large number of parameter variations. The non-linear FE model was developed using the finite element analysis software DIANA. The modelling approach studied crack propagation in dependence on the stiffness of the restraints as well as distance between the restraints. The results of non-linear FE analysis outcome into the plots assessing crack propagation of concrete elements with the geometry comparable to infinite sheet. Furthermore, the case study was performed for novel thin-walled sandwich elements made of fiber-reinforced HPC. The results of the case study proved that the proposed approach fits reasonably well with the observations on site, i.e. the ability to predict when crack growth becomes unstable and when structural macro-cracking is expected to appear.

## 8.1 Optimization problem

Early age cracking has always been an issue for concrete structures, but this issue is being emphasized with the use of high performance (HPC) and high strength concretes (HSC) due to (i) some HPC (especially HSC) are more brittle than normal concretes (Henrik Stang & Østergaard, 2003) (ii) HPC promote the design of more slender and more thin-walled structures resulting in more fragile elements as facing larger consequences of cracking and more severe drying. New types of concrete have been constantly developed in order to meet the increasing demand for improved mechanical properties and durability. However, the improved and densified microstructure of these new types of concrete leads to a significant increase in the volume changes which occur during the hardening of the material, i.e. in autogenous shrinkage (Farhat et al., 2007). Due to these adverse mechanisms, interest in characterizing the full description of the behaviour of early age concrete has increased dramatically in the last two or three decades, see e.g. (Pichler et al., 2007), (Bernardet al., 2003), (Schlangen et al., 2007). Nearly all the governing material parameters have undergone intensive research and the existing body of knowledge provides a basis for the calculation of the stress evolution which, in turn, represents a tool for predicting whether cracking will occur or not. However, the experimental investigation and the modelling of the early age concrete after crack initiation has occurred is scarce (Østergaard, 2003). Thus, there is a growing need for analysis predicting the occurrence of cracking as well as the severity of the related consequences.

Though – from a design point of view – cracking is, in many cases simply unacceptable, localized cracking with very small crack openings and crack lengths is an acceptable and un-avoidable phenomenon in practice. The robustness of a structure

with regards to cracking is characterized according to the fact that small cracks created by local overload remain small (invisible and subjected to self-healing processes) or result in catastrophic crack propagation.

From an analysis point-of-view it is extremely difficult to undertake the full analysis of crack propagation and even crack initiation in early age concrete because of the following main reasons:

- The free shrinkage – drying as well as autogenous shrinkage is difficult to predict (Shiotani et al., 2003), (Bažant & Raftshol, 1982).
- Knowing the free shrinkage, the stress analysis associated with constrained shrinkage at early ages is difficult and highly non-linear due to aging (strength and elastic stiffness) viscoelastic behaviour.
- The analysis for crack propagation is even more difficult due to the non-linear nature of the crack propagation analysis and the aging (van Mier & van Vliet, 2002).

Østergaard (2003) investigated the possible influence of time-dependent effects in the fracture mechanical properties on the cracking behavior in early age. The reason for this has been the known fact that viscoelasticity of the bulk material is very important for the determination of the stress evolution in early age, and thus, this could also be the case for the crack. However, it has not been possible to determine any rate effects or viscoelastic effects of the crack in early age.

The issue of early age crack propagation has been found to be a practical issue in the development of thin-walled sandwich elements using HPC and HSC (see Fig. 8.1), where the restraints of the shear connectors are found to give rise to unacceptable cracking openings (Hodicky et al., 2013a). These type of constraints lead to cracks that are in general visible to the unaided eye, i.e. they are referred to as macro cracks. The present paper presents a rough approach to analyze for the robustness of thin-walled sandwich panels at early ages. The approach investigates the constrained shrinkage that the external HPC plate is subjected to.

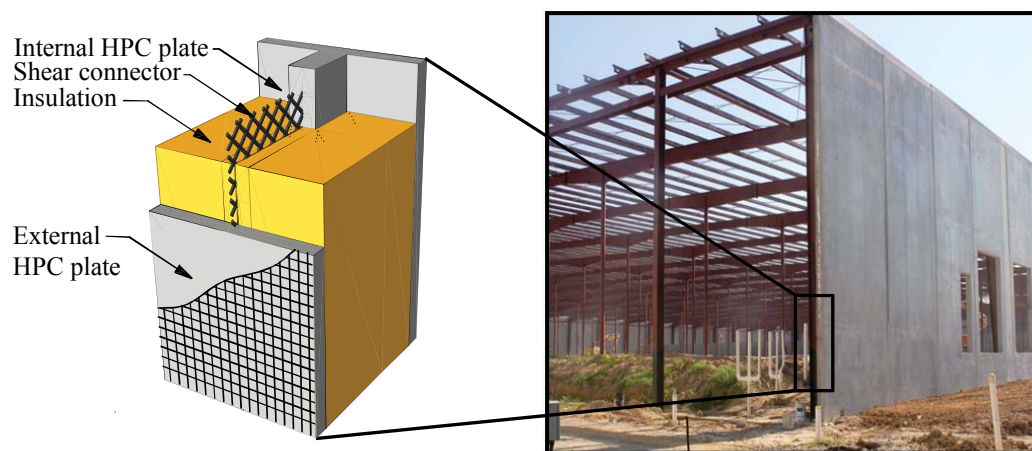


Figure 8.1. *Field application of typical thin-walled sandwich panel.*

## 8.2 Theoretical background

In HPC and HSC, propagation of a crack may be stable, stationary, or unstable due to the presence of a crack arrest mechanism in the inelastic zone around the crack tip. The stable crack growth means that the crack propagates only when the applied load or displacement increases, whereas the unstable crack growth means that the crack may propagate even though the applied load decreases or is kept constant. The stationary crack propagation represents a critical state between the stable and unstable crack growths (Shah, 1995).

In the last two decades, the tensile behaviour of non-fiber and fiber reinforced HPC and HSC is mostly described by the concepts of the Fictitious Crack Model (FCM). However, the application of the FCM for HPC and HSC is still under debate and Linear Elastic Fracture Mechanics (LEFM) is often used instead to model these brittle materials. The most commonly used non-linear FCM was originally developed by Hillerborg et al. (1976). This model is able to closely describe the fracture properties of concrete. Nevertheless, the determination of softening curves consisting of stress-crack opening relationships can cause particular difficulties due to the influence of specimen's own weight in early-aged HPC and HSC like in the case of the uniaxial tensile test and three point bending (Østergaard et al., 2004). Another option is the wedge splitting test setup (WST), which is made for indirect determination of the softening curve, see e.g. (Walter et al., 2005), (Löfgren et al., 2007), (Linsbauer, 1990). The WST was originally proposed by Linsbauer & Tschegg (1986) and later developed by Brühwiler & Wittmann (1990). Its main advantage lies in its simplicity and stability. Moreover, it was proven by Østergaard et al. (2004) and Hansen et al. (1998) that the test is suitable for early-aged HPC and HSC because it does not introduce effects caused by the self-weight of the specimen. The cohesive law for HPC and HSC can be consequently obtained by using an inverse analysis approach, see e.g. (Roelfstra & Wittmann, 1986), (Skocek & Stang, 2008), (Kurihara et al., 2000).

### 8.2.1 Fictitious Crack Model

In the FCM, a crack in concrete is conceptually divided into two parts, a fictitious crack that transfers stresses and a part that is stress free, see Fig. 8.2. At the tip of the crack, a process zone exists which consists of a number of micro cracks which weaken the material. In the continuation of the process zone, a localized crack is formed. This localized crack can transfer stress thanks to aggregate interlock. After a certain crack opening is reached, no more aggregate interlocking takes place and the crack becomes stress free. It should be noted that the fracture process of HPC and HSC to a large extent depends on the aggregates and their bond to the matrix (Prado & van Mier, 2003). The aggregates may become the weak link and aggregate rupture may occur, which reduces the bridging effect and results in a more brittle fracture processes (Löfgren, 2005). The FCM allows for the modelling of the entire crack including the process-zone in one model. At

the crack tip, the cohesive stress is equal to the tensile strength,  $f_t$ , and as the crack opens, the cohesive stresses,  $\sigma = \sigma_w(w)$ , decrease as a function of the opening,  $w$ . The relationship between crack opening and stress is described through a cohesive law, where the area under the curve is defined as the fracture energy,  $G_F$  (see Fig. 8.2(b)).

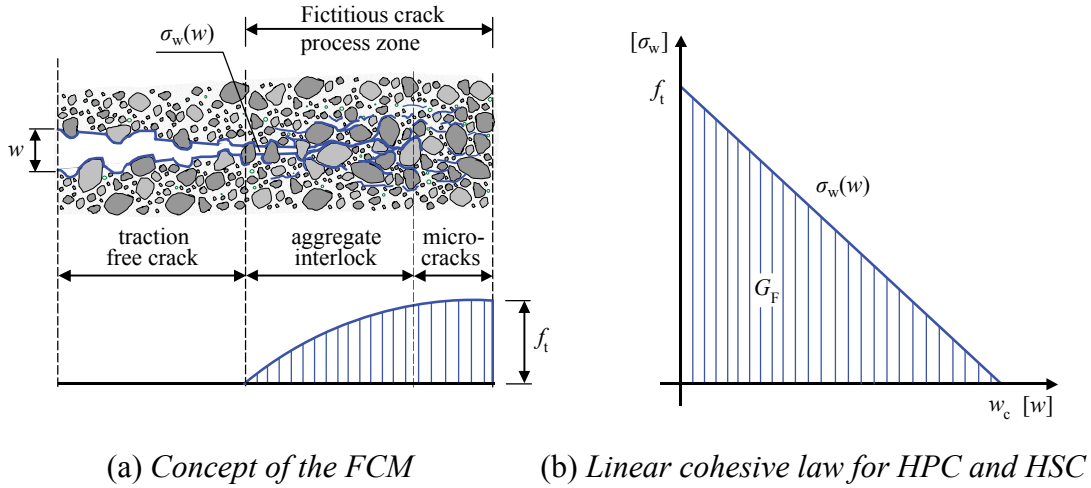


Figure 8.2. Concept of the fictitious crack model (FCM).

The FCM was originally developed for mode I cracks only, but it can be extended to mode II and mixed mode crack propagation. However, the propagation of cracks under mixed modes is a research area that is currently undergoing progressive development, see e.g. Walter et al. (2005) and Carol et al. (1997). The brittleness of a cohesive material can be described using the characteristic length,  $l_{ch}$ :

$$l_{ch} = \frac{EG_F}{f_t^2} \quad (8.1)$$

Apart from modeling of crack propagation in pure concrete material, the FCM model has also successfully been applied to model crack propagation in fiber-reinforced concrete materials, see e.g. Østergaard & Olesen (2005) and Löfgren et al. (2005).

### 8.3 Basic hypothesis

Stang et al. (2007) performed a numerical investigation on crack propagation in centrally cracked infinite sheet for a material with a linear cohesive law. It was observed that a crack propagates stably as long as the crack length,  $a$ , is smaller than the characteristic length,  $l_{ch}$ . For larger crack lengths, the applied far-field stress decreases and the crack growth becomes unstable. Thus, the characteristic length,  $l_{ch}$ , (Eq. 8.1) can according to Stang et al. (2007) be used to predict when the crack growth becomes unstable. The external HPC plate can be perceived as an infinite sheet restrained by individual points representing shear connectors as shown in Fig. 8.3. The sheet is imposed to shrinkage,  $\varepsilon_s$ . In linear elastic analysis when imposed shrinkage,  $\varepsilon_s > f_t/E$ , the

zone,  $b$ , will develop where tensile (principle) stress,  $\sigma_I$ , exceeds the tensile strength of concrete,  $f_t$  ( $\sigma_I > f_t$ ). The size of this zone,  $b$ , depends on how much the imposed shrinkage,  $\varepsilon_s$ , is greater than  $f_t/E$ . Thus, it is expected that:

- large imposed shrinkage,  $\varepsilon_s$ , results in large zone,  $b$ , and tendency to unstable crack growth
- small fracture energy,  $G_F$ , results in small characteristic length,  $l_{ch}$ , and tendency to unstable crack growth
- large distance,  $l$ , results in large zone,  $b$ , and tendency to unstable crack growth when imposed shrinkage,  $\varepsilon_s$ , is greater than  $f_t/E$

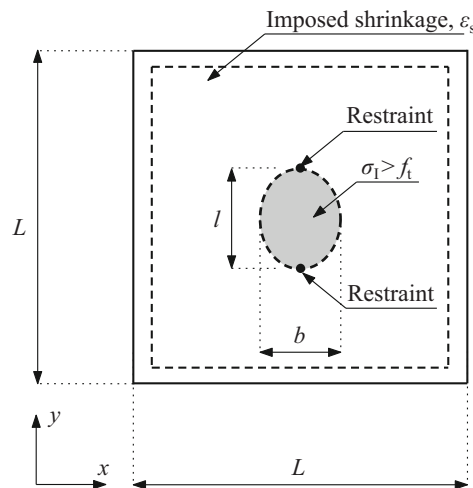


Figure 8.3. *Schematic representation of an infinite sheet with two restraints and imposed shrinkage.*

Thus, the critical state between the stable and unstable crack growth is expected to be predicted by the width of the zone,  $b$ , in which the tensile (principle) stress,  $\sigma_I$ , exceeds the tensile strength of concrete,  $f_t$  in a linear elastic analysis:

$$b \approx 2l_{ch} \quad (8.2)$$

## 8.4 Parametric study

Two models were established for the presented parametric study: a 3D linear elastic model and a 3D non-linear model. A 3D non-linear FE model was applied to verify the use of simplified linear elastic theory. To arrive at some general conclusions, a number of simulations on crack propagation were carried out for infinitely large sheets, to obtain some general results. All the simulations were made for the sheets imposed by shrinkage,  $\varepsilon_s$ . The material parameters employed in the parametric study are summarized in Table 8.1. These parameters correspond to the typical values for concretes used in the industry (Bamforth et al., 2007), (Bažant, 2002), (Brühwiler & Wittmann, 1990), (Tang et al., 1996). The parametric study was performed using the random combinations of the parameters from Table 8.1.

Table 8.1 *Material parameters used for parametric study*

| Parameter   | Min. value | Max. value |
|-------------|------------|------------|
| $l$ [mm]    | 100        | 1000       |
| $G_f$ [N/m] | 20         | 300        |
| $f_t$ [MPa] | 2          | 7          |
| $E$ [MPa]   | 25000      | 50000      |

### 8.4.1 Non-linear FE model

The model was developed using the finite element analysis software DIANA with pre- and post-processor FX+ (TNO DIANA, 2011). The analysed square sheet had a length,  $L$ , equal to 2000 mm and the thickness of the sheet was 20 mm. The symmetry of the sheet allowed for only half of the sheet to be considered in the FE model. The applied element was an eight-node isoperimetric solid brick element ( $HX24L$ ). The sheet was restrained along the x and y-axis by two centrally located restraints spaced at a distance of  $l$  as depicted in Fig. 8.4a. Due to the presence of restraints in the sheet and imposed shrinkage, the formation of a crack is expected to appear in the middle of these restraints. Therefore, a discrete crack was prescribed at the centre of the sheet. Plane quadrilateral interface elements ( $Q24IF$ ) were defined at the location of prescribed cracking, such that these elements would ensure a connection between the two adjacent planes of the 3D sheets. Moreover, a simple linear softening FCM was assigned to the interface elements, see Fig. 8.2b. The un-cracked material was assumed to be linear elastic with Young's modulus,  $E$ , until the tensile strength,  $f_t$ , was reached. After crack initiation the material softened and followed the cohesive law. The area under the cohesive stress versus crack opening curve is interpreted as the fracture energy,  $G_F$ , according to Fig. 8.2b.

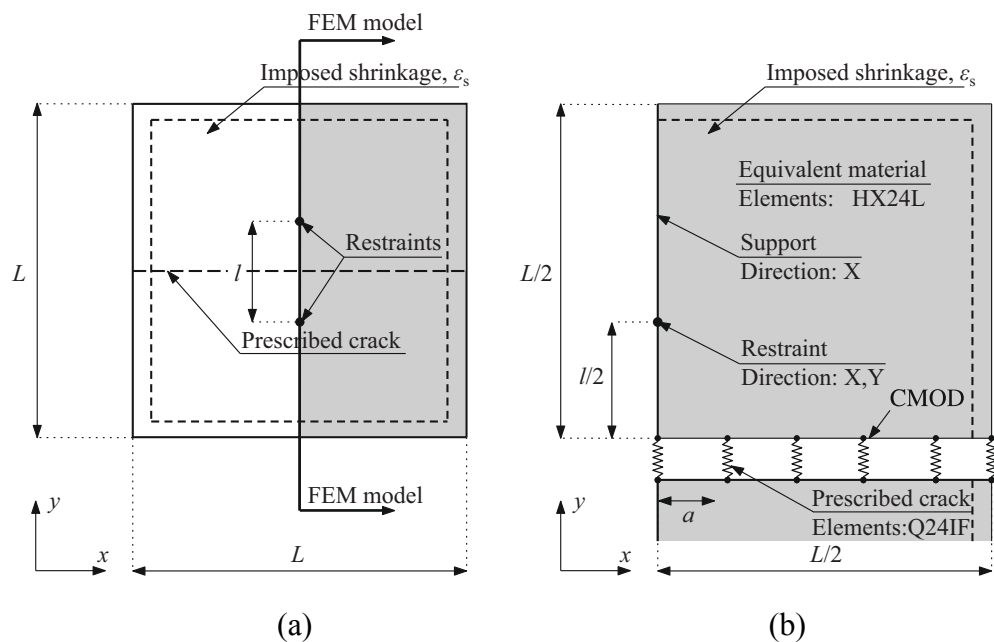


Figure 8.4. (a) The full geometry of the considered sheet (b) Overview of the developed FE model including type of elements and boundary conditions.



Furthermore, plane stress-strain behaviour was assumed along the thickness of the sheet. Fig. 8.4b provides an overview of the 3D model along with the associated element types and boundary conditions. The mesh size was adopted to provide satisfactory convergence. Firstly, by investigating the stress field in the sheet before crack propagation, it was verified that the stresses were independent of boundaries, i.e. that the cracked sheet effectively behaved like an infinite sheet.

### 8.4.2 Linear elastic FE model

The procedure for the establishment of the linear elastic FE model was identical to the non-linear model. The only difference was that the prescribed crack in the middle of the sheet was omitted.

## 8.5 Results and discussion

The results of the parametric investigation for the linear elastic FE model are presented in terms of a curve introducing a dimensionless parameter,  $\alpha$ , as shown in Eq. 8.3

$$\alpha = \frac{\sigma_1}{E \varepsilon_s} \quad (8.3)$$

The parameter,  $\alpha$ , is the ratio between tensile (principle) stress,  $\sigma_1$ , Young's modulus of concrete and imposed shrinkage,  $\varepsilon_s$ . With the increase of imposed shrinkage,  $\varepsilon_s$ , parameter,  $\alpha$ , is decreased and the size of zone,  $b$ , further develops.

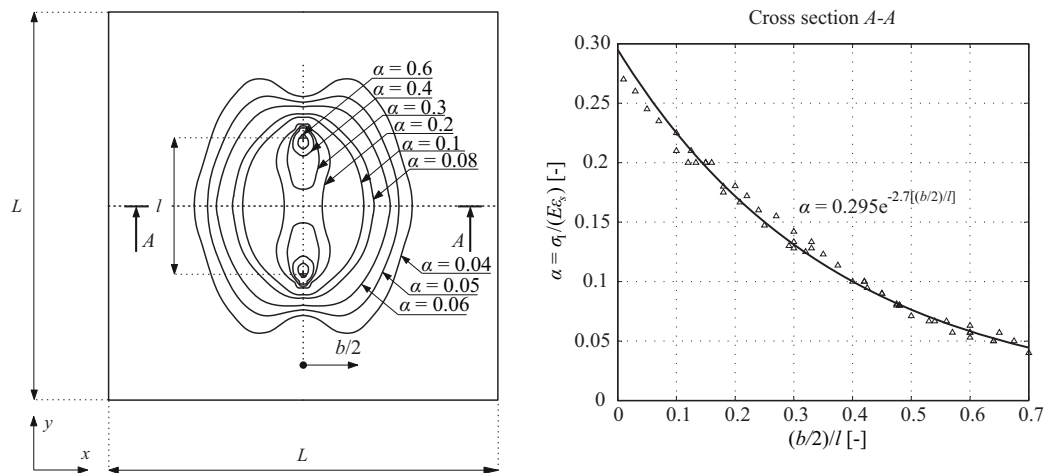


Figure 8.5. Dependencies of parameter,  $\alpha$ , for linear elastic FE model.

Analyzing 214 parameter variations it has been shown numerically that all results narrow down to a single master curve, see Fig. 8.5 right. The function of the master curve can be described according to an exponential decay (Eq. 8.4):

$$\alpha = 0.295 e^{-2.7 \left[ \frac{b/2}{l} \right]} \quad (8.4)$$

A direct comparison of the FE results pertaining to the linear elastic and non-linear analyses has revealed that the initial assumption to predict the critical state between the stable and unstable crack growth ( $b \approx 2l_{ch}$ ) is invalid for the case of an infinite sheet restrained by individual points. It has been shown numerically that the results of the non-linear analysis are highly dependent on the distance between the restraints,  $l$ . Hence, the results of the parametric investigation for the non-linear FE model are presented in terms of curves introducing a dimensionless crack length,  $a/l$ , and a dimensionless crack opening,  $w/l$ , as an inverse function of the dimensionless parameter,  $\alpha$ . Accordingly, the dimensionless crack length can be defined as the ratio of crack length to the distance between the restraints, while, the dimensionless crack opening represents the ratio of crack opening to distance between restraints. The inverse function of dimensionless parameter,  $\alpha$ , can be thought of the extent of imposed shrinkage,  $\varepsilon_s$ , that is required to propagate the crack between two restraints. In order to normalize the results, the dimensionless parameter,  $\beta$ , is also introduced:

$$\beta = \frac{l}{l_{ch}} \quad (8.5)$$

where the dimensionless parameter,  $\beta$ , represents the ratio of the distance between the restraints,  $l$ , and characteristic length,  $l_{ch}$ . Fig. 8.6 depicts 11 different curves depending on the dimensionless parameter  $\beta$ .

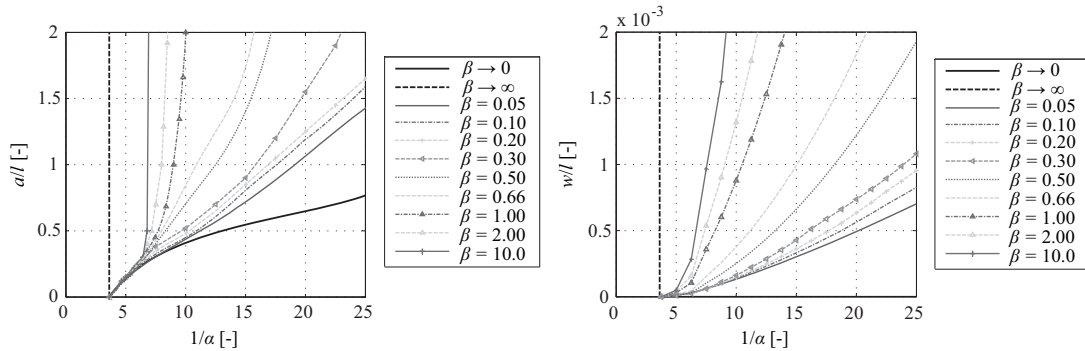


Figure 8.6. (a) Dimensionless crack length,  $a/l$ , as function of inverse function of dimensionless parameter,  $\alpha$ , for normalized results of the dimensionless parameter,  $\beta$ . (b) Dimensionless crack opening,  $w/l$ , as function of inverse function of dimensionless parameter,  $\alpha$ , for normalized results of the dimensionless parameter,  $\beta$ .

The theoretical boundaries are presented by two individual curves. The upper boundary represents the curve,  $\beta \rightarrow \infty$ , where the concrete is assumed to be infinitely brittle ( $l_{ch} \rightarrow 0$ ), meaning that when the tensile strength of concrete is exceeded in the center of the plate, the crack propagates immediately in an unstable manner. The lower boundary is represented by the curve,  $\beta \rightarrow 0$ , where the concrete is assumed to be infinitely stiff ( $l_{ch} \rightarrow \infty$ ). The lower boundary curve corresponds to the solution of the linear FE analysis. Based on the parameters presented in Table 8.1, the dimensionless

parameter,  $\beta$ , varies within the range 0.05 to 10. Looking at Fig. 8.6, it was found out that in order to propagate the crack in the centre of the plate, imposed shrinkage,  $\varepsilon_s$ , should be approximately four times greater than  $f_t/E$ . Generally, when imposed shrinkage,  $\varepsilon_s$ , is up to six times greater than  $f_t/E$ , all the solutions approximately follow the linear FE solution. Further increase of imposed shrinkage,  $\varepsilon_s$ , leads to a deviation from the linear FE solution. The rate function, the extent of deviation of the non-linear FE solution from the linear FE solution depends on the dimensionless parameter,  $\beta$ . Increase of the dimensionless parameter,  $\beta$ , leads to situation when unstable crack growth occurs. The results revealed that the crack propagates stably as long as the values of the dimensionless parameter,  $\beta$ , are below 1. As such, the results of the dimensionless parameter,  $\beta$ , above 1 lead to unstable crack propagation. Thus, one can predict critical imposed shrinkage in the structure, which will either lead to unstable crack propagation or will give to the designer possibility to change the type of concrete and spacing between restraints in order to avoid unstable crack propagation. Designers may use the given parametric study for self-evaluation of their concrete elements with the geometry comparable to infinite sheet under the assumption of fully fixed restraints. Interpolation between the curves can be made for dimensionless parameters,  $\beta$ , different than those indicated in the Fig. 8.6. It is recommended that for the design of thin-walled sandwich elements that the dimensionless parameter,  $\beta$ , is kept below the value of 1, which is further applied in the case study.

## 8.6 Case study

The case study was performed for novel thin-walled sandwich elements made of fiber-reinforced HPC developed in Denmark. The width of the elements was 3.584 m and height 4.48 m. Those elements experienced structural macro-cracking between four weeks to three months after casting. The studied sandwich elements consisted of an internal layer of insulation and two HPC plates. The thicknesses of the HPC plates were 20 mm, whereas the internal HPC plate was strengthened by the HPC ribs being 50 mm wide and 120 mm high. The HPC ribs were reinforced with 12 mm diameter rebar. The welded steel truss-connectors with 4 mm diameter were used to keep the plates together and the panel intact during handling. The insulation layer consisted of expanded polystyrene (EPS) with a thickness of 200 mm. Fig. 8.7 schematically depicts a drawing of the sandwich element together with the detail of the shear connector used for the presented case study.

### 8.6.1 Material properties

The HPC mix design applied in this study is shown in Table 8.2. The developments of the mechanical properties – Young's modulus,  $E_{cm}$ , compressive strength,  $f_{cm,cube}$ , tensile strength (wedge splitting test),  $f_{ctm,sp}$ , fracture energy,  $G_{Fm}$ , as well as characteris-

tic length,  $l_{\text{chm}}$ , were investigated in detail as a function of time. All the tests were performed at room temperature ( $20 \pm 2$  °C).

Table 8.2 HPC mix design ( $\text{kg/m}^3$ )

| Mix                                | HPC  |
|------------------------------------|------|
| Cement (CEM I 52.5 R)              | 495  |
| CA, granite, 2-5 mm                | 868  |
| FA, sea gravel, 0.1-1.5 mm         | 782  |
| Silica fume                        | 55   |
| Super-plasticizer                  | 11   |
| Glass fibers                       | 4.0  |
| Polypropylene fibers               | 2.0  |
| Total dry mass                     | 2206 |
| Water-cementitious material ratio  | 0.25 |
| Water-cementitious material ratio* | 0.27 |

\*including the water content of the superplasticizer

The compressive strength and static elastic modulus were determined according to Eurocode 2 (Bamforth et al., 2007). The specimen geometry for mechanical tests is specified in Table 8.3.

Table 8.3 Specimen geometry for different tests

| Test                   | Specimen geometry      |
|------------------------|------------------------|
| Compressive strength   | W/H/L = 40/40/40 mm    |
| Tensile strength       | W/H/L = 100/100/100 mm |
| Static elastic modulus | W/H/L = 100/100/100 mm |

The mean values of mechanical properties for HPC are presented in Table 8.4. At the given age, 12 specimens were tested to gain a representative behaviour for each test. The reinforcement and shear connectors were made from steel with a Young's modulus,  $E_s$ , equal to  $2 \cdot 10^5$  MPa and minimum yield strength guaranteed by the producer,  $f_{yk}$ , to be equal to 420 MPa.

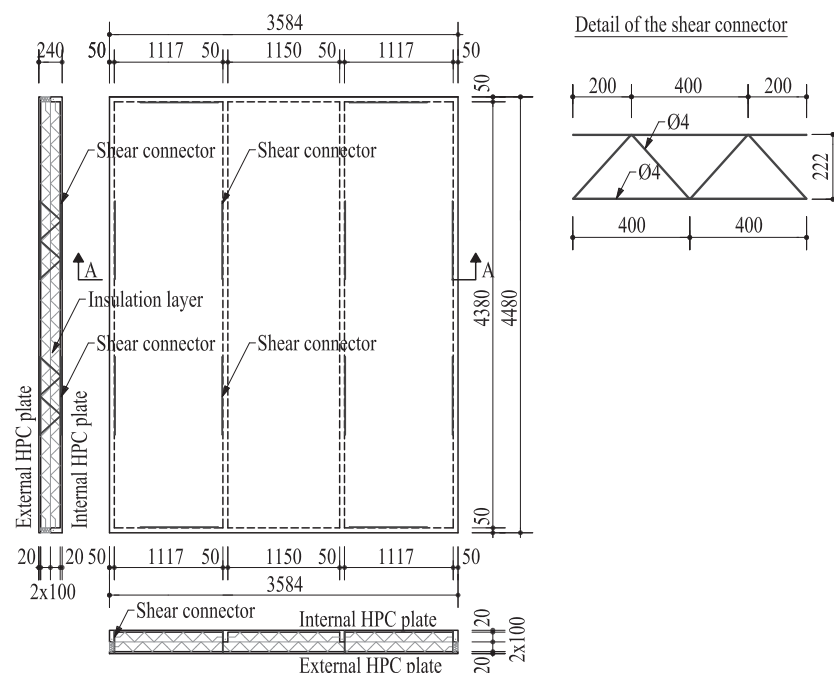


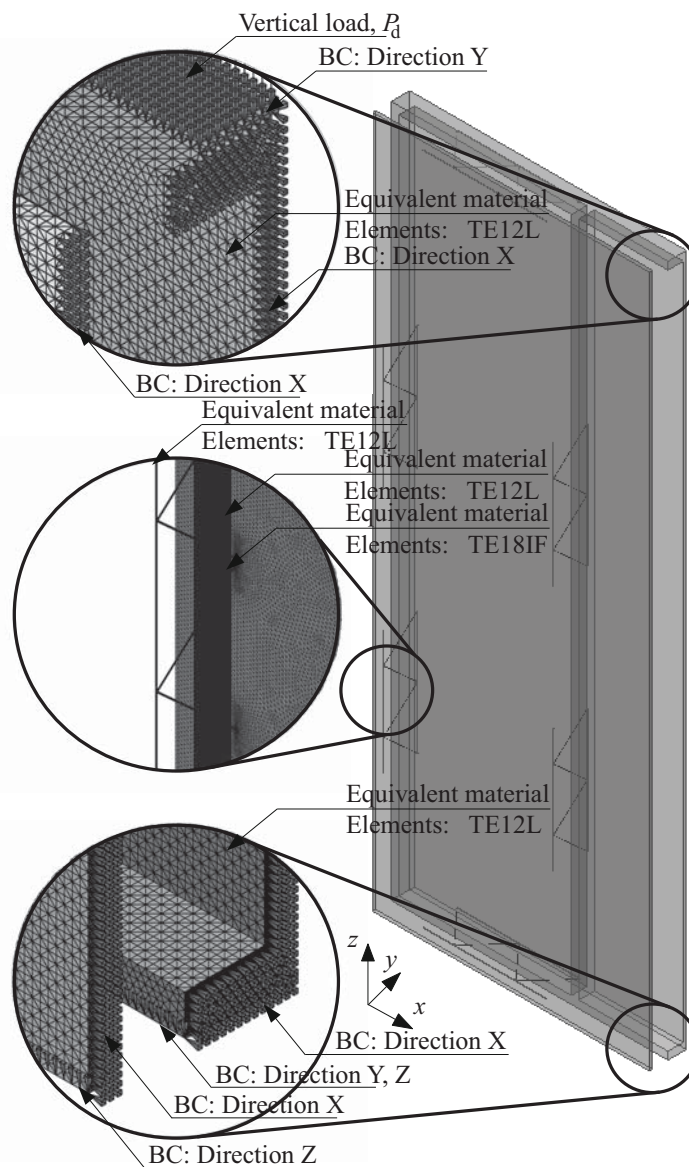
Figure 8.7. Drawing of the thin-walled sandwich element together with the detail of the shear connector used for the case study.

Table 8.4 *Mean values of mechanical properties of HPC*

| Mix | Age<br>(days) | $f_{cm,cube}$<br>(MPa) | $f_{cm,sp}$<br>(MPa) | $E_{cm}$<br>(GPa) | $G_{fm}$<br>(N/m) | $l_{chm}$<br>(mm) |
|-----|---------------|------------------------|----------------------|-------------------|-------------------|-------------------|
| HPC | 1             | 47.4                   | 3.4                  | 25.0              | 158.2             | 342               |
|     | 3             | 64.9                   | 4.8                  | 45.5              | 161.0             | 317               |
|     | 7             | 65.0                   | 5.9                  | 48.5              | 167.8             | 233               |
|     | 28            | 81.6                   | 6.5                  | 52.3              | 168.9             | 209               |
|     | 56            | 85.2                   | 6.7                  | 54.2              | 173.6             | 209               |

### 8.6.2 FE model

The FE model for the case study was also developed using the finite element analysis software DIANA with pre- and post-processor FX+ (TNO DIANA, 2011). An overview of the model developed in FX+ and the corresponding elements and model definitions are described in Fig. 8.8.

Figure 8.8. *Overview of the developed model.*

The symmetry of the sandwich panel allowed for only half of the panel to be considered in the FE model. The FE model was established as a phased analysis for 56 days. The applied element for HPC, shear connectors and reinforcement was a four-node, three-side isoparametric solid pyramid element (*TE12L*). Interface elements (*TE18IF*) were used for the embedded parts of reinforcement and shear connectors into the HPC. No bond-slip was prescribed for the interface between the reinforcement, shear connectors and HPC, such that perfect bond was assumed. In regards to the rebar and shear connectors, a simple elasto-plastic law was applied. The presence of the insulation layer was disregarded from the FEM analysis. Some researchers used the same approach under the assumption that the bond between concrete plates and insulation becomes discontinuous during shipping or erection or due to cyclic differential volume changes during the service life of the panel (Salmon, 1997), (Benayoune et al., 2008), (Benayoune et al., 2007), (Benayoune et al., 2006).

The applied vertical loads correspond to the design load transferred by roof,  $P_d$ , and the self-weight of the sandwich element,  $G$ . The design load,  $P_d$ , equivalent to 52.1 kN/m, was applied two weeks after the production of the elements. The vertical loads were simulated by pressure load applied to the upper rib of the internal HPC plate, as shown in Fig. 8.8. In order to ensure this condition in practice the connections between the sandwich elements and the slabs are designed to only transfer the vertical load and do not transfer moments (simply supported slabs over neoprene pads installed on the top surface of the internal HPC plate). Furthermore, the adopted mesh size was found to yield satisfactory convergence.

The time dependent effective shrinkage,  $\varepsilon_s^e$ , was imposed on the sandwich element over a period of 56 days. The effective autogenous shrinkage,  $\varepsilon_s^{a,e}$ , and drying shrinkage,  $\varepsilon_s^d$ , was measured in previous research campaigns and is summarized in Fig. 8.9.

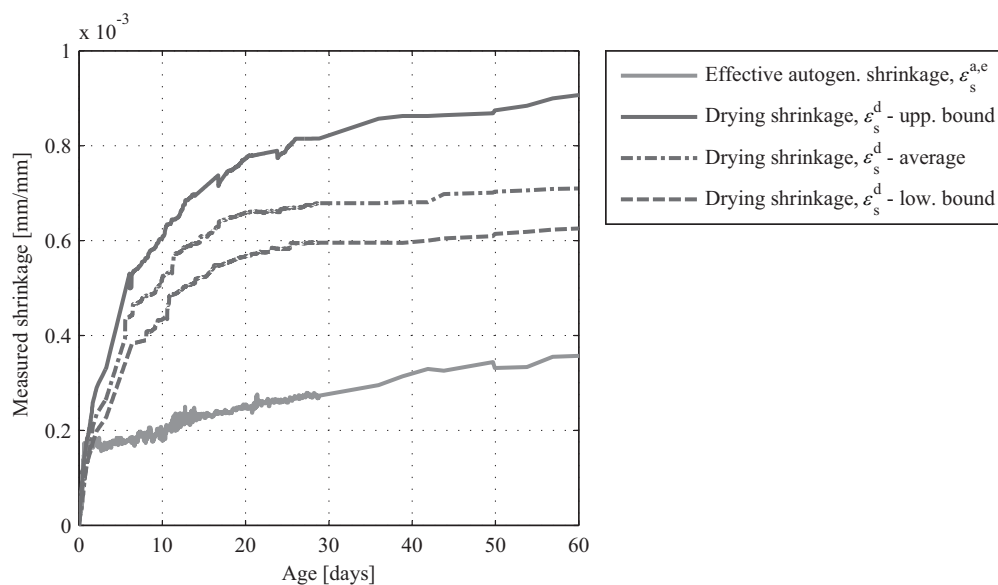


Figure 8.9. Measured shrinkage,  $\varepsilon_s$ , over a period of 56 days.

More details pertaining to the campaign can be found in the author's ref. (Hodicky, 2015). The effective drying shrinkage,  $\varepsilon_s^{d,e}$ , was not measured in the scope of the previous research campaigns. Thus, the effective drying shrinkage was recalculated based on measured drying shrinkage,  $\varepsilon_s^d$ , and relaxation functions over time for a similar type of HPC found in literature (Habel, 2004). The effective autogenous shrinkage,  $\varepsilon_s^{a,e}$ , and effective drying shrinkage,  $\varepsilon_s^{d,e}$ , are depicted in Fig. 8.10. The effective drying shrinkage,  $\varepsilon_s^{d,e}$  is presented as upper and lower bound as well as an average curve based on eight measurements. In addition to the four curves, the superposition of the effective autogenous shrinkage,  $\varepsilon_s^{a,e}$ , and effective drying shrinkage,  $\varepsilon_s^{d,e}$ , are plotted.

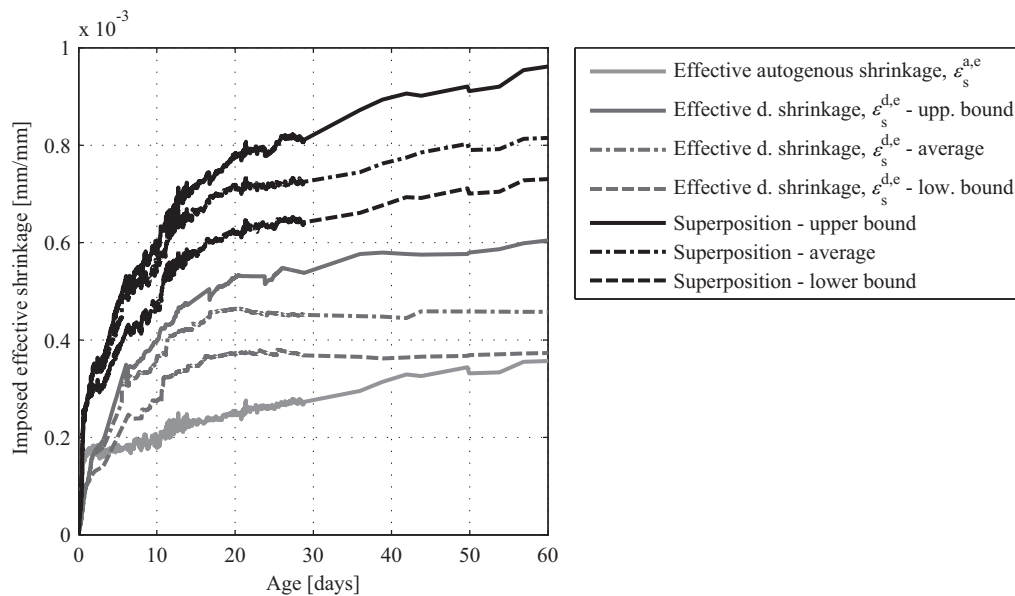


Figure 8.10. *Imposed effective shrinkage,  $\varepsilon_s^e$ , over a period of 56 days.*

### 8.6.3 Results and discussion

Based on modelling work presented in the previous section, the tensile (principle) stress,  $\sigma_I$ , exceeded the tensile strength of concrete,  $f_t$ , in the vicinity of the shear connectors. As was already mentioned in the previous section (Section 8.5), to evaluate the risk of early age cracking in concrete elements with the geometry comparable to an infinite sheet under the assumption of fully fixed restraints, Fig. 8.6 may be used. However, in real case applications, the restraints may have different stiffness properties than fully fixed restraints. In order to use Fig. 8.6 in different scenarios other than fully fixed restraints, the stiffness of the restraints,  $k$ , have to be evaluated. To address a different degree of stiffness, a large number of parameter variations have been investigated using a linear elastic FE model. The stiffness of the restraints,  $k_c$ , in the case study was measured experimentally and found to be equal to  $3.1 \cdot 10^6$  N/m.

The results of the parametric investigation related to the restraint's stiffness for the linear elastic FE model are presented in Fig. 8.11. Based on the comparison of the dimensionless parameter,  $\alpha$ , for the given stiffness of the restraint,  $k$ , and fully fixed re-



straint ( $k = \infty$ ), the reduction factor,  $\gamma$ , may be obtained. Therefore, in order to directly use the Fig. 8.6 and evaluate the risk of early age cracking for the given elements, the values of the imposed effective shrinkage,  $\varepsilon_s^e$ , should be adapted using the reduction factor,  $\gamma$ .

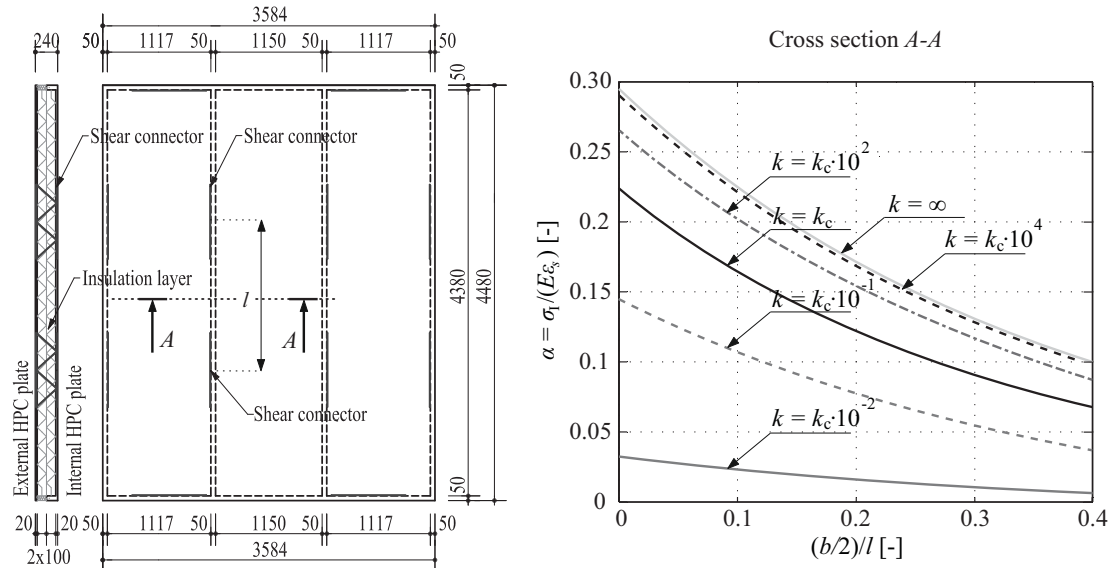


Figure 8.11. Dependencies of restraint's stiffness on the parameter,  $\alpha$ , for linear elastic FE model.

For simplicity only the upper bound of imposed effective shrinkage,  $\varepsilon_s^e$ , is considered in the assessment. Assessment risk of cracking for the thin-walled sandwich elements made of the HPC is depicted in Fig. 8.12.

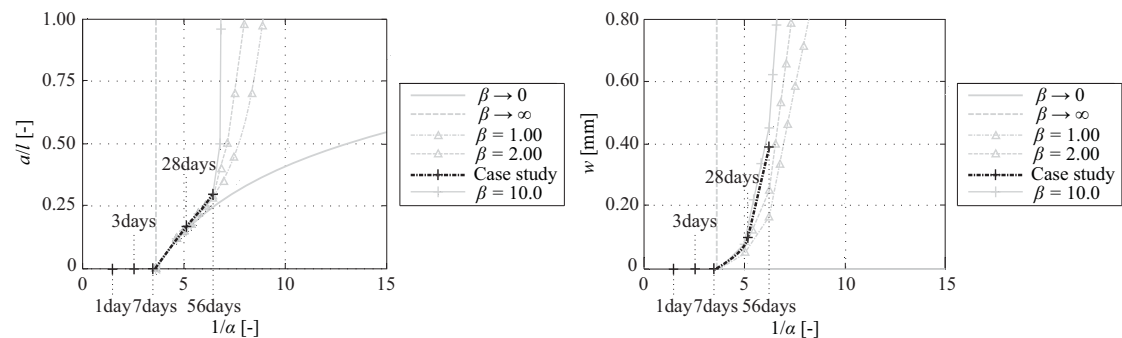


Figure 8.12. Assessment risk of cracking for the thin-walled sandwich elements made of the HPC over a period of 56 days.

Fig. 8.12 presents the analysis for 56 days, where it can be observed that the crack between the restraints starts to propagate approximately after eight days. The crack opening,  $w$ , was observed to be approximately 0.10 mm at 28 days and 0.40 mm at 56 days after casting of the elements. The modelling work proved that proposed approach fits very well with the observation on site, i.e. the structural macro-cracking appeared between four weeks to three months after casting as previously mentioned.



## 8.7 Conclusion

The paper presented a rough approach to analyze the robustness of thin-walled sandwich panels at early ages. The approach investigated the external HPC plate subjected to a constrained shrinkage load,  $\varepsilon_s$ . A parametric study of an infinitely large sheet was analyzed for 214-parameter variations. It has been shown numerically that the results of the non-linear analysis are highly dependent on the distance between the restraints,  $l$ . The results of the non-linear analysis were plotted into 11 different curves as a function of the dimensionless parameter  $\beta$ . The theoretical boundaries were presented by two individual curves. It was discovered that in order to propagate the crack in the centre of the plate, imposed shrinkage,  $\varepsilon_s$ , should to be approximately four times greater than  $f_t/E$ . Generally, when imposed shrinkage,  $\varepsilon_s$ , is up to six times greater than  $f_t/E$ , all the solutions approximately follow the linear FE solution. Further increase of imposed shrinkage,  $\varepsilon_s$ , was found to lead to the deviation from the linear FE solution. The rate function, the deviation of the non-linear FE solution from the linear FE solution depended on the dimensionless parameter,  $\beta$ . An increase of the dimensionless parameter,  $\beta$ , caused unstable crack growth to occur. The results also revealed that the crack propagated stably as long as the values of dimensionless parameter,  $\beta$ , were below 1. Accordingly, the results of of dimensionless parameter,  $\beta$ , above 1 led to unstable crack propagation.

Even though the parametric study has been undertaken only for a linear elastic softening material, the conclusion should also hold for variations of the softening branch, as long as the fracture energy,  $G_F$ , and critical crack opening,  $w_c$ , are related to the initial slope of the non-linear softening relationship. The proposed model showed that the theory and associated assumptions presented in the present paper are applicable with reasonable accuracy.

Further, the case study was performed for novel thin-walled sandwich elements made of fiber-reinforced HPC. The results of the case study proved that the proposed approach fits reasonably well with the observations on site, i.e. the ability to predict when crack growth becomes unstable and when structural macro-cracking is expected to appear.

## 8.8 Acknowledgments

The authors would like to acknowledge the Danish National Advanced Technology Foundation and Connovate for financial support.

## Chapter 9

### Journal paper 4

Title: Cost Optimization of Load Carrying Thin-walled Precast High Performance Concrete Sandwich Panels

Authors: Kamil Hodicky, Sanne Hansen, Thomas Hulin, Jacob W. Schmidt and Henrik Stang

Published in: Journal of Structural and Multidisciplinary Optimization

## Abstract

The paper describes a procedure to find the structurally and thermally efficient design of load-carrying thin-walled precast High Performance Concrete Sandwich Panels (HPCSP) with an optimal economical solution. A systematic optimization approach is based on the selection of material's performances and HPCSP's geometrical parameters as well as on material cost function in the HPCSP design. Cost functions are presented for High Performance Concrete (HPC), insulation layer, reinforcement and include labour-related costs. The present study reports the economic data corresponding to specific manufacturing process and actual financial parameters for the Danish pre-fabrication industry. The strength based design of HPCSP is in competence with the format of Eurocode 2 and takes into account failure modes related to flexure, shear, HPCSP buckling/slenderness, local HPC plate buckling and maximum deflections. The solution of the optimization problem is performed in the computer package software Matlab® with SQPlab package and integrates the processes of HPCSP design, quantity take-off and cost estimation. The proposed optimization process outcomes in complex HPCSP design proposals to achieve minimum cost of HPCSP.

## 9.1 Introduction

According to the European Union (EU, 2010) residential and commercial buildings are responsible for about 40% of the total energy consumption and CO<sub>2</sub> emissions in Europe. Ambitious targets for energy consumption of new buildings are being implemented, and by the year 2020 nearly zero energy buildings will become a requirement in the European Union. As a consequence of these requirements as well as general requirements for increased efficiency and sustainability, the building sector is experiencing a growing demand for modular, light and strong building elements. These elements need to have a high degree of insulation, a long lifetime, a low CO<sub>2</sub> emission, a low consumption of raw materials, and an attractive surface with minimum maintenance. Thus, finding the balance between structural performances and economically optimal solution in building design is needed. Load carrying thin-walled precast High Performance Concrete Sandwich Panels (HPCSP) are an interesting option for future low or plus energy building constructions in countries with low seismic activity. Such elements are structurally, thermally and sustainably efficient elements for exterior walls in multi-stories residential, commercial and warehouse buildings. The HPCSP have several beneficial features such as high quality, proven durability, fast erection, and attractive architectural appearance (Einea et al., 1994).

HPCSP consists of two precast High Performance Concrete (HPC) plates and a layer of insulation that separates the two HPC plates. Shear connectors penetrate the insulation layer and join the two HPC plates. In most cases, the HPC plates are reinforced by rebars and/or reinforcing mesh made of steel or various types of Fiber Rein-

forced Polymer (FRP) materials. A typical HPCSP geometry is given in Figure 9.1, where the panel height is ( $h_w$ ) and length ( $L$ ), respectively;  $t_b$ ,  $t_f$ ,  $t_r$  and  $t_{ins}$  are the thicknesses of the internal HPC plate, external HPC plate, rib structure and insulation layer, respectively;  $w_r$  denotes width of the rib structure;  $t$  is the total thickness of the HPCSP.

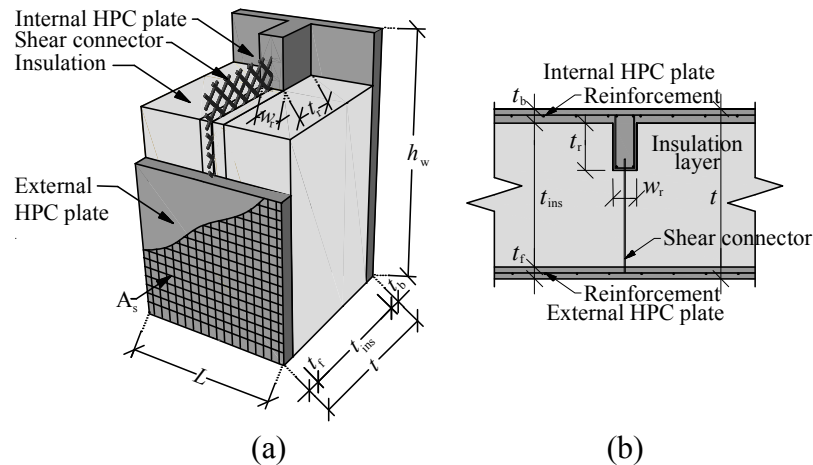


Figure 9.1. Typical HPC sandwich panel geometry a) 3-D view b) Top view.

The structural behaviour of HPCSP is usually stated in the literature as corresponding to that of multi-layered beams with deformable interlayer connection (Ranzi, 2008; Sousa Jr & da Silva, 2010; Gara et al., 2012). The degree of interaction between the various layers provided by the shear connector is referred to as the degree of composite interaction. The HPCSP may be designed with various degrees of composite interaction: non-composite, partial composite or full composite (S. H. Rizkalla et al., 2009). Two main categories of connectors exist: non-shear connectors and shear connectors. Non-shear connectors are used in non-composite HPCSP primarily to resist the tensile forces required to maintain integrity of the panel by keeping two HPC plates attached. Shear connectors are anchored in the external and internal HPCSP in a way that provide adequate stiffness and strength to create significant composite behaviour of the panel to resist the ultimate and service loads. The connections between the plates have traditionally been made by using bent reinforcing bars or various specially-designed steel or non-metallic connectors (Frankl et al., 2008).

Recently, the sandwich panel design concept has leaped forward by the introduction of FRP shear connectors, due to the relatively high stiffness combined with its relatively low thermal conductivity compared to steel (Soriano & Rizkalla, 2013). Wade et al. (1988) performed the first attempt to use Glass Fiber Reinforced Polymer (GFRP) connectors for insulated concrete sandwich walls. Salmon et al. (1997) introduced GFRP bars formed in a truss orientation substituting metal wire trusses. The experimental investigation showed that the use of GFRP resulted in 84 % composite interaction compared to 88 % for steel truss connectors. Following the same concept, Maximos et al. (2007), Morcoux et al. (2010) and Lameiras et al. (2013a, 2013b) studied different shapes of GFRP shear connectors to obtain full composite interaction.

Rizkalla et al. (2009) and Hodicky (2015) focused on using Carbon Fiber Reinforced Polymer (CFRP) and Basalt Fiber Reinforced Polymer (BFRP) shear connector grids. Tests indicated that the use of CFRP and BFRP shear connector grids enabled development of composite interaction with minimum thermal bridges, enabling a consistent insulating value of the panel. It is seen from research that increasing the degree of composite interaction between two HPC plates using any type of connectors increases the structural capacity of the HPCSP making it more structurally efficient. However, increasing the degree of composite interaction may lead to lower thermal efficiency of the panel due to the creation of thermal bridges (Wade et al., 1988). Undesirable thermal deflection of HPCSP may occur due to thermal gradients over the thickness of the element. The thermal deflections in long HPCSP can be significant and may cause cracking due to solar exposure. Recent research and development work indicates that load-bearing thin-walled HPCSP are prone to structural cracking due to the combined effect of shrinkage and high temperature differentials (Hodicky et al., 2013a). The bond between the insulation and HPC plates provides some shear transfer, but this bond can diminish over time and thus will not provide full strength over the life time of the panel (Salmon et al., 1997). The insulation layer mainly provides thermal efficiency of the HPCSP and its efficiency depends on the thickness and type of the insulation material as well as the amount and type of penetrations through insulation layer.

In the literature minimum cost design of reinforced concrete structures (Kanagasundaram & Karihaloo, 1990; Fadaee & Grierson, 1996) is generally related to beams (Al-Salloum & Husainsiddiqi, 1994; Barros, Martins, & Barros, 2005), columns (Kanagasundaram & Karihaloo, 1991) and footings (Camp & Assadollahi, 2013). Several authors have attempted to optimize concrete sandwich panels (Maximos et al., 2007; Morcoux et al., 2010; Hassan & Rizkalla, 2010; Naito et al., 2012). Their work focused on how to experimentally reach a full composite interaction in standard thick-walled concrete sandwich elements and fulfil the requirements for thermal properties and material reduction. None of these authors addressed material cost of those elements. Papanicolaou & Triantafillou (2002, 2004) performed a minimum material cost design of thick-walled concrete sandwich panels with pumice aggregate concrete (PAC) core in combination with foam core for the case of in-plane and out-plane loading. However, their work was limited to concrete sandwich panel used in countries with high seismic activity. Full composite behaviour of the panels was considered in this campaign. The literature reveals that there is a lack of methods, guidelines and optimization studies in the design of load carrying thin-walled HPCSP.

The scope of the research summarized in this paper is to present a general optimization procedure of HPCSP obtaining an optimal economical solution (minimum material cost) subjected to structural and thermal constraints – given the load cases. The economic data correspond to specific manufacturing process and actual financial parameters for the Danish prefabrication industry. A quick, accurate and systematic optimization procedure to HPCSP design is proposed. The tool integrates the processes of HPCSP design, quantity take-off and cost estimation. The proposed optimization

procedure results in complex of HPCSP design recommendations, which fulfil the requirement of minimum cost for those elements.

## 9.2 Optimization problem

In the present work material cost is minimized while fulfilling requirements to structural and thermal performance. In the cost function only those costs that contain the design variables are included, and the economy is achieved by changing these variables to minimize the cost function. Quantitative data regarding statistical behaviour of production parameters has to be taken into account. This implies cost data collection from current and previous projects and materials suppliers to create a reference database. Although the economic data of raw materials vary across regions and countries and are influenced by local energy costs, labour and material resources, attention should not be focused on single cost values. The present study reports the economic data corresponding to actual financial costs for the Danish prefabrication industry. Hence, the present cost study is used to draw useful conclusions on relative influences of design variables and variations on the HPCSP cost and consequently to propose the optimum design solution. The work includes the material costs and ignores others such a transportation and assembly costs of HPCSP. Further, the cost associated with the production facilities is not taken into consideration as the cost is considered to be included in fixed production plant investment costs. It should be noted that the proposed optimization procedure refers to specific manufacturing process. Therefore, the labour-related cost in this study includes molding, mixing and casting of HPC, the placement of reinforcement and insulation layer.

In the literature the term of HPC is typically assigned to a concrete with characteristic compressive strength,  $f_{ck}$ , between 50 MPa to 120 MPa (Aïtcin, 2011). The present study focuses on the HPC with strengths in the same range. Tensile strengths and modulus of elasticity of HPC are derived from the compressive strength (Bamforth et al., 2007). It is assumed that the minimum HPC cover requirements are satisfied and reinforcement is fully protected against corrosion. It is assumed that the panel height ( $h_w$ ), length ( $L$ ), load, thermal transmittance of HPCSP, type and materials for shear connectors/reinforcement are fixed prior optimization procedure. Only steel reinforcement and shear connectors are considered in the present study. The strength based design of HPCSP is in competence with the format of Eurocode 2. Further, the optimization process considers, whereas the rib construction is beneficial and cost efficient for design or not. Finally, boundary conditions must be specified taking into account subgrade friction, temperature gradients over the thickness and connections between HPCSP. In the present study a simply supported HPCSP is considered.

### 9.2.1 Formulation of the optimization problem

Mathematically, the optimization problem is formulated by minimizing the objective function  $f(x)$  (Fadaee & Grierson, 1996; Papanicolaou & Triantafillou, 2002, 2004).

$$\text{minimize } f(x) \quad (9.1)$$

where the  $x$  is subjected to the equality (9.2a), inequality (9.2b) and boundary constraints (9.2c), respectively.

$$y_i(x) = 0 \quad (9.2a)$$

$$y_i(x) \leq 0 \quad (9.2b)$$

$$x_{\min} \leq x \leq x_{\max} \quad (9.2c)$$

where vector  $x$  stands for design variables,  $x_{\min}$  and  $x_{\max}$  are the lower and upper bounds for the variables, respectively;  $f(x)$  is the objective function that returns a scalar value and  $y(x)$  is vector function that expresses the constraints in terms of equality and/or inequality evaluated at  $x$ . Formulation of the optimization problem in the sense of minimum cost design of HPCSPs is highly dependent on careful selection of the optimization variables. Generally, the optimization variables are the ones required for detailed description of the system (Arora, 2012). Different design variables can be assigned to the design of the HPCSP, e.g. HPCSP thickness, degree of composite interaction, reinforcement ratio, composition of the HPCSP and choice of materials. However, it is preferred to constrain their number, so only the most important cost components are considered in the objective function. To address key issues in a practical application case, the design variables vector  $x$  is taken to be equal to

$$x = \{k, f_{cd}, \rho_{sw}, t_b, t_f, t_r, w_r, t_{ins}, t\} \quad (9.3)$$

where  $k$  is the degree of composite interaction,  $f_{cd}$  is the design value of HPC compressive strength,  $\rho_{sw}$  stands for the reinforcement ratio. It is assumed that compressive strength can be used as an independent optimization variable. In practise, however, changing compressive strength has a number of associated consequences such as:

1. HPC mix must be designed to minimize autogenous shrinkage
2. Provide adequate strength to meet the design load
3. High early age strength (time-related production cycles)
4. Durability (life time up to 100 years)
5. Improved crack control (avoiding damage risks during lifting, transport and assembly)
6. Maximum aggregate in case of thin-walled HPCSPs size should not exceed 10mm

The lower and upper bound of the design variables vector applied in this study are given below

$$x_{\min} = \{0, 35.7 \text{ MPa}, 2.0 \%, 10 \text{ mm}, 10 \text{ mm}, 50 \text{ mm}, 50 \text{ mm}, 160 \text{ mm}, 180 \text{ mm}\} \quad (9.4a)$$

$$x_{\max} = \{1, 85.7 \text{ MPa}, 4.0 \%, 70 \text{ mm}, 70 \text{ mm}, 150 \text{ mm}, 150 \text{ mm}, 400 \text{ mm}, 500 \text{ mm}\} \quad (9.4b)$$

where 0 and 1 assigns non-composite interaction and full composite interaction, respectively. The minimum and maximum degree of reinforcement is specified in accordance with Eurocode 2 (CEN, 2010). The geometric variables are based on practical consideration, since standard limits do not exist. The total thickness of the HPCSP is the sum of individual thicknesses of the internal HPC plate, external HPC and insulation layer, respectively. Often thinner wall thickness, thus thinner insulation layer is desirable as it gives more square meters for living areas in areas where the build density is high and/or the size of the building site is limited. Thus, the lower and upper bound of total thickness of the HPCSP is constraint to 180 mm and 500 mm, respectively.

### 9.2.2 Objective function

Generally, the objective of HPCSP development is to establish the elements with an optimal economical solution (minimum material cost) subjected to structural and thermal constraints. The cost function is described as the sum of material cost functions that already include other costs, such as labour cost per unit volume; mixing, casting of HPC mix and reinforcing of HPC plates and transport of raw materials. The total cost of HPCSP,  $C$  per unit width (1m') is shown beneath:

$$C = t_b h_w 1\text{m}' C_{\text{HPC}} + t_f h_w 1\text{m}' C_{\text{HPC}} + t_r w_r h_w C_{\text{HPC}} + (t_{\text{ins}} 1\text{m}' - t_r w_r) h_w C_{\text{ins}} + \gamma_s \rho_{\text{sw}} (t_b 1\text{m}' + t_f 1\text{m}' + t_r w_r) h_w C_{\text{sh}} \quad (9.5)$$

where  $C_{\text{HPC}}$  and  $C_{\text{ins}}$  stand for the cost per unit volume of the HPC plates and insulation layer, respectively;  $C_{\text{sh}}$  is the cost of shear connectors/reinforcement per unit weight;  $\gamma_s$  stands for shear connectors/reinforcement density (density of steel).

### 9.2.3 Design prerequisites

The HPCSP used as a wall panel is subjected to both horizontal and vertical loads. It is considered that the vertical load is transferred through the slabs to the load-bearing HPCSP and into the foundations through the internal HPC plates that face the interior of the building. The lateral wind loads  $w_d$  are resisted by the HPCSP spanning between slabs or the slabs and foundations. The slabs are considered to act as horizontal diaphragms taking the horizontal loads into the shear walls. The vertical loads corre-



spond to self-weight and the loads transferred by the slabs. This vertical load is acting on the upper rib of the internal HPC plate. In order to assure this condition in practice, the floor slabs are resting on neoprene pads installed on the upper rib of the internal HPC plate, see Figure 9.2.

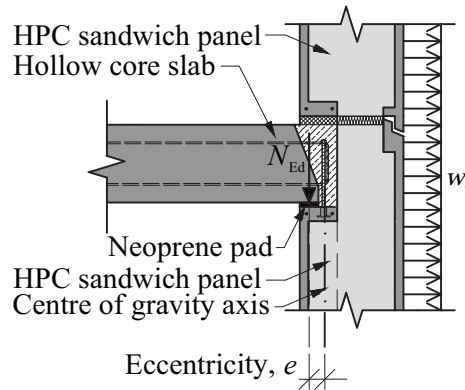


Figure 9.2. *Schematic representation of slab support conditions and forces transferred by the slab.*

It should be noted that actions during handling, transportation and erection have not been taken into consideration in this work. Design bending moment  $M_{Ed}$  is calculated according Eq. 9.6

$$M_{Ed} = N_{Ed}e + \frac{1}{8}w_d h_w^2 \quad (9.6)$$

where  $e$  is an eccentricity of vertical load.

#### 9.2.4 Constraints

All the design constraints should be carefully set before its optimization process. A proper selection of constraints leads to faster convergence solutions and significant reduction of computation time. The Ultimate and Serviceability Limit State (ULS and SLS) serve as key design constraints. Thus, for any given design variables vector  $x$ , the ULS constraints are the following:

$$y_1 = M_{Ed} - M_{Rd} \leq 0 \quad (9.7a)$$

$$y_2 = V_{Ed} - V_{Rd} \leq 0 \quad (9.7b)$$

$$y_3 = N_{Ed} - N_{Rd} \leq 0 \quad (9.7c)$$

$$y_4 = \sigma_{cd,max} - \sigma_{cr,min} = 0 \quad (9.7d)$$

where  $M$ ,  $V$  and  $N$  are bending moment, shear and compressive axial loads (with the subscripts Ed and Rd representing design values and limit states), respectively;  $\sigma_{cd,max}$  is the maximum design compressive stress in HPC and  $\sigma_{cr,min}$  is the minimum critical compressive stress for local buckling of the HPC plates.

SLS constraints related to maximum deflections are prescribed by national codes and standards, see e.g. CEN (2010). Further, design of HPCSP has to limit any structural cracking:

$$y_5 = \delta_y \leq h_w/300 \quad (9.7e)$$

$$y_6 = \sigma_{ctd,max} - \sigma_{ct,crack} = 0 \quad (9.7f)$$

where  $\delta_y$  is maximum deflection of HPCSP,  $\sigma_{ctd,max}$  is the maximum design principle stress in HPC and  $\sigma_{ct,crack}$  is the tensile stress when cracks occur.

Finally, the thermal resistance requirement has to be set as a design constraint. The insulation thickness and type for walls are not prescribed directly by national codes and standards, but there are indirect constraints which relate to the required U-value for walls in form of a national energy performance requirement which limits the total energy consumption of buildings (Energy Styrelsen, 2014). For 2015, the energy performance requirement in Denmark is 31-51 kWh/m<sup>2</sup>/year depending on the type and size of the building and for 2020, the energy performance requirement is 20-25 kWh/m<sup>2</sup>/year depending on type of the building. Hansen (2012a) performed an economical optimization of building elements, such as walls, roof, floor, joints, ventilations units, to find the optimal economical solution with specific constraints such as the insulation thickness/U-value of the walls based on the energy performance requirement for nearly zero energy buildings. The result showed that the maximum U-value should be about 0.14 W/m<sup>2</sup>K for the 2015 demands and about 0.07 W/m<sup>2</sup>K for the 2020 demands. For highly insulated HPCSP, i.e. elements where at least 60 mm insulation layer is unbroken by rib structure, the insulation portion of the U-value is predominant. Thus, the part of the U-value that comes from the HPC plates and the heat transfer coefficients can be ignored for simplicity (Hansen, 2012b). The constraint for the insulation type and thickness is given in Eq. 9.7g

$$U \leq U_{max} \Leftrightarrow \frac{1}{R_{si} + \frac{t_b}{\lambda_{HPC}} + \frac{t_f}{\lambda_{HPC}} + \frac{t_r}{\lambda_{rib}} + \frac{t_{ins}}{\lambda_{ins}} + R_{se}} \Rightarrow y_7 = \frac{1}{\frac{t_{ins}}{\lambda_{ins}} + \frac{t_r}{\lambda_{rib}}} - U_{max} \leq 0 \quad (9.7g)$$

where  $R_{si}$  and  $R_{se}$  is the inner and outer heat transfer coefficient, respectively;  $\lambda_{HPC}$ ,  $\lambda_{ins}$ ,  $\lambda_{rib}$  is the thermal conductivity for the HPC, insulation layer and rib structure, respectively. Thermal conductivity of rib structure is calculated as:

$$\lambda_{rib} = \frac{(w_r \lambda_{HPC} + (w_{br} - w_r) \lambda_{ins})}{w_{br}} \quad (9.8)$$

where  $w_{br}$  is the distance between the ribs.

### 9.3 Ultimate and serviceability limit state analysis of HPCSP

The thin-walled HPCSP may reach failure due to flexure, shear, global buckling, and local buckling due to compression of the HPC plates. Also cracking in HPC plates or exceeding maximum deflections should be addressed.

For any given bending moment  $M_{Ed}$  and axial force  $N_{Ed}$ , the corresponding stresses in the internal and external HPC plates can be determined by assuming full composite interaction using stress compatibility and equilibrium of the HPCSP section. The assumed stress distribution in this case is illustrated in Figure 9.3, top right part.

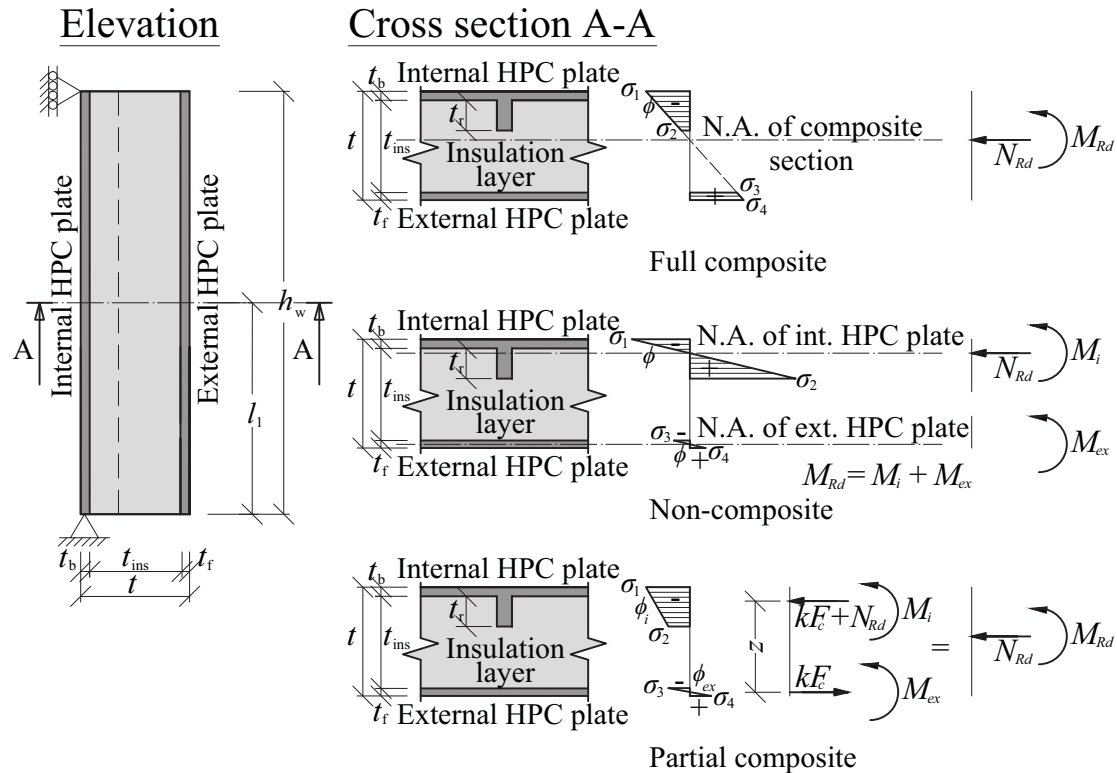


Figure 9.3. *Strain distribution in HPCSPs with full composite, non-composite and partial composite interaction.*

The stresses  $\sigma_{1-4}$  are calculated as superposition of axial and flexural stresses.

$$\sigma_{1-4} = \sigma_{\text{axial}} + \sigma_{\text{flexural}} \quad (9.9)$$

where axial stresses are constant along the HPCSP height and calculated as

$$\sigma_{\text{axial}} = \frac{N_{Ed}}{A_{cb}} \Rightarrow N_{Rd} \geq \sigma_{\text{axial}} A_{cb} \quad (9.10)$$

where  $A_{cb}$  is area of the internal HPC plate.

### 9.3.1 Flexural failure mode

Traditionally, a full composite interaction arises when no slip occurs at the interface of two material layers. Therefore, there is a linear strain distribution over the whole section with the neutral axis at the centroid of the composite section. The non-composite interaction arises when no shear connection is established and the two HPC plates behave independently. Hence, there are two neutral axes at the centroid of the internal and external HPC plate. The presence of shear forces at the interface of the HPC plates and the insulating layer provides the mechanism for partial composite interaction. The following assumptions are made for the analysis of this case (Ranzi et al., 2006; Hassan & Rizkalla, 2010; Frankl et al., 2011):

1. The shear connectors between the HPC plates are assumed continuous along the length of the HPCSP.
2. The strain distributions along the depth of the internal and external HPC plate, respectively, are linear.
3. This model neglects the effects on any flexural stresses in the insulation layer, which can be expected to be very small.
4. The relative displacements between internal and external HPC plates are assumed to be equal at any point along the lengths. Hence, the curvature of the internal and external HPC plates is consistent at all loading stages as expressed in Eq. 7.11.

$$\phi_i = \phi_{ex} \quad (9.11)$$

where  $\phi_i$  and  $\phi_{ex}$  corresponds to the curvature of the internal and external HPC plate, respectively.

#### 9.3.1.1 Full composite interaction

Considering a simply supported HPCSP under uniformly distributed lateral load  $w_d$  (suction in the external HPC plate) acting along the entire height of the HPCSP, see Figure 9.4.

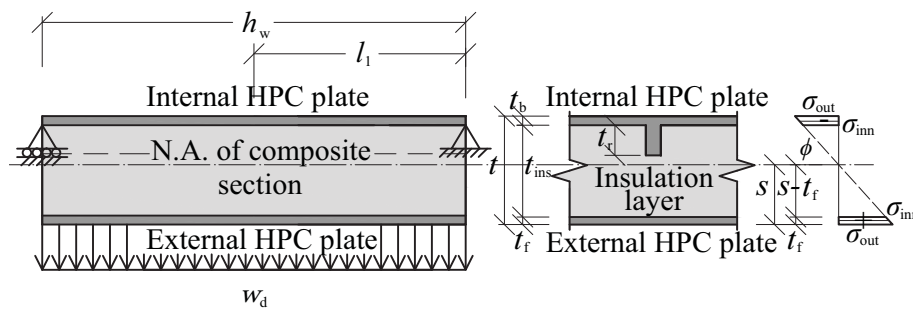


Figure 9.4. *Full composite HPCSP - Flexural stress distribution.*

The external HPC plate tends to lengthen, and conversely the internal HPC plate tends to shorten. At any vertical cross section of the HPCSP the uniform load induces a bending moment. Let  $\sigma_{\text{out}}$  denote the magnitude of the flexural stresses on the outer fibers at a cross section located at distance  $l_1$  from the end of the HPCSP. The familiar relationship

$$\sigma_{\text{out}} = \frac{M_{\text{Ed}}}{W_{\text{FC}}} \quad (9.12)$$

where  $W_{\text{FC}}$  represents the section modulus of the HPCSP, relates the bending moment to the maximum magnitude of the flexural bending stress at the cross section. The shear force at the interface between HPC plates and insulation layer maintains the equilibrium of the HPC plates. The required total horizontal shear force per unit width at the interface  $F_c$  can be evaluated at the interface of the external HPC plate and established by

$$F_c = \int_A \sigma \, dA = \frac{1}{2} t_f (\sigma_{\text{out}} + \sigma_{\text{inn}}) \quad (9.13)$$

where  $A$  is the cross sectional area of the HPC plate per unit width,  $\sigma_{\text{inn}}$  and  $\sigma_{\text{out}}$  denotes the magnitude of the flexure stresses on the inside and outside of the external HPC plate in the uniformly loaded, simply supported HPCSP. The magnitude of the shear force  $F_c$  varies linearly with the location  $l_1$  along the height of the HPCSP. The maximum value of  $F_c$  is found for  $l_1 = h_w/2$ .

### 9.3.1.2 Partial composite interaction

An interaction force  $F$  smaller than  $F_c$ , implies partial composite interaction. Thus, the degree of composite interaction  $k$  can be evaluated by

$$k = \frac{F}{F_c} \quad (9.14)$$

The horizontal shear force  $kF_c$  acting on the external HPC plate must be

$$F = kF_c = \int_A \sigma \, dA = \frac{1}{2} (\sigma_{\text{out}} c_{\text{out}} - \sigma_{\text{inn}} c_{\text{inn}}) \quad (9.15)$$

where Figure 9.5 defines  $c_{\text{out}}$  and  $c_{\text{inn}}$ . Algebraic manipulation of Eq. 9.15 leads to the expression for the distance from the outer and inner HPC fibers to the neutral face for the external HPC plate, respectively, as

$$c_{\text{out}} = \frac{t_f + ks}{2} \quad \text{and} \quad c_{\text{inn}} = \frac{t_f - ks}{2} \quad (9.16)$$

When  $k = 0$  (non-composite interaction),  $c_{\text{out}} = c_{\text{inn}} = t_f/2$ . For values of  $k$  lying from 0 to 1, the HPC plates support the load-induced bending moment through combination of individual HPC plate bending and axial force, hence  $c_{\text{out}} \geq t_f/2$  and  $c_{\text{inn}} \leq t_f/2$ . The magnitude of the resultant of the flexural stress distribution on either HPC plate must be  $kF_c$ .

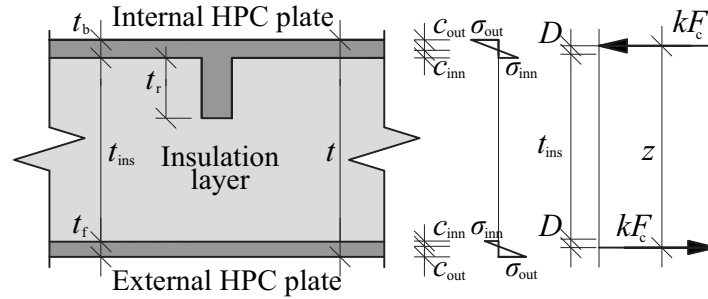


Figure 9.5. *Flexural strain distribution and their resultants.*

Further, this resultant of the forces induced by the flexural stresses on a single HPC plate must act at the centroid of the flexural stress distribution. The distance from the inside of HPC plate to the centroid of the stress distribution on the external HPC plate is

$$D = \frac{t_f}{3} \left( 1 + \frac{1}{k} \right) \quad (9.17)$$

The load-induced moment carried by a simply supported HPCSP to the horizontal shear force  $kF_c$  transferred between the HPC plates can be expressed as

$$\begin{aligned} M_{\text{Rd}} &= kF_c z = kF_c (2D + t_{\text{ins}}) = F_c \left[ \frac{2t_f}{3} (1 + k) + kt_{\text{ins}} \right] \\ &= t_f (\sigma_{\text{out}} + \sigma_{\text{inn}}) \left( \frac{t_f}{3} + \frac{kt_f}{3} + \frac{kt_{\text{ins}}}{2} \right) \end{aligned} \quad (9.18)$$

The magnitude of horizontal shear force, which is transferred by shear connectors to each HPC plate, must be equal. In order to evaluate stresses for partial composite interaction, the effective section modulus has to be introduced. Eq. 9.12 relates stresses on the outer fibers at a section located of HPCSP to the bending moment at that section. Rearranging Eq. 9.12 gives the effective section modulus for HPCSP as

$$\frac{W_{\text{eff}}}{W_{\text{FC}}} = \frac{M_{\text{Rd}}}{M_{\text{Ed}}} \quad (9.19)$$

Required tension reinforcement is calculated from

$$A_s = \frac{M_{Ed}}{f_{yd}z} \quad (9.20)$$

where  $f_{yd}$  is the design strength for reinforcement. Required amount of reinforcement has to be checked with minimum and maximum reinforcement requirements specified in Eurocode 2 (CEN, 2010).

### 9.3.2 Shear failure mode

The magnitude of the shear connectors demand is commonly computed using one of three methods (Naito et al., 2012). Technique 1 computes the shear demand from the flexural capacity of the section. This method is recommended by the Precast/Prestressed Concrete Institute (PCI Committee on Precast Sandwich Wall Panels, 2011). Technique 2 computes the shear demand assuming elastic response and considering the first moment of the area above the shear connector. Since the derivation of this method is based on the elastic response of the member, the accuracy is poor after cracking. Technique 3 approximates the shear connector demand from the transverse shear forces acting on the HPCSP. This method is recommended by ACI 318 (ACI Committee 318, 2008). In present paper the shear capacity of HPCSP can be expressed as

$$V_{Rd} = n\gamma_{sh}q_{sh} \quad (9.21)$$

where  $n$  is number of shear connectors required at a certain cross-section,  $\gamma_{sh}$  is partial safety coefficient for material and  $q_{sh}$  is shear flow capacity of the shear connector. The evaluation of shear flow capacity based on experimental studies for different types of shear connectors used in practise can be found in Maximos et al. (2007), Hassan & Rizkalla (2010), Morcous et al. (2010), Naito et al. (2012) and Hodicky et al. (2013b).

### 9.3.3 Global HPCSP buckling

Eurocode 2 (CEN, 2010) states the buckling problem can be ignored, if slenderness  $\lambda$  (Eq. 9.22a) is less than slenderness limit  $\lambda_{lim}$ . The slenderness limit can be expressed by Eq. 9.22b

$$\lambda = \frac{l_0}{i} \quad (9.22a)$$

$$\lambda_{lim} = \frac{20ABC}{\sqrt{\frac{N_{Ed}}{A_c f_{cd}}}} \quad (9.22b)$$

where  $l_0$  is the effective length,  $i$  is the radius of gyration and  $A_c$  represents the concrete area; coefficients  $A$ ,  $B$ ,  $C$  are assumed to have minimum values specified in Eurocode 2 (CEN, 2010). If  $\lambda > \lambda_{\text{lim}}$  HPCSP must be designed for an additional moment caused by its curvature at ultimate conditions, using Nominal Stiffness or Nominal Curvature method for calculation of reinforcement, see e.g. Eurocode 2 (CEN, 2010) and Lluca et al. (2013).

#### 9.3.4 Local HPC plate buckling

The HPC plates are subjected to in-plane axial loading and act as slender columns stabilized by the insulation layer. Under the in-plane axial loading the HPC plates may become wavy, see Figure 9.6.

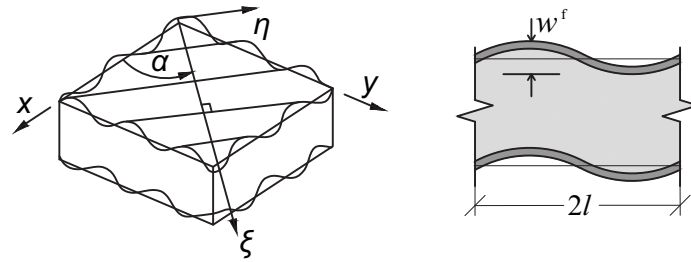


Figure 9.6. *Face local buckling of HPC plates.*

The structural defects in the form of a HPC plate indentation can be idealized as sinusoidal waves with amplitude  $w^f$ , as shown in Figure 9.6 right. For full composite HPCSP, face local buckling is unlikely to occur, unless manufacturing defects are present in one of the HPC plates due to insufficient concreting. The waves may propagate in two directions. However, in our analysis we consider only waves in one direction, since generally the waves in one direction dominate (Kollár & Springer, 2009). The wave length  $2l$  depends on the material and on the geometry of the HPCSP. The analysis considers that wave length is “long” such that  $l/t \gg 1$ . The following analytical approach is presented by Allen (1969), Kollár & Springer (2009), Vasiliev & Morozov (2013). The critical stress  $\sigma_{\text{cr,min}}$  at which de-bonding between insulation layer and HPC plates occurs due to local buckling of the HPC plate is given as

$$\sigma_{\text{cr,min}} = \frac{E_{\text{HPC}}}{12} \left( \frac{t_{\text{min}}}{t_{\text{ins}}} \right)^2 \mathcal{G}^2 + E_{\text{ins}} \left( \frac{t_{\text{ins}}}{t_{\text{min}}} \right)^2 f(\mathcal{G}) \quad (9.23)$$

where

$$\mathcal{G} = \frac{\pi t_{\text{ins}}}{l} \quad (9.24a)$$

$$f(\mathcal{G}) = \frac{2}{\mathcal{G}} \frac{(3 - \nu_c) \sinh \mathcal{G} \cosh \mathcal{G} + (1 + \nu_c) \mathcal{G}}{(1 + \nu_c)(3 - \nu_c)^2 \sinh^2 \mathcal{G} - (1 + \nu_c)^3 \mathcal{G}^2} \quad (9.24b)$$



$E_{\text{HPC}}$  and  $E_{\text{ins}}$  is the elastic modulus of HPC and insulation layer, respectively;  $\nu_c$  represents the Poisson's ratio of the HPC;  $t_{\min}$  denotes minimum thickness of HPC plates, i.e.  $\min(t_b, t_f)$ . For certain insulation material, the critical value of  $\vartheta$  is determined by solving  $d\sigma_{\text{cr}}/d\vartheta = 0$  for  $\vartheta$ .

### 9.3.5 Deflections and cracking in the HPCSP

The maximum deflections of HPCSP  $\delta_y$ , may be expressed by Eq. 9.25 as superposition of deflections caused by eccentricity of axial load  $N_{\text{Ed}}$  and lateral wind loads  $w_d$ .

$$\delta_y = \frac{N_{\text{Ed}} e h_w^2}{16EI} + \frac{5}{384} \frac{w_d h_w^4}{EI} \quad (9.25)$$

Assessment of cracking in HPCSP is performed based on Section 9.3.1, where the maximum design principle stress  $\sigma_{\text{ctd,max}}$  is taken into account. It is assumed that the tensile stress when cracks occur  $\sigma_{\text{ct,crack}}$  corresponds to characteristic tensile strength for a given HPC (Bamforth et al., 2007).

## 9.4 Material cost function

### 9.4.1 HPC plates

The HPC cost is generally expressed as a linear or non-linear function of its compressive strength for high-strength concretes (Papanicolaou & Triantafillou, 2002, 2004). In the present study HPC mix designs are compiled from 249 set of mixtures found in the literature (Mehta & Aïtcin, 1990; Rougeron & Aïtcin, 1994; Chang & Peng, 2001; Bharatkumar et al., 2001; Donza et al., 2002; Alves et al., 2004; Lim et al., 2004; Buhler, 2008; Nawy, 2008; Baykasoğlu et al., 2009; Brandt, 2009; Ozbay et al., 2010; Phelan, 2011; Megat Johari et al., 2011; Lee et al., 2012) and shown in Figure 9.7.

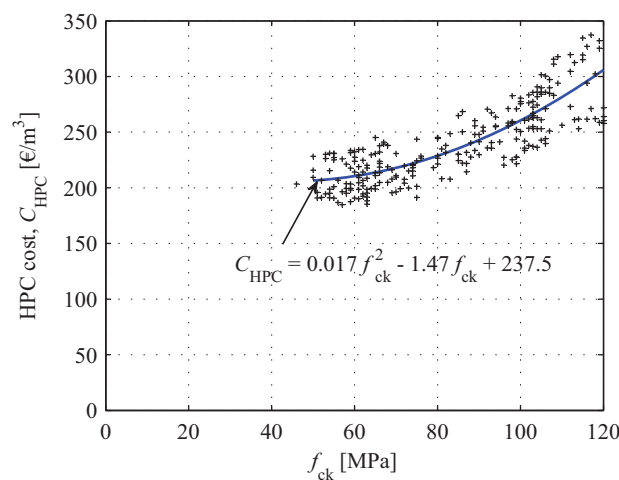


Figure 9.7. *The relationship between HPC cost and characteristic compressive strength.*

None of the HPC mixes contained fibres. The HPC cost varies within the range 205 and 305 €/m<sup>3</sup>. Individual material and labour costs are listed in Table 9.1.

Table 9.1 *Material and labour cost for HPC plates*

| Material and labour function         | Cost [€/kg] |
|--------------------------------------|-------------|
| Cement                               | 0.095       |
| Fine aggregate                       | 0.020       |
| Coarse aggregate                     | 0.034       |
| Fly ash                              | 0.272       |
| Microsilica                          | 0.408       |
| Ground granulated blast furnace slag | 0.136       |
| Superplasticizer                     | 2.040       |
| Mixing/Placement/Reinforcing         | 0.025       |
| Transport of raw materials           | 0.020       |

A second order polynomial fit resulted in a relationship that provides unit HPC cost ( $C_{\text{HPC}}$ , in €/m<sup>3</sup>) as a function of the characteristic HPC compressive strength

$$C_{\text{HPC}} = 0.017f_{ck}^2 - 1.47f_{ck} + 237.5 \quad [\text{€/m}^3] \quad (9.26)$$

The total unit cost of HPC plates is equal to the sum of material and labour costs for all stages of production.

#### 9.4.2 Insulation layer

Often thinner wall thickness, thus thinner insulation layer will be desirable as it will give more square meters for living areas. The optimum insulation layer corresponds to low thermal transmittance at minimum insulation cost. The cost function for insulation layers can be described by a linear function with an increasing cost/thickness gradient as shown in Figure 9.8 left. In case of no constraint to the maximum thickness of the panel, meaning that an insulation layer of 280 mm polystyrene or an insulation layer of 160 mm PIR will be equal to the 2015 Energy requirement, see Figure 9.8 right. The cost values for insulation values are equal to  $C_{\text{ins}} = 86 - 312 \text{ €/m}^3$  depending on type of insulation material. These values represent typical costs of the Danish market.

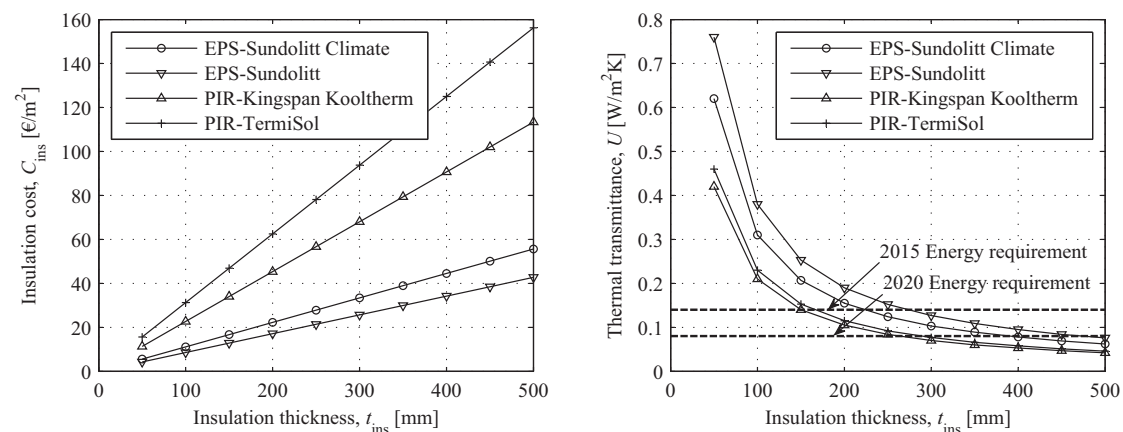


Figure 9.8. *Assessment of insulation cost and thermal transmittance.*

### 9.4.3 Shear connectors and reinforcement

The number and position of shear connectors and degree of reinforcement depend on the required structural systems. Steel provides relatively cheap solutions but can negatively influence thermal efficiency of HPCSP. An interesting option is to use different kind of FRP materials which do not significantly affect thermal efficiency. However, the cost may be higher in comparison with steel. The cost function of shear connecting system/reinforcement equals the individual costs of used materials. The typical cost value for steel shear connectors and reinforcement for the Danish market is equal to  $C_{sh} = 0.77 \text{ €/kg}$ .

## 9.5 Optimization procedure

The minimum cost design for HPCSP at hand is a non-linear optimization problem, since both the objective function and the constraints are non-linear functions of the optimization variables of the problem. For such a problem, the commercial software Matlab® with SQPlab (a Matlab solver for nonlinear optimization and optimal control problems) package was used (The MathWorks, Inc, 2013). The computer program flow chart shown in Figure 9.9 provides the main steps of the optimization procedure. The initiation of the optimization process requires the estimation of an initial optimization variables vector ( $x_o$ ). Theoretically, the closer the initial vector  $x_o$  is to the optimal design variables vector  $x_{opt}^{theor}$ , the faster the solution convergence is expected. In the present study the total number of iterations did not differ significantly with the selection of starting point in design space. For HPCSP the optimal design variables vector  $x_{opt}^{theor}$  is given in Eq. 9.27

$$x_{opt}^{theor} = \{k_{min}, f_{cd,min}, \rho_{sw,min}, t_{b,min}, t_{f,min}, t_{r,min}, w_{r,min}, t_{ins,min}, t_{min}\} \quad (9.27)$$

Table 9.2 *Key design parameters and characteristics*

|                           | Pre-assigned parameters  |
|---------------------------|--|
| 1. Geometrical parameters | • Panel's dimensions ( $h_w, t, L$ )   |
| 2. Cost data              | • HPC cost ( $C_{HPC}$ )<br>• Insulation cost ( $C_{ins}$ )<br>• Steel/FRP cost ( $C_{sh}$ )   |
| 3. Insulation data        | • Coefficient of thermal conductivity for HPC ( $\lambda_{HPC}$ )<br>• Coefficient of thermal conductivity for insulation ( $\lambda_i$ )  |
| 4. Material properties    | • Characteristic strength values ( $f_{ck}, f_{ck,ins}, f_{ctk}, f_{tk,ins}, f_{yk}$ )<br>• Partial safety coefficients ( $\gamma_{HPC}, \gamma_{ins}, \gamma_{sh}$ )<br>• Modulus of elasticity ( $E_{HPC}, E_{ins}, E_{sh}$ )<br>• Shear connectors/reinforcement density ( $\gamma_s$ ) |
| 5. Design requirements    | • Design bending moment ( $M_{Ed}$ )<br>• Design shear ( $V_{Ed}$ )<br>• Design axial load ( $N_{Ed}$ )<br>• Desired HPCSP's thermal transmittance ( $U$ )<br>• Deflection criterion ( $\delta_y$ )  |

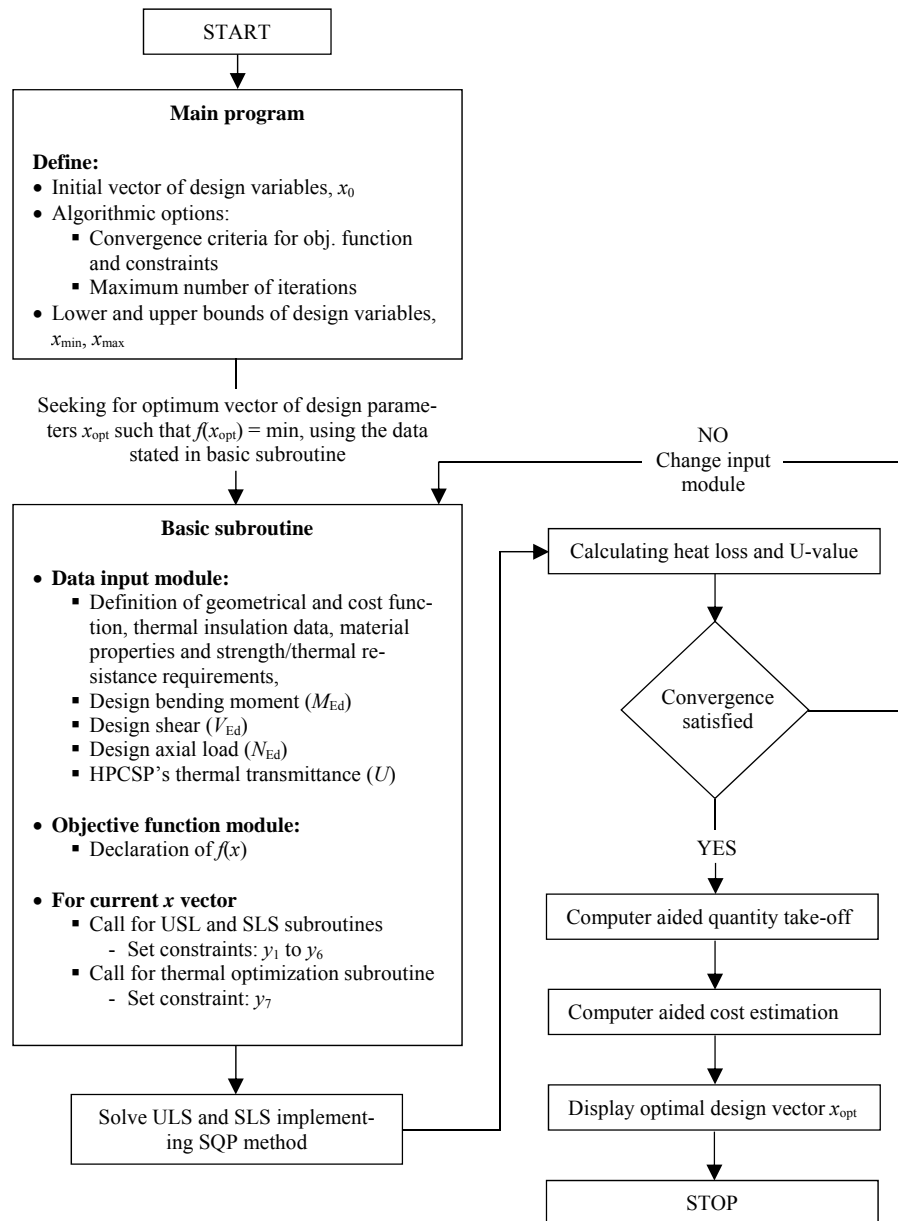


Figure 9.9. *Computer program flow chart.*

For any set of the design performance demands ( $N_{Ed}$ ) exceeding the ultimate HPCSP's capacity ( $N_{Rd}$ ) that corresponds to the components of  $x_{opt}^{theor}$ , HPCSP cost increases, as one or more design variables has to be modified to accommodate the demands. Minimum HPCSP cost is assured when the condition  $N_{Ed} = N_{Rd}(x_{opt}^{theor})$ . Hence, the bending moment and shear become active constraints. When shear becomes active constraint, the minimum cost is obtained by proper adjustment of shear reinforcement, keeping the remaining design components minimum as specified in Eq. 9.27. To adapt moment requirements when flexure arises as active constraint, vertical reinforcement and HPC plate thicknesses are adjusted in the sense to ensure minimum HPCSP cost. Similarly, when SLS becomes active constraint, HPC plate thicknesses are adjusted in order to keep minimum HPCSP cost. Table 9.2 summarizes the key design parameters related to the HPCSP considered in the present study.

Optimization procedure as study case is performed for one meter strip of simply supported HPCSP with height,  $h_w$  equals to 3000 mm. HPCSP is loaded by design axial force  $N_{Ed}$  equal to  $1.25 \cdot 10^5$  N (loads corresponding to two stories building) and the lateral wind loads  $w_d$  equal to  $3.0 \cdot 10^3$  N/m<sup>2</sup>. Thickness of the insulation layer is for simplicity constrained to 160 mm using PIR. The galvanised welded wire mesh made with  $\phi 3$  wires of high yield steel is used as shear connector with shear-flow capacity  $q = 7.3$  kN/mm (Gara et al., 2012b). The upper and lower bound on the optimization variables are specified in Eq. 9.4. Three different HPCSP structures are considered, i.e. HPCSP without rib structure, HPCSP with rib structure spanning 1/3 of the insulation layer thickness ( $t_r = 50$  mm) and width of the rib equal to  $w_r = 50$  mm; and HPCSP with rib structure spanning 2/3 of the insulation layer thickness ( $t_r = 100$  mm) and  $w_r = 50$  mm. Moreover, six different interaction scenarios are chosen, i.e. full composite interaction, 80 % full composite interaction, 60 % full composite interaction, 40 % full composite interaction, 20 % full composite interaction and non-composite interaction.

## 9.6 Results and discussion

Influences of composite interaction on HPCSP cost for the case study HPCSP without rib structure, HPCSP with rib structure spanning 1/3 of the insulation layer thickness ( $t_r = 50$  mm) and width of the rib equal to  $w_r = 50$  mm, HPCSP with rib structure spanning 2/3 of the insulation layer thickness ( $t_r = 100$  mm) and width of the rib equal to  $w_r = 50$  mm are illustrated in Fig. 9.10, Fig. 9.11 and Fig. 9.12, respectively. All minimum HPCSP costs for one meter strip are summarized in Table 9.3.

Table 9.3 *Minimum HPCSP cost for one meter strip*

| Degree of composite interaction | Type of HPCSP structure   |                 |                |    |                            |                 |                |    |                            |                 |                |    |
|---------------------------------|---------------------------|-----------------|----------------|----|----------------------------|-----------------|----------------|----|----------------------------|-----------------|----------------|----|
|                                 | Without rib structure [€] | $t_b, t_r$ [mm] | $f_{ck}$ [MPa] | AC | Rib structure 50/50 mm [€] | $t_b, t_r$ [mm] | $f_{ck}$ [MPa] | AC | Rib structure 50/100mm [€] | $t_b, t_r$ [mm] | $f_{ck}$ [MPa] | AC |
| FC                              | 123.6                     | 10;10           | 110            | B  | 126.1                      | 10;10           | 110            | B  | 128.7                      | 10;100          | 100            | B  |
| 80%                             | 197.0                     | 10;75           | 100            | B  | 194.0                      | 70;10           | 90             | C  | 170.8                      | 40;13           | 110            | B  |
| 60%                             | 215.3                     | 10;5            | 90             | B  | 216.4                      | 10;100          | 90             | B  | 198.8                      | 70;11           | 100            | C  |
| 40%                             | 228.3                     | 10;105          | 90             | B  | 229.8                      | 10;110          | 80             | B  | 226.7                      | 10;100          | 90             | B  |
| 20%                             | 237.9                     | 10;120          | 80             | B  | 240.2                      | 10;120          | 80             | B  | 238.4                      | 10;120          | 80             | B  |
| NC                              | 246.2                     | 10;130          | 80             | B  | 247.5                      | 10;130          | 80             | B  | 246.7                      | 10;125          | 80             | B  |

FC is full composite; NC denotes non-composite; AC is active constraint, B is buckling and C represents cracking limit.

In case of full composite interaction, the active constraint is buckling failure mode for thicknesses of internal HPC plate up to 20 mm. For larger thicknesses of the internal HPC plate, cracking limit becomes decisive active constraint for external HPC plates. With increasing thickness of internal HPC plate the HPCSP cost increases as well. It is observed that minimum HPCSP cost is reached for full composite interaction for thickness of internal HPC plate of 10 mm and HPC mix with characteristic compres-

sive and tensile strength, 110 MPa and 6 MPa, respectively. In case of full composite interaction, there is no obvious difference in optimum HPCSP cost in dependence of type of HPCSP structure. This phenomenon is caused due to overall stiffness  $EI$  of the HPCSP structure increases only by 5 % for HPCSP with rib structure in the case of full composite interaction.

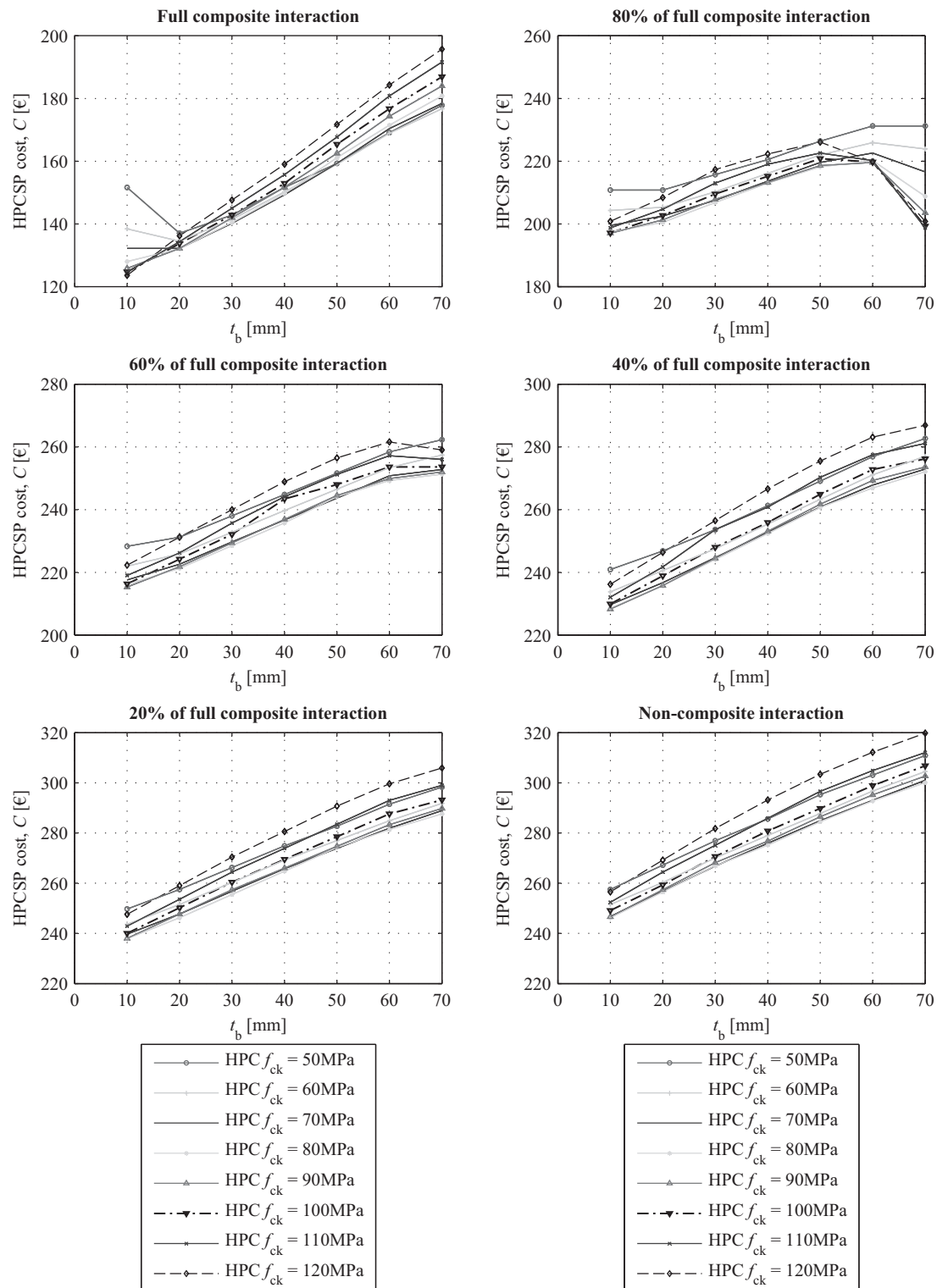


Figure 9.10. Influences of composite interaction on HPCSP cost – HPCSP without rib structure.

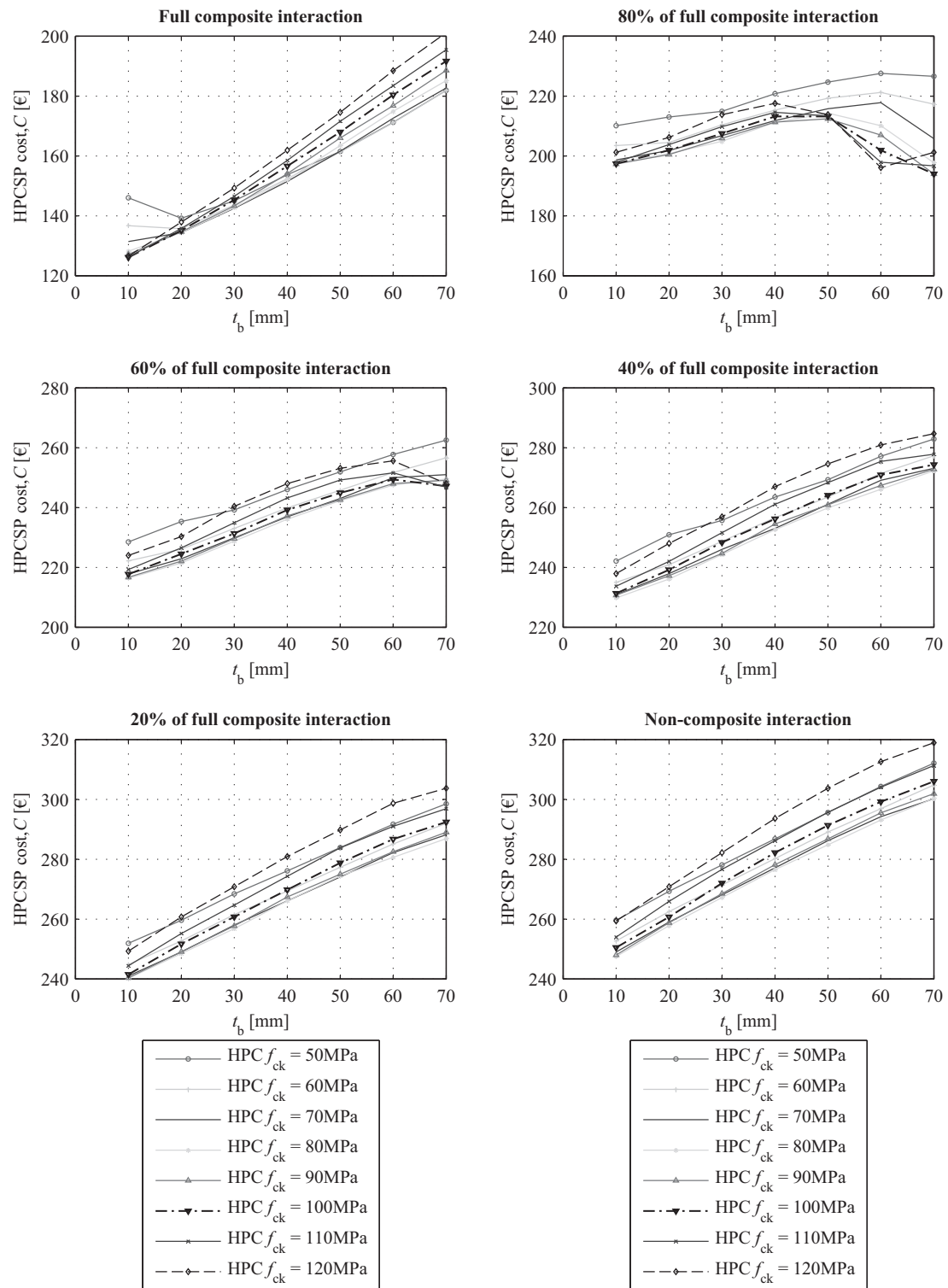


Figure 9.11. Influences of composite interaction on HPCSP cost – HPCSP with rib structure spanning  $1/3$  of the insulation layer thickness ( $t_r = 50\text{ mm}$ ) and width of the rib equal to  $w_r = 50\text{ mm}$ .

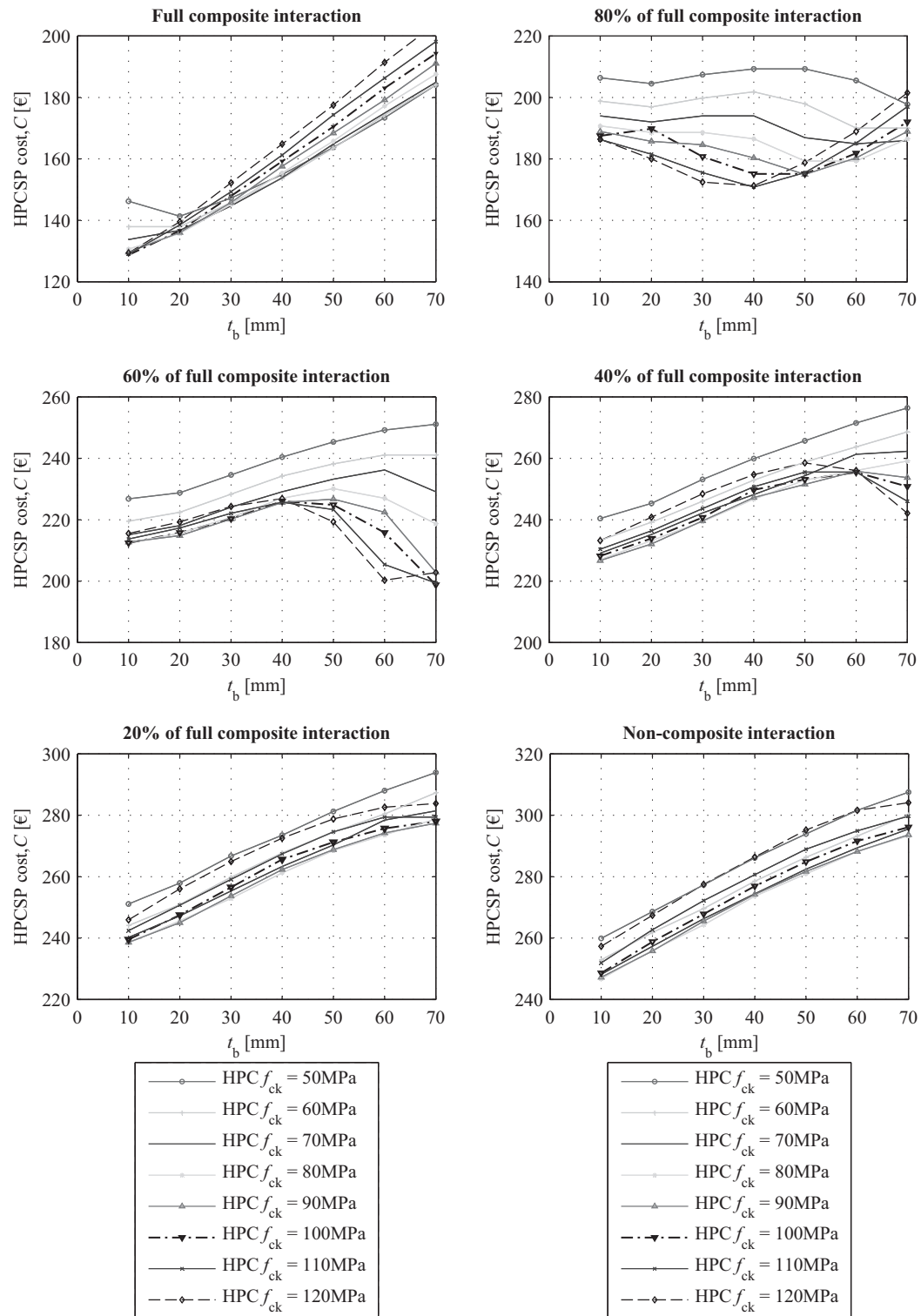


Figure 9.12. Influences of composite interaction on HPCSP cost – HPCSP with rib structure spanning 2/3 of the insulation layer thickness ( $t_r = 100\text{ mm}$ ) and width of the rib equal to  $w_r = 50\text{ mm}$ .

Reducing the degree of composite interaction from full composite interaction to 80 % of full composite interaction leads to increase HPCSP cost in about 60 %. Active constraint is buckling failure mode in the case 80 % of full composite interaction for thicknesses of the internal HPC plate up to 50 mm. For thicknesses of the internal



HPC plate above 50 mm, the thickness of the external HPC significantly reduces and cracking limit of the external HPC plate becomes decisive active constraint for given HPC mixes. Implementing HPCSP with rib structure 50/50 mm and rib structure 50/100 mm leads to reduction in HPCSP cost by 2 % and 15 %, respectively, in direct comparison with HPCSP without rib structure. The minimum cost for 80 % of full composite interaction is for thickness of internal HPC plate of 40 mm and 110 MPa HPC mix.

Decrease of degree of composite interaction generally leads to increase of HPCSP cost. Minimum HPCSP cost in the case of 60% composite interaction differs about 74 % of the full composite interaction. Also in this solution implementing HPCSP with rib structure 50/50 mm and rib structure 50/100 mm leads to reduction in HPCSP cost, i.e. 1% and 8%, respectively, in comparison with HPCSP without rib structure. The minimum cost for 60 % of full composite interaction is for thickness of internal HPC plate of 70 mm and HPC mix with characteristic compressive and tensile strength, 100 MPa and 5.5 MPa, respectively.

Continuing with decreasing degree of composite interaction, the rate of increasing HPCSP cost is reducing. The increase of HPCSP cost is about 85 %, 92 % and 100 % in comparison with full composite interaction for the cases 40% of full composite interaction, 20 % of full composite interaction and non-composite interaction, respectively. The type of HPCSP structure has negligible effect on HPCSP cost for degrees of composite interaction below 60 %.

The minimum cost for 40 % of full composite interaction is found for the thickness of internal HPC plate of 10 mm and HPC mix with characteristic compressive and tensile strength, 90 MPa and 5 MPa, respectively. In case of 20 % of full composite interaction and non-composite interaction the minimum HPCSP cost is observed for thickness of internal HPC plate of 10 mm and HPC mix with characteristic compressive and tensile strength, 80 MPa and 4.8 MPa, respectively. It was observed that with decreasing degree of composite interaction need for HPC mixes with high compressive strength is diminished. This fact is caused by the need of fulfilment buckling failure mode constraint. As a consequence of this constraint, thicknesses of HPC plates are significantly increased. As shown in Fig. 9.7, HPC cost is governed by a non-linear function and cost for HPC mixes with characteristic compressive strength above 80 MPa rapidly increases. Hence, increase of thicknesses of HPC plates and use of HPC with compressive strength above 80 MPa leads to higher HPCSP costs.

Total cost of shear connectors and reinforcement is about 10 % and 20 % of total HPCSP cost in case of full composite and non-composite interaction, respectively. Design of full composite HPCSP requires a high amount of shear connectors in comparison with non-composite and partial composite interaction. However, the amount of reinforcement used for non-composite and partial composite HPCSP is significantly larger than in the case of full composite HPCSP. This can be explained due to greater thicknesses of HPC plates for non-composite and partial composite HPCSP and fulfilment of requirement for the minimum degree of reinforcement.

The resulting  $U$ -value corresponding to minimum HPCSP cost for case of HPCSP without rib structure is equal to  $0.136 \text{ W/(m}^2\text{K)}$ . Inclusion of rib structure 50/50 mm leads to increase of  $U$ -value by 27%. Further increase of rib structure results in loss of  $U$ -value up 100 % in comparison with HPCSP without rib structure. The internal and external HPC plates account for less than 1.0 % of HPCSP  $U$ -value. Metallic and FRP shear connectors in general cause  $U$ -value loss of 3 %.

## 9.7 Parametric study

The previous section revealed that stability of thin-walled HPCSP is in most cases the decisive constraint. Parametric studies for cases of local HPC plate buckling and global HPCSP buckling were performed to further study of these phenomena. The individual subroutines specified in Section 9.5 are used to perform parametric study. Geometry of HPCSP and loading correspond to values typically used in precast industry.

### 9.7.1 Local HPC plate buckling

The minimum critical stress for local HPC plate buckling  $\sigma_{cr,min}$ , is considered for critical value for the insulating material's elastic modulus  $E_{ins}$ , equal to 3 MPa (EPS-insulation), various ratios  $(t/t_{ins})$  in correspondence to Eq. 9.23 and different values of  $\vartheta$ . The general dependency of  $\sigma_{cr,min}$  on values  $\vartheta$  for different ratios  $(t/t_{ins})$  is graphically shown in Figure 9.13. For any given set of components from Eq. 9.4, local HPC plate buckling constraint is activated when the maximum HPC plate compressive stress is equal to  $\sigma_{cr,min}$ .

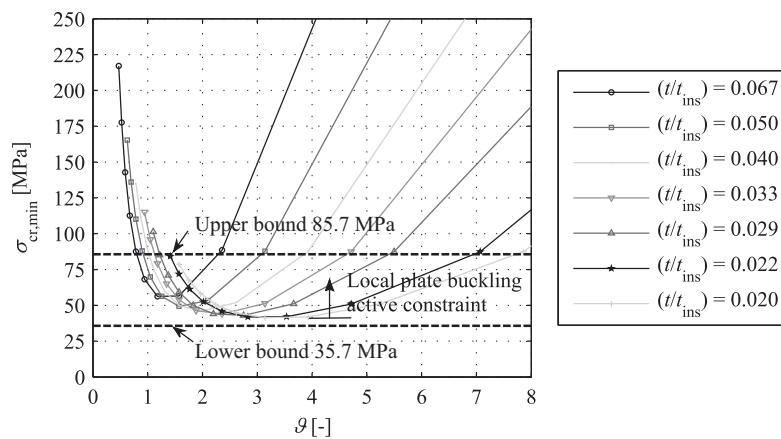


Figure 9.13. The dependency  $\sigma_{cr,min}$  on values  $\vartheta$  for different ratios  $(t/t_{ins})$ .

### 9.7.2 Global HPCSP buckling

Assuming the height of HPCSP ( $h_w$ ) in range of 2750 to 3500 mm with minimum insulation layer thickness of 160 mm (using the best insulation material on the market) for energy performance requirement 2015, the thicknesses of HPC plates vary from 10 to 70 mm ( $t_b$  is equal to  $t_f$ ); design axial load  $N_{Ed}$  in range of  $5 \cdot 10^4$  to  $2 \cdot 10^5$  N. Depend-

ences of  $\lambda$  on  $\lambda_{lim}$  and design axial load  $N_{Ed}$  for full composite interaction are shown in Figure 9.14. For design axial load bellow  $5 \cdot 10^4$  N, the full composite interaction always fulfil condition  $\lambda \leq \lambda_{lim}$ . An increase of design axial load above  $1 \cdot 10^5$  N leads to an increase of the thicknesses of the HPC plates to fulfil  $\lambda_{lim}$  criteria, i.e. about 20 mm for  $1.5 \cdot 10^5$  N and 30 mm for  $2 \cdot 10^5$  N in dependency on HPC and height of HPCSP. In case of non-composite interaction it is very unlikely to reach limit condition  $\lambda \leq \lambda_{lim}$ , even for minimum design axial load as shown in Figure 9.15. Therefore, it is necessary to implement rib structure and/or increase HPC plate thicknesses in design of HPCSP.

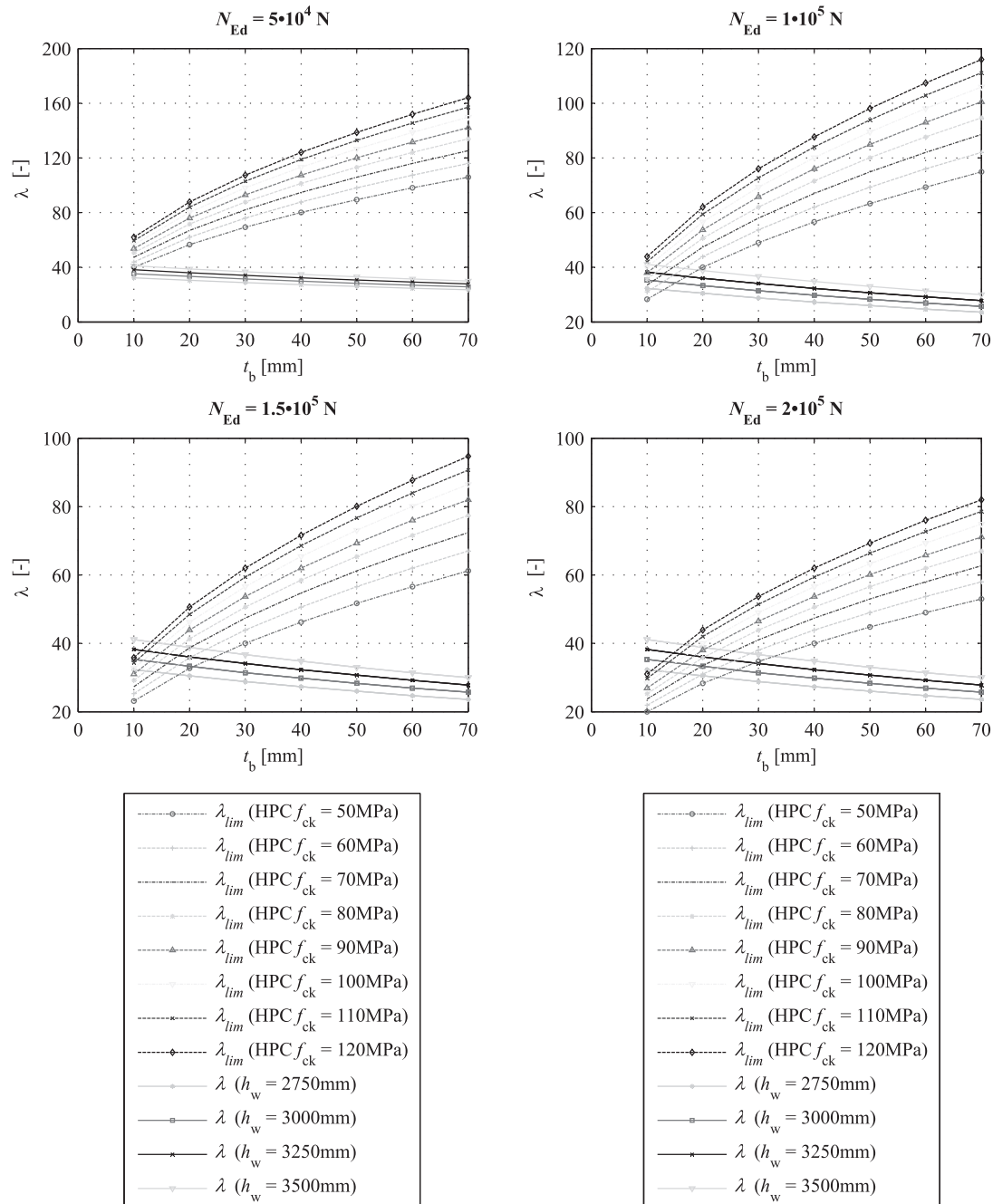


Figure 9.14. Dependences of  $\lambda$  on  $\lambda_{lim}$  and design axial load  $N_{Ed}$  for full composite interaction.

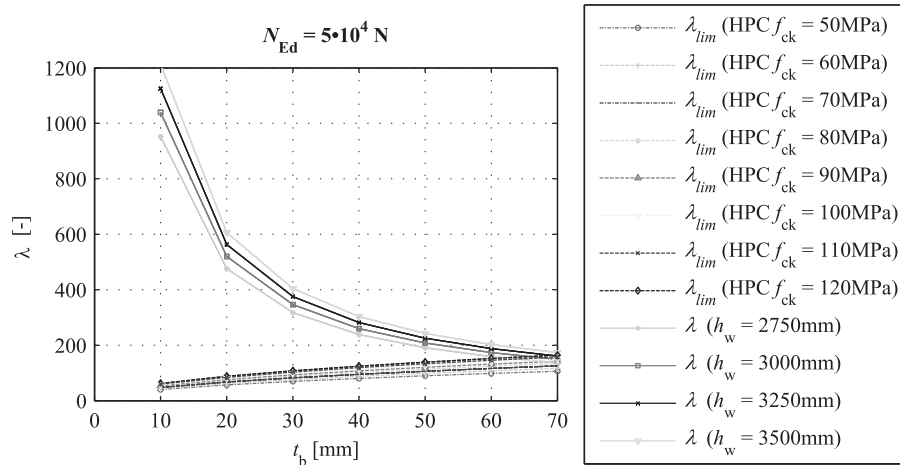


Figure 9.15. Dependences of  $\lambda$  on  $\lambda_{lim}$  for non-composite interaction.

## 9.8 Conclusions

In this study, the optimum design of HPCSP is investigated to address a minimum cost. The optimization process involves minimization of HPCSP cost function subjected to given constraints specified by performance demands. The optimization process is expressed for the case of load-carrying thin-walled HPCSP made of HPC plates and insulation layer. A quick and accurate systematic optimization approach is based on material cost function in the HPCSP design. Cost functions are presented for HPC, insulation layer, reinforcement and include labour-related costs. The present study reports the economic data corresponding to specific manufacturing process and actual financial parameters for the Danish prefabrication industry. The present optimization is performed in computer package software Matlab® with SQPlab package and integrates the processes of HPCSP design, quantity take-off and cost estimation.

The following general conclusions can be outlined from the optimization procedure presented in this paper.

- 1) Minimum HPCSP cost is obtained for the case full composite interaction and HPCSP without rib structure.
- 2) Reduction of fully composite interaction leads to increase of HPCSP cost up to 100 %.
- 3) Rib structure has beneficial effect on minimum HPCSP cost for panels designed between 60 to 100 % of full composite interaction.
- 4) The type of HPCSP rib structure has negligible effect on HPCSP cost for degrees of full composite interaction below 60 %.
- 5) With decreasing degree of composite interaction need for HPC mixes with high compressive strength is diminished. It is found out that minimum HPCSP cost for HPCSP designed between 80 to 100 % of full composite interaction is HPC mix with characteristic compressive strength of 110 MPa. HPCSP designed between 60 to 80 % of full composite interaction an optimum HPC mix is with characteristic compressive strength of 100 MPa. For all other composite inter-

actions optimum HPC mix is with characteristic compressive strength of 80 MPa.

- 6) The best thermal properties of HPCSP favour with HPCSP without rib structure. HPCSP with rib structure spanning 1/3 and 2/3 of insulation layer thickness result in U-value loss of 27 % and 100 %, respectively.
- 7) Metallic and FRP shear connectors in general cause U-value loss of 3 % and 1.5 %, respectively.
- 8) Total cost of shear connectors and reinforcement is about 10 % and 20 % of total HPCSP cost in case of full composite and non-composite interaction, respectively.
- 9) Local HPC plate buckling is not typically decisive design parameter when insulation material has elastic modulus  $E_{ins}$ , larger than 3 MPa.

It should be mentioned that establishment of HPCSP with 100 % full composite interaction is very difficult in precast industry. There are always some losses in the bond between HPC plates and insulation layer. Based on author's experiences these losses are in the most cases caused by shrinkage of HPC plates, and by formation of air pockets between HPC plates and insulation layer interface. HPC mix should be designed to minimize autogenous shrinkage, provide high early age strength and improved crack control. This involves study of optimum fiber content and durability. Moreover, HPC mix has to provide adequate strength to meet the design load. The variety of production plants and production method for HPCSP with combination with the diversity between individual countries should be considered and taken into account if precise HPCSP cost estimations are needed. Nevertheless, the different economic conditions do not change optimization procedure outlined in present study. Further research is intended in implementing proposed optimization procedure to FEM code together with quantity take-off computer program and computer aided cost estimation. Investigation will consider predicting optimal design dimensions, mixture proportions and structural designs and systems during whole production process. It will ease implementing new optimization parameters and restrains, such as maximum CO<sub>2</sub> emissions, energy consumption, and type of formwork or curing method. Moreover, it will allow possibility of using different HPC mixes for the external and internal HPC plates. Finally, the more systematic cost database is necessary to establish to higher reliability cost prediction formulation for HPCSP.

## 9.9 Acknowledgments

The authors greatly thank to the Danish National Advanced Technology Foundation and Connovate for the financial support. Thanks are extended to Bryant Miller for language proofreading.

# Chapter 10

## Conclusions and recommendations for further work

The main conclusions of this Ph.D. thesis are presented in the following. Conclusions are drawn for experimental work, numerical investigation and optimization of precast thin-walled HPC Sandwich Panels. In addition, recommendations for future work are given.

### 10.1 Conclusions

#### **Material characterization of HPC including time dependent fracture properties**

The chapter 3 discussed the wedge splitting test setup and inverse analysis algorithm for various multi-linear softening curves. In particular it addressed the question about the amount of information that can be retrieved from the WST using inverse analysis. The fracture behaviour of three fiber reinforced and regular HPC were investigated. The wedge splitting test setup with 48 cubical specimens was used experimentally and the cracked non-linear hinge model based on the fictitious crack model was applied for the interpretation of the results. The stress-crack opening relationships were extracted by using inverse analysis algorithm for various multi-linear softening curves. The fracture mechanics parameters such as crack opening displacement (COD), fracture energy and characteristic length were experimentally determined. Experiments were performed at 1, 3, 7 and 28 days. Fracture energy,  $G_f$ , was found to increasing with age, while the characteristic length,  $L_{ch}$ , was found to decrease.

The conclusions that can be drawn from chapter 3 are that:

- The wedge splitting test is suitable test method for assessment of fracture properties of regular and glass-polypropylene fiber reinforced HPC.
- The test method is easy to handle and the execution is relatively fast.
- Using the inverse analysis, the both elastic and fracture properties may be interpreted from the test results as a bi-linear or multi-linear stress-crack opening relationship.
- The refinement of the softening curves reflects in improved accuracy of the WST simulation in comparison with bi-linear softening curves with acceptable increase of computational time.

### **Material characterization of HPC including time dependent shrinkage**

The chapter 4 contained a description of experimental setup that allows measurement of effective shrinkage in HPC, which develops on an elastic inhomogeneity embedded in HPC matrix undergoing shrinkage during hydration (autogenous shrinkage). The chapter also presented the analysis necessary to perform an interpretation of the experimental results and to determine effective shrinkage in the HPC matrix. Furthermore, the mechanical properties of three fiber reinforced and regular HPC were investigated in detail as function of time.

### **Small scale and semi-full scale specimens of thin-walled concrete sandwich panels**

Chapter 5 discussed experimental and numerical investigation of thin-walled concrete sandwich panel system using the BFRP and CFRP connecting systems. The experimental program included testing of small scale specimens by applying shear (push-off) loading and semi-full scale specimens by flexural loading. Numerical investigations were based on 3-D linear elastic finite element analysis.

From the work presented in Chapter 5 the following conclusion can be drawn:

- *Push-off test:* The HPCSPs made of CFC/HCFC Kingspan Free Rigid Phenolic insulation showed higher initial shear stiffness in comparison with those made with expanded polystyrene (EPS). Nevertheless, the panels with EPS reached higher ultimate shear strength likely due to higher bond capacity. The panels reinforced with BFRP grid reached similar initial shear stiffness as well ultimate shear strength as the panels reinforced with CFRP grid.
- *Flexural test:* The results of the panels subjected to four-point bending showed no obvious difference in the overall capacity between the specimens with EPS insulation and BFRP grid, and the specimens with CFRP grid. In general, the specimens with EPS insulation provided a higher overall bending capacity in comparison with the CFC/HCFC Kingspan Free Rigid Phenolic insulation. The

observed flexural behaviour in comparison with the theoretical composite and non-composite action indicated that the specimens behave only with partial composite action i.e. 53 % composite action. The partial composite behaviour is caused by a combination of buckling of FRP grid, compression of insulation and shear slip between insulation layer and HPC plates.

- *Numerical modelling*: Numerical investigations were based on 3-D linear elastic finite element analysis using commercial software Abaqus. Results from the numerical investigations were compared with experimental results of small and semi-scale specimens for the validation of the design procedure. A good correlation was observed between the results in the linear elastic range.

Chapter 6 included an experimental program designed to investigate the behaviour of 46 small segments representing typical sandwich panels using the CFRP grid/rigid foam as shear mechanism. Various parameters believed to affect the shear flow strength for this CFRP grid/foam system were examined. The parameters that were considered are the spacing between lines of CFRP grids and the thickness of the rigid foam. The research reported in this paper was conducted to determine the characteristics of the shear transfer mechanism of the CFRP grid/rigid foam. A nonlinear 3D FEM analysis was performed to model the behaviour of the test specimens and to study the behaviour of PCSP. A parametric study was performed to predict the shear flow strength of different FRP materials.

From the work presented in Chapter 6 the following conclusion can be drawn:

- The observed failure modes were shear cracking and/or shear sliding for rigid foam, whereas the CFRP grid exhibited rupturing of the CFRP grid in tension and buckling of the CFRP grid in compression.
- Increasing the spacing between the vertical lines of the CFRP grid increased the overall shear flow strengths due to an increase of the bonded contact concrete/rigid foam interface area. However, it showed a decrease in overall shear stresses due to the increase of the interface surface area in comparison to the increase of the measured load capacity.
- The FEM results were in good agreement with measured values.
- A spreadsheet program was used to establish the factors for design equations to predict the shear flow strengths for given CFRP grid/EPS foam systems.
- The results of parametric study showed that panels with a CFRP grid have higher shear flow strength in comparison with panels with vertical BFRP and GFRP grids. Panels with vertical BFRP and GFRP grids have lower shear flow strength than panels with CFRP grids by 5 - 10 and 10 - 25 %, respectively, using the same cross section of the strands and spacing of the grid.



### Full scale specimens of thin-walled concrete sandwich panels

Chapter 7 reported an experimental and numerical investigation of two full scale pre-cast concrete sandwich panels exposed to uniformly distributed flexural loading. The testing of the panels was performed in a vertical position using a test frame built at DTU. Two setup configurations were used to study different boundary conditions. A nonlinear 3D FEM analysis was performed to model the behaviour of the test specimens and to study the behaviour of precast concrete sandwich panels.

From the work presented in Chapter 7 the following conclusion can be drawn:

- The observed failure modes of the panels were horizontal cracking in the rib structure of the back plates and horizontal cracking with combination of vertical cracking around ribs and shear connectors in the front plates. The panel #01 - test setup 1 also experienced one significant vertical crack in the rib. The foam failed with combination of cracking and/or shear sliding. Some parts of foam remained well bonded to the concrete after testing.
- None of the panels exhibited pull-out of BFRP grid from the concrete or rupturing of BFRP grid.
- The FEM results were found in good agreement with measured values. The crack development was studied using Aramis optical strain measurement in the panel #02. The results of FE analysis showed reasonable agreement with the Aramis measurements.

### Assessment of risk of early age cracking in thin-walled sandwich panels

Chapter 8 presented a rough approach to analyze the robustness of thin-walled sandwich panels at early ages. The approach investigated the external HPC plate subjected to constrained shrinkage load,  $\varepsilon_s$ . The results of non-linear analysis are plotted into the curves in dependence on dimensionless parameter  $\beta$ . Parametric study of infinitely large sheet was analyzed for 214-parameter variations. Further, the case study was performed for novel thin-walled sandwich elements made of fiber-reinforced HPC.

From the work presented in Chapter 8 the following conclusion can be drawn:

- The results of non-linear analysis are highly dependent on the distance between the restraints,  $l$ .
- It was found out that in order to propagate the crack in the centre of the plate, imposed shrinkage,  $\varepsilon_s$ , should be approximately 4 times greater than  $f_t/E$ . Generally, when imposed shrinkage,  $\varepsilon_s$ , is up to 6 times greater than  $f_t/E$ , all the solutions approximately follow the linear FE solution. Further increase of imposed shrinkage,  $\varepsilon_s$ , leads to deviation from linear FE solution.
- The rate function, how much deviates non-linear FE solution from linear FE solution depends on the dimensionless parameter,  $\beta$ . Increase of the dimension-

less parameter,  $\beta$ , leads to situation when unstable crack growth occurs. The results also revealed that the crack propagates stable as long as the values of dimensionless parameter,  $\beta$ , are below 1. The results of dimensionless parameter,  $\beta$ , above 1 lead to unstable crack propagation.

- The results of the case study proved that proposed approach fits reasonably with observation on site, i.e. the ability to predict when crack growth becomes unstable and when structural macro-cracking is expected to appear.

### **Optimization of precast thin-walled HPC sandwich panels**

Chapter 9 of this Ph.D. thesis dealt with cost optimization of load carrying thin-walled precast HPC sandwich panels. The optimization approach is based on the selection of material's performances and panel's geometrical parameters as well as on material cost functions in the sandwich panel design. The strength based design of sandwich panels is in competence with the format of Eurocode 2. Cost functions are presented for HPC, insulation layer, reinforcement and include labour-related costs. The present study reports the economic data corresponding to specific manufacturing process and actual financial parameters for the Danish prefabrication industry. The present optimization is performed in computer package software Matlab® with SQPlab package and integrates the processes of HPCSP design, quantity take-off and cost estimation.

From the work presented in Chapter 9 the following conclusion can be drawn:

- Minimum HPCSP cost is obtained for the case full composite interaction and HPCSP without rib structure.
- Reduction of fully composite interaction leads to increase of HPCSP cost up to 100 %.
- Rib structure has beneficial effect on minimum HPCSP cost for panels designed between 60 to 100 % of full composite interaction.
- The type of HPCSP rib structure has negligible effect on HPCSP cost for degrees of full composite interaction below 60 %.
- With decreasing degree of composite interaction need for HPC mixes with high compressive strength is diminished. It is found out that minimum HPCSP cost for HPCSP designed between 80 to 100 % of full composite interaction is HPC mix with characteristic compressive strength of 110 MPa. HPCSP designed between 60 to 80 % of full composite interaction an optimum HPC mix is with characteristic compressive strength of 100 MPa. For all other composite interactions optimum HPC mix is with characteristic compressive strength of 80 MPa.
- The best thermal properties of HPCSP favour with HPCSP without rib structure. HPCSP with rib structure spanning 1/3 and 2/3 of insulation layer thickness result in U-value loss of 27 % and 100 %, respectively.

- Metallic and FRP shear connectors in general cause U-value loss of 3 % and 1.5 %, respectively.
- Total cost of shear connectors and reinforcement is about 10 % and 20 % of total HPCSP cost in case of full composite and non-composite interaction, respectively.
- Local HPC plate buckling is not typically decisive design parameter when insulation material has elastic modulus  $E_{\text{ins}}$ , larger than 3 MPa.

## 10.2 Recommendations for further work

Based on the findings and conclusions of this Ph.D. study, the following recommendations for further work are listed:

### **Material characterization of HPC including time dependent fracture properties**

The present work was limited to Glass and Polypropylene fibers in HPC. The suggested future work is recommended:

- To investigate the effect to varying material parameters on the fracture behaviour as determined by the WST and inverse analysis, i.e. different volumes of carbon and basalt fiber reinforced polymers in HPC.

### **Material characterization of HPC including time dependent shrinkage**

The study of time dependent shrinkage was limited to investigation of Glass and Polypropylene fibers in HPC during period of 4000 hours. It is recommended that further study is performed:

- To investigate the effect to varying material parameters on time dependent shrinkage, i.e. different volumes of carbon and basalt fiber reinforced polymers in HPC.
- Long-term measurement of time-dependent shrinkage.
- To provide more statistically reliable data collection of time dependent shrinkage.

### **Testing of thin-walled concrete sandwich panels**

It was already mentioned in the Chapter 1 that the main limitation of the present works lays in the testing possibility. Indeed, testing and especially the full scale testing remains an expensive process where many things can go wrong, which makes repetitions costly. Further, the work has been limited to investigating HPC sandwich panels reinforced with metallic, BFRP and CFRP grids in combination with loose Glass and Polypropylene fibers. The further development is needed:

- To provide more statistically relevant test results in term of full scale testing.

- To study the resistance of thin-walled concrete sandwich panels due to damaging effects from deicing chemicals and freeze thaw cycles.
- To study durability and fatigue resistance of thin-walled concrete sandwich panels.
- To study long-term behaviour of FRP/foam shear transfer mechanism for thin-walled concrete sandwich panels.
- To perform study on different kind of FRP shear connectors and foams, and evaluate their FRP/foam shear transfer mechanisms for thin-walled concrete sandwich panels.
- To evaluate the bond-slip relationship by means of pull-out tests between different kinds of FRP shear connectors and HPC.

### **Numerical investigation of thin-walled concrete sandwich panels**

Although, comparisons between experimental and numerical results presented in chapter 6 and chapter 7 indicate that the model is capable describing the shear transfer mechanism of the CFRP grid/rigid foam as well as behaviour of two full scale precast concrete sandwich panels exposed to uniformly distributed flexural loading, further development is needed.

- To model all phases of constructions, i.e. to predict the behaviour of thin-walled concrete sandwich panels since beginning of casting to the assembly of the panels and during whole lifetime of the elements.
- To provide more precise tool evaluating risk of early age cracking and crack developments in thin-walled sandwich panels.

### **Optimization of precast thin-walled HPC sandwich panels**

Despite the fact that, the results presented in Chapter 9 indicate the potential of predicting optimal design dimensions, further development work is needed.

- To assess Life Cycle Assessment (LCA) of thin-walled concrete sandwich panels
- To consider predicting optimal design dimensions, mixture proportions and structural designs and systems during whole production process.
- To implement new optimization parameters and restrains, such as maximum CO<sub>2</sub> emissions, energy consumption, and type of formwork or curing method. Moreover, implement possibility of using different HPC mixes for the external and internal HPC plates.
- To establish more systematic cost database for higher reliability cost prediction formulation for HPCSP.



## Additional publications (not included in the thesis)

### Journal papers:

Hodicky K., Hulin T.: 'A thin-walled High Performance Concrete Sandwich System reinforced with BFRP shear connectors'. In *Journal: Beton*, 2013, Issue: 6, pp: 56-61.

Hulin T., Maluk Ch., Bisby L., Hodicky K., Schmidt J.W., Stang H.: 'Experimental studies on the fire behaviour of high performance concrete thin plates'. In *Journal: Fire Technology*, 2015. (accepted for publication).

Hulin T., Lauridsen D.H., Hodicky K., Schmidt J.W., Stang H.: 'Influence of basalt FRP mesh reinforcement on high performance concrete thin plates at high temperatures'. In *Journal: ASCE Journal of Composites for Construction*, 2015. (accepted for publication).

Hulin T., Hodicky K., Schmidt J.W., Stang H.: 'Experimental investigations of sandwich panels using high performance concrete thin plates exposed to fire'. In *Journal: Materials and Structures*, 2015. (submitted).

Hulin T., Hodicky K., Schmidt J.W., Stang H.: 'Sandwich panels with high performance concrete thin plates at elevated temperatures – numerical studies'. In *Journal: Materials and Structures*, 2015 (accepted for publication).

Krejcirikova B., Ottosen L.M., Goltermann P., Hodicky K.: 'Incinerated sewage sludge ash as alternative binder in cement-based materials; effect on mortar characteristic'. In *Journal: Waste Management*, 2015 (submitted).

### Conference papers:

Hodicky K., Hulin T., Schmidt J.W., Stang H.: 'Optimization process for thin-walled High Performance Concrete sandwich panels'. In *Proceedings: 5<sup>th</sup> International Conference on Structural Engineering, Mechanics and Computation (SEMC 2013)*, 2013, Cape Town, South Africa.

Hodicky K., Hulin T., Schmidt J.W., Stang H.: 'Optimization process for thin-walled High Performance Concrete sandwich panels'. In *Proceedings: 4<sup>th</sup> Fourth International fib Congress*, 2014, Mumbai, India.

Hodicky K., Sopal G., Rizkalla S., Hulin T., Stang H.: 'FRP shear transfer mechanism for precast concrete sandwich panels'. In *Proceedings: fib symposium*, 2015, Copenhagen, Denmark.

Hulin T., Hodicky K., Schmidt J.W., Nielsen J.H., Stang H.: 'A model for spalling of HPC thin plates exposed to fire'. In *Proceedings: 5<sup>th</sup> International Conference on Structural Engineering, Mechanics and Computation (SEMC 2013)*, 2013, Cape Town, South Africa.

Hulin T., Hodicky K., Schmidt J.W., Nielsen J.H., Stang H.: 'Fire performance of basalt FRP mesh reinforced HPC thin plates'. In *Proceedings: 4<sup>th</sup> Asia-Pacific Conference on FRP in Structures (APFIS 2013)*, 2013, Melbourne, Australia.

Krejcirikova B., Goltermann P., Hodicky K.: 'Incinerated sewage sludge ash as alternative binder in cement-based materials'. In *Proceedings: 2<sup>nd</sup> International Conference Wastes*, 2013, Braga, Portugal.

# Bibliography

- ACI Committee 318. (2008). *Building Code Requirements for Structural Concrete and Commentary*. American Concrete Institute.
- ACI Committee 533. (2012). *533R-11 Guide for Precast Concrete Wall Panels*. American Concrete Institute.
- ACI Committee 544. (2002). *State-of-the-Art Report on Fiber Reinforced Concrete*.
- Aİtcin, P.-C. (2011). *High Performance Concrete*. CRC Press.
- Aİtcin, P. C., Neville, A. M., & Acker, P. (1997). Integrated view of shrinkage deformation. *Concrete International*, 19(9). Retrieved from <http://trid.trb.org/view.aspx?id=577721>
- Aİtcin, P.-C. (2000). Cements of yesterday and today: Concrete of tomorrow. *Cement and Concrete Research*, 30(9), 1349–1359. [http://doi.org/10.1016/S0008-8846\(00\)00365-3](http://doi.org/10.1016/S0008-8846(00)00365-3)
- Aİtcin, P. C. (2003). The durability characteristics of high performance concrete: a review. *Cement and Concrete Composites*, 25(4–5), 409–420. [http://doi.org/10.1016/S0958-9465\(02\)00081-1](http://doi.org/10.1016/S0958-9465(02)00081-1)
- Allen, H. G. (1969). *Analysis and design of structural sandwich panels*. Pergamon. Retrieved from <http://www.sciencedirect.com/science/article/pii/B9780080128702500018>
- Al-Salloum, Y. A., & Husainsiddiqi, G. (1994). Cost-Optimum Design of Reinforced Concrete (RC) Beams. *Structural Journal*, 91(6). <http://doi.org/10.14359/1539>
- Alves, M. F., Cremonini, R. A., & Dal Molin, D. C. C. (2004). A comparison of mix proportioning methods for high-strength concrete. *Cement and Concrete Composites*, 26(6), 613–621. [http://doi.org/10.1016/S0958-9465\(03\)00036-2](http://doi.org/10.1016/S0958-9465(03)00036-2)
- Arora, J. S. (2012). *Introduction to Optimum Design* (3rd ed.). Boston: Academic Press. Retrieved from <http://www.sciencedirect.com/science/article/pii/B9780123813756000334>
- ASTM. (2011). *C496/C496M-11 Standard test method for splitting tensile strength of cylindrical concrete specimens*. West Conshohocken, PA.
- ASTM. (2014a). *C39/C39M-14 Standard test method for compressive strength of cylindrical concrete specimens*. West Conshohocken, PA.
- ASTM. (2014b). *C469/C469M-14 Standard test method for static modulus of elasticity and Poisson's ratio of concrete in compression*. West Conshohocken, PA.
- ASTM. (2014c). *D3039D3039M-14 Standard test method for tensile properties of polymer matrix composite materials*. West Conshohocken, PA.



- ASTM 1550-02. (2003). *Standard Test Method for Flexural Toughness of Fiber Reinforced Concrete (Using Centrally Loaded Round Panel)*. ASTM International.
- ASTM C1018-97. (1997). *Standard Test Method for Flexural Toughness and First-Crack Strength of Fiber-Reinforced Concrete (Using Beam With Third-Point Loading)*. ASTM International. Retrieved from <http://www.astm.org/doiLink.cgi?C1018>
- Bache, H. H. (1989). Fracture Mechanics in Integrated Design of New, Ultra-strong Materials and Structures. *RILEM Technical Committee 90-FMA, Fracture Mechanics Two Concrete Applications (L. Elfgren, Ed.) - Fracture Mechanics of Concrete Structures. From Theory Two Applications*, 382–398.
- Balaguru, P. N., & Shah, S. P. (1992). *Fiber-reinforced cement composites*. McGraw-Hill.
- Bamforth, P., Chisholm, D., Gibbs, J., & Harrison, T. (2007). *Properties of Concrete for use in Eurocode 2*. The Concrete Centre.
- Banthia, N., & Sheng, J. (1996). Fracture toughness of micro-fiber reinforced cement composites. *Cement and Concrete Composites*, 18(4), 251–269. [http://doi.org/10.1016/0958-9465\(95\)00030-5](http://doi.org/10.1016/0958-9465(95)00030-5)
- Banthia, N., & Trottier, J.-F. (1995). Test Methods for Flexural Toughness Characterization of Fiber Reinforced Concrete: Some Concerns and a Proposition. *ACI Materials Journal*, 92(1), 48–57. <http://doi.org/10.14359/1176>
- Barragán, B. E. (2002). *Failure and toughness of steel fiber reinforced concrete under tension and shear* (PhD Dissertation). Universitat Politècnica de Catalunya, Barcelona, Spain. Retrieved from <http://upcommons.upc.edu/handle/10803/5905>
- Barr, B., Gettu, R., Al-Oraimi, S. K. A., & Bryars, L. S. (1996). Toughness measurement — the need to think again. *Cement and Concrete Composites*, 18(4), 281–297. [http://doi.org/10.1016/0958-9465\(96\)00021-2](http://doi.org/10.1016/0958-9465(96)00021-2)
- Barros, M. H. F. M., Martins, R. a. F., & Barros, A. F. M. (2005). Cost optimization of singly and doubly reinforced concrete beams with EC2-2001. *Structural and Multidisciplinary Optimization*, 30(3), 236–242. <http://doi.org/10.1007/s00158-005-0516-2>
- Baykasoğlu, A., Öztaş, A., & Özbay, E. (2009). Prediction and multi-objective optimization of high-strength concrete parameters via soft computing approaches. *Expert Systems with Applications*, 36(3, Part 2), 6145–6155. <http://doi.org/10.1016/j.eswa.2008.07.017>
- Bažant, Z. P. (2002). Concrete fracture models: testing and practice. *Engineering Fracture Mechanics*, (2), 165–205. [http://doi.org/10.1016/S0013-7944\(01\)00084-4](http://doi.org/10.1016/S0013-7944(01)00084-4)

- Bažant, Z. P., & Raftshol, W. J. (1982). Effect of cracking in drying and shrinkage specimens. *Cement and Concrete Research*, 12(2), 209–226. [http://doi.org/10.1016/0008-8846\(82\)90008-4](http://doi.org/10.1016/0008-8846(82)90008-4)
- Benayoune, A., Samad, A. A. A., Abang Ali, A. A., & Trikha, D. N. (2007). Response of pre-cast reinforced composite sandwich panels to axial loading. *Construction and Building Materials*, 21(3), 677–685. <http://doi.org/10.1016/j.conbuildmat.2005.12.011>
- Benayoune, A., Samad, A. A. A., Trikha, D. N., Abang Ali, A. A., & Ashrabov, A. A. (2006). Structural behaviour of eccentrically loaded precast sandwich panels. *Construction and Building Materials*, 20(9), 713–724. <http://doi.org/10.1016/j.conbuildmat.2005.02.002>
- Benayoune, A., Samad, A. A. A., Trikha, D. N., Ali, A. A. A., & Ellinna, S. H. M. (2008). Flexural behaviour of pre-cast concrete sandwich composite panel – Experimental and theoretical investigations. *Construction and Building Materials*, 22(4), 580–592. <http://doi.org/10.1016/j.conbuildmat.2006.11.023>
- Bennett, D. (2002). *Innovation in concrete*. London, UK: Thomas Telford Publishing.
- Bentur, A. (2002). Cementitious Materials—Nine Millennia and A New Century: Past, Present, and Future. *Journal of Materials in Civil Engineering*, 14(1), 2–22. [http://doi.org/10.1061/\(ASCE\)0899-1561\(2002\)14:1\(2\)](http://doi.org/10.1061/(ASCE)0899-1561(2002)14:1(2))
- Bentur, A. (2003). *Report 25: Early Age Cracking in Cementitious Systems - Report of RILEM Technical committee TC 181-EAS: Early age cracking shrinkage induced stresses and cracking in cementitious systems*. RILEM Publications.
- Bentur, A., & Mindess, S. (2006). *Fibre Reinforced Cementitious Composites, Second Edition*. CRC Press.
- Bernard, O., Ulm, F.-J., & Lemarchand, E. (2003). A multiscale micromechanics-hydration model for the early-age elastic properties of cement-based materials. *Cement and Concrete Research*, 33(9), 1293–1309. [http://doi.org/10.1016/S0008-8846\(03\)00039-5](http://doi.org/10.1016/S0008-8846(03)00039-5)
- Betterman, L. R., Ouyang, C., & Shah, S. P. (1995). Fiber-matrix interaction in micro-fiber-reinforced mortar. *Advanced Cement Based Materials*, 2(2), 53–61. [http://doi.org/10.1016/1065-7355\(95\)90025-X](http://doi.org/10.1016/1065-7355(95)90025-X)
- Bharatkumar, B. H., Narayanan, R., Raghuprasad, B. K., & Ramachandramurthy, D. S. (2001). Mix proportioning of high performance concrete. *Cement and Concrete Composites*, 23(1), 71–80. [http://doi.org/10.1016/S0958-9465\(00\)00071-8](http://doi.org/10.1016/S0958-9465(00)00071-8)
- Brameshuber, W. (2006). *Report 36: Textile Reinforced Concrete - State-of-the-Art Report of RILEM TC 201-TRC*. RILEM Publications.

- Brandt, A. M. (1994). *Cement-based Composites: Materials, Mechanical Properties and Performance*. CRC Press.
- Brandt, A. M. (2009). *Cement-Based Composites: Materials, Mechanical Properties and Performance, Second Edition*. CRC Press. Retrieved from <http://www.crcpress.com/product/isbn/9780415409094>
- Brühwiler, E., & Wittmann, F. H. (1990). The wedge splitting test, a new method of performing stable fracture mechanics tests. *Engineering Fracture Mechanics*, 35(1–3), 117–125. [http://doi.org/10.1016/0013-7944\(90\)90189-N](http://doi.org/10.1016/0013-7944(90)90189-N)
- Buhler, E. R. (2008). High Percentage Recovered Mineral Component (Silica Fume) in Extreme Concrete Exposure and Exceptional Concrete Durability Applications. Presented at the Concrete Technology Forum. Focus on Sustainable Development. Retrieved from <http://trid.trb.org/view.aspx?id=919739>
- Bunn, W. G. (2011). *CFRP Grid/Rigid Foam Shear Transfer Mechanism for Precast, Prestressed Concrete Sandwich Wall Panels* (MSc Thesis). Civil Engineering. North Carolina State University, Raleigh, North Carolina, USA.
- Bush Jr., T. D., & Stine, G. L. (1994). Flexural behavior of composite precast concrete sandwich panels with continuous truss connectors. *PCI Journal*, 39(2), 112–121.
- Bush Jr., T. D., & Wu, Z. (1998). Flexural analysis of prestressed concrete sandwich panels with truss connectors. *PCI Journal*, 43(5), 76–101.
- Bygningsreglementet 01.01.2014 - BR10. (n.d.). Retrieved January 30, 2015, from <http://byggningsreglementet.dk/br10/0/42>
- Caldarone, M. A. (2008). *High-Strength Concrete: A Practical Guide*. CRC Press.
- Camp, C. V., & Assadollahi, A. (2013). CO<sub>2</sub> and cost optimization of reinforced concrete footings using a hybrid big bang-big crunch algorithm. *Structural and Multidisciplinary Optimization*, 48(2), 411–426. <http://doi.org/10.1007/s00158-013-0897-6>
- Carol, I., Prat, P. C., & López, C. M. (1997). Normal/Shear Cracking Model: Application to Discrete Crack Analysis. *Journal of Engineering Mechanics*, 123(8), 765–773. [http://doi.org/10.1061/\(ASCE\)0733-9399\(1997\)123:8\(765\)](http://doi.org/10.1061/(ASCE)0733-9399(1997)123:8(765))
- CEB-FIP Model Code 1990. (1993). *CEB-FIP Model Code 1990: Design Code*. Fédération internationale du béton (fib).
- CEN. (2006a). EN 14889-1: Fibres for concrete - Part 1: Steel fibres. Definition, specifications and conformity. CEN European Committee for Standardization.
- CEN. (2006b). EN 14889-2: Fibres for concrete - Part 2: Polymer fibres - Definition, specification and conformity. CEN European Committee for Standardization.

- CEN. (2010). *Eurocode 2: Design of concrete structures EN 1992-1-1*. European Committee for Standardisation. Brussels.
- Chang, P.-K., & Peng, Y.-N. (2001). Influence of mixing techniques on properties of high performance concrete. *Cement and Concrete Research*, 31(1), 87–95. [http://doi.org/10.1016/S0008-8846\(00\)00439-7](http://doi.org/10.1016/S0008-8846(00)00439-7)
- Collins, F. T. (1954). Precast Concrete Sandwich Panels for Tilt-Up Construction. *ACI Journal Proceedings*, 51, 149–164. <http://doi.org/10.14359/11671>
- Connovate. (2015). Connovate. Retrieved March 26, 2015, from <http://www.connovate.dk/>
- Cornelissen, H. A. W., Hordijk, D. A., & Reinhardt, H. W. (1986). Experimental determination of crack softening characteristics of normalweight and lightweight concrete. Delft University of Technology. Retrieved from <http://resolver.tudelft.nl/uuid:08c29b39-5c60-4ab6-b9d5-643d11007f7c>
- Cotterell, B., & Mai, Y. W. (1995). *Fracture Mechanics of Cementitious Materials*. CRC Press.
- Dela, B. F. (2000). *Eigenstresses in Hardening Concrete* (PhD Dissertation). Department of Structural Engineering and Materials, Technical University of Denmark, Kgs. Lyngby.
- De Larrard, F., & Sedran, T. (2002). Mixture-proportioning of high-performance concrete. *Cement and Concrete Research*, 32(11), 1699–1704. [http://doi.org/10.1016/S0008-8846\(02\)00861-X](http://doi.org/10.1016/S0008-8846(02)00861-X)
- Dhir, R. K., Hewlett, P. C., & Csetenyi, L. J. (2002). *Innovations and Developments in Concrete Materials and Construction: Proceedings of the International Conference Held at the University of Dundee, Scotland, UK on 9-11 September 2002*. Thomas Telford.
- Dick-Nielsen, L. (2008). *Modeling of ECC Materials using Numerical Formulations based on Plasticity* (PhD Dissertation). Technical University of Denmark, Kgs. Lyngby.
- Donza, H., Cabrera, O., & Irassar, E. F. (2002). High-strength concrete with different fine aggregate. *Cement and Concrete Research*, 32(11), 1755–1761. [http://doi.org/10.1016/S0008-8846\(02\)00860-8](http://doi.org/10.1016/S0008-8846(02)00860-8)
- EFNARC. (1996). *European Specification for Sprayed Concrete*. European Federation of Producers and Applicators of Specialist Products for Structures.
- Einea, A., Salmon, D. C., Fogarasi, G. J., Culp, T., & Tadros, M. K. (1991). State-of-the-Art of Precast Concrete Sandwich Panel. *PCI Journal*, 36(6), 78–98.
- Einea, A., Salmon, D. C., Tadros, M. K., & Culp, T. (1994). A new structurally and thermally efficient precast sandwich panel system. *PCI J*, 39(4), 90–101.

- Elser, M., Tschegg, E. K., & Stanzl-Tschegg, S. E. (1996). Fracture behaviour of polypropylene-fibre-reinforced concrete under biaxial loading: An experimental investigation. *Composites Science and Technology*, 56(8), 933–945. [http://doi.org/10.1016/0266-3538\(96\)00057-7](http://doi.org/10.1016/0266-3538(96)00057-7)
- Energy Styrelsen. (2014). Bygningsreglementet 31.12.2014. Retrieved from <http://bygningsreglementet.dk/br10/0/42>
- Erki, M. A., & Rizkalla, S. H. (1993). FRP reinforcement for concrete structures. *Concrete International*, 15(6), 48–53.
- Eshelby, J. D. (1957). The Determination of the Elastic Field of an Ellipsoidal Inclusion, and Related Problems. *Proceedings of the Royal Society of London A: Mathematical, Physical and Engineering Sciences*, 241(1226), 376–396. <http://doi.org/10.1098/rspa.1957.0133>
- EU. (2010). European Commission - PRESS RELEASES - Press release - Energy efficiency: delivering the 20% target. Retrieved March 6, 2015, from [http://europa.eu/rapid/press-release\\_MEMO-08-699\\_en.htm](http://europa.eu/rapid/press-release_MEMO-08-699_en.htm)
- European Commission - PRESS RELEASES - Press release - Energy efficiency: delivering the 20% target. (n.d.). Retrieved January 28, 2015, from [http://europa.eu/rapid/press-release\\_MEMO-08-699\\_en.htm](http://europa.eu/rapid/press-release_MEMO-08-699_en.htm)
- Fadaee, M. J., & Grierson, D. E. (1996). Design optimization of 3D reinforced concrete structures. *Structural Optimization*, 12(2-3), 127–134. <http://doi.org/10.1007/BF01196945>
- Farhat, F. A., Nicolaides, D., Kanellopoulos, A., & Karihaloo, B. L. (2007). High performance fibre-reinforced cementitious composite (CARDIFRC) – Performance and application to retrofitting. *Engineering Fracture Mechanics*, 74(1–2), 151–167. <http://doi.org/10.1016/j.engfracmech.2006.01.023>
- fib Special Activity Group 5. (1999). fib Model Code for Concrete Structures 1990. Retrieved May 3, 2015, from <http://www.ernst-und-sohn.de/en/fib-model-code-for-concrete-structures-2010>
- Frankl, B., Lucier, G., Hassan, T., & Rizkalla, S. (2011). Behavior of Precast, Prestressed Concrete Sandwich Wall Panels Reinforced with CFRP Grid. *PCI Journal*, 56(2), 88–111.
- Frankl, B., Lucier, G., Rizkalla, S., Blaszkak, G., & Harmon, T. (2008). Structural Behavior of Insulated Prestressed Concrete Sandwich Panels Reinforced with FRP Grid. In *4th International Conference on FRP Composites in Civil Engineering*. Zurich, Switzerland.
- Freedman, S. (1999). Loadbearing architectural precast concrete wall panels. *PCI Journal*, 44(5), 92–115.

- Gara, F., Ragni, L., Roia, D., & Dezi, L. (2012). Experimental tests and numerical modelling of wall sandwich panels. *Engineering Structures*, 37, 193–204. <http://doi.org/10.1016/j.engstruct.2011.12.027>
- Gilbert, R. I. (2001). Shrinkage, Cracking and Deflection the Serviceability of Concrete Structures. *Electronic Journal of Structural Engineering*, 1(1), 2–14.
- Glavind, M. (1992). *Evaluation of the Compressive Behaviour of Fibre Reinforced High Strength Concrete* (PhD Dissertation). Technical University of Denmark, Kgs. Lyngby.
- Glech, H. (2007). New Carbon Fiber Reinforcement Advances Sandwich Wall Panels. *Structure Magazine*, 61–63.
- GOM mbH. (2015). ARAMIS Software: GOM. Retrieved April 8, 2015, from <http://www.gom.com/3d-software/aramis-software.html>
- Gopalaratnam, V. S., & Gettu, R. (1995). On the characterization of flexural toughness in fiber reinforced concretes. *Cement and Concrete Composites*, 17(3), 239–254. [http://doi.org/10.1016/0958-9465\(95\)99506-O](http://doi.org/10.1016/0958-9465(95)99506-O)
- Gopalaratnam, V. S., Shah, S. P., Batson, G. B., Criswell, M., Ramakishnan, V., & Wecharatana, M. (1991). Fracture Toughness of Fiber Reinforced Concrete. *ACI Materials Journal*, 88(4), 339–353. <http://doi.org/10.14359/1840>
- Griffith, A. A. (1921). The Phenomena of Rupture and Flow in Solids. *Royal Society of London Philosophical Transactions Series A*, 221, 163–198. <http://doi.org/10.1098/rsta.1921.0006>
- Hansen, E. J. D. P., Aassved Hansen, E., Stang, H., & Hassanzadeh, M. (1998). *Determination of the Fracture Energy of Concrete*. SP Swedish National Testing and Research Institute.
- Hansen, S. (2012a). Economical optimization of building elements for use in design of nearly zero energy buildings. In *5th International Building Physics Conference* (pp. 49–55). Kyoto, Japan.
- Hansen, S. (2012b). Optimization of the thermal bridge effect of ribs in sandwich panels of High Performance Concrete. In *11th International Conference on Sustainable Energy Technologies*. Vancouver, Canada.
- Hansen, S. (2015). *Optimization of thermal performance of sandwich panel of high performance concrete* (Ph.D. Thesis). Technical University of Denmark, Kgs. Lyngby.
- Hariri, K. (2000). *Bruchmechanisches Verhalten jungen Betons. Laser-Speckle-Interferometrie und Modellierung der Rißprozeßzone* (Vol. 509). Deutscher Ausschluß für Stahlbeton.

- Hassan, R., Yusoff, M., Ismail, Z., Amin, N. M., & Fadzil, M. A. (2014). *InCIEC 2013: Proceedings of the International Civil and Infrastructure Engineering Conference 2013*. Springer Science & Business Media.
- Hassan, T. K., & Rizkalla, S. H. (2010). Analysis and design guidelines of precast, prestressed concrete, composite load-bearing sandwich wall panels reinforced with CFRP grid. *PCI Journal*, 55(2), 147–164.
- Hearle, J. W. S. (2001). *High-performance Fibres*. Textile Institute.
- Hillerborg, A. (1980). Analysis of fracture by means of the fictitious crack model, particularly for fibre reinforced concrete. *International Journal of Cement Composites*, 2(4), 177–184.
- Hillerborg, A., Modéer, M., & Petersson, P.-E. (1976). Analysis of crack formation and crack growth in concrete by means of fracture mechanics and finite elements. *Cement and Concrete Research*, 6(6), 773–781. [http://doi.org/10.1016/0008-8846\(76\)90007-7](http://doi.org/10.1016/0008-8846(76)90007-7)
- Hodicky, K. (2015). *Analysis and development of Advanced Sandwich Elements for Sustainable Buildings* (PhD Dissertation). Civil Engineering, Technical University of Denmark.
- Hodicky, K., Hulin, T., Schmidt, J. W., & Stang, H. (2013a). Assessment risk of fracture in thin-walled fiber reinforced and regular High Performance Concretes sandwich elements. In *Proceedings of the 8th International Conference on Fracture Mechanics of Concrete and Concrete Structures* (pp. 1257–1266). Toledo, Spain.
- Hodicky, K., Hulin, T., Schmidt, J. W., & Stang, H. (2013b). Structural performance of new thin-walled concrete sandwich panel system reinforced with bfrp shear connectors. In *Proceedings of the fourth asia-pacific conference on frp in structures*. Melbourne, Australia.
- Hordijk, D. A., & Reinhardt, H. W. (1991). Local approach to fatigue of concrete. TU Delft, Delft University of Technology. Retrieved from <http://resolver.tudelft.nl/uuid:fa87147b-8201-47ed-83d7-b812b09c5fbb>
- Hulin, T. (2015). *Advanced Sandwich Elements for Sustainable Buildings - Integrated Structural and Materials Modelling* (Ph.D. Thesis). Technical University of Denmark, Kgs. Lyngby.
- IEA - Energy efficiency. (n.d.). Retrieved January 30, 2015, from <http://www.iea.org/aboutus/faqs/energyefficiency/>
- Jansson, A., Löfgren, I., & Gylltoft, K. (2010). Flexural Behaviour of members with a combination of steel fibres and conventional reinforcement. *Nordic Concrete Research*, 2/2010(42), 155–171.

- Jensen, O. M., & Hansen, P. F. (2001). Autogenous deformation and RH-change in perspective. *Cement and Concrete Research*, 31(12), 1859–1865. [http://doi.org/10.1016/S0008-8846\(01\)00501-4](http://doi.org/10.1016/S0008-8846(01)00501-4)
- Kabir, M. Z. (2005). Structural Performance of 3-D Sandwich Panels Under Shear and Flexural Loading. *Scientia Iranica*, 12(4), 402–408.
- Kanagasundaram, S., & Karihaloo, B. L. (1990). Minimum cost design of reinforced concrete structures. *Structural Optimization*, 2(3), 173–184. <http://doi.org/10.1007/BF01836566>
- Kanagasundaram, S., & Karihaloo, B. L. (1991). Minimum-cost reinforced concrete beams and columns. *Computers & Structures*, 41(3), 509–518. [http://doi.org/10.1016/0045-7949\(91\)90145-C](http://doi.org/10.1016/0045-7949(91)90145-C)
- Kang, J.-S., Won, D.-H., & Kang, Y.-J. (2011). Large Displacement Behaviors of Foam-Insulated Concrete Sandwich Panels Subjected to Uniform Pressure. *Journal of the Korean Society for Advanced Composite Structures*, 2(4), 35–43.
- Karihaloo, B. L. (1995). *Fracture Mechanics and Structural Concrete*. Harlow, Essex, England; New York: Longman Pub Group.
- Kazem, H., Bunn, W. G., Seliem, H., Rizkalla, S., & Glech, H. (2014). Durability and Long Term behaviour of FRP/Foam Shear Transfer Mechanism for Concrete Sandwich Panels. *PCI Journal*, (submitted).
- Khoury, G. A. (2008). Polypropylene fibres in heated concrete. Part 2: Pressure relief mechanisms and modelling criteria. *Magazine of Concrete Research - MAG CONCR RES*, 60(3), 189–204. <http://doi.org/10.1680/macr.2007.00042>
- Kim, J., & You, Y.-C. (2015). Composite Behavior of a Novel Insulated Concrete Sandwich Wall Panel Reinforced with GFRP Shear Grids: Effects of Insulation Types. *Materials*, 8, 899–913. <http://doi.org/10.3390/ma8030899>
- Kim, Y. J., Messenger, H., & Harmon, T. (2010). Composite insulated precast wall panels with shear transfer provided by carbon fiber grid. In *3rd fib International Congress*. Washington, USA.
- Kingspan. (2015). Fordele ved Kooltherm isolering fra Kingspan Insulation. Retrieved April 7, 2015, from <http://www.kingspaninsulation.dk/Produkt/Kooltherm.aspx>
- Knack, I. (2011). The use of PP fibres in tunnel construction to avoid explosive concrete spalling in case of fire. New test results for the clarification of the mode of action. In *2nd International RILEM Workshop on Concrete Spalling due to Fire Exposure*. Delft, The Netherlands.



- Kollár, L. P., & Springer, G. S. (2009). *Mechanics of Composite Structures* (1 edition). Place of publication not identified: Cambridge University Press.
- Kurihara, N., Kunieda, M., Kamada, T., Uchida, Y., & Rokugo, K. (2000). Tension softening diagrams and evaluation of properties of steel fiber reinforced concrete. *Engineering Fracture Mechanics*, 65(2–3), 235–245. [http://doi.org/10.1016/S0013-7944\(99\)00116-2](http://doi.org/10.1016/S0013-7944(99)00116-2)
- Lameiras, R., Barros, J., Azenha, M., & Valente, I. B. (November 2013b). Development of sandwich panels combining fibre reinforced concrete layers and fibre reinforced polymer connectors. Part II: Evaluation of mechanical behaviour. *Composite Structures*, 105, 460–470. <http://doi.org/10.1016/j.compstruct.2013.06.015>
- Lameiras, R., Barros, J., Valente, I. B., & Azenha, M. (November 2013a). Development of sandwich panels combining fibre reinforced concrete layers and fibre reinforced polymer connectors. Part I: Conception and pull-out tests. *Composite Structures*, 105, 446–459. <http://doi.org/10.1016/j.compstruct.2013.06.022>
- Lawler, J. S., Wilhelm, T., Zampini, D., & Shah, S. P. (2003). Fracture processes of hybrid fiber-reinforced mortar. *Materials and Structures*, 36(3), 197–208. <http://doi.org/10.1007/BF02479558>
- Lee, B., & Pessiki, S. (2008). Experimental Evaluation of Precast, Prestressed Concrete, Three-Wythe Sandwich Wall Panels. *PCI Journal*, 53(2), 95–115.
- Lee, J.-H., Yoon, Y.-S., & Kim, J.-H. (2012). A new heuristic algorithm for mix design of high-performance concrete. *KSCE Journal of Civil Engineering*, 16(6),
- Lim, C.-H., Yoon, Y.-S., & Kim, J.-H. (2004). Genetic algorithm in mix proportioning of high-performance concrete. *Cement and Concrete Research*, 34(3), 409–420. <http://doi.org/10.1016/j.cemconres.2003.08.018>
- Linsbauer, H. N. (1990). Application of the methods of fracture mechanics for the analysis of cracking in concrete dams. *Engineering Fracture Mechanics*, 35(1–3), 541–551. [http://doi.org/10.1016/0013-7944\(90\)90229-A](http://doi.org/10.1016/0013-7944(90)90229-A)
- Linsbauer, H. N., & Tschegg, E. K. (1986). Fracture energy determination of concrete with cube-shaped specimens. *Zement Und Beton*, 31, 38–40.
- Li, V. C. (1993). From Micromechanics to Structural Engineering. *Doboku Gakkai Ronbunshu*, 1993(471), 1–12. [http://doi.org/10.2208/jscej.1993.471\\_1](http://doi.org/10.2208/jscej.1993.471_1)
- Li, V. C. (1995). New Construction Materials Proliferate in Japan. *Civil Engineering—ASCE*, 65(8), 38–41.
- Li, V. C., & Maalej, M. (1996). Toughening in cement based composites. Part II: Fiber reinforced cementitious composites. *Cement and Concrete Composites*, 18(4), 239–249. [http://doi.org/10.1016/0958-9465\(95\)00029-1](http://doi.org/10.1016/0958-9465(95)00029-1)

- Lluka, D., Guri, M., Hajdari, V., & Ndoj, A. (2013). The design of slender rc columns. In *2nd International Balkans Conference on Challenges of Civil Engineering*. Tirana, Albania. Retrieved from <http://ecs.epoka.edu.al/index.php/bccce/bccce2013/paper/view/421>
- Löfgren, I. (2005a). *Fibre-reinforced Concrete for Industrial Construction* (PhD Dissertation). Chalmers University of Technology, Department of Civil and Environmental Engineering, Göteborg, Sweden.
- Löfgren, I. (2005b). Fibre-reinforced Concrete for Industrial Construction - a fracture mechanics approach to material testing and structural analysis.
- Löfgren, I., Stang, H., & Olesen, J. F. (2005). Fracture Properties of FRC Determined through Inverse Analysis of Wedge Splitting and Three-Point Bending Tests. *Journal of Advanced Concrete Technology*, 3(3), 423–434. <http://doi.org/10.3151/jact.3.423>
- Löfgren, I., Stang, H., & Olesen, J. F. (2007). The WST method, a fracture mechanics test method for FRC. *Materials and Structures*, 41(1), 197–211. <http://doi.org/10.1617/s11527-007-9231-3>
- Lorman, W. R., & Wiehle, C. K. (1953). Assembly-line technique results in low-cost concrete construction at forrestal village. *Civil Engineering (New York)*, 23(11), 58–62.
- Losch, E. (2003). Bowing of insulated precast concrete wall panels. *PCI Journal*, 48(6), 126–129.
- Lura, P., & Jensen, O. M. (2006). Measuring techniques for autogenous strain of cement paste. *Materials and Structures*, 40(4), 431–440. <http://doi.org/10.1617/s11527-006-9180-2>
- Lura, P., Jensen, O. M., & van Breugel, K. (2003). Autogenous shrinkage in high-performance cement paste: An evaluation of basic mechanisms. *Cement and Concrete Research*, 33(2), 223–232. [http://doi.org/10.1016/S0008-8846\(02\)00890-6](http://doi.org/10.1016/S0008-8846(02)00890-6)
- Mackerle, J. (2002). Finite element analyses of sandwich structures: a bibliography (1980–2001). *Engineering Computations*, 19(2), 206–245.
- Mahadevan, M. G. (2009). *Textile Spinning, Weaving and Designing*. Chandigarh, IND: Global Media.
- Marti, P., Pfyl, T., Sigrist, V., & Ulaga, T. (1999). Harmonized test procedures for steel fiber-reinforced concrete. *ACI Materials Journal*, 96(6). Retrieved from <http://trid.trb.org/view.aspx?id=639327>
- Maruyama, I., Kameta, S., Suzuki, M., & Sato, R. (2006). Cracking of high strength concrete around deformed reinforcing bar due to shrinkage. In *International*

*RILEM-JCI Seminar on Concrete Durability and Service Life Planning*. Dead Sea, Israel.

- Maximos, H. N., Pong, W. A., Tadros, M. K., & Martin, L. D. (2007). *Behavior and Design of Composite Precast Prestressed Concrete Sandwich Panels with NU-Tie*. Lincoln, USA: University of Nebraska.
- Megat Johari, M. A., Brooks, J. J., Kabir, S., & Rivard, P. (2011a). Influence of supplementary cementitious materials on engineering properties of high strength concrete. *Construction and Building Materials*, 25(5), 2639–2648. <http://doi.org/10.1016/j.conbuildmat.2010.12.013>
- Megat Johari, M. A., Brooks, J. J., Kabir, S., & Rivard, P. (2011b). Influence of supplementary cementitious materials on engineering properties of high strength concrete. *Construction and Building Materials*, 25(5), 2639–2648. <http://doi.org/10.1016/j.conbuildmat.2010.12.013>
- Mehta, P. K., & Aïtcin, P.-C. (1990). Microstructural basis of selection of materials and mix proportions for high strength concrete. *ACI Special Publication*, 121, 265–286.
- Metelli, G., Bettini, N., & Plizzari, G. (2011). Experimental and numerical studies on the behavior of concrete sandwich panels. *European Journal of Environmental and Civil Engineering*, 15(10), 1465–1481.
- Mikeska, T. (2014). *Energy performance of ventilation, heating and cooling systems integrated in sandwich panel of high performance concrete* (Ph.D. Thesis). Technical University of Denmark, Kgs. Lyngby.
- Morcous, G., Tadros, M. K., Lafferty, M., & Gremel, D. (2010). Optimised NU sandwich panel system for energy, composite action and production efficiency. In *3rd International fib Congress*. Washington, USA.
- Mortensen, A. (2006). *Concise Encyclopedia of Composite Materials*. Elsevier.
- Naaman, A. E. (2003). Engineered Steel Fibers with Optimal Properties for Reinforcement of Cement Composites. *Journal of Advanced Concrete Technology*, 1(3), 241–252.
- Naaman, A. E., & Reinhardt, H. W. (1996). *High Performance Fiber Reinforced Cement Composites 2: Proceedings of the International Workshop*. CRC Press.
- Naito, C., Hoemann, J., Beacraft, M., & Bewick, B. (2012). Performance and Characterization of Shear Ties for Use in Insulated Precast Concrete Sandwich Wall Panels. *Journal of Structural Engineering*, 138(1), 52–61. [http://doi.org/10.1061/\(ASCE\)ST.1943-541X.0000430](http://doi.org/10.1061/(ASCE)ST.1943-541X.0000430)

- Nanakorn, P., & Horii, H. (1996). A fracture-mechanics-based design method for SFRC tunnel linings. *Tunnelling and Underground Space Technology*, 11(1), 39–43. [http://doi.org/10.1016/0886-7798\(96\)00050-8](http://doi.org/10.1016/0886-7798(96)00050-8)
- National Instruments. (2013). LabVIEW (Version 2013). Austin, Texas, USA: National Instruments.
- Nawy, E. G. (2008). *Concrete Construction Engineering Handbook*. CRC Press.
- Nelson, P. K., Li, V. C., & Kamada, T. (2002). Fracture Toughness of Microfiber Reinforced Cement Composites. *Journal of Materials in Civil Engineering*, 14(5), 384–391. [http://doi.org/10.1061/\(ASCE\)0899-1561\(2002\)14:5\(384\)](http://doi.org/10.1061/(ASCE)0899-1561(2002)14:5(384))
- Neville, A. (2011). *Properties of concrete* (5th ed.). Prentice Hall.
- Neville, A., & Aïtcin, P.-C. (1998). High performance concrete—An overview. *Materials and Structures*, 31(2), 111–117. <http://doi.org/10.1007/BF02486473>
- Nielsen, K. E. C. (1971). *Aggregate stresses in concrete* (PhD Dissertation). Royal Institute of Technology, Stockholm.
- Nijhawan, J. C. (1998). Insulated wall panels - interface shear transfer. *PCI Journal*, 43(3), 98–101.
- Olesen, J. F. (2001). Fictitious crack propagation in fibre reinforced concrete beams. *Journal of Engineering Mechanics*, 127(3), 272–281.
- Østergaard, L. (2003, October). *Early Age Fracture Mechanics and Cracking of Concrete: Experiments and Modelling* (PhD Dissertation). Civil Engineering, Technical University of Denmark.
- Østergaard, L., Lange, D., & Stang, H. (2004). Early-age stress–crack opening relationships for high performance concrete. *Cement and Concrete Composites*, 26(5), 563–572. [http://doi.org/10.1016/S0958-9465\(03\)00074-X](http://doi.org/10.1016/S0958-9465(03)00074-X)
- Østergaard, L., & Olesen, J. F. (2005). Method for determination of tensile properties of ECC. I: Formulation and parameter variations. *Proceedings of the International Workshop on High Performance Fiber Reinforced Cementitious Composites in Structural Applications*, 60–67.
- Ozbay, E., Gesoglu, M., & Guneyisi, E. (2010). Transport properties based multi-objective mix proportioning optimization of high performance concretes. *Materials and Structures*, 44(1), 139–154. <http://doi.org/10.1617/s11527-010-9615-7>
- Pantelides, C., Surapaneni, R., & Reaveley, L. (2008). Structural Performance of Hybrid GFRP/Steel Concrete Sandwich Panels. *Journal of Composites for Construction*, 12(5), 570–576. [http://doi.org/10.1061/\(ASCE\)1090-0268\(2008\)12:5\(570\)](http://doi.org/10.1061/(ASCE)1090-0268(2008)12:5(570))

- Papanicolaou, C. G., & Triantafillou, T. C. (2002). Minimum cost design of concrete sandwich panels made of HPC faces and PAC core: the case of in-plane loading. *Structural Concrete*, 3(4), 167–181. <http://doi.org/10.1680/stco.2002.3.4.167>
- Papanicolaou, C. G., & Triantafillou, T. C. (2004). Analysis and minimum cost design of concrete sandwich panels under out-of-plane loading. *Structural Concrete*, 5(1), 11–27. <http://doi.org/10.1680/stco.2004.5.1.11>
- PCI Committee on Precast Sandwich Wall Panels. (2011). State of the art of Precast/Prestressed concrete sandwich wall panels. *PCI Journal*, 56(2), 131–176.
- Pessiki, S., & Mlynarczyk, A. (2003). Experimental evaluation of the composite behavior of precast concrete sandwich wall panels. *PCI Journal*, 48(2), 54–71.
- Phelan, W. S. (2011). Self-consolidating concrete (SCC): Today and Tomorrow. *Structure Magazine*, 33–35.
- Phillips, G. O., & Hongu (Eds.). (1997). *Front Matter*. Woodhead Publishing. Retrieved from <http://www.sciencedirect.com/science/article/pii/B9781855733343500016>
- Pichler, C., Lackner, R., & Mang, H. A. (2007). A multiscale micromechanics model for the autogenous-shrinkage deformation of early-age cement-based materials. *Engineering Fracture Mechanics*, 74(1–2), 34–58. <http://doi.org/10.1016/j.engfracmech.2006.01.034>
- Prado, E. P., & van Mier, J. G. M. (2003). Effect of particle structure on mode I fracture process in concrete. *Engineering Fracture Mechanics*, 70(14), 1793–1807. [http://doi.org/10.1016/S0013-7944\(03\)00125-5](http://doi.org/10.1016/S0013-7944(03)00125-5)
- Ranzi, G. (2008). Locking problems in the partial interaction analysis of multi-layered composite beams. *Engineering Structures*, 30(10), 2900–2911. <http://doi.org/10.1016/j.engstruct.2008.04.006>
- Ranzi, G., Gara, F., Leoni, G., & Bradford, M. A. (2006). Analysis of Composite Beams with Partial Shear Interaction Using Available Modelling Techniques: A Comparative Study. *Comput. Struct.*, 84(13–14), 930–941. <http://doi.org/10.1016/j.compstruc.2005.12.003>
- Rao, G. A., & Prasad, B. K. R. (2002). Fracture energy and softening behavior of high-strength concrete. *Cement and Concrete Research*, 32(2), 247–252. [http://doi.org/10.1016/S0008-8846\(01\)00667-6](http://doi.org/10.1016/S0008-8846(01)00667-6)
- Reinhardt, H. W. (1984). Fracture Mechanics of an Elastic Softening Material like Concrete. Delft University of Technology. Retrieved from <http://resolver.tudelft.nl/uuid:7e908683-e816-4c4f-928f-03103ed2780e>

- RILEM TC 162-TDF. (2002). *Brite Euram Project nr: BE 97-4163, Test and Design Methods for Steel Fibre Reinforced Concrete*.
- Rizkalla, S. H., Hassan, T. K., & Lucier, G. (2009). FRP Shear Transfer Mechanism for Precast, Prestressed Concrete Sandwich Load-Bearing Panels. *ACI Special Publication*, 265, 603–625.
- Rizkalla, S., Lucier, G., & Dawood, M. (2012). Innovative Use of FRP for the Precast Concrete Industry. *Advances in Structural Engineering*, 15(4), 565–574. <http://doi.org/10.1260/1369-4332.15.4.565>
- Roelfstra, P. E., & Wittmann, F. H. (1986). A Numerical Method to Link Strain Softening with Fracture in Concrete, 163–175.
- Romualdi, J. P., & Batson, G. B. (1963). Mechanics of Crack Arrest in Concrete. *Journal of the Engineering Mechanics Division*, 89(3), 147–168.
- Romualdi, J. P., & Mandel, J. A. (1964). Tensile Strength of concrete Affected by Uniformly Distributed and Closely Spaced Short Lengths of wire Reinforcement. *ACI Journal Proceedings*, 61(6), 657–672. <http://doi.org/10.14359/7801>
- Rossi, P., & Chanvillard, G. (2000). *PRO 15: 5th RILEM Symposium on Fibre-Reinforced Concretes (FRC) - BEFIB' 2000*. RILEM Publications.
- Rougeron, P., & Aïtcin, P.-C. (1994). Optimization of the Composition of a High-Performance Concrete. *Cement, Concrete, and Aggregates*, 16(2), 115–124.
- Saertex. (2013). NCF - Non Crimp Fabrics for the composite industry - preforms - textile stitch bonded constructions - aramid - carbon - glass - multiaxials - Saertex. Retrieved February 9, 2015, from <http://www.saertex.com/produkt>
- Salmon, D. C., Einea, A., Tadros, M. K., & Culp, T. (1997). Full scale testing of precast concrete sandwich panels. *ACI Structural Journal*, 94(4), 354–362.
- Sato, R., Xu, M., & Yang, Y. (1999). Stresses due to autogenous shrinkage in high strength concrete and its prediction. *Autogenous Shrinkage of Concrete*, 351–362.
- Schaffer, S. J. (1998). Irving J. Gill, Progressive Architect Part II: Creating a Sense of Place. *The Journal of San Diego History*, 44(1). Retrieved from <http://www.sandiegohistory.org/journal/98winter/gill2.htm>
- Scheffler, C., Förster, T., Mäder, E., Heinrich, G., Hempel, S., & Mechtcherine, V. (2009). Aging of alkali-resistant glass and basalt fibers in alkaline solutions: Evaluation of the failure stress by Weibull distribution function. *Journal of Non-Crystalline Solids*, 355(52–54), 2588–2595. <http://doi.org/10.1016/j.jnoncrysol.2009.09.018>
- Schladitz, F., Frenzel, M., Ehlig, D., & Curbach, M. (2012). Bending load capacity of reinforced concrete slabs strengthened with textile reinforced concrete. *Engi-*

- neering Structures*, 40, 317–326.  
<http://doi.org/10.1016/j.engstruct.2012.02.029>
- Schlangen, E., Koenders, E. A. B., & van Breugel, K. (2007). Influence of internal dilation on the fracture behaviour of multi-phase materials. *Engineering Fracture Mechanics*, 74(1–2), 18–33.  
<http://doi.org/10.1016/j.engfracmech.2006.01.033>
- Shah, S., & Carpinteri, A. (Eds.). (1990). *Fracture Mechanics Test Methods For Concrete* (1 edition). CRC Press.
- Shah, S. P. (1992). Do Fibers Increase the Tensile Strength of Cement-Based Matrix? *ACI Materials Journal*, 88(6). <http://doi.org/10.14359/1195>
- Shah, S. P. (1995). *Fracture Mechanics of Concrete: Applications of Fracture Mechanics to Concrete, Rock and Other Quasi-Brittle Materials*. John Wiley & Sons.
- Shah, S. P., & Weiss, W. J. (2000). High Strength Concrete: Strength, Permeability, and Cracking. In *PCI/FHWA International Symposium on High Performance Concrete* (pp. 331–340). Orlando, Florida.
- Shah, S. P., Weiss, W. J., & Yang, W. (1997). Shrinkage cracking in High Performance Concrete. In *PCI/FHWA International Symposium on High Performance Concrete* (pp. 148–158). New Orleans, USA.
- Shiotani, T., Bisschop, J., & Van Mier, J. G. M. (2003). Temporal and spatial development of drying shrinkage cracking in cement-based materials. *Engineering Fracture Mechanics*, 70(12), 1509–1525. [http://doi.org/10.1016/S0013-7944\(02\)00150-9](http://doi.org/10.1016/S0013-7944(02)00150-9)
- Skocek, J., & Stang, H. (2008). Inverse analysis of the wedge-splitting test. *Engineering Fracture Mechanics*, 75(10), 3173–3188.  
<http://doi.org/10.1016/j.engfracmech.2007.12.003>
- Smarter Building Systems. (2010). Basalt Rebar, Basalt Mesh, Basalt Fabric, Basalt Fiber and Chopped Fiber. Smarter Green Building Materials. Retrieved from <http://smarter-building-systems.com/>
- Sopal, G. J. (2013). *Use of CFRP Grid as shear transfer mechanism for Precast Concrete Sandwich Wall Panels* (PhD Dissertation). North Carolina State University, Raleigh, USA.
- Sopal, G., Rizkalla, S., & Sennour, L. (2013). CFRP Grid For Concrete Sandwich Panels. In *4th Asia-Pacific Conference on FRP in Structures*. Melbourne, Australia.
- Soriano, J., & Rizkalla, S. (2013). Use of FRP Grid for the Composite Action of Concrete Sandwich Panels. In *FRPRCS11 – 11th International Symposium on Fi-*

- ber Reinforced Polymer for Reinforced Concrete Structures*. Guimarães, Portugal.
- Sousa Jr, J. B. M., & da Silva, A. R. (2010). Analytical and numerical analysis of multilayered beams with interlayer slip. *Engineering Structures*, 32(6), 1671–1680. <http://doi.org/10.1016/j.engstruct.2010.02.015>
- Springenschmid, R. (Ed.). (1994). *Thermal Cracking in Concrete at Early Ages: Proceedings of the International RILEM Symposium*. London: CRC Press.
- Stang, H. (1996). Significance of shrinkage-induced clamping pressure in fiber-matrix bonding in cementitious composite materials. *Advanced Cement Based Materials*, 4(3–4), 106–115. [http://doi.org/10.1016/S1065-7355\(96\)90079-6](http://doi.org/10.1016/S1065-7355(96)90079-6)
- Stang, H., Gettu, R., & Barr, B. (2000). *Test Methods for the Characterization of Steel Fiber Reinforced Concrete - A State-of-the-Art Report. Report of Sub-task 1.1 Test and Design Methods for Steel Fiber Reinforced Concrete Brite-EuRam Project BRPR-CT98-0813 (DG12-BRPR)* (p. 51).
- Stang, H., Olesen, J. F., Poulsen, P. N., & Dick-Nielsen, L. (2007). On the application of cohesive crack modeling in cementitious materials. *Materials and Structures*, 40(4), 365–374. <http://doi.org/10.1617/s11527-006-9179-8>
- Stang, H., & Østergaard, L. (2003). Cracking and Fracture in Early Age Concrete. *Advances in Cement and Concrete*, 257–268.
- Sule, M., & van Breugel, K. (2004). The effect of reinforcement on early-age cracking due to autogenous shrinkage and thermal effects. *Cement and Concrete Composites*, 26(5), 581–587. [http://doi.org/10.1016/S0958-9465\(03\)00078-7](http://doi.org/10.1016/S0958-9465(03)00078-7)
- Tada, H., Paris, P. C., & Irwin, G. R. (2000). *The Stress Analysis of Cracks Handbook, Third Edition*. Three Park Avenue New York, NY 10016-5990: ASME. Retrieved from <http://ebooks.asmedigitalcollection.asme.org/book.aspx?bookid=230>
- Taylor, M., Lydon, F. D., & Barr, B. I. G. (1997). Toughness measurements on steel fibre-reinforced high strength concrete. *Cement and Concrete Composites*, 19(4), 329–340. [http://doi.org/10.1016/S0958-9465\(97\)00036-X](http://doi.org/10.1016/S0958-9465(97)00036-X)
- The MathWorks, Inc. (2013). MATLAB (Version R2013a). Natick, Massachusetts: The MathWorks Inc.
- Thorenfeldt, E., Tomaszewicz, A., & Jensen, J. J. (1987). Mechanical properties of high-strength concrete and applications in design. In *Proceedings of the Symposium on the Utilization of High Strength Concrete*. Stavanger, Norway: Tapir.
- TNO DIANA. (2011). Finite Element Analysis User's Manual - Release 9.4.4. TNO.



- Twachtman, Q. (1936). *Concrete building construction*. Google Patents. Retrieved from <http://www.google.com/patents/US2065355>
- Ulfkjær, J., Krenk, S., & Brincker, R. (1995). Analytical Model for Fictitious Crack Propagation in Concrete Beams. *Journal of Engineering Mechanics*, 121(1), 7–15. [http://doi.org/10.1061/\(ASCE\)0733-9399\(1995\)121:1\(7\)](http://doi.org/10.1061/(ASCE)0733-9399(1995)121:1(7))
- Van de Velde, K., Kiekens, P., & Van Langenhove, L. (2003). Basalt fibres as reinforcement for composites. In *10th Int. Conf. on Composites/Nano Engineering*. University of New Orleans, New Orleans.
- Van Mier, J. G. M. (1996). *Fracture Processes of Concrete*. CRC Press, Boca Raton, Florida. Retrieved from <http://www.crcpress.com/product/isbn/9780849391231>
- Van Mier, J. G. M., & van Vliet, M. R. A. (2002). Uniaxial tension test for the determination of fracture parameters of concrete: state of the art. *Engineering Fracture Mechanics*, 69(2), 235–247. [http://doi.org/10.1016/S0013-7944\(01\)00087-X](http://doi.org/10.1016/S0013-7944(01)00087-X)
- Vasiliev, V. V., & Morozov, E. (2013). *Advanced Mechanics of Composite Materials (Third Edition)* (3rd ed.). Boston: Elsevier. Retrieved from <http://www.sciencedirect.com/science/article/pii/B9780080982311010013>
- Vetrotex. (2011). Vetrotex Technical Information - Saint-Gobain Vetrotex. Retrieved February 9, 2015, from <http://www.vetrotextextiles.com/TechnicalInformation>
- Vonk, R. A. (1992). *Softening of concrete loaded in compression* (PhD Dissertation). Technical University of Eindhoven.
- Wade, T. G., Porter, M. L., & Jacobs, D. R. (1988). *Glass-Fiber Composite Connectors for Insulated Concrete Sandwich Walls*. Ames, USA: Engineering Research Institute, Iowa State University.
- Walter, R., Olesen, J. F., Stang, H., Walter, R., Olesen, J. F., & Stang, H. (2005). Interface Mixed Mode Model. *11th International Conference on Fracture*.
- Walter, R., Østergaard, L., Olesen, J. F., & Stang, H. (2005). Wedge splitting test for a steel-concrete interface. *Engineering Fracture Mechanics*, 72, 2565–2583. <http://doi.org/10.1016/j.engfracmech.2005.06.001>
- Wei, B., Cao, H., & Song, S. (2010). Tensile behavior contrast of basalt and glass fibers after chemical treatment. *Materials & Design*, 31(9), 4244–4250. <http://doi.org/10.1016/j.matdes.2010.04.009>
- Williams Portal, N., Lundgren, K., Wallbaum, H., & Malaga, K. (2014). Sustainable Potential of Textile-Reinforced Concrete. *Journal of Materials in Civil Engineering*, accepted for publication. [http://doi.org/10.1061/\(ASCE\)MT.1943-5533.0001160](http://doi.org/10.1061/(ASCE)MT.1943-5533.0001160)

- Woltman, G., Tomlinson, D., & Fam, A. (2013). Investigation of Various GFRP Shear Connectors for Insulated Precast Concrete Sandwich Wall Panels. *Journal of Composites for Construction*, 17(5), 711–721. [http://doi.org/10.1061/\(ASCE\)CC.1943-5614.0000373](http://doi.org/10.1061/(ASCE)CC.1943-5614.0000373)
- Wu, Z., Wang, X., & Wu, G. (2012). Advancement of structural safety and sustainability with basalt fiber reinforced polymers. In *International Conference on Fiber-Reinforced Polymer (FRP) Composites in Civil Engineering*. International Institute for FRP in Construction (IIFC).
- Yin, S. Y., Xu, S., & Li, H. (2013). Improved mechanical properties of textile reinforced concrete thin plate. *Journal of Wuhan University of Technology-Mater. Sci. Ed.*, 28(1), 92–98. <http://doi.org/10.1007/s11595-013-0647-z>
- Yun, Y.-W., Jang, I.-Y., & Wang, W.-W. (2012). Early-age autogenous shrinkage of high-performance concrete columns by embedded Fiber Bragg-Grating sensor. *KSCE Journal of Civil Engineering*, 16(6), 967–973. <http://doi.org/10.1007/s12205-012-0811-6>
- Zhejiang GBF Basalt Fiber Co., LTD. (2015). Basalt Reinforcing Mesh, Basalt Reinforcing Mesh Manufacturer, Supplier, Factory - Zhejiang GBF Basalt Fiber Co., LTD. Retrieved April 7, 2015, from <http://www.basaltfiber-gbf.com/basalt-reinforcing-mesh-supplier.html>
- Zheng, Z., & Feldman, D. (1995). Synthetic fibre-reinforced concrete. *Progress in Polymer Science*, 20(2), 185–210. [http://doi.org/10.1016/0079-6700\(94\)00030-6](http://doi.org/10.1016/0079-6700(94)00030-6)
- Zipprodt, R. R. (1935). Recent Noteworthy Developments In Concrete's Use In Housing Developments. *ACI Journal Proceedings*, 31(5), 462–477. <http://doi.org/10.14359/8356>

This Ph.D. thesis proposes a framework for analysis and optimization of the precast thin-walled High Performance Concrete Sandwich Panels. The present framework is led at three levels. The material level and the structural level are described through experimental and numerical investigations. The third level is concerned about structural and cost optimization of the proposed sandwich system. Finally, the study is performed to assess the risk of early age cracking and to analyse the robustness of thin-walled sandwich panels at early ages.

**DTU Civil Engineering**  
Technical University of Denmark

Brovej, Building 118  
2800 Kongens Lyngby  
Tel. 45251700

[www.byg.dtu.dk](http://www.byg.dtu.dk)

ISBN 9788778774224  
ISSN 1601-2917